

**HOST CELL PROTEIN IMPURITIES AND PROTEIN-PROTEIN  
INTERACTIONS IN DOWNSTREAM PURIFICATION OF MONOCLONAL  
ANTIBODIES**

by

Nicholas E. Levy

A dissertation submitted to the Faculty of the University of Delaware in partial fulfillment of the requirements for the degree of Doctor of Philosophy in Chemical Engineering

Summer 2014

© 2014 Nicholas E. Levy  
All Rights Reserved

UMI Number: 3642330

All rights reserved

INFORMATION TO ALL USERS

The quality of this reproduction is dependent upon the quality of the copy submitted.

In the unlikely event that the author did not send a complete manuscript and there are missing pages, these will be noted. Also, if material had to be removed, a note will indicate the deletion.



UMI 3642330

Published by ProQuest LLC (2014). Copyright in the Dissertation held by the Author.

Microform Edition © ProQuest LLC.

All rights reserved. This work is protected against unauthorized copying under Title 17, United States Code



ProQuest LLC.  
789 East Eisenhower Parkway  
P.O. Box 1346  
Ann Arbor, MI 48106 - 1346

**HOST CELL PROTEIN IMPURITIES AND PROTEIN-PROTEIN  
INTERACTIONS IN DOWNSTREAM PURIFICATION OF MONOCLONAL  
ANTIBODIES**

by

Nicholas E. Levy

Approved: \_\_\_\_\_  
Abraham M. Lenhoff, Ph.D.  
Chair of the Department of Chemical and Biomolecular Engineering

Approved: \_\_\_\_\_  
Babatunde A. Ogunnaike, Ph.D.  
Dean of the College of Engineering

Approved: \_\_\_\_\_  
James G. Richards, Ph.D.  
Vice Provost for Graduate and Professional Education

I certify that I have read this dissertation and that in my opinion it meets the academic and professional standard required by the University as a dissertation for the degree of Doctor of Philosophy.

Signed:

---

Abraham M. Lenhoff, Ph.D.  
Professor in charge of dissertation

I certify that I have read this dissertation and that in my opinion it meets the academic and professional standard required by the University as a dissertation for the degree of Doctor of Philosophy.

Signed:

---

Kelvin H. Lee, Ph.D.  
Member of dissertation committee

I certify that I have read this dissertation and that in my opinion it meets the academic and professional standard required by the University as a dissertation for the degree of Doctor of Philosophy.

Signed:

---

Christopher J. Roberts, Ph.D.  
Member of dissertation committee

I certify that I have read this dissertation and that in my opinion it meets the academic and professional standard required by the University as a dissertation for the degree of Doctor of Philosophy.

Signed:

---

Edward R. Lyman, Ph.D.  
Member of dissertation committee

## ACKNOWLEDGEMENTS

I am very grateful for the help and guidance I received from many different people during my graduate studies at the University of Delaware. Faculty members, fellow graduate students, friends and family all helped me throughout this challenging experience. I would like to specifically thank a few people who were particularly important to me throughout my graduate career.

First, I would like to thank Bramie Lenhoff and Kelvin Lee for giving me the opportunity to work on a fantastic thesis project. I would also like to thank Bramie for his guidance and support throughout my graduate career. As an advisor, Bramie allowed me enough freedom to develop into an independent researcher without letting me get too far off track. Bramie's guidance has helped me to grow as both a scientist and a person.

I am thankful to have been a member of the Chemistry-Biology Interface (CBI) program at Delaware. CBI was an important part of my graduate experience that contributed to my development as a scientist and resulted in great friendships and collaborations.

I would also like to thank the Lenhoff and Lee group members for their help and support. Kristin Valente performed many of the proteomic analyses that are found throughout this thesis. Without her efforts and expertise my work would not have been possible. Steve Traylor and Brian Bowes helped me get started in the lab when I first joined the Lenhoff group, and Harun Koku went out of his way to help me with computational work towards the end of my graduate career. Rahul Bhambure and Jim

Angelo were great office-mates and helped me in the lab during my last few years in the Lenhoff group.

I would like to thank Amalie Tuerk for her endless love and support. I am very lucky to have Amalie in my life. I am also fortunate to have an amazing group of friends in Colburn and beyond. Peter Beltramo and Kyle Doolan have been great friends throughout my graduate career. When I needed a break from Delaware I could always count on my friends from the University of Maryland (Fauci, Dan, KK, Justin, Julie, Ted, Evie and Greg) or Lexington (Ben, Sol and Toma) to cheer me up and show me a good time.

I am very lucky to have such a loving and supportive family. My parents provided me with incredible opportunities throughout my life and made me believe I could succeed in any endeavor. The love, support and friendship of my sister helped me through some of the more difficult periods of graduate school. I am also fortunate to have an amazing extended family. I am grateful to my grandparents, aunts and uncles and cousins for their love, support and unforgettable summers on Cape Cod.

## TABLE OF CONTENTS

LIST OF TABLES .....	xi
LIST OF FIGURES .....	xiii
ABSTRACT .....	xxi

### Chapter

1	INTRODUCTION .....	1
1.1	Motivation and Goals .....	1
1.2	Monoclonal Antibody Structure .....	2
1.3	Platform MAb Manufacturing .....	5
1.3.1	Upstream Processes .....	5
1.3.2	Clarification and Protein A Affinity Chromatography .....	8
1.3.3	Chromatographic Polishing .....	11
1.3.3.1	Ion-Exchange Chromatography .....	11
1.3.3.2	Hydrophobic Interaction Chromatography .....	12
1.3.3.3	Multimodal Chromatography .....	13
1.4	Formulation .....	13
1.5	Host Cell Protein Impurities .....	14
1.6	Proteomics in Bioprocessing .....	16
1.7	Phase Behavior .....	18
1.8	Protein-Protein Interactions .....	19
2	MATERIALS AND METHODS .....	21
2.1	Materials and Solutions .....	21
2.2	Instantaneous Phase Boundaries .....	23
2.3	ANS Fluorescence .....	24
2.4	Oligomerization Measurements .....	25
2.4.1	Dynamic Light Scattering .....	25
2.4.2	Analytical Ultracentrifugation .....	26
2.5	Fragment Generation and Purification .....	26
2.6	Cell Culture .....	27

2.7	Protein A Affinity Purification of MABs .....	28
2.8	Protein-Protein Interactions.....	29
2.9	HCP-MAB CIC.....	31
2.10	Proteomic Methods.....	32
	2.10.1 Sample Preparation.....	32
	2.10.2 Two-Dimensional Gel Electrophoresis (2-DE).....	32
	2.10.3 Mass Spectrometry .....	33
2.11	Calculation of HCP Parameters.....	34
2.12	MAB-HCP Interaction Orientation Calculations .....	34
2.13	Recombinant Lipoprotein Lipase (LPL) Production .....	35
	2.13.1 <i>E. coli</i> Expression of CHO LPL .....	35
	2.13.2 LPL Purification .....	36
	2.13.3 LPL Refolding.....	37
2.14	LPL Activity Assay .....	38
2.15	Yeast Surface Display (YSD) of LPL .....	39
3	HOST CELL PROTEIN IMPURITIES IN PROTEIN A AFFINITY PURIFICATION OF MONOCLONAL ANTIBODIES.....	40
	3.1 Introduction .....	40
	3.2 Total HCP Product Association .....	41
	3.3 Cross-Interaction Chromatography (CIC): MAB-CHO HCP.....	44
	3.4 Cross-Interaction Chromatography: MAB-Insulin .....	55
	3.5 Interaction Orientation of MAb and Associated HCP Impurities .....	56
	3.6 Conclusions .....	63
4	HOST CELL PROTEIN IMPURITIES IN MONOCLONAL ANTIBODY PLATFORM PURIFICATION POLISHING STEPS .....	65
	4.1 Introduction .....	65
	4.2 Binding Capacity of Polishing Resins.....	66
	4.3 Total Product Association in Polishing Columns.....	67
	4.4 Cross-Interaction Chromatography: HCP-MAB Association in HIC.....	70
	4.5 HCP Fractionation: Cation-Exchange Chromatography .....	75
	4.6 HCP Fractionation: Anion-Exchange Chromatography.....	80
	4.7 HCP Fractionation: Hydrophobic Interaction Chromatography .....	87
	4.8 HCP Fractionation: Multimodal Chromatography .....	91
	4.9 HCP Homology Models .....	97
	4.10 Conclusions .....	103

5	EFFECTS OF LIPOPROTEIN LIPASE AS AN IMPURITY IN MONOCLONAL ANTIBODY DOWNSTREAM PROCESSING AND FORMULATIONS.....	105
5.1	Introduction .....	105
5.2	Lipase Catalysis.....	106
5.3	LPL Production .....	109
5.3.1	Expression in <i>E. coli</i> .....	109
5.3.2	CHO LPL Purification.....	111
5.4	Characterization of LPL Interaction with MAbs.....	115
5.4.1	LPL-MAb CIC.....	116
5.4.2	LPL-MAb Yeast Surface Display .....	117
5.5	Enzymatic Activity of CHO LPL Expressed in <i>E. coli</i> .....	122
5.6	Native CHO LPL Activity.....	126
5.7	Conclusions .....	128
6	MONOCLONAL ANTIBODY SELF-INTERACTIONS AND INSTANTANEOUS PHASE BEHAVIOR .....	130
6.1	Introduction .....	130
6.2	MAb Instantaneous Phase Boundaries .....	131
6.2.1	Instantaneous Phase Boundaries in Different Salts .....	133
6.2.2	Instantaneous Phase Boundaries: Dependence on Solution pH .....	135
6.3	Co-Precipitation with HCP Product-Associated Impurity .....	138
6.4	MAb Self-Interactions.....	140
6.4.1	$B_{22}$ Values as a Function of Solution pH.....	147
6.5	ANS Fluorescence.....	149
6.6	MAb D and MAb $D_M$ Instantaneous Phase Boundary and $B_{22}$ Comparison .....	156
6.7	Conclusions .....	160
7	MONOCLONAL ANTIBODY OLIGOMERIZATION AND FRAGMENT INTERACTION STRENGTH .....	162
7.1	Introduction .....	162
7.2	MAb Oligomerization Tendencies .....	163
7.3	Fragment Interactions.....	172

7.3.1	IDEC-152 Fragment Interactions .....	173
7.3.2	Mill04 Fragment Interactions .....	175
7.3.3	MAb B Fragment Interactions.....	177
7.3.4	MAb C Fragment Interactions.....	179
7.4	Calculation of Full MAb Interaction from Fragments .....	181
7.4.1	Stoichiometric Mixing-Rule Model .....	181
7.4.2	Three-Sphere Model.....	182
7.5	Conclusions .....	188
8	CONCLUSIONS AND RECOMMENDATIONS FOR FUTURE WORK ..	190
8.1	Conclusions .....	190
8.1.1	HCP Impurities in MAb Bioprocessing .....	190
8.1.2	MAb-MAb Interactions and Phase Boundaries.....	193
8.2	Future Work .....	194
8.2.1	Improved Upstream Technology.....	194
8.2.2	Yeast-Surface Display Technology Development .....	195
8.2.3	High-Throughput Product-Association Method Development .	196
8.2.4	MAb-HCP Interaction Calculations .....	197
8.2.5	HCP Analysis for Alternative Cell Lines .....	197
	REFERENCES.....	199
Appendix		
A	IDENTIFIED 2-DE SPOTS FOR PROTEIN A PRODUCT ASSOCIATION .....	220
A.1	Quantification of Missing Spots from 2-DE Images.....	220
A.1.1	MAb D HCP-CIC 2-DE Analysis: Protein A Solution Conditions.....	222
A.1.2	MAb D <sub>M</sub> HCP-CIC 2-DE Analysis: Protein A Solution Conditions.....	226
A.1.3	IDEC-152 HCP-CIC 2-DE Analysis: Protein A Solution Conditions.....	229
A.1.4	Mill04 HCP-CIC 2-DE Analysis: Protein A Solution Conditions.....	231

A.1.5	Mill04 Fab HCP-CIC 2-DE Analysis: Protein A Solution Conditions.....	234
A.1.6	Mill04 Fc HCP-CIC 2-DE Analysis: Protein A Solution Conditions.....	236
B	IDENTIFIED 2-DE SPOTS FOR HIC PRODUCT ASSOCIATION .....	239
B.1	Quantification of Missing Spots from 2-DE Images.....	239
B.1.1	MAb D HCP-CIC 2-DE Analysis: HIC Conditions.....	241
B.1.2	MAb D <sub>M</sub> HCP-CIC 2-DE Analysis: HIC Conditions .....	242
C	MAB FRAGMENT PURIFICATION .....	243
C.1	MAb B Fc Chromatographic Purification .....	243
C.2	MAb C Fc Chromatographic Purification .....	244
C.3	IDEC-152 Fc Chromatographic Purification.....	245
C.4	Mill04 Fc Fragment Purification .....	247
D	LIPOPROTEIN LIPASE DNA SEQUENCE .....	249
D.1	Synthesized CHO LPL Sequence.....	249
E	PERMISSION LETTERS .....	251

## LIST OF TABLES

Table 2.1: Extinction coefficients of available mAbs. ....	23
Table 2.2: Fc purification methods for papain-digested mAbs. ....	27
Table 3.1: CHO HCP impurities with attractive interactions to mAbs D, D <sub>M</sub> , IDEC-152 and Mill04 at 150 mM NaCl, pH 7.4. ....	53
Table 3.2: CHO HCP impurities with attractive interactions to Mill04, Mill04 Fab and Mill04 Fc at 150 mM NaCl, pH 7.4. ....	54
Table 4.1: Binding capacities of HCP on polishing columns. ....	67
Table 4.2: CHO HCP impurities with attractive interactions to mAbs D and D <sub>M</sub> at pH 7.0, 1 M ammonium sulfate. ....	74
Table 4.3: Shotgun proteomic results for fractions A-D of SP Sepharose FF gradient elution of CHO HCP impurities. Proteins in italics also associate with mAbs in protein A affinity chromatography. ....	78
Table 4.4: Shotgun proteomic results for fractions A-D of Q Sepharose FF gradient elution of CHO HCP impurities. Proteins in italics associate with mAbs in protein A affinity chromatography. ....	85
Table 4.5: Shotgun proteomic results for fractions A-D of Butyl Sepharose FF gradient elution of CHO HCP impurities. Proteins in italics associate with mAbs in protein A affinity chromatography. ....	90
Table 4.6: Shotgun proteomic results for fractions A-D of Capto MMC gradient elution of CHO HCP impurities. Proteins in italics associate with mAbs in protein A affinity chromatography. ....	95
Table 4.7: HCP impurities found to associate with at least two mAbs in protein A purification and also difficult to remove in polishing steps. ....	104
Table 5.1: Candidate protein A wash solutions adapted from previous work (Shukla and Hinckley, 2008). ....	119

Table A.1: Integrated HCP spot volume in ‘flow-through’ gel divided by integrated HCP spot volume in ‘load’ gel for protein A loading conditions. .... 221

Table B.1: Integrated HCP spot volume in ‘flow-through’ gel divided by integrated HCP spot volume in ‘load’ gel for HIC loading conditions..... 239

## LIST OF FIGURES

Figure 1.1: Monoclonal antibody crystal structure (rcsb.org). The two heavy chains are shown in red and the two light chains are shown in yellow. The Fc-domain is the lower portion of the ‘Y’ shaped molecule, and the two upper branches of the ‘Y’ are Fab domains.....	3
Figure 1.2: IgG generalized structure showing the constant light ( $C_L$ ), variable light ( $V_L$ ), constant heavy ( $C_H$ ) and variable heavy ( $V_H$ ) loops (adapted from Thermo Fisher Scientific Inc.) .....	6
Figure 1.3: Typical mAb platform manufacturing process scheme adapted from (Shukla et al., 2007b). .....	7
Figure 1.4: Crystal structure of human Fc domain (yellow) and fragment B of protein A ligand (orange) (PDB ID: 1FC2) (Deisenhofer, 1981). .....	9
Figure 1.4: Two-dimensional gel of CHO HCP from serum-free null CHO cell culture. The majority of impurities are high molecular weight and slightly acidic. Gel parameters: 3-10 NL IPG strips, 12% Tris polyacrylamide gel, stained with Sypro Ruby.....	15
Figure 3.1: HCP content in protein A product fraction for purification of null CHO supernatant compared to purification of null CHO supernatant spiked with one of 3 different mAbs (D, $D_M$ , IDEC-152). Error bars represent chromatography replicates.....	42
Figure 3.2: 2-DE images of product fraction of protein A affinity purification of (A) mAb D spiked into null CHO supernatant and (B) 2-DE image of only mAb D.....	43
Figure 3.3: Typical chromatogram from HCP-mAb CIC run. HCP A280 is shown in black and conductivity in grey. The high-salt and low pH column elution steps are in the shaded region.....	45
Figure 3.4: Analyzed 2-DE load (left column) and flow-through (right column) gels for HCP CIC of mAbs D and $D_M$ . Indicated spots on ‘load’ gels are absent from corresponding flow-through gels and represent strongly interacting HCPs. Individual spot analysis and larger images are in Appendix A.1. ....	47

Figure 3.5: Analyzed 2-DE load (left column) and flow-through (right column) gels for HCP CIC of IDEC-152 and Mill04. Indicated spots on ‘load’ gels are absent from corresponding flow-through gels and represent strongly interacting HCPs. Individual spot analysis and larger images are in Appendix A.1. ....	48
Figure 3.6: Analyzed 2-DE load (left column) and flow-through (right column) gels for HCP CIC of Mill04 Fab and Fc. Indicated spots on ‘load’ gels are absent from corresponding flow-through gels and represent strongly interacting HCPs. Individual spot analysis and larger images are in Appendix A.1. ....	49
Figure 3.7: Calculated properties of HCP impurities found to associate to mAb D ( $\square$ ), mAb D <sub>M</sub> ( $\times$ ), IDEC-152 (+) and Mill04 ( $\Delta$ ) in protein A solutions.....	55
Figure 3.8: Second osmotic virial cross-coefficient ( $B_{23}$ ) measured by cross-interaction chromatography of insulin with mAb D, D <sub>M</sub> , IDEC-152, Mill04, Mill04 Fab and Fc at pH 7.4 and varying sodium chloride concentration. ....	56
Figure 3.9: Histogram of the distribution of the non-electrostatic interaction well depths from 300,000 randomly-sampled configurations of nidogen-1 and the Fc domain. The inset histogram shows the tail of the distribution.....	60
Figure 3.10: The highest affinity configuration of nidogen-1 (red) and the human IgG2 Fc domain (blue) with a well depth of 23.5 kT.....	61
Figure 3.11: Histogram of the distribution of the non-electrostatic interaction well depths from 180,000 randomly sampled configurations of lipoprotein lipase and the Fc domain. The inset histogram shows the tail of the distribution.....	62
Figure 3.12: The highest-affinity configuration of lipoprotein lipase (red) and the human IgG2 Fc domain (blue), with a well depth of 33.5 kT. ....	63
Figure 4.1: Excess HCP due to HCP-mAb product association in protein A, CEX and MMC columns for three mAbs.....	69
Figure 4.2: Estimated properties of HCP impurities found to associate to mAb D ( $\square$ ) and mAb D <sub>M</sub> ( $\times$ ) in HIC solution conditions. ....	74

Figure 4.3: Null CHO supernatant chromatographic behavior on SP Sepharose FF at pH 4.5, eluted with 0-1 M NaCl linear gradient elution. Red trace is A280; blue trace is conductivity. Fractions A-D were collected for shotgun proteomic analysis. ....	78
Figure 4.4: Estimated isoelectric point, net charge, hydrophobicity and size of identified HCP species from chromatographic fractions of SP Sepharose FF gradient elution. ....	79
Figure 4.5: Gel-based chromatograms of identified CHO HCP impurities on SP Sepharose FF with linear gradient elution. ....	80
Figure 4.6: Null CHO supernatant chromatographic behavior on Q Sepharose FF, at pH 7.0 with 0-1 M NaCl linear gradient elution. Red trace is A280; blue trace is conductivity. Fractions A-D were collected for shotgun proteomic analysis. ....	84
Figure 4.7: Estimated isoelectric point, net charge, hydrophobicity and size of HCP species from chromatographic fractions of Q Sepharose FF gradient elution. ....	86
Figure 4.8: Gel-based chromatograms of identified CHO HCP impurities on Q Sepharose FF with linear gradient elution. ....	87
Figure 4.9: Null CHO supernatant chromatographic behavior on Butyl Sepharose FF, with loading at pH 7.0 and elution using a linear gradient from 1 M to 0 M ammonium sulfate. Red trace is A280; blue trace is conductivity. Fractions A-D were collected for shotgun proteomic analysis. ....	90
Figure 4.10: Estimated isoelectric point, net charge, hydrophobicity and size of HCP species from chromatographic fractions of Butyl Sepharose FF gradient elution. ....	91
Figure 4.11: Null CHO supernatant chromatographic behavior on Capto MMC, with loading at pH 4.5 and elution using a linear gradient to 1 M NaCl, pH 8.5. Red trace is A280; blue trace is conductivity. Fractions A-D were collected for shotgun proteomic analysis. ....	94
Figure 4.12: Gel-based chromatogram of HCP impurities on Capto MMC with simultaneous salt and pH gradient elution. ....	96

Figure 4.13: Estimated isoelectric point, net charge, hydrophobicity and size of HCP species from chromatographic fractions of Cpto MMC gradient elution.....	97
Figure 4.14: Nidogen-1 homology model with calculated surface charge at pH 7.0. Negative (red) and positive (blue) charges are indicated. ....	99
Figure 4.15: Legumain homology model with calculated surface charge at pH 7.0. Negative (red) and positive (blue) charges are indicated. ....	100
Figure 4.16: Tubulointerstitial nephritis antigen-like homology model with calculated surface charge at pH 7.0. Negative (red) and positive (blue) charges are indicated. ....	100
Figure 4.17: Homology model of nidogen-1 with surface charges indicated for pH 4.5. Negative (red) and positive (blue) charges are indicated. ....	101
Figure 4.18: Homology model of nidogen-1 with surface hydrophobicity indicated. Hydrophobic (gold) and hydrophilic (blue) regions are indicated. ....	102
Figure 5.1: Catalytic hydrolysis by lipase of lipids into carboxylic acid and an alcohol. ....	108
Figure 5.2a: Structure of polysorbate 20. Ester bond is a possible target for hydrolysis by lipases. ....	108
Figure 5.2b: Structure of polysorbate 80. Ester bond is a possible target for hydrolysis by lipases. ....	109
Figure 5.3: Silver-stained reducing SDS-PAGE of non-induced (A) and induced (B) LPL-producing <i>E. coli</i> cell cultures. ....	110
Figure 5.4: Ni-NTA affinity purification of recombinant CHO LPL with 250 mM imidazole step elution.....	111
Figure 5.5a: The flow-through fraction (A) and elution fraction (B) of LPL Ni-NTA affinity purification on silver-stained reducing SDS-PAGE. ....	114
Figure 5.5b: Anti-His western blot of the LPL Ni-NTA affinity purification flow-through fraction (A) and elution fraction (B). ....	114
Figure 5.6: RP-HPLC gradient elution (45 min 0-100% acetonitrile linear gradient, C <sub>18</sub> column, 1 mL/min) of refolded LPL (blue) and LPL solubilized in 6 M guanidine HCl (red).....	115

Figure 5.7: LPL-mAb osmotic second virial cross-coefficient ( $B_{23}$ ) at pH 7.4 as a function of sodium chloride concentration.....	117
Figure 5.8: LPL-mAb binding measured using YSD of CHO LPL for 4 mAbs in PBS with a concentration of 500 nM mAb. ....	120
Figure 5.9: Titration of CHO LPL expressed on the yeast surface with mAb D to measure equilibrium binding constant $K_D$ .....	121
Figure 5.10: Representative chromatogram of ADAM-labeled degraded and non-degraded polysorbate 80.....	124
Figure 5.11: Digestion rate of polysorbate 80 by CHO LPL (produced in <i>E. coli</i> ) in different solution conditions at 37 °C for 24 hours. ....	125
Figure 5.12: Digestion rate of polysorbate 20 by CHO LPL (produced in <i>E. coli</i> ) in different solution conditions at 37 °C for 24 hours. No measurable digestion was found at pH 6.0. ....	126
Figure 5.13: Polysorbate 80 degradation after 48 hours of incubation at 37 °C with CHO supernatant and LPL knockdown CHO supernatant.....	128
Figure 6.1: Instantaneous phase boundaries of mAbs at pH 7.0 in ammonium sulfate solutions. ....	133
Figure 6.2: Instantaneous phase boundaries of mAbs at pH 7.0 in lithium sulfate solutions.....	134
Figure 6.3: Instantaneous phase boundaries of mAbs at pH 5.0 in ammonium sulfate solutions. ....	137
Figure 6.4: Instantaneous phase boundaries of mAbs at pH 5.0 in lithium sulfate solutions.....	138
Figure 6.5: Instantaneous phase boundaries of mAb D with and without 9.6 $\mu\text{g/mL}$ of insulin at pH 7.0 in various concentrations of ammonium sulfate....	140
Figure 6.6: Osmotic second virial coefficients of mAbs at pH 7.0 in ammonium sulfate solutions, measured using self-interaction chromatography. ....	145
Figure 6.7: Osmotic second virial coefficients of mAbs at pH 7.0 in lithium sulfate solutions, measured using self-interaction chromatography. ....	146
Figure 6.8: Osmotic second virial coefficients of mAbs at pH 7.0 in sodium chloride solutions, measured using self-interaction chromatography. ...	147

Figure 6.9: Osmotic second virial coefficients of mAbs at pH 5.0 in ammonium sulfate solutions, measured using self-interaction chromatography. ....	148
Figure 6.10: Osmotic second virial coefficients of mAbs at pH 5.0 in lithium sulfate solutions, measured using self-interaction chromatography. ....	149
Figure 6.11: ANS fluorescence in solutions of mAb B, plotted together with the instantaneous phase boundary and $B_{22}$ at pH 7.0 for ammonium sulfate (open symbols) and lithium sulfate (filled symbols) solutions. MAb samples with visible phase separation during ANS fluorescence measurements are indicated ( $\Delta$ ). ....	152
Figure 6.12: MAb C ANS fluorescence, instantaneous phase boundary and $B_{22}$ at pH 7.0 with ammonium sulfate (open symbols) and lithium sulfate (filled symbols). MAb samples with visible phase separation during ANS fluorescence measurements are indicated ( $\Delta$ ). ....	153
Figure 6.13: MAb D ANS fluorescence, instantaneous phase boundary and $B_{22}$ at pH 7.0 with ammonium sulfate (open symbols) and lithium sulfate (filled symbols). MAb samples with visible phase separation during ANS fluorescence measurements are indicated ( $\Delta$ ). ....	154
Figure 6.14: MAb $D_M$ ANS fluorescence, instantaneous phase boundary and $B_{22}$ at pH 7.0 with ammonium sulfate (open symbols) and lithium sulfate (filled symbols). MAb samples with visible phase separation during ANS fluorescence measurements are indicated ( $\Delta$ ). ....	155
Figure 6.15: ANS fluorescence vs. $B_{22}$ for mAbs D, $D_M$ , B and C in ammonium sulfate (open symbols) and lithium sulfate (filled symbols) at pH 7.0. ....	156
Figure 6.16: Instantaneous phase boundaries of mAb D as a function of pH with different concentrations of ammonium or lithium sulfate. ....	158
Figure 6.17: Instantaneous phase boundaries of mAb $D_M$ as a function of pH with different concentrations of ammonium or lithium sulfate. ....	159
Figure 6.18: $B_{22}$ values of mAbs D and $D_M$ and the cross-interaction of mAbs D and $D_M$ at pH 7.0 in ammonium and lithium sulfate solutions. ....	160
Figure 7.1: Dynamic light scattering results for six different mAbs in solutions of ammonium and lithium sulfate and sodium chloride at pH 7.0 after 24 hours of incubation at room temperature. ....	166

Figure 7.2: Analytical ultracentrifugation of 5 mg/mL mAb B and 5 mg/mL IDEC-152 in ammonium and lithium sulfate at pH 7.0. ....	168
Figure 7.3: Analytical ultracentrifugation of 5 mg/mL Mill04 in ammonium and lithium sulfate and sodium chloride solutions at pH 7.0. ....	169
Figure 7.4: Analytical ultracentrifugation of 5 mg/mL mAb C in ammonium and lithium sulfate solutions at pH 7.0. ....	171
Figure 7.5: IDEC-152 fragment interaction strengths in sodium chloride, ammonium and lithium sulfate salts at pH 7.0. ....	175
Figure 7.6: Mill04 fragment interaction strengths in ammonium and lithium sulfate solutions at pH 7.0. ....	177
Figure 7.7: MAb B fragment interaction strengths in ammonium and lithium sulfate solutions at pH 7.0. ....	179
Figure 7.8: MAb C fragment interaction strengths in various concentrations of ammonium and lithium sulfate at pH 7.0. ....	181
Figure 7.9: Second osmotic virial coefficients measured by SIC for mAbs B, C, IDEC-152 and Mill04 at pH 7.0 in ammonium and lithium sulfate, and calculated $B_{22}$ values from two different fragment interaction models. ....	187
Figure B.1: Analyzed 2-DE ‘load’ (left column) and ‘flow-through’ (right column) gels for HCP CIC of mAb D and mAb $D_M$ in HIC loading conditions. Indicated spots on ‘load’ gels are absent from corresponding ‘flow-through’ gels and represent strongly interacting HCPs. ....	240
Figure C.1: Chromatographic purification of mAb B Fc on SP Sepharose FF at pH 4.5 with a 25 CV linear gradient from 0 to 0.5 M NaCl. The first peak is the Fc domain and the second peak is undigested mAb. ....	244
Figure C.2: Chromatographic purification of mAb C Fc on SP Sepharose FF at pH 4.5 with a linear gradient from 0 to 1 M NaCl over 20 CVs. The first peak is Fc and the second peak is intact mAb. Subsequent runs at more gradual gradient resulted in better peak separation. ....	245
Figure C.3: Chromatographic purification of IDEC-152 Fc on QAE 550 at pH 8.5 with a linear salt gradient from 0 to 0.4 M NaCl over 15 CVs. Undigested mAb is found in the ‘flow-through’ and Fc fragment is in the elution fraction. ....	246

Figure C.4: Chromatographic purification of Mill04 Fc on SP 650S at pH 5.5 with a linear salt gradient from 0 to 0.5 M NaCl over 20 CVs. The first peak is Fc, the second peak is Fc-Fab and last peak is full mAb. .... 248

Figure D.1. CHO LPL sequence synthesized by Life Technologies. N-del (1-6) and BamHI (1378-1383) restriction enzyme sites are highlighted in yellow. .... 250

## **ABSTRACT**

Monoclonal antibodies (mAbs) have become increasingly important as protein therapeutics over the last few decades. MAbs can be engineered to achieve high binding affinity to a wide array of desired biological targets. Despite having different therapeutic targets, mAbs have nearly identical amino acid sequences and biophysical properties. The high degree of similarity among different mAb products has led to the development of platform manufacturing processes in many companies.

Downstream purification processes for mAbs are designed based on a platform process that is empirically tuned to optimize impurity removal for each new product. A more fundamental understanding of impurities and the product itself would provide insights into the rational design of efficient downstream processes. The first part of this thesis is focused on host cell protein (HCP) impurities, and the main objectives are to identify and characterize HCP impurities and their behavior in a typical downstream platform purification process. In protein A affinity chromatography – the capture step used in the majority of mAb platform purification processes – HCP impurities were found to associate to mAb products due to strongly attractive interactions. By coupling cross-interaction chromatography to proteomic analysis, specific HCP impurities that associate with different mAbs were identified. A subset of HCPs associates with all or most mAb products. Additionally, a unique population of HCPs associates with each mAb product; minor changes to the primary amino acid sequence were found to have a potentially significant impact on the population of associated HCPs.

HCP impurities were also studied in non-affinity platform chromatographic processes. Product-association was found to be an important mechanism through which HCPs can co-purify with mAbs in all chromatographic modes studied. HCP impurities with similar chromatographic behavior to those of mAbs were also identified. This work has identified many difficult-to-remove HCPs and provided mechanistic insight that will aid future downstream process development.

Lipoprotein lipase is a specific HCP impurity that was persistent in many different chromatographic purification processes and was studied in greater detail in this thesis. This particular HCP associates with most mAbs with high affinity. Also, it was found that lipoprotein lipase can enzymatically degrade nonionic surfactants that are commonly included in mAb formulations to prevent product aggregation. Enzymatic degradation of nonionic surfactants by lipoprotein lipase in mAb formulations could negatively affect product quality by inducing mAb aggregation or precipitation.

The final aspect of this work was to compare mAb self-interaction strengths and instantaneous phase boundaries in various solution conditions and to explore the underlying molecular basis for such interactions. In solutions of sulfate salts most of the mAbs studied had nearly identical self-interaction trends and instantaneous phase boundaries. However, the divergent behavior of two nearly identical mAbs shows the potential impact of minor structural changes on product molecules. Overall, there is a qualitative correlation between self-interactions and phase boundary location, but due to mAb anisotropy, quantitative correlations and predictions of mAb properties are difficult.

Measurements of mAb fragment interactions provide further insight into different oligomerization patterns and the origin of attractive self-interactions for various mAbs. Although many mAbs were found to have similar self-interaction properties, the domain-level interactions have greater variability. Fab-Fab, Fc-Fc and ‘hinge’ region interactions were identified as the source of highly attractive self-interactions for different mAbs. Because mAbs are large, anisotropic molecules that are sensitive to minor structural changes, detailed domain-based analysis provides greater insight into oligomerization mechanisms and potentially allows engineering of more stable mAbs.

# Chapter 1

## INTRODUCTION

### 1.1 Motivation and Goals

Monoclonal antibody (mAb) therapeutics are currently the fastest growing sector of the pharmaceutical industry (Li and Zhu, 2010). The FDA has approved 40 mAb therapeutics that account for approximately 38.5% of the biologics market (Aggarwal, 2014). MAb molecular properties are highly conserved from product to product, which enables the use of a ‘platform’ purification process for most mAbs. The ‘platform’ purification process is usually empirically optimized using design of experiments methods (Guiochon and Beaver, 2011). A more mechanistic understanding of these frequently utilized processes would greatly aid in future process development endeavors.

The first part of this work aims to provide a better understanding of impurities in downstream processing. The specific class of impurities investigated is host cell proteins (HCP) derived from Chinese hamster ovary (CHO) cells. The first objective is to identify the specific CHO HCPs that are difficult to remove in typical mAb downstream processes. The second objective is to determine why the identified HCP species are difficult to remove. Identification of specific HCP species and the properties that make them difficult to remove will allow for significant process improvements.

The second major aspect of this work was to study the consequences of HCP impurities that are not removed, and are present in final product formulations. The

most frequent concern regarding HCP impurities is the possibility of antigenic responses from human patients. Two clinical trials were recently canceled due to patient immune response to CHO HCP impurities (Gutiérrez et al., 2012). In addition to antigenic responses in patients, previous work has shown that certain HCP impurities with enzymatic activity can impact final product quality (Gao et al., 2010). The potential for product degradation due to HCP enzymatic activity is studied here for a particular HCP.

The final aspect of this work is to compare mAb self-interaction strengths and instantaneous phase boundaries in various solution conditions. The objective is to determine the variability of self-interaction strength from mAb to mAb. The impact of minor mutations to the mAb amino acid sequences is also investigated. In order to better understand the different interaction strengths and oligomerization behavior of some mAbs, the interactions of Fc and Fab domains are measured. Overall, the goal of this work is to better understand the importance of different protein-protein interactions in bioprocessing of mAb therapeutics.

## **1.2 Monoclonal Antibody Structure**

Antibodies are large protein molecules (approximately 150 kDa) with a characteristic 'Y' shape consisting of three similarly sized lobes (Figure 1.1). Antibodies are highly similar from product to product. The most dramatic differences in primary and secondary structure occur near the antigen-binding domain (Figure 1.2) (Hamilton, 2001).

Antibody molecules consist of four peptide chains, two heavy chains and two light chains. Heavy chains have a molecular weight of approximately 50 kDa and light chains of 25 kDa. Each mAb has two identical heavy chains and two identical light

chains. The heavy chains are linked to each other by a series of disulfide bonds in the 'hinge' region of the antibody (Figure 1.2). The 'hinge' region allows the two antigen-binding domains the flexibility to bind two separate antigens. Each heavy chain is linked to one light chain via a single disulfide bond – between the constant heavy and constant light regions – and through various non-covalent interactions (Goldsby, 2003).

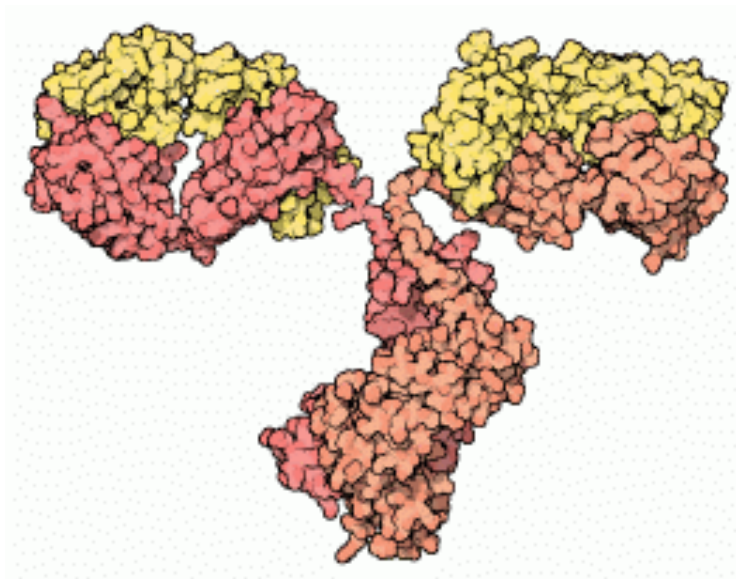


Figure 1.1: Monoclonal antibody crystal structure (rcsb.org). The two heavy chains are shown in red and the two light chains are shown in yellow. The Fc-domain is the lower portion of the 'Y' shaped molecule, and the two upper branches of the 'Y' are Fab domains.

Antibodies contain multiple constant and variable domains. The domains consist of loops (approximately 60 amino acids long) created by intra-chain disulfide bonds. Heavy chains have three or four constant domains (depending on antibody class) and a single variable domain and light chains have one constant and one

variable domain (Figure 1.2) (Goldsby, 2003). Constant domain sequences depend on mAb class and subclass. The first 110 amino-terminal residues in the light and heavy chains constitute the variable domain responsible for antigen binding – also known as the complementarity-determining region (CDR) (Goldsby, 2003).

There are five major classes of antibodies: IgG, IgM, IgA, IgD and IgE. The different classes are distinguished from each other by the constant heavy chain domain (Hamilton, 2001). IgG is the most commonly used antibody class for mAb therapeutics (Reichert, 2012). Within the IgG class there are four antibody subtypes: IgG1, IgG2, IgG3 and IgG4 (Hamilton, 2001). IgG1 is the most commonly used for therapeutic applications by a significant margin; there is also a small number of IgG2 products on the market (Reichert, 2012). IgG molecules from any two different subclasses are typically 90-95% homologous in constant domains (Steward, 1984). In this work IgG1 and IgG2 mAbs are studied.

The largest structural difference among subclasses exists in the ‘hinge’ region. IgG1 antibodies have a hinge region containing 15 residues and two inter-heavy chain disulfide bonds. This allows for sufficient flexibility that each of the two Fab domains can fully rotate on its axis (Hamilton, 2001). IgG2 antibodies have only 12 residues in the hinge region and four disulfide bonds. The combination of a shorter hinge and more inter-chain covalent bonds makes IgG2 molecules less flexible (Hamilton, 2001).

Previous studies have examined the flexibility of different mAbs by measuring the Fab-Fab angle in mAb crystal structures. For example, crystallized Ko1 – a human IgG1 – forms an angle of 132 degrees between Fab fragments. B12 is another human IgG1 and was found to have a Fab-Fab angle of 148 degrees when crystallized.

Crystallized murine IgG1 61.1.3 has a Fab-Fab angle of 115 degrees. The crystal structure of Mcg, another human IgG1, has an angle of 180 degrees, which represents more of a 'T' than a 'Y' shape (Saphire et al., 2002). The Fab-Fab angles in mAb crystal structures indicate the range of different possible conformations of mAbs in solution.

### **1.3 Platform MAb Manufacturing**

MAb industrial manufacturing processes are nearly identical across the biopharmaceutical industry (Rathore et al., 2013). The molecular similarities among mAb products and the availability of protein A affinity resins has allowed for the development of a platform manufacturing process, which can be divided into 'upstream' and 'downstream' processes. The upstream processes consist of mammalian cell culture and the downstream consist of initial harvest and purification processes (Figure 1.3).

#### **1.3.1 Upstream Processes**

MAbs are most commonly produced in mammalian host cells in order to achieve proper glycosylation patterns and protein folding. Due to product secretion by mammalian host cells, cell lysis is not necessary in mAb manufacturing. Compared to upstream processes using bacterial host cells, mammalian processes have relatively 'cleaner' harvest material with less intra-cellular HCP and cellular debris. Although there are alternative host cells used by some manufacturers, the majority of mAbs are produced in Chinese hamster ovary (CHO) cell culture (Jayapal et al., 2007). In the last 20 years, mAb titers in CHO cell cultures have increased approximately 20-fold (De Jesus and Wurm, 2011). Cellular productivity is on the order of 50 pg/cell/day and

final titers can routinely reach 1-5 mg/mL or higher (Butler and Meneses-Acosta, 2012; De Jesus and Wurm, 2011; Lim et al., 2010). Upstream fermentation processes use fed-batch reactors with chemically defined media. Bovine serum was historically used, but due to regulatory concerns animal derived media are now avoided (Butler and Meneses-Acosta, 2012).

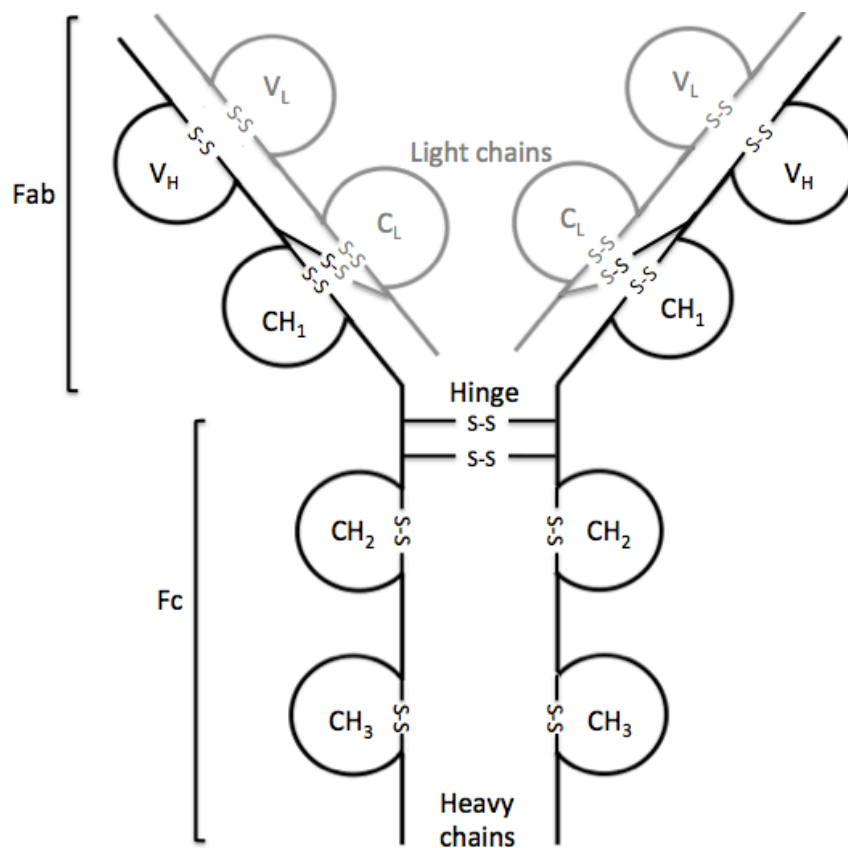


Figure 1.2: IgG generalized structure showing the constant light (C<sub>L</sub>), variable light (V<sub>L</sub>), constant heavy (C<sub>H</sub>) and variable heavy (V<sub>H</sub>) loops (adapted from Thermo Fisher Scientific Inc.).

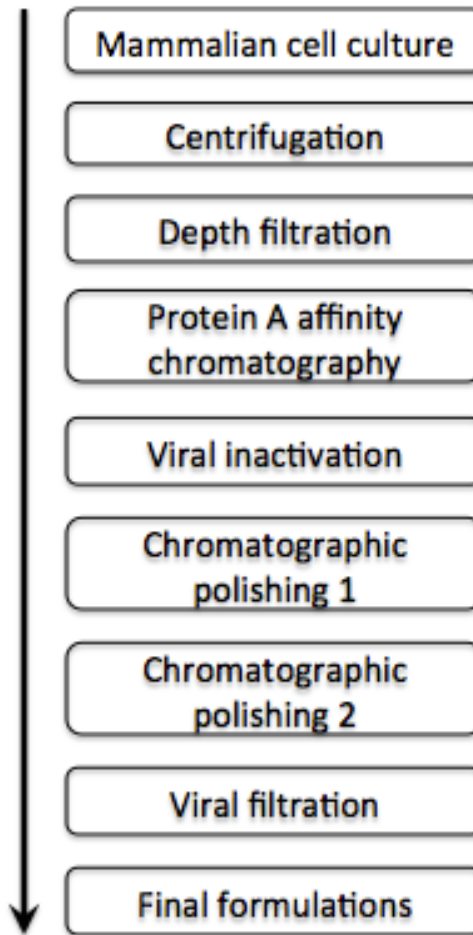


Figure 1.3: Typical mAb platform manufacturing process scheme adapted from (Shukla et al., 2007b).

CHO cells secrete the mAb product molecules along with HCPs, which must be removed in subsequent purification processes. The population of secreted HCPs changes depending on a number of factors, including length of fermentation, temperature, and cell viability (Jin et al., 2010; Tait et al., 2011). Many of the changes in HCP profile throughout the course of a fermentation process are a consequence of increased cell lysis (Tait et al., 2011). Null cell lines – those not producing a mAb

product – were found to have minimal differences in HCP content compared to production lines (Jin et al., 2010). Null cells are used in this work for generating representative HCP samples.

### **1.3.2 Clarification and Protein A Affinity Chromatography**

Primary recovery and clarification are the first steps in platform downstream purification. In large-scale platform manufacturing processes, clarification generally consists of continuous centrifugation followed by depth filtration (Liu et al., 2010). Centrifugation is used to remove larger cell debris and depth filtration removes smaller cellular debris and can also provide clearance of host cell DNA, HCP and virus (Liu et al., 2010). The largely cellulosic depth filtration membranes can remove impurities via size exclusion, hydrophobic interaction, or electrostatics (Liu et al., 2010). Charged depth filters are used for removing endotoxin and host cell DNA (Gerba and Hou, 1985). HCP impurity populations are highly dependent on clarification processes (Hogwood et al., 2012). Although primary recovery and clarification have been shown to influence HCP clearance, they are not studied here.

The cornerstone of mAb platform purification processes is protein A affinity chromatography. The high binding capacity, specificity and impurity clearance of protein A affinity chromatography allows for platform processing to accommodate most mAbs. The protein A ligand has been shown to bind the Fc domain of different IgG molecules. Crystallographic studies have determined the interaction to include residues in both the CH<sub>2</sub> and CH<sub>3</sub> domains on the Fc. The interaction between the ligand and the Fc involves 1,234 Å<sup>2</sup> of solvent-accessible surface area and is primarily hydrophobic. The crystal structure of the mAb-ligand complex is shown in Figure 1.4 (Deisenhofer, 1981).

This highly specific and strong interaction has made protein A affinity chromatography the most effective capture step for most mAb platforms. Additionally, the high flow rate, high binding capacities between pH 6.0 and 8.0 and up to 20 mS/cm conductivity (25-50 mg/mL in many cases) allow for washes to remove many different impurities (Ghose et al., 2007; Swinnen et al., 2007; Zou et al., 2010). The disadvantage of protein A as a capture step is the considerable cost and limited lifespan of protein A resin. One of the most commonly used protein A resins, MabSelect SuRe, has a dynamic binding capacity of 35 mg/mL human IgG at a residence time of 2.4 min, according to the manufacturer (GE Healthcare). The cost of the resin is on the order of \$5,000 per 200 mL resin. Typically protein A columns are limited to approximately 200 cycles.

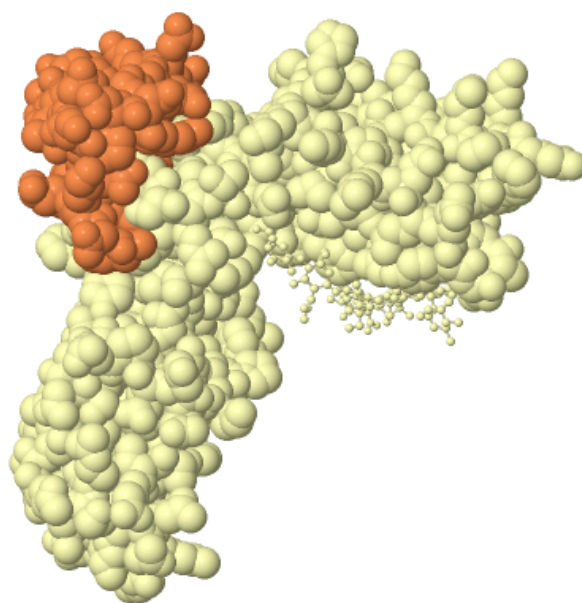


Figure 1.4: Crystal structure of human Fc domain (yellow) and fragment B of protein A ligand (orange) (PDB ID: 1FC2) (Deisenhofer, 1981).

The cell culture supernatant can be directly loaded onto the protein A column after clarification processes. The majority of host cell DNA (~99.9%) is usually removed in protein A processing (Tugcu et al., 2007), HCP can be removed to around 100-500 ppm in most cases (Tarrant et al., 2012), viral clearance of 2.5-5 log<sub>10</sub> reduction value (LRV) is common (Miesegeas et al., 2010) and product yields are typically between 95 and 100% (Tugcu et al., 2007). Following loading, the column is re-equilibrated with loading buffer. Column washes designed to provide additional clearance of specific impurities such as HCP or host cell DNA can then be applied to the column (Shukla and Hinckley, 2008). This is followed by lowering the pH to ~3 to elute the mAb product. Most processes take advantage of the low pH elution and perform a viral inactivation – low pH hold for ~1 hour – that provides considerable viral reduction (Marichal-Gallardo and Álvarez, 2012).

Another drawback to protein A purification is the low-pH elution. MAbs are often not as stable at the elution pH and aggregation at this step can be significant. Numerous studies have characterized mAb aggregation at pH lower than 4.0 (Arosio et al., 2011; Hari et al., 2010; Shukla et al., 2007a). The aggregates formed due to the low pH must be removed in subsequent steps.

Although protein A chromatography is costly, the high binding capacity, specificity, impurity clearance and high yield for almost all mAb products make protein A difficult to replace. The work completed in Chapter 3 is focused on better understanding the process and improving it, rather than replacing it with an alternative capture step.

### **1.3.3 Chromatographic Polishing**

After protein A capture and viral inactivation there are usually 1-3 additional ‘polishing’ steps in the downstream platform process. These steps are non-affinity chromatographic operations. The goal of polishing steps is to remove trace impurities that remain after protein A capture. Trace impurities include HCP, host cell DNA, product molecule fragments and aggregates, virus, and leached protein A ligand. Three of the more commonly implemented chromatographic modes are studied in this work and are introduced further below.

#### **1.3.3.1 Ion-Exchange Chromatography**

Ion-exchange chromatography has two major applications in platform purification of mAbs; depending on the operating conditions, ion-exchange columns are used as a flow-through step or a bind-and-elute step. In most mAb processes, anion-exchange (AEX) columns are operated at neutral pH in flow-through mode. Most mAbs are slightly basic and will not bind to the AEX resin at these conditions. The flow-through AEX step usually directly follows the low-pH viral inactivation. The main purpose of this step is viral clearance – about half of all existing viral clearance studies are for flow-through AEX steps. Flow-through AEX processes have been shown consistently to reduce model virus by about 5 LRV (Miesegaes et al., 2012; Miesegaes et al., 2010). AEX has also been shown to remove host cell DNA by 1 to 2 LRV (Weaver et al., 2013) and HCP from around 100 to 10 ppm, depending on process conditions (Wang et al., 2007).

Cation-exchange chromatography (CEX) is also commonly used as a polishing step. Most often, CEX is run at an acidic pH and the highly positively-charged mAb will bind to the column. Dynamic binding capacities vary from mAb to mAb and resin

to resin, but they are often between 40 and 70 mg/mL (Fogle et al., 2012). A salt gradient or a pH gradient is used to elute the mAb. CEX bind-and-elute is usually used for mAb aggregate and fragment clearance, although it does provide clearance of additional impurities. To achieve appropriate final aggregate levels, yields are often between 70 and 85% (Fogle and Persson, 2012). Certain model retroviruses can also be removed by CEX polishing (Connell-Crowley et al., 2011). Due to the required high-salt elution, the product pool often requires desalting before subsequent processing.

### **1.3.3.2 Hydrophobic Interaction Chromatography**

Hydrophobic interaction chromatography (HIC) is another common polishing process, primarily used for removing product aggregate and fragments. HIC columns are usually operated in bind-and-elute mode. High salt concentrations are necessary during loading to promote mAb binding to the hydrophobic ligand. Ammonium sulfate or sodium chloride at concentrations between 1 and 2 M are common for loading and generally achieve binding between 10 and 20 mg/mL (Chen et al., 2008). Gradient elution is then performed with a gradient down to 0 M salt. HIC processes have been demonstrated to remove HCP, high and low molecular weight impurities, and leached protein A ligand (Chen et al., 2008; Hunter et al., 2009).

While HIC processes offer good selectivity, the binding capacities are lower than for most other resins. The high salt concentrations necessary for loading can present difficulties with phase behavior and high viscosities as well.

### **1.3.3.3 Multimodal Chromatography**

Multimodal chromatographic (MMC) ligands have more than one interaction mechanism. Frequently they have both ion-exchange and HIC characteristics (Kallberg et al., 2012). MMC has been suggested as an alternative capture step due to favorable selectivity, less harsh elution compared to protein A affinity chromatography, better resin lifetime and lower cost of materials (Touaille et al., 2011). One additional advantage over protein A capture is the aggregate removal capability of MMC resins (Touaille et al., 2011). The CEX-MMC resin, Capto MMC, is reported to have mAb binding capacities of 60-90 mg/mL (GE Healthcare). MMC processing has been shown to reduce HCP by 25-50% while maintaining reasonable product yield (Wolfe et al., 2014).

## **1.4 Formulation**

Following mAb purification processes, the final drug substance must be formulated for storage and administration to patients. Most mAb therapeutics require large dosages because they must be administered in stoichiometric quantities; dosages can frequently be as high as 1 gram. MAb therapeutics delivered as infusions are formulated between 1-10 mg/mL; mAbs delivered as subcutaneous injections are usually in excess of 50 mg/mL (Daugherty and Mrsny, 2006). In either case, the final formulation must be sufficiently pure, stable and safe for injection. The biggest concerns for product stability are aggregate formation and denaturation (Manning et al., 2010; Wang et al., 2006). The high concentrations of mAb can add to the difficulty of developing stable formulations (Shire et al., 2004).

The majority of FDA-approved mAb therapeutics are formulated in phosphate, histidine or acetate buffer between pH 5.0 and 7.0 with a variety of excipients and

surfactants (Daugherty and Mrsny, 2006; Wang et al., 2006). Surfactants are the most common additive to mAb formulations and serve to prevent aggregation (Kiese et al., 2008). Polysorbate 20 and 80 are two of the most frequently-used surfactants in formulations, largely due to the low concentrations needed and low toxicity. The addition of polysorbates reduces aggregation due to shaking and agitation of mAb solutions (Wang et al., 2008). Although the mechanism of polysorbate protection of mAbs is not completely understood, it has been theorized that polysorbate competes with mAb for adsorption to air-liquid and glass-liquid interfaces and thus prevents surface-induced denaturation and aggregation. It has also been theorized that surfactants interact with hydrophobic patches on mAb product molecules and thus prevent mAb-mAb interactions that lead to aggregation (Mahler et al., 2005).

### **1.5 Host Cell Protein Impurities**

HCP impurities are a class of impurities that must be removed from all cell-derived protein therapeutics. The FDA does not specify a maximum level of HCP content; HCP levels must be consistent and well-characterized from batch to batch (FDA, 1999). CHO cell culture supernatant contains a complex population of HCPs, the majority of which are slightly acidic. A two-dimensional gel in Figure 1.4 shows the total population of CHO HCP in a serum-free suspension culture. The majority of species are in the upper left quadrant, indicating relatively high molecular weight and acidic isoelectric point.

This complex mixture of HCP impurities enters the downstream purification process and must be reduced to low levels due to regulatory concerns. Typically HCP concentrations are reduced to 1-100 ppm for final product formulations (Champion et al., 2005). One of the primary concerns is the possibility of HCP impurities causing

antigenic effects in human patients (Singh et al., 2012). All products will have trace HCP levels, although the levels may be below the level of detection. It is impossible to predict the human response to trace HCP impurities, but it is hypothesized that the more dissimilar to human proteins, the more likely an impurity is to elicit an immune response in humans (Wang et al., 2009). While it is uncommon, two clinical trials were recently canceled due to anti-CHO responses in human patients (Gutiérrez et al., 2012). In addition to adverse health of the patient, HCP contaminants with enzymatic activity can potentially harm product quality as well (Gao et al., 2010; Robert et al., 2009).

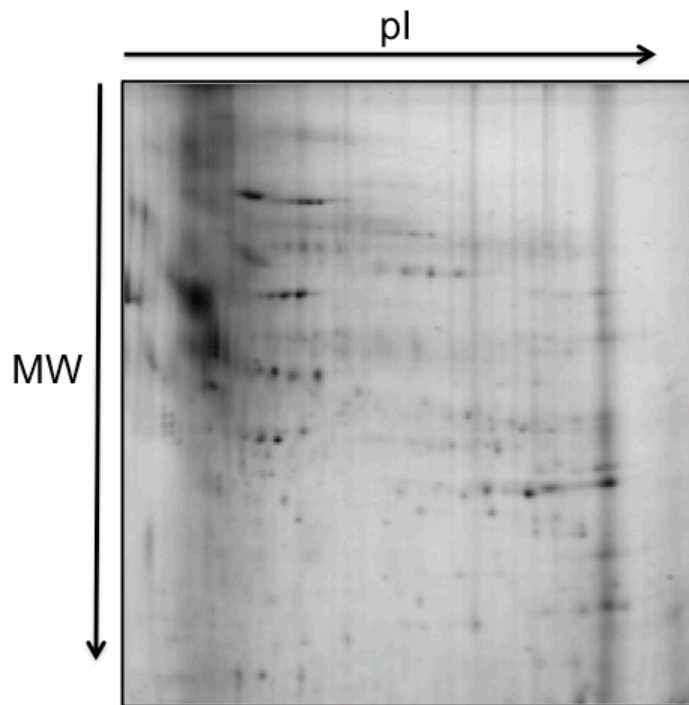


Figure 1.4: Two-dimensional gel of CHO HCP from serum-free null CHO cell culture. The majority of impurities are high molecular weight and slightly acidic. Gel parameters: 3-10 NL IPG strips, 12% Tris polyacrylamide gel, stained with Sypro Ruby.

## 1.6 Proteomics in Bioprocessing

Most downstream purification processes for recombinant protein therapeutics use enzyme-linked immunosorbent assays (ELISA) to monitor the HCP content of process intermediates and final purified product. There are inherent difficulties with measuring HCP content in mAb process intermediates. Generally the mAb product concentration in these solutions is between 1 and 100 mg/mL. The HCP concentration is orders of magnitude lower and the specific HCP species present are unknown. ELISA measurements rely on a polyclonal antibody mixture raised against null HCP (Tscheliessnig et al., 2013). It is likely that some HCP impurities did not elicit an immune response and are not detected by the polyclonal primary antibodies. It is also possible that some HCP impurities are detected by multiple antibodies, thus showing a larger-than-accurate signal. There is some evidence supporting the use of ELISAs for multiple cell lines, as very few detectable changes in protein populations between different CHO lines have been detected (Krawitz et al., 2006). However, if different ELISA kits are used to measure the HCP concentration in a single sample, there is significant variability. A side-by-side comparison of four ELISAs showed how unrealistic a generic ELISA is and casts doubt on the accuracy of ELISA-based HCP measurements (Schwertner and Kirchner, 2010).

Clearly the information gathered from an ELISA is limited, but it is a quick and relatively inexpensive HCP detection method. HCP thresholds based on total concentrations are not informative. There is a realistic possibility that antigenic impurities, harmful to human patients, are undetected by ELISA. A possibility also exists that significant cost and development time is spent lowering HCP concentrations for impurities that are being over-detected or have no harmful effects on human patients.

With proteomic analysis methods such as two-dimensional gel electrophoresis (2-DE) and mass spectrometry, considerably more detailed information can be ascertained regarding HCP impurities. Two-dimensional gel electrophoresis has been used for identification of HCP species in bioprocessing (Grzeskowiak et al., 2009; Hogwood et al., 2012; Levy et al., 2013) and sample preparation methods for CHO samples have been optimized (Valente et al., 2012). Doneanu et al. used LC/LC/MS to identify and quantify HCP impurities in the product fraction of a protein A affinity purification (Doneanu et al., 2012). A modified approach has been developed in which polyclonal antibodies for ELISA are immobilized onto a chromatographic resin. The immobilized polyclonal antibody column is then used to collect enriched HCP samples after each mAb purification step, followed by mass spectrometry analysis of the enriched sample (Bomans et al., 2013). A similar approach used a protein A affinity column to deplete product molecules and identify HCP impurities at low concentrations by LC/MS (Thompson et al., 2014).

The sensitivity of LC/LC/MS for reliable identification and quantification of individual HCP was determined to be approximately 13 ppm for individual proteins. This was accomplished by spiking known quantities of impurities into samples. The LC/LC/MS method developed was then used to identify the 20 most abundant HCP impurities in an *E. coli*-derived Fc-fusion formulation (Schenauer et al., 2012). It has recently been suggested that capillary isoelectric focusing can be coupled to high-resolution mass spectrometry in order to identify HCP populations in mAb bioprocessing as well (Zhu et al., 2012). Overall, the available technology for identifying HCP impurities has advanced rapidly and allows for valuable information in process development.

## 1.7 Phase Behavior

Protein salting-out has a number of applications and consequences in mAb processing. Previously, purification steps have been designed that take advantage of protein salting-out in which the protein of interest is selectively precipitated from a more complex mixture (Chick and Martin, 1913; Cohn et al., 1946; Judge et al., 1995). Also, as discussed above, HIC processes are used in mAb purification to remove mAb aggregates and other trace impurities. Most of these operations require high concentrations of ammonium sulfate or sodium chloride (Chen et al., 2008; Kramarczyk et al., 2008) and precipitation would be detrimental to the process. Finally, in many cases crystallization is utilized to perform structural analysis of mAb products. Obtaining diffraction-quality crystals is often difficult, as it requires finding solution conditions conducive to forming an ordered solid phase rather than an amorphous solid phase (McPherson, 2004). Slightly acidic solutions of ammonium sulfate and polymer have resulted in mAb crystals (Harris et al., 1995; Roussel, 1999). Generally, protein concentrations a few percent lower than those that result in amorphous precipitate, or instantaneous phase separation, are conducive to crystal growth (McPherson, 1982). Thus identifying the location of instantaneous phase separation boundaries can assist in developing crystallization experiments. Instantaneous phase separation is also described as rapid demixing or spinodal decomposition (Dumetz et al., 2008b). Nucleation-dependent phase separations such as crystallization or liquid-liquid phase separation can be observed at lower salt or protein concentrations and longer incubation times (Feher and Kam, 1984; Galkin and Vekilov, 2001; Sear, 1999; Shih et al., 1992).

## 1.8 Protein-Protein Interactions

Previous work has shown a clear correlation of protein-protein interactions for model proteins (Dumetz et al., 2008b; Dumetz et al., 2008c; Tessier et al., 2002b; Tessier et al., 2004a) as well as mAbs (Lewus et al., 2011) with phase behavior. It is expected that net attractive interactions lead to the formation of a protein-rich dense phase. Previously it has been theorized that for globular proteins the relative strength of attraction can lead to different forms of phase behavior such as ordered crystals – for more moderately attractive proteins – or amorphous dense phases for highly attractive interactions (George and Wilson, 1994). The proposed range of moderately attractive protein-protein interactions that lead to high-quality crystals is termed the ‘crystallization slot’ (George and Wilson, 1994).

Proteins are highly anisotropic molecules; despite the anisotropy, protein-protein interactions are represented here as second osmotic virial coefficients ( $B_{22}$  values).  $B_{22}$  appears in the virial expansion for osmotic pressure (McQuarrie, 2000), which has the form:

$$\frac{\Pi}{kT} = c + B_{22}c^2 + \dots$$

where  $\Pi$  is the osmotic pressure,  $T$  is temperature,  $c$  is protein concentration and  $k$  is Boltzmann’s constant.  $B_{22}$  represents solution non-ideality due to two-body protein-protein interactions in solution and is related to molecular interactions via a Boltzmann-weighted average over all possible configurations. Osmotic pressure and  $B_{22}$  have been used historically for the study of various protein properties (Adams et al., 1978; Kupke, 1960).

The conditions studied here – high salt concentrations for crystallization, precipitation or HIC processes – have sufficiently high salt concentrations that long-

range electrostatics are screened out. The protein-protein interactions studied in the present work are ‘salting-out’ interactions. Different salts have different propensities for promoting protein-protein interactions, characterized by the Hofmeister series (Hofmeister, 1888; Kunz et al., 2004). It has been hypothesized that kosmotropic salts interact strongly with water, resulting in structured water molecules around salt ions and desolvation of protein molecules, whereas chaotropic salts tend to break the structure of water and increase protein solvation (Curtis et al., 2000).

Protein-protein and protein-salt interactions in solution are complex and have many contributing factors. In this work, the primary concern is two-body protein-protein interaction strengths in different solution environments. For protein self-interactions at high salt concentrations, short-range interactions dominate (Curtis et al., 1998; Elcock and McCammon, 2001), which depend highly on protein geometry (Neal et al., 1998).

## Chapter 2

### MATERIALS AND METHODS

This chapter describes materials and methods used throughout the thesis. A large portion of the materials, including the mAbs and buffer solutions, are used in multiple chapters. Many of the methods described here, such as protein-protein interactions (Section 2.8) and HCP cross-interaction chromatography, are common to multiple chapters, while some methods are used only in single chapters.

#### 2.1 Materials and Solutions

Ammonium sulfate (A2939), lithium sulfate (L6375), bis-tris (B7535), glutaraldehyde (G5882), ethanolamine (E9508), L-histidine (H8000) and EDTA (E9884) were purchased from Sigma (St. Louis, MO). Tris HCl (BP153), sodium phosphate (7558), calcium chloride (C70), L-arginine (BP370), sodium chloride (S271), sodium acetate (S209), MES (172595000), ANS (82-76-8), guanidine HCl (50-01-1), polysorbate 20 (Tween® 20, BP337), and polysorbate 80 (Tween® 80, BP338) were purchased from Fisher (Pittsburgh, PA). 9-Anthryldiazomethane (ADAM) was purchase from Setareh Biotech, LLC (Eugene, OR). EnzyChrom™ Free Fatty Acid Assay Kit was purchased from BioAssay Systems (Hayward, CA).

Solutions were made using DI water further purified using an EMD Millipore Milli-Q ® system (Billerica, MA) and pH-adjusted using small amounts of concentrated sodium hydroxide or hydrochloric acid solutions. Unless otherwise noted

the pH was maintained at 7.0 by 10 mM sodium phosphate, at 6.0 by 10 mM MES, or at 5.0 by 10 mM sodium acetate.

IDEC-151, an IgG4, and IDEC-152, an IgG1, were donated by Biogen Idec (San Diego, CA); both are human antibodies with variable regions derived from primates. IDEC-151 was delivered lyophilized and was rehydrated to a concentration of 69 mg/mL, and IDEC-152 was delivered in formulation buffer at 49 mg/mL. MAbs A, B and C are IgG1s that were donated by Genentech (South San Francisco, CA). They have theoretically calculated pIs of 9.25, 7.85 and 9.35, respectively, and were delivered in formulation buffers at 3.2, 22 and 100 mg/mL, respectively. MAbs D and D<sub>M</sub>, provided by Amgen Inc. (Seattle, WA), are closely related IgG2s that differ only in that two Arg residues near the CDRs of mAb D are mutated to an Ala and a Thr in mAb D<sub>M</sub>. These two mAbs were provided in formulation buffer at 150 and 32.2 mg/mL, respectively. Finally, Mill04 (EMD Millipore, Bedford, MA) is an IgG1-κ that was provided in buffer at 60 mg/mL.

The purity of each mAb was checked by gel electrophoresis and all were used without further purification. Buffer exchanges were carried out in Slide-A-Lyzer cassettes (66810, 66380) from Pierce Biotechnology (Rockford, IL) or in Fisherbrand regenerated cellulose 6,000-8,000 nMWCO dialysis tubing by dialyzing three times against the final buffer for at least 4 hours each at  $4 \pm 1^\circ\text{C}$ . Solutions were concentrated using Amicon® ultracentrifugal filter units (UFC8-030-96) from EMD Millipore. All centrifugal protein concentration procedures were run in an Eppendorf Centrifuge 5810R. Protein concentrations were determined from UV absorbance at 280 nm, measured using a Perkin-Elmer Lambda 4B spectrophotometer or a Thermo Scientific NanoDrop 2000 spectrometer. The extinction coefficients of the mAbs used

were provided by the manufacturers or calculated from dilution curves of solutions of known concentration and are listed in Table 2.1.

Table 2.1: Extinction coefficients of available mAbs.

<b>Molecule ID</b>	<b><math>\epsilon</math> (mL mg<sup>-1</sup>cm<sup>-1</sup>)</b>
MAb A	1.16
MAb B	1.73
MAb C	1.57
MAb D	1.47
MAb D <sub>M</sub>	1.47
IDEC-151	1.86
IDEC-152	1.61
Mill04	1.53

## 2.2 Instantaneous Phase Boundaries

Instantaneous phase boundaries were determined using a batch method. First, a protein stock solution was prepared by buffer-exchanging the mAb of interest into a buffer solution, containing only buffering salts, at the desired pH. The triple buffer-exchanged protein solution was then concentrated using Amicon ultracentrifugal filters and the final protein concentration was measured by absorbance at 280 nm. A corresponding high-salt buffer solution was prepared containing the same buffering salt, the same pH and 2 M ammonium sulfate or lithium sulfate.

To determine the location of the instantaneous phase boundary, the three solutions described above were mixed in small batch experiments to a total volume of 20  $\mu$ L. For a given final salt concentration, the boundary was determined by preparing a series of solutions differing in final mAb concentration. The protein stock solution was always added last to avoid high local salt concentration effects. Upon addition of the protein stock solution, the solution was aspirated and monitored closely. If the solution was clear after aspiration, the next batch was prepared at a slightly higher

protein concentration. If the solution was cloudy after mixing, the subsequent batch was at a slightly lower protein concentration. The instantaneous boundary for each salt concentration was located between protein concentrations with and without phase separation. This procedure was carried out at decreasing salt concentrations until phase separation could not be observed. For all instantaneous phase boundary plots, the error bars represent the solution composition of the experimental conditions on either side of the boundary.

### **2.3 ANS Fluorescence**

ANS fluorescence was used to shed light on the driving forces of mAb self-association at high salt concentrations. The methods used were adapted from previous work on mAb aggregation pathways (Kayser et al., 2011; Rubin et al., 2012). 8-anilino-1-naphthalenesulfonic acid (ANS) ammonium salt was purchased from Sigma. ANS stock solutions were made at 1 mM in ultrapure water and were sterile-filtered before use.

Experiments were carried out in white opaque polystyrene 96-well plates (Pierce, Rockford, IL). Each well was filled with 200  $\mu$ L of solution. All solutions contained an identical concentration of ANS (60  $\mu$ M) and an identical concentration of mAb (1 mg/mL) with varying salt concentrations. Each trial was run in triplicate. The background fluorescence for each salt concentration was obtained from an identical solution (salt, ANS, pH) without mAb. The fluorescence was measured in a Synergy2 Microplate Spectrometer/Fluorimeter (Biotek, Winooski, VT) with an excitation wavelength of 360 nm and an emission wavelength of 460 nm. Fluorescence measurements were made immediately following solution preparation.

## **2.4 Oligomerization Measurements**

The tendency of different mAbs to form soluble oligomers was determined using two methods: dynamic light scattering and analytical ultracentrifugation.

### **2.4.1 Dynamic Light Scattering**

Methods for dynamic light scattering (DLS) were adapted from those previously used (Lewus, 2011). All mAb solutions were buffer-exchanged to the appropriate pH with no additional salt. MAb solutions were then mixed with low-salt buffer and high-salt buffer to obtain the appropriate salt concentration (NaCl, ammonium sulfate or lithium sulfate) and mAb concentration (5 mg/mL). The mAb solutions were then sterile-filtered into light-scattering vials.

Light-scattering vials purchased from Fisher (Pittsburgh, PA) were prepared by soaking in NOCHROMIX® (Godax Laboratories, Cabin John, MD) solution for at least 1 hour, followed by rinsing and soaking in ultrapure water for another hour. The vials were then rinsed at least 5 times, covered with Teflon tape and dried overnight in a vacuum oven.

DLS measurements were taken using identical methods to those described previously (Lewus, 2011). Measurements were made with a Lexel Laser Inc. helium-neon laser operating at 100-200 mV coupled with a Brookhaven Instruments Corporation goniometer, detector and correlator. Analysis was performed using Brookhaven Instruments Corporation dynamic light scattering software 3.34. The samples were all run at 25 °C and the viscosity was assumed to be the solvent viscosity. The average hydrodynamic diameter was taken from a quadratic fit of the intensity autocorrelation function collected over 2 minutes. Samples were all run in duplicate.

#### **2.4.2 Analytical Ultracentrifugation**

Analytical ultracentrifugation (AUC) was performed using a Beckman Coulter ProteomeLab XL-I analytical ultracentrifuge equipped with a 4-hole An-60 Ti rotor, controlled by the accompanying data analysis software. AUC methods were adapted from those in previous work (Lewus, 2011). Experiments with different mAbs were performed at 40,000 rpm for at least 10 hours at 25 °C. Interference rather than absorbance was used for measuring concentration profiles, as the initial mAb concentrations were held constant at 5 mg/mL. 400  $\mu$ L of sample and 400  $\mu$ L of solvent were loaded into 2-channel centerpieces with sapphire windows. All protein solutions were prepared using the same methods as those described for DLS.

Post-run analysis was performed using SEDFIT version 12.52 to determine a continuous distribution of sedimentation coefficients (continuous  $c(S)$  model) (Brown and Schuck, 2006). The continuous distribution of sedimentation coefficients was fit for appropriate ranges of sedimentation coefficients for each mAb while using the frictional ratio and meniscus position as adjustable parameters. The density and viscosity of all solvents were interpolated from values in International Critical Tables (Washburn, 1926) and the partial specific volume for all fits was measured for IDEC-152 and reported previously as 0.697 mL/g (Lewus, 2011). This was used for all mAbs as material was not available in large quantities and differences from mAb to mAb are expected to be small. Reported sedimentation coefficients were normalized to standard conditions of 20 °C in water.

#### **2.5 Fragment Generation and Purification**

Fab and Fc fragments were generated using immobilized papain from Pierce Biotechnology (Rockford, IL). IDEC-152 was digested using immobilized papain for

6 hours at 37 °C. MAbs B, C and Mill04 were digested overnight at 37 °C. Fragments were purified first using protein A affinity chromatography; the flow-through, which contained pure Fab fragments, was collected. The low-pH eluate was collected and buffer-exchanged into the appropriate loading buffer for the second column using Amicon® ultracentrifugal filter units (10 kDa nMWCO). The buffer-exchanged eluate was then injected into a 1 mL AP-Minicolumn packed with AEX or CEX resin, washed with 15 column volumes (CVs) of loading buffer and eluted using a linear salt gradient to separate Fc fragments from undigested mAb. The conditions used in the second column for each mAb are shown in Table 2.2 and chromatograms are in Appendix C. Each Fc fragment had different chromatographic properties. To achieve adequate separation of Fc domains from undigested mAb, different resins and process conditions were used.

Table 2.2: Fc purification methods for papain-digested mAbs.

<b>Molecule</b>	<b>Resin</b>	<b>Operating pH</b>	<b>Gradient</b>
MAb B	SP Sepharose FF <sup>1</sup>	4.5	0-500 mM NaCl, 25 CV
MAb C	SP Sepharose FF <sup>1</sup>	4.5	0-1 M NaCl, 20 CV
IDEC-152	Toyopearl QAE 550 <sup>2</sup>	8.5	0-400 mM NaCl, 15 CV
Mill04	Toyopearl SP 650S <sup>2</sup>	5.5	0-500 mM NaCl, 20 CV

1: Resin from GE Healthcare (Piscataway, NJ)

2: Resins from Tosoh Bioscience (King of Prussia, PA)

## 2.6 Cell Culture

A null CHO-K1 cell line (ATCC, Manassas, VA) was adapted to adherent serum-free growth in SFM4CHO-A media (Hyclone Laboratories Inc., Logan, UT), as described previously (Kumar et al., 2008). Cultures were seeded at  $5 \cdot 10^4$  cells/mL in T-75 culture flasks and incubated for 3 – 4 days in a 37 °C cell culture incubator with

5% CO<sub>2</sub> and 80% relative humidity until the final cell density reached  $1 \cdot 10^6$  cells/mL at 97 – 99% viability.

CHO cells were adapted to suspension culture in 125 mL shake flasks containing SFM4CHO suspension media (Hyclone Laboratories Inc.) to source HCP for Fc fragment experiments and HCP retention experiments (Chapter 4). The extracellular CHO HCPs were harvested by decanting the cell supernatant, removing the residual cells by centrifugation (180 g, 5 min), and stored at -20 °C until further use.

CHO cell culture supernatant was buffer-exchanged into protein A loading buffer using Slide-A-Lyzer cassettes from Pierce Biotechnology (Rockford, IL) by dialyzing three times against the final buffer for at least 4 hours each at 4 °C. The supernatant was then concentrated using Amicon® ultracentrifugal filter units (10 kDa nMWCO) from EMD Millipore (Bedford, MA) and was filtered using Millex 0.22 µm syringe filters from EMD Millipore.

## **2.7 Protein A Affinity Purification of MAbs**

A series of protein A affinity chromatography purifications were completed to determine the total amount of HCP that associates with various mAbs. The investigation was performed similarly to previous work (Shukla and Hinckley, 2008; Tarrant et al., 2012), but excluding the use of ELISA. An AP-Minicolumn (5 mm i.d.) was packed with approximately 1 mL of rProtein A Sepharose Fast Flow resin from GE Healthcare (Piscataway, NJ) according to the manufacturer's specifications. Three different 10 mL solutions were prepared for loading. The first mixture consisted of CHO supernatant that was buffer-exchanged into protein A loading buffer (20 mM sodium phosphate, 150 mM NaCl, pH 7.4). The second mixture contained an equal

volume of buffer-exchanged supernatant that was spiked with purified mAb to a final concentration of 1.5 mg/mL and equilibrated overnight. The third mixture contained only buffer and 1.5 mg/mL mAb as the spiked sample. The mAb concentration was chosen to simulate typical primary capture conditions (Butler and Meneses-Acosta, 2012; De Jesus and Wurm, 2011; Lim et al., 2010).

Identical purification procedures were followed for these three solutions, using an ÄKTA Purifier 900 using Unicorn 5.11 software (GE Healthcare, Piscataway, NJ). The sample was loaded onto the prepared protein A column using the sample pump, followed by a five column-volume wash and elution in low-pH buffer. The entire low-pH eluate was collected for all protein A affinity purifications to represent the product fraction. Product fractions from the three purifications were analyzed using a BCA assay (Pierce Biotechnology, Rockford, IL) to determine total protein concentrations. Each chromatographic experiment was run in triplicate. The known amount of mAb and the protein contribution from the HCP-only sample were subtracted from the results for the spiked sample to determine the total amount of HCP in the product fraction due to product association.

## **2.8 Protein-Protein Interactions**

Interactions of mAbs and mAb fragments were measured by self-interaction chromatography (SIC) and cross-interaction chromatography (CIC) (Lewus et al., 2011; Tessier et al., 2004a; Tessier et al., 2004b). For these measurements, the relevant mAbs or mAb fragments were immobilized separately onto Toyopearl AF-Amino-650 chromatographic particles (Tosoh Bioscience, King of Prussia, PA) using glutaraldehyde chemistry as previously described (Lewus et al., 2011). The immobilization density was measured using a Micro BCA™ Protein Assay Kit (Pierce

Biotechnology, Rockford, IL). Resin carrying the immobilized mAb or fragment was flow-packed into a 1 mL AP-Minicolumn at a flowrate of 2 mL/min water for 1 hour. The packing quality was verified by measuring the asymmetry using an acetone pulse. Asymmetry between 0.9 and 1.3 was considered acceptable.

Self-interaction chromatography (SIC) was used to determine the second osmotic virial coefficient ( $B_{22}$ ). This method has previously been shown to provide results that agree in general with those obtained using other methods of measuring  $B_{22}$  (Ahamed et al., 2005; Tessier et al., 2002a; Valente et al., 2005). The procedures used for SIC measurements on mAbs are described in detail elsewhere (Lewus et al., 2011). Isocratic retention of the injected sample was measured in the immobilized protein column and a blank column. A volume of 100-200  $\mu$ L with a mAb concentration of 1-5 mg/mL was injected using an Akta A900 Autosampler (GE Healthcare) at a constant flow rate of 0.1 mL/min. The retention factor  $k'$  was calculated as

$$k' = \frac{V_R - V_0}{V_0}$$

where  $V_R$  is the retention volume in the immobilized-protein column and

$$V_0 = V_p' \frac{V_a}{V_a'} - V_{immob}$$

where  $V_p'$ ,  $V_a'$  and  $V_a$  are the retention volumes of mobile-phase protein in the blank column, acetone in the blank column and acetone in the immobilized-protein column, respectively.  $V_{immob}$  is the total volume of immobilized protein.  $B_{22}$  was calculated using

$$B_{22} = B_{HS} - \frac{k'}{\rho_S \phi}$$

where  $B_{HS}$  is the hard-sphere contribution to  $B_{22}$ , based on the sphere of equivalent volume to the mAb,  $\phi$  is the surface area accessible to mobile phase proteins, estimated by extrapolating from previous results (DePhillips and Lenhoff, 2000), and  $\rho_S$  is the surface density of the immobilized protein (Tessier et al., 2002b).

Cross-interaction chromatography (CIC) (Cheng et al., 2008; Teske et al., 2004; Tessier et al., 2004a; Tessier et al., 2004b) was used to measure osmotic second virial cross-coefficients ( $B_{23}$ ) of various mAb fragments as well as interactions of insulin and lipoprotein lipase with different mAbs. CIC methods and calculations are almost identical to those for SIC, except that two different proteins are used in the mobile and stationary phases.

## **2.9 HCP-MAb CIC**

Cross-interaction chromatography (CIC) (Cheng et al., 2008; Teske et al., 2004; Tessier et al., 2004a; Tessier et al., 2004b) was used to probe the interactions of a complex mixture of HCP with a single mAb. It was also used to measure osmotic second virial cross-coefficients ( $B_{23}$ ) of insulin with immobilized mAbs and mAb fragments.

HCPs were prepared for CIC by concentrating them in Amicon® centrifugal ultrafiltration filters, 10 kDa nMWCO, to 100 times the original concentration, followed by buffer exchange into protein A loading buffer (Section 2.7). Adherent CHO cell culture supernatant was used for all CIC work except that for CIC with Fc fragment, for which suspension cell culture supernatant was used. A 200  $\mu$ L injection into the immobilized mAb column was followed by a 10 mL isocratic elution at the solution conditions being tested. The procedure was terminated with a high-salt

elution (2 M NaCl) and a low-pH (pH 3.0) elution to remove any HCP impurities very strongly bound to the immobilized mAb.

## **2.10 Proteomic Methods**

Proteomic analysis was performed using two-dimensional electrophoresis (2-DE) and/or mass spectrometry (MS). Various fractions from CIC experiments were analyzed using 2-DE and the HCP populations of these fractions were compared to the total HCP that was injected into the immobilized mAb column.

### **2.10.1 Sample Preparation**

Approximately 1 mg of each CHO HCP-containing sample was precipitated using trichloroacetic acid (TCA) on ice for a minimum of 1 hour, followed by centrifugation (14,000 g for 5 minutes) and two acetone (Fisher Scientific, Fair Lawn, NJ) wash-centrifugation cycles (14,000 g for 5 minutes). The protein pellet was dried under argon.

### **2.10.2 Two-Dimensional Gel Electrophoresis (2-DE)**

2-DE was performed as described previously (Valente et al., 2012). Materials and equipment were obtained from Bio-Rad Laboratories (Hercules, CA) unless otherwise specified. Briefly, precipitated proteins were resolubilized in rehydration solution (8 mM tris, 8 M urea, 30 mM DTT, 2% CHAPS (Sigma-Aldrich Chemical Co.), 0.4% BioLytes, and trace bromophenol blue), which was used to rehydrate 18 cm, pH 3–10 nonlinear Immobiline DryStrips (GE Healthcare). Isoelectric focusing (IEF) was performed using a PROTEAN IEF Cell for 100,000 Vh, after which IEF gels were sequentially equilibrated with DTT and iodoacetamide (Sigma-Aldrich Chemical Co.). SDS-PAGE was performed using 12 %T, 2.6 %C polyacrylamide slab

gels measuring 18 cm x 16 cm x 1.5 mm. Gels were stained with SYPRO Ruby (Molecular Probes, Eugene, OR) and imaged on an FLA-3000 Fluorescent Image Analyzer (Fujifilm Corp., Tokyo, Japan). Gel images were analyzed and compared using ImageMaster 2D Platinum Software v5.0 (GE Healthcare). Spots were detected using the auto-detect feature and manually edited to remove artifacts. Spot matching was manually completed by comparing images of the CIC fractions to those of the total HCP supernatant that was loaded onto the CIC column. Spots of interest were either manually excised and stored at -80 °C or compared to a reference gel with previously identified spots using ImageMaster software.

### **2.10.3 Mass Spectrometry**

Gel plugs containing spots of interest were subjected to in-gel digestion using trypsin (Promega Corporation, Madison, WI). The resulting peptides were desalted and concentrated using ZipTips (EMD Millipore) and spotted onto stainless steel target plates with  $\alpha$ -cyano-4-hydroxycinnamic acid (Sigma-Aldrich Chemical Co.) matrix. Analysis by matrix-assisted laser desorption/ionization tandem time-of-flight (MALDI-TOF/TOF) MS was performed as described previously (Hayduk et al., 2004) on an Applied Biosystems 4800 MALDI TOF/TOF Analyzer (Framingham, MA). Data were acquired in positive ion MS reflector mode and MS/MS, then submitted for Mascot v2.2 (Matrix Science Ltd., London, UK) database searches through GPS Explorer software v3.6 (Applied Biosystems). Spectra were searched against translations of the CHO genome (Xu et al., 2011) and the NCBI nr database (downloaded July 15, 2009), and identifications with 95% confidence or greater were accepted.

## 2.11 Calculation of HCP Parameters

Molecular properties of CHO HCPs were calculated from primary amino acid sequences. The protein molecular weight was calculated by the addition of average isotopic masses of amino acids in the primary amino acid sequence; posttranslational modifications were not considered. The isoelectric point (pI) and protein net charge were estimated using pK<sub>a</sub> values of free amino acids, as described previously (Bjellqvist et al., 1993). The Grand Average of Hydropathy (GRAVY) was calculated as the sum of hydropathy values for every residue divided by the number of residues (Kyte and Doolittle, 1982). Calculations were performed on the ExPASy server (Gasteiger et al., 2005). The radius of a sphere of equivalent volume for each HCP was extrapolated from previous results (Neal and Lenhoff, 1995).

## 2.12 MAb-HCP Interaction Orientation Calculations

To determine highly attractive orientations of HCP impurities and mAbs, a number of calculations were performed using molecular mechanics methods. The methodology and code for these calculations was adapted from previous work (Asthagiri et al., 1999; Neal et al., 1998; Quang et al., 2014) that was designed to calculate second osmotic virial coefficients by estimating the configurational integral of the potential of mean force using Monte Carlo methods. In this work, rather than calculate B<sub>22</sub>, the goal was to identify highly attractive orientations of HCPs and mAbs. The original code was adapted to allow for use of atomic structural data for two different molecules. The first input was a homology structure of an HCP and the second was the crystal structure of a human IgG2 Fc domain.

Rather than calculate an average interaction strength, the two proteins were randomly oriented with respect to each other and placed 100 Å apart. As they were

moved closer to each other the interaction free energy was calculated by ignoring electrostatics and considering only short-range interactions. Short-range (non-electrostatic) interactions were based on OPLS parameters (Jorgensen and Tirado-Rives, 1988). For center-to-center separation distances less than 5 Å for a particular pair of atoms, an atomistic Lennard-Jones potential was used and for larger separation distances a continuum Lifshitz-Hamaker method was used (Asthagiri et al., 1999).

## **2.13 Recombinant Lipoprotein Lipase (LPL) Production**

### **2.13.1 *E. coli* Expression of CHO LPL**

The Chinese hamster LPL gene sequence (UniProKB entry G3H6V7) was synthesized by Life Technologies. The synthesized sequence included NdeI and BamHI restriction enzyme sites at the 5' and 3' ends respectively (Appendix D). To assist the purification of LPL, a six His tag sequence was also added between the last codon of LPL and the BamHI site. The vector pMK-RQ, containing LPL, and pET11a were separately transformed and amplified in NEB5 $\alpha$  competent cells and purified by QIAGEN QIAprep spin columns. Both pMK-RQ and pET11a were double-digested by NdeI and BamHI at 37 °C for 3 hours and purified by agarose gel electrophoresis. The digested LPL sequence and pET11a were extracted from the gel using a QIAGEN QIAquick kit. LPL was ligated to pET11a using T4 ligase at room temperature for 3 hours and the resulting plasmid was then transformed into NEB5 $\alpha$  competent cells and plated on Amp-LB agar plates. Twelve positive colonies were selected and 5 mL overnight cultures were grown. The plasmids of twelve clones were purified and digested using NdeI and BamHI restriction enzymes. Positive clones were confirmed by agarose gel electrophoresis and all twelve clones had positive bands corresponding

to the size of the LPL gene sequence. Sequencing of two clones was performed at the University of Delaware Sequencing and Genotyping Center and both clones were found to contain perfectly matched sequences as the synthesized LPL gene sequence.

The LPL-containing pET11a plasmid was then transformed into BL21 competent cells in SOC broth and plated on ampicillin. Colonies were selected and cultures were grown overnight to seed the production culture. Production of recombinant CHO LPL was done at the 750 mL scale. Induction was commenced at 0.4 OD with the addition of 400  $\mu$ M IPTG, followed by LPL expression for 3 hours.

### **2.13.2 LPL Purification**

After induction of the production cell line, the cultures were collected and distributed into 50 mL tubes and centrifuged at 1000 g for 10 minutes to pellet the cells using an Eppendorf 5810R centrifuge (Hamburg, Germany). The supernatant was discarded and the cell pellets frozen for future use.

Cell pellets were thawed in lysis buffer – 75 mM tris, 120 mM NaCl, 5 mM EDTA, pH 7.7 – which also contained protease inhibitors. The cells were lysed in an M-110L Pneumatic Microfluidizer from Microfluidics (Westwood, MA) at 9000 psi while being maintained at 5 °C. LPL-containing cells were passed through the homogenizer for at least 6 full cycles.

Cell lysate, containing LPL inclusion bodies, was then ultracentrifuged in a Beckman Coulter Optima™ L-100 XP Ultracentrifuge at 40,000 g for 1 hour in order to pellet the inclusion bodies. The inclusion bodies were then scraped out of the centrifuge tube and stored at -20 °C for future use.

The inclusion bodies were solubilized in 6 M guanidine HCl, 300 mM NaCl, 10 mM imidazole, 20 mM sodium phosphate and protease inhibitors at pH 7.4.

HisPur™ Ni-NTA resin from Thermo Scientific was packed in a 1 mL AP-Minicolumn and equilibrated using 25 CVs of 6 M guanidine HCl buffer at a flow rate of 1 mL/min. The solubilized LPL was loaded onto the column at 0.5 mL/min. This was followed by a 10 CV wash with loading buffer. The LPL was then eluted with 16 CVs of 20 mM sodium phosphate, 300 mM NaCl, 6 M guanidine HCl, 250 mM imidazole, pH 7.4 at a flow rate of 1 mL/min. The column was then regenerated with 10 CVs of 20 mM MES, 0.1 M NaCl, pH 5.0 followed by 10 CVs ultrapure water and 10 CVs of 20% ethanol.

### **2.13.3 LPL Refolding**

LPL inclusion bodies were recovered after purification and diluted in 6 M guanidine HCl to a final OD of 0.4. The solubilized protein was then reduced with the addition of DTT to a final concentration of 15 mM.

A solution of refold buffer was made including 50 mM tris, 600 mM L-arginine, 2.5 mM calcium chloride and 5 mM cysteine at pH 8.5. The arginine is intended to prevent aggregation and there is evidence from previous work that calcium chloride can assist in proper folding of LPL into active dimers (Zhang et al., 2005).

A volume of refolding buffer 50 times larger than the volume of solubilized inclusion bodies was stirred gently with a magnetic stir bar at 5 °C until the temperature was equilibrated. The LPL inclusion body solution was then added at ~0.2 mL/min using a peristaltic pump. The nozzle of the pump was submerged in the refolding buffer. After the addition of LPL was complete, gentle stirring was continued for 12 hours at constant temperature. To remove small amounts of precipitate following the refolding step the entire refolding solution was sterile-filtered.

## 2.14 LPL Activity Assay

Measurements of LPL activity against polysorbate 20 and polysorbate 80 were carried out in various solution conditions. Refolded LPL was buffer-exchanged into the appropriate buffer prior to the activity assay. The conditions investigated were pH 5.0, pH 6.0 and pH 6.8 and the buffers used were 10 mM sodium acetate, pH 5.0, 10 mM L-histidine, pH 6.0, and 50 mM bis-tris, pH 6.8. Polysorbate 20 or 80 was added to the buffer-exchanged LPL with a final concentration of 0.23 mM. Some samples also had either 10 mM calcium chloride or 10 mM sodium chloride. The polysorbate and LPL solutions were then incubated at 37 °C with constant mixing for 24 hours.

The polysorbate degradation assay was adapted from previous work (Khosravi et al., 2002) that was designed to measure degraded polysorbate 20 from pancreatic lipase, but for this work it was also used to detect degradation products of polysorbate 80.

270  $\mu$ M ADAM in methanol was added to each sample in a 3:1 ratio of ADAM solution to sample. The ADAM conjugation was carried out at room temperature using opaque 1.6 mL Eppendorf tubes with constant mixing for at least 6 hours. Following conjugation the samples were centrifuged at 13,000 g for 6 minutes (Eppendorf miniSpin centrifuge, Hamburg, Germany) and the supernatant was added to HPLC sample vials. A Viva C18 150 x 4.6 mm column from Restek (Bellefonte, PA) was used with a Shimadzu Prominence UFLC (Kyoto, Japan). The mobile phase was 97% acetonitrile, 3% methanol. Samples were all run in triplicate on the HPLC with injection volumes of 10  $\mu$ L and a flow rate of 1 mL/min for 13 minutes per sample. The absorbance at 254 nm was analyzed for the characteristics peaks of degraded polysorbate 20, 80 or triglyceride. The EnzyChrom™ Free Fatty Acid Kit

was used as a secondary method to confirm the results of the HPLC assay described by directly measuring the release of fatty acid by lipase.

### **2.15 Yeast Surface Display (YSD) of LPL**

Yeast surface display (YSD) was used to measure the interaction of LPL with different mAbs and mAb fragments. Existing methods were followed (Boder and Wittrup, 1997; Chao et al., 2006). However, rather than an scFv, CHO LPL was fused to Aga2p and expressed in yeast cells. As described in the previous methods, there is an HA tag between the Aga2p and the LPL and a c-Myc tag on the c-terminal end of LPL. Soluble protein was labeled at a labeling ratio of 1.5 with amine-reactive Alexa Fluor 647 (Life Technologies, Grand Island, NY) and incubated with the surface expressing cells for 45 minutes. Flow cytometry was then used to measure the relative binding of soluble protein to the surface anchored LPL. Controls were run with a non-immune scFv in place of LPL on the yeast surface. To measure the  $K_D$  of LPL-mAb a titration was completed with increasing concentrations of soluble protein.

## Chapter 3

### HOST CELL PROTEIN IMPURITIES IN PROTEIN A AFFINITY PURIFICATION OF MONOCLONAL ANTIBODIES

#### 3.1 Introduction

Protein A affinity chromatography is the workhorse of mAb platform purification processes in that it serves as an efficient capture step and removes the majority of HCP impurities as well as most other impurities. However, not all HCP impurities are removed by the protein A step, and identification of persistent HCPs in the protein A step and more importantly the reasons that these particular HCP impurities are retained can be valuable in future efforts to optimize downstream process design.

There are two major mechanisms by which HCPs can enter the product fraction of the protein A affinity step, or any bind-and-elute type of chromatographic purification. The first mechanism is product association (Luhrs et al., 2009; Shukla and Hinckley, 2008; Tarrant et al., 2012), which refers to strongly attractive interactions that certain HCPs have with the mAb product molecule, resulting in binding to the mAb. The HCP species is then carried through the process in association with the mAb, both in binding to the protein A or other ligand and in elution into the product fraction. The second mechanism for HCP retention in a chromatographic operation is co-elution, which refers to HCP species that bind to either the chromatographic ligand or the resin backbone and are then eluted into the product fraction as impurities. A more complete understanding of the relative

importance of co-elution and product association and identification of HCPs that follow each of the two mechanisms can provide much-needed mechanistic knowledge of HCP impurity retention, which can aid in future process synthesis efforts.

The first goal of this chapter is to determine the overall importance of HCP-mAb product-association in protein A affinity chromatography. The second goal is to identify specific HCP impurities that associate with mAbs in a typical protein A process. Overall, this work will provide an improved understanding of HCP impurities in protein A affinity purification of mAbs.

### **3.2 Total HCP Product Association**

The total HCP content in the product fraction of protein A affinity purifications with and without mAb spiked into the starting material is shown in Figure 3.1 for three different mAbs. These results are consistent with those reported by previously (Shukla and Hinckley, 2008; Sisodiya et al., 2012) as they show an increase in HCP in the product fraction when a mAb is included; the observed increase in HCP is presumably due to HCP-mAb association.

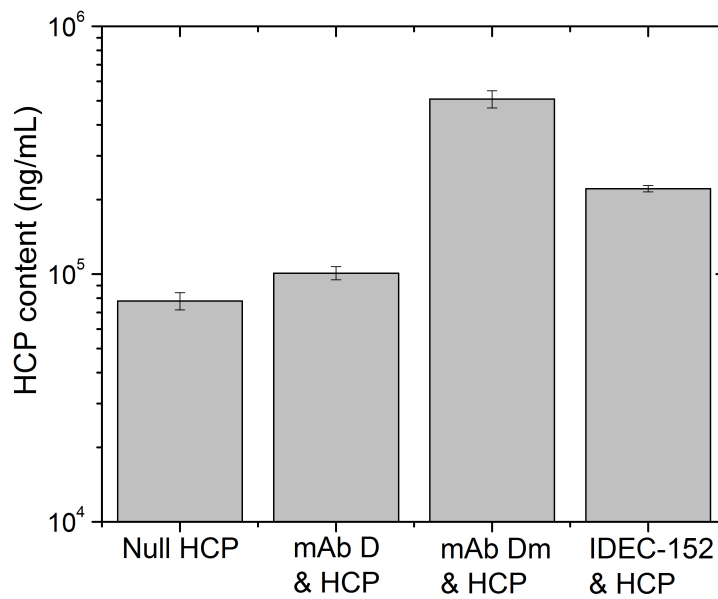


Figure 3.1: HCP content in protein A product fraction for purification of null CHO supernatant compared to purification of null CHO supernatant spiked with one of 3 different mAbs (D, D<sub>M</sub>, IDEC-152). Error bars represent chromatography replicates.

These results also demonstrate the variability in total product association with different mAbs. As shown in Figure 3.1, mAb D<sub>M</sub> gives rise to the largest amount of HCP in the eluate whereas the increase in the presence of mAb D is very small. Although mAbs D and D<sub>M</sub> differ by only 2 charged residues near the CDR, this relatively minor difference has a very large impact on total product association. This considerable difference in total associating HCP could be caused by a single abundant species that binds appreciably more strongly to the mutated molecule or it could be due to binding of a number of different HCP species. These alternatives are not easily distinguished because the method used in developing Figure 3.1 indicates only total

product association as opposed to determining specific HCP species responsible for the interaction.

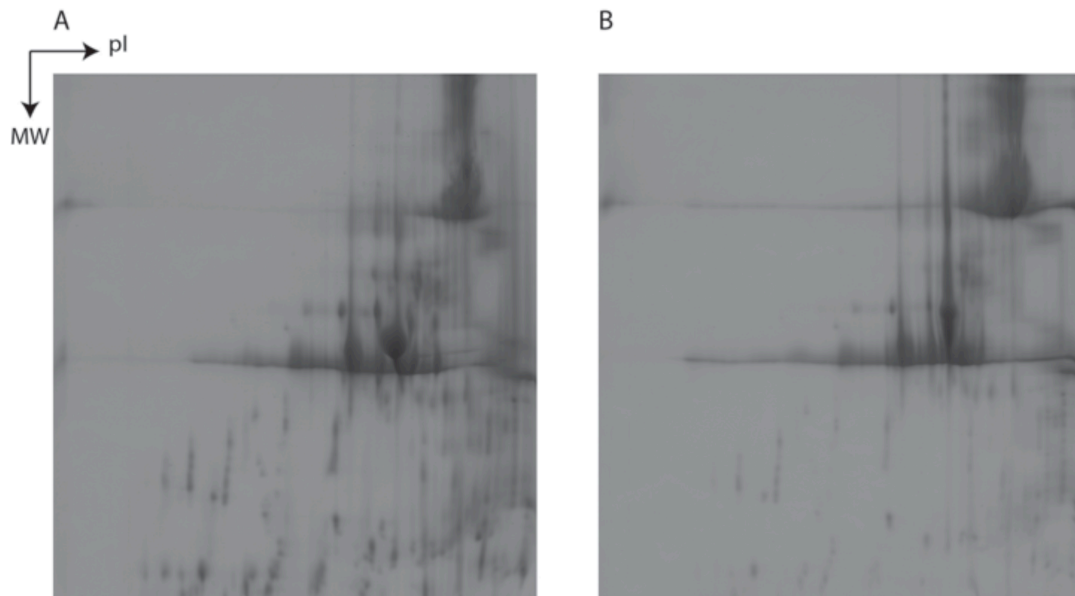


Figure 3.2: 2-DE images of product fraction of protein A affinity purification of (A) mAb D spiked into null CHO supernatant and (B) 2-DE image of only mAb D.

2-DE was used to monitor HCPs that persist through a typical protein A affinity purification process and appear in the product fraction. A representative example (Figure 3.2) compares 2-DE images for product fractions of protein A affinity purifications of null CHO supernatant spiked with mAb D (Figure 3.2A) and an equivalent quantity of only mAb D (Figure 3.2B). Given the inherent order-of-magnitude difference between the HCP and mAb concentrations, the heavy and light chains of the mAb obstruct most of the gel, hindering the ability to observe HCP impurities. It is therefore difficult to monitor both the mAb product and HCP

impurities simultaneously using a method such as 2-DE. Despite this uncertainty and the low HCP concentrations compared to those of the mAb, the HCP concentration is still likely unacceptable in terms of final purity. Sypro Ruby has been reported to detect protein concentrations as low as 0.3-1.0 ng (Tscheliessnig et al., 2013); however, it has been shown that for in-process samples, where HCP is in the ppm range, 2-DE is unlikely to provide significant information about HCP populations (Jin et al., 2010).

### **3.3 Cross-Interaction Chromatography (CIC): MAb-CHO HCP**

Measuring and identifying the complete set of HCP impurities in the product fraction of protein A affinity purification is informative and has been done previously for a similar system (Doneanu et al., 2012). However, this previous work did not provide information about the mechanisms by which specific HCP impurities are retained in the product fraction. CIC was used here to measure interactions between CHO HCP and various mAb products, and was coupled to 2-DE and MS to obtain identities of the specific strongly associating HCP impurities for each mAb. Procedures for each of the 4 mAbs and the Fc and Fab fragments of Mill04 were run in duplicate. A typical CIC chromatogram is shown in Figure 3.3. The majority of HCP content is found in the flow-through fraction, and the column wash yields a secondary peak containing strongly interacting HCP.

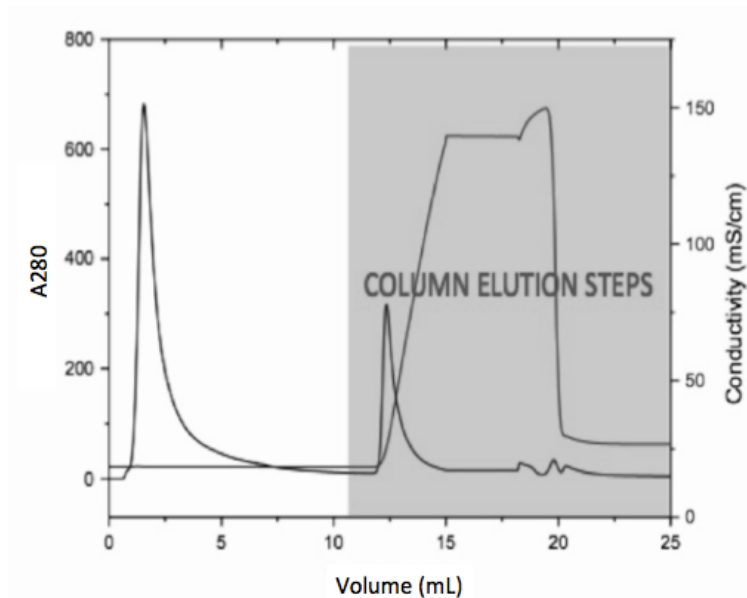


Figure 3.3: Typical chromatogram from HCP-mAb CIC run. HCP A280 is shown in black and conductivity in grey. The high-salt and low pH column elution steps are in the shaded region.

Direct identification of the strongly interacting HCPs was not possible as the relatively low concentration of HCP in the secondary peak was not sufficient for detection by 2-DE. In addition, very strongly interacting HCP species may be retained following elution and not appear in the secondary peak at all. The interacting HCP impurities were therefore instead identified by comparing 2-DE images of the CIC flow-through, containing non-interacting HCPs, to those of the CIC feed, containing all CHO HCPs. Spots that were detected on the feed image and absent from the flow-through image correspond to HCPs that associate strongly with the mAb being tested and thus remain in the column during isocratic elution. Missing spots in the flow-through were determined either by a  $> 2x$  decrease in integrated spot volume using Image Master software or by qualitative changes based on visual inspection. Further

details can be found in Appendix A. These identified spots are marked on the feed gel and were either excised for further identification or compared to a reference gel with previously identified spots, as can be seen in Figures 3.4-3.6. The proteins identified as strongly associating HCPs are listed for each mAb and the Fab and Fc domains of Mill04 in Tables 3.1 and 3.2. As noted above, mAbs D and D<sub>M</sub> differ by only 2 residues near the CDR, while IDEC-152 and Mill04 are unrelated products. Not surprisingly, mAbs D and D<sub>M</sub> share 9 strongly interacting HCPs but each also has strong associations with a number of HCPs that do not interact with the other. As was shown in Figure 3.1, the total amount of HCP association was dramatically changed by the mutation from mAb D to D<sub>M</sub>. Here it can be seen that there is a significant change in the population of interacting HCP species due to the two-residue mutation.

IDEC-152 and Mill04, which are unrelated products, differ considerably more with each other and with mAbs D and D<sub>M</sub>. However, there were 4 HCP impurities that associated strongly with all 4 mAbs, and 5 additional species that associated with 3 of the 4 mAbs tested. These results show a baseline set of HCP impurities that appear to bind strongly to all mAbs and additional HCPs that bind to smaller subsets of mAbs or only single mAbs. The smaller subsets may be due to HCPs with high affinity for the hyper-variable region or different IgG subtypes or specific constructs. The 9 HCP that bind to at least 3 of the mAbs tested are likely interacting with one of the constant domains of these mAbs.

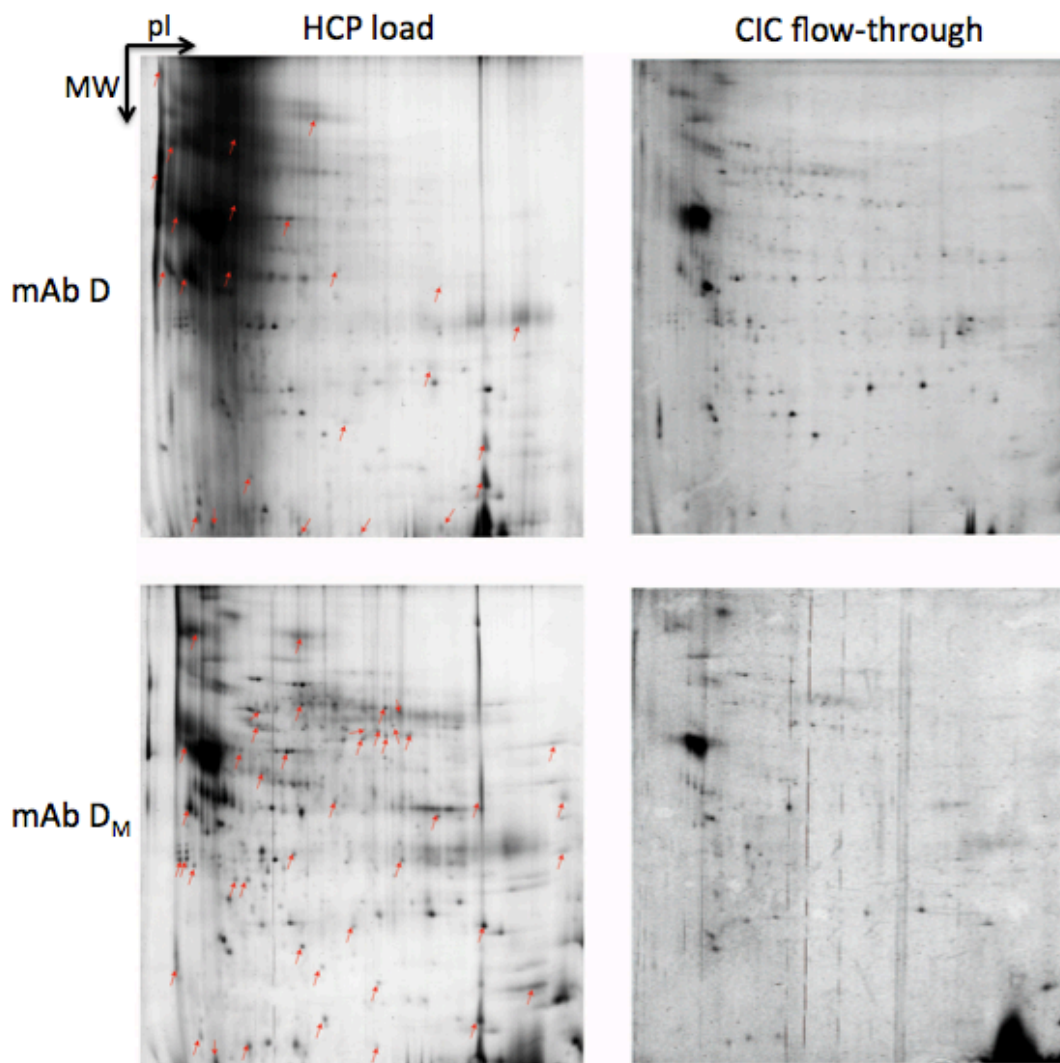


Figure 3.4: Analyzed 2-DE load (left column) and flow-through (right column) gels for HCP CIC of mAbs D and D<sub>M</sub>. Indicated spots on 'load' gels are absent from corresponding flow-through gels and represent strongly interacting HCPs. Individual spot analysis and larger images are in Appendix A.1.

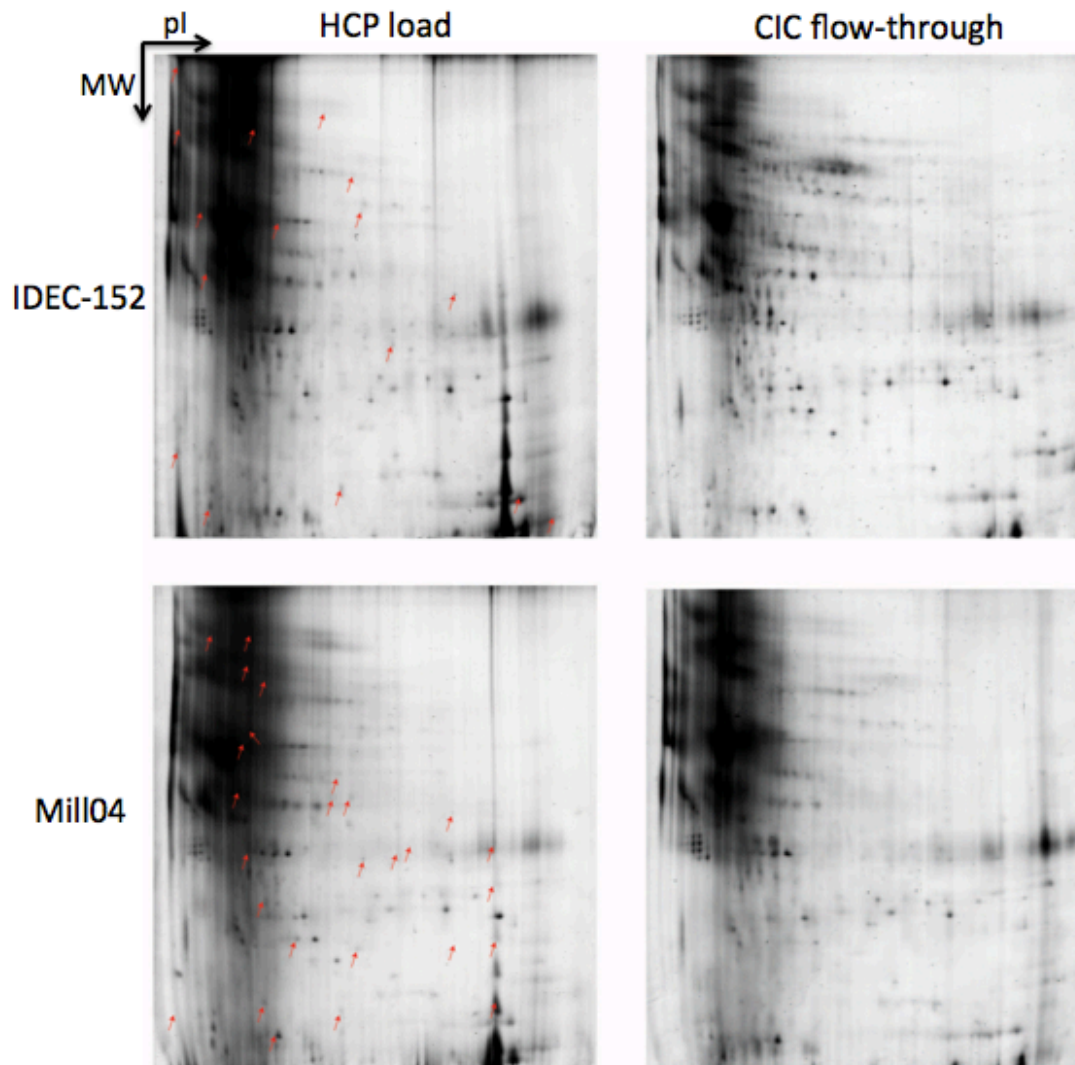


Figure 3.5: Analyzed 2-DE load (left column) and flow-through (right column) gels for HCP CIC of IDEC-152 and Mill04. Indicated spots on 'load' gels are absent from corresponding flow-through gels and represent strongly interacting HCPs. Individual spot analysis and larger images are in Appendix A.1.

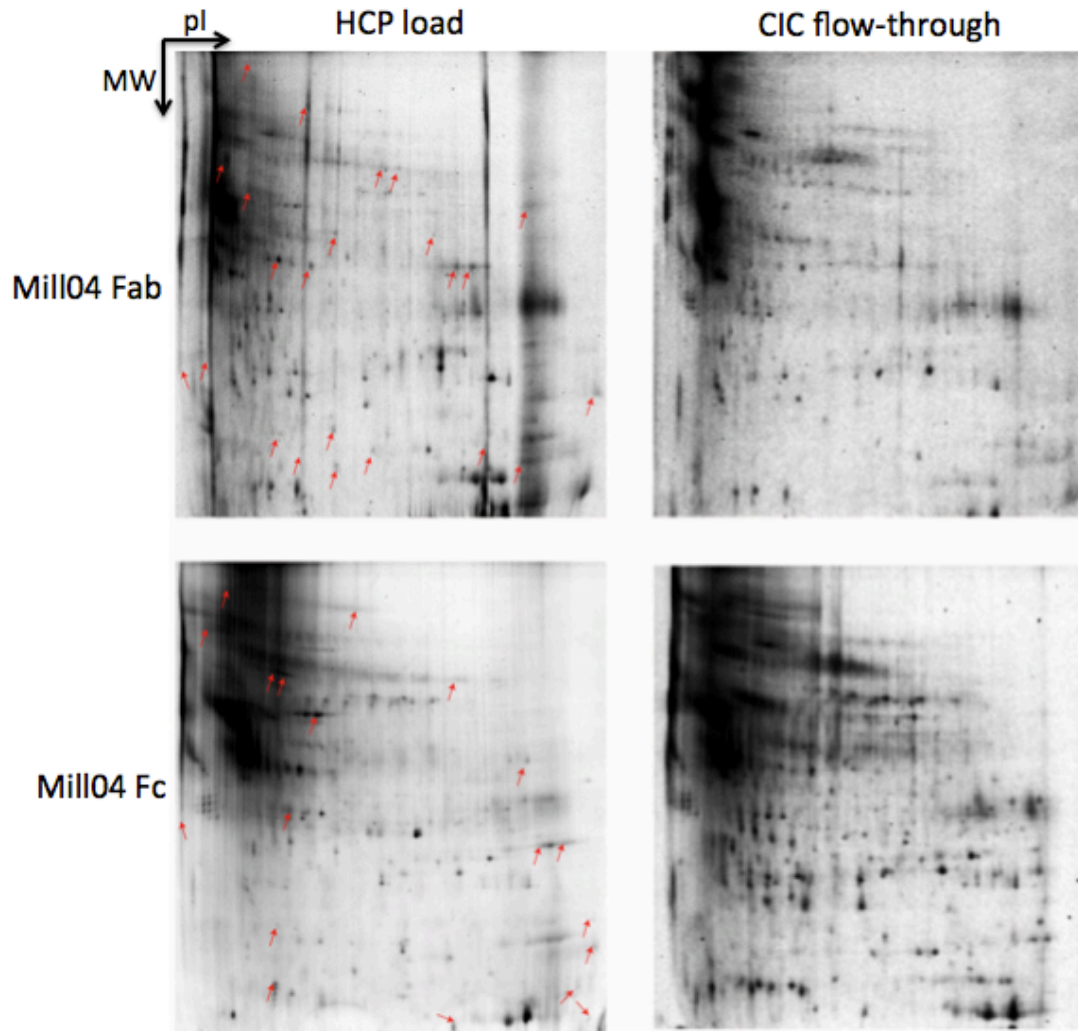


Figure 3.6: Analyzed 2-DE load (left column) and flow-through (right column) gels for HCP CIC of Mill04 Fab and Fc. Indicated spots on 'load' gels are absent from corresponding flow-through gels and represent strongly interacting HCPs. Individual spot analysis and larger images are in Appendix A.1.

Lipoprotein lipase, nidogen-1, heat shock protein, actin and clusterin were all found in this study to bind to at least 2 mAbs, and they were also previously identified as HCP impurities found in protein A product fractions for mAb purification (Doneanu et al., 2012). The results here, using mAbs unrelated to those used by Doneanu et al., are further evidence that this group of HCP binds to one of the constant regions of mAbs.

CIC experiments were also completed for Mill04 Fab and Fc. Images of the analyzed 2-DE feed and flow-through gels are shown in Figure 3.6. It was anticipated that the associating HCP for the Mill04 Fab and Fc domains would be similar to those for Mill04. The results from the 2-DE and MS analysis showed only 4 associated HCP that were also identified for the full mAb. For Mill04 Fc, 4 out of 8 interacting HCP were identified as also interacting strongly with Mill04. It is plausible that the additional interacting HCP are associating to an epitope on the Fc that is not accessible in the full molecule.

It was previously shown that clusterin binds multivalently to the Fab and Fc domains of IgGs (Wilson and Easterbrook-Smith, 1992). Therefore the finding here that clusterin binds to all mAbs and the Fab that were tested is consistent with previous observations, but clusterin was not identified as strongly attracted to Mill04 Fc. Insulin was also found to bind to all mAbs tested, but did not interact with Mill04 Fab or Fc. It is possible that the inconsistencies for clusterin and insulin are a result of using suspension cell culture for Fc CIC that may have contained less clusterin and insulin than the adherent cell culture, making them difficult to detect. Nidogen-1 binds strongly to mAbs D, D<sub>M</sub>, IDEC-152, Mill04 and Mill04 Fc, but does not bind to Mill04 Fab. This suggests that nidogen-1 binds to the Fc region of IgG molecules.

The majority of the interacting HCPs found are slightly acidic proteins. About a third of the interacting proteins have previously been reported as being secreted, with the remaining two-thirds all characterized as intracellular proteins (The UniProt Consortium, 2011). Abundant intracellular proteins, such as actin, are likely released into the extracellular space from a small amount of cell lysis during culture. The mechanism of release of low-abundance intracellular proteins, such as V-type proton ATPase subunit S1, is unknown; however, it is possible that these proteins may be actively secreted by a non-classical secretory pathway, as has been reported for heat shock protein 70 (Mambula et al., 2007).

A mechanistic basis for predicting HCP binding would allow streamlining of the process of identifying candidates for product association. Several protein parameters were calculated according to the methods outlined in Section 2.11 and are shown in Figure 3.7 as scatter plots of calculated net charge at pH 7.0 versus molecular weight and of the radius of a sphere of equivalent volume versus estimated hydrophobicity for the HCP impurities found to associate in protein A affinity chromatography. The estimated hydrophobicity was expressed as the grand average of hydropathicity (GRAVY) (Kyte and Doolittle, 1982). Negative values correspond to more hydrophilic and positive values to more hydrophobic proteins. The estimated protein parameters provide some insights into HCP-mAb association.

The HCP impurities found to associate with mAbs in protein A solutions tend to have calculated net charges between -20 and 0, with a few outliers that are either slightly positive or highly negatively-charged. The majority of secreted HCP impurities are slightly acidic (Jin et al., 2010). At the solution pH used for protein A processes, mAbs are generally positively-charged (Lehermayr et al., 2011). At low salt

concentrations, such as in protein A loading, HCP associations are likely attributed to charge-charge interactions.

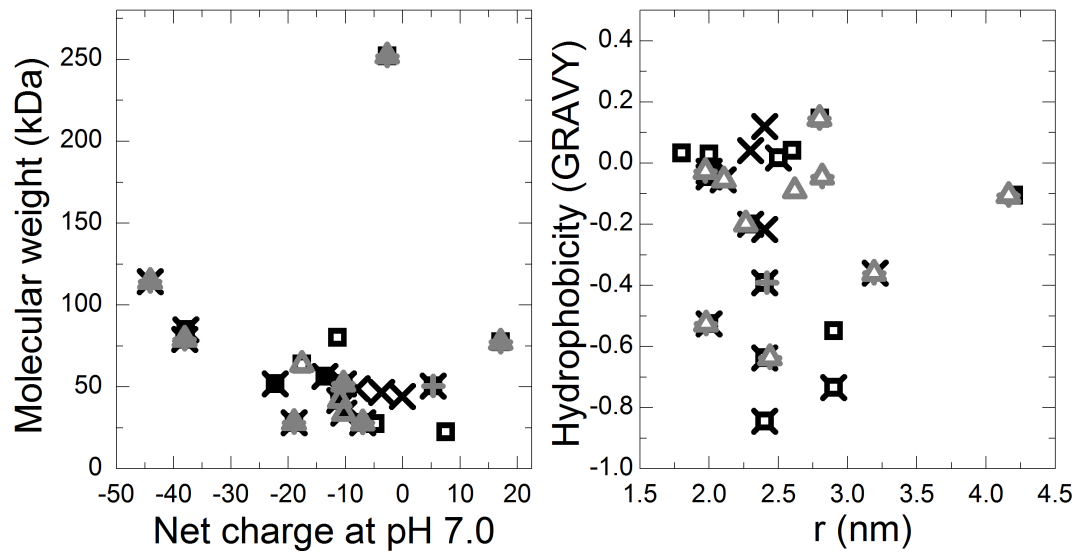
The HCPs that associate with mAbs in protein A columns show very little dependence on estimated hydrophobicity. The hydrophobicity estimates for this group of HCPs are spread out evenly across the more hydrophilic side of the GRAVY scale. HCP molecular size and weight do not appear to have a significant correlation with mAb interactions. The associating HCPs have similar molecular weights to the majority of secreted HCPs (Jin et al., 2010).

Table 3.1: CHO HCP impurities with attractive interactions to mAbs D, D<sub>M</sub>, IDEC-152 and Mill04 at 150 mM NaCl, pH 7.4.

Protein ID	MAb D	MAb D <sub>M</sub>	IDEC-152	Mill04	Location	MW (kDa)
Neural cell adhesion molecule	-	+	+	+	Cell membrane	17.9
Renin receptor	-	+	-	+	Cell membrane	33.9
Lipoprotein lipase	+	+	+	-	Cell membrane, secreted	50.5
Chondroitin sulfate proteoglycan 4	+	-	+	+	Cell membrane, cell projection, membrane	153.8
Alpha-enolase	-	+	-	-	Cytoplasm, cell membrane	15.5
Galectin-3-binding protein	+	-	-	+	Membrane	63.8
G-protein coupled receptor 56	+	-	+	+	Membrane	77.4
V-type proton ATPase subunit S1	-	+	-	-	Membrane, vacuole	28.1
Nidogen-1	+	+	+	+	Basement membrane, extracellular matrix	30.1
ATP synthase subunit beta, mitochondrial	+	+	-	-	Mitochondrion inner membrane	56.3
Vimentin	+	+	-	-	Cytoplasm	53.7
Heat shock protein	+	+	-	-	Cytoplasm	32.6
Actin	+	+	-	+	Cytoplasm	41.5
Peroxirodoxin 1	-	-	-	-	Cytoplasm, melanosome	22.3
SPARC	+	+	+	+	Secreted	28.2
Clusterin	+	+	+	+	Secreted	51.8
Complement C1r-a sub-component	+	-	-	-	Extracellular	80.1
Metalloproteinase inhibitor 1	+	-	-	-	Secreted	22.4
Insulin	+	+	+	+	Secreted	28.1
Cathepsin D	-	+	-	-	Lysosome, melanosome	44.9
Sulfated glycoprotein 1	+	-	-	-	Lysosome	27.4
Lysosomal protective protein	-	-	-	-	Lysosome	54

Table 3.2: CHO HCP impurities with attractive interactions to Mill04, Mill04 Fab and Mill04 Fc at 150 mM NaCl, pH 7.4.

<b>Protein ID</b>	<b>Mill04</b>	<b>Mill04 Fab</b>	<b>Mill04 Fc</b>	<b>Location</b>	<b>MW (kDa)</b>
Neural cell adhesion molecule	+	-	-	Cell membrane	17.9
Renin receptor	+	+	-	Cell membrane	33.9
Lipoprotein lipase	-	-	+	Cell membrane, secreted	50.5
Chondroitin sulfate proteoglycan 4	+	+	-	Cell membrane, cell projection, membrane	153.8
Galectin-3-binding protein	+	-	+	Membrane	63.8
G-protein coupled receptor 56	+	-	+	Membrane	77.4
Nidogen-1	+	-	+	Basement membrane, extracellular matrix	30.1
ATP synthase subunit beta, mitochondrial	-	-	+	Mitochondrion inner membrane	56.3
Actin	+	-	+	Cytoplasm	41.5
Peroxirodoxin 1	-	-	+	Cytoplasm, melanosome	22.3
SPARC	+	+	-	Secreted	28.2
Clusterin	+	+	-	Secreted	51.8
Insulin	+	-	-	Secreted	28.1
Lysosomal protective protein	-	-	+	Lysosome	54



analysis shows that if a high-salt wash is applied, the insulin is likely to be easily removed prior to product elution. These results are unique to insulin; CIC with additional product-associated impurities is necessary to assess the effectiveness of high-salt washes in general.

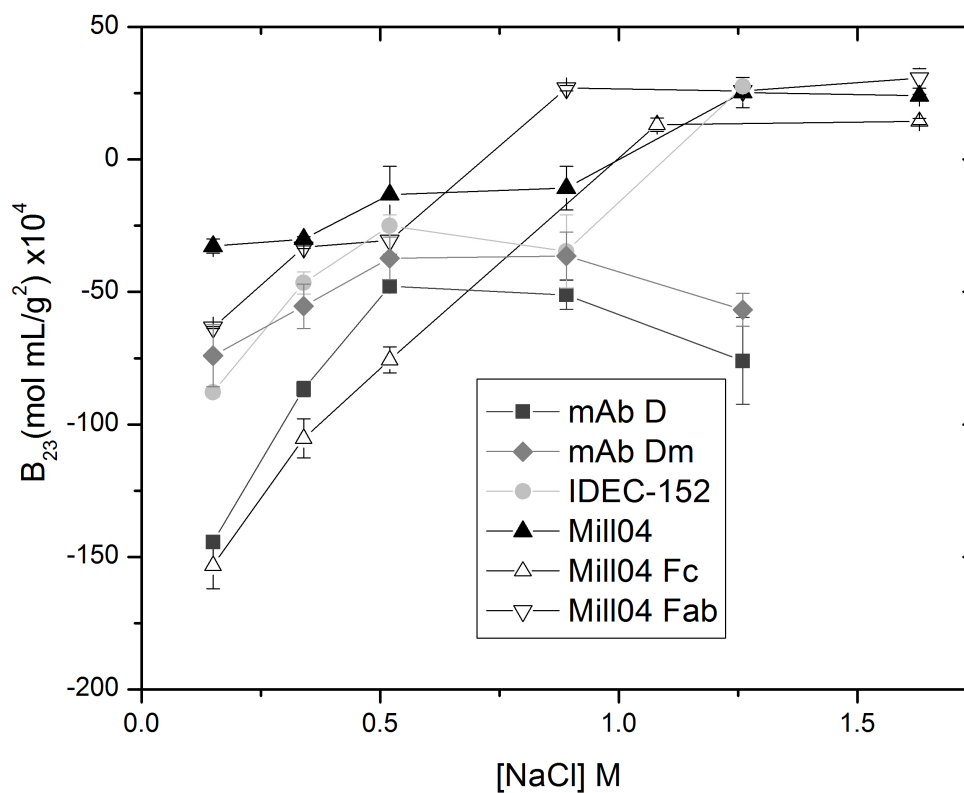


Figure 3.8: Second osmotic virial cross-coefficient ( $B_{23}$ ) measured by cross-interaction chromatography of insulin with mAb D,  $D_M$ , IDEC-152, Mill04, Mill04 Fab and Fc at pH 7.4 and varying sodium chloride concentration.

### 3.5 Interaction Orientation of MAb and Associated HCP Impurities

Nidogen-1 associates with mAbs D,  $D_M$ , IDEC-152 and Mill04 and lipoprotein lipase associates with mAbs D,  $D_M$  and IDEC-152 in protein A affinity

chromatography. To understand better these mAb-HCP interactions, non-electrostatic interaction well depths at randomly sampled mAb-HCP orientations were calculated using molecular mechanics methods and code that were adapted from previous work (Asthagiri et al., 1999; Neal et al., 1998; Quang et al., 2014), as described further in Section 2.12. Homology structures of nidogen-1 and lipoprotein lipase were developed on the SWISS-MODEL workspace (Arnold et al., 2006). The mAb structure used in these calculations is the previously solved crystal structure of a human IgG2 Fc domain (Teplyakov et al., 2013).

The non-electrostatic interaction well depths were first calculated for nidogen-1 interacting with the Fc domain of a human IgG2 Fc. For computational purposes, only half of the Fc structure was used, and only the solvent-accessible space was explored. The histogram of the distribution of non-electrostatic well depths for 300,000 randomly-sampled orientations of nidogen-1 and the Fc domain is shown in Figure 3.9. This distribution is similar to previous results for non-electrostatic protein-protein interactions (Quang et al., 2014). Interactions in the majority of orientations are only weakly attractive. The inset indicates the most attractive orientations that were found.

The most attractive orientations were studied in further detail. Small angular perturbations around the nominal orientations for these interactions were further explored. For nidogen-1 and Fc, the most attractive orientation that was found has a well depth of -23.5 kT and is shown in Figure 3.10. The residues on the Fc domain that are closest to nidogen-1 in this attractive orientation are from the highly solvent-exposed domain responsible for binding to the protein A ligand (Deisenhofer, 1981).

The non-electrostatic interaction well depths were also calculated for a lipoprotein lipase homology structure and the human IgG2 Fc domain. The histogram of the distribution of non-electrostatic well depths for 180,000 randomly sampled orientations of lipoprotein lipase and the Fc domain is shown in Figure 3.11. This distribution of well depths is similar to those for the nidogen-1-Fc results and similar to previous findings (Quang et al., 2014). However, there are a small number of more highly attractive interactions with well depths beyond 20 kT. Localized searches around the most attractive orientation indicated a highly attractive configuration of lipoprotein lipase and human Fc with a well depth of -33.5 kT. This high-affinity configuration is shown in Figure 3.12. Similarly to the nidogen-1 result, the lipoprotein lipase-Fc interaction involves the portion of the Fc domain responsible for protein A binding (Deisenhofer, 1981).

These results neglect electrostatics and consider only half of the Fc domain. An intact mAb has two identical sites that can bind to the protein A ligand. These findings suggest that those sites can also bind nidogen-1 or lipoprotein lipase. Because each mAb will bind only to a single protein A ligand during purification, it is possible that nidogen-1 or lipoprotein lipase could bind to the same domain on the opposite side of the Fc domain and be carried through to the product fraction. Based on this result it is unlikely that mutations can be made to the mAb product to decrease HCP-association without compromising protein A affinity, which would negatively impact platform processing.

In evaluating the significance of the computational results, a key question concerns the accuracy of the interaction free energy estimates. The force field used (Asthagiri et al., 1999) was parameterized against experimental protein-protein

interaction free energy data and therefore should account to a reasonable approximation for all contributions, including hydration effects. However, small structural perturbations, including tightly bound water molecules (Asthagiri et al., 2005; Paliwal et al., 2005) and bound ions (Gillespie et al., 2014) can attenuate otherwise highly attractive contacts by virtue of their disruption of the geometric complementarity of the apposing surfaces. Therefore a potential source of error in this computational analysis is the absence of explicit solvent molecules and ions. The attractive interactions identified here are largely due to mAb-HCP orientations with high surface complementarity, and it is possible that the actual mAb-HCP affinity can be lower than the affinity calculated here because of uncertainties in the interaction parameters and the absence from the analysis of potentially disruptive effects such as solvent molecules and ions.

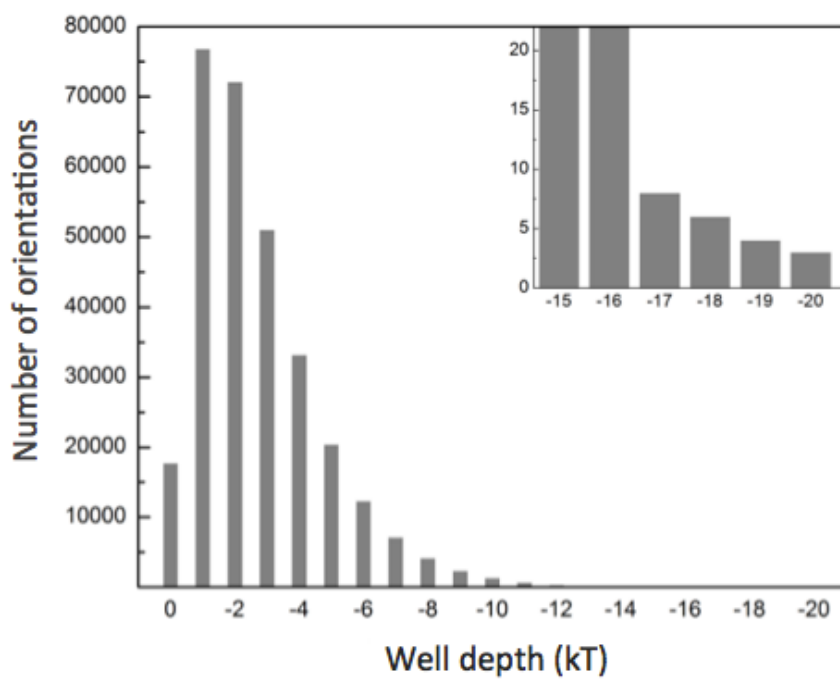


Figure 3.9: Histogram of the distribution of the non-electrostatic interaction well depths from 300,000 randomly-sampled configurations of nidogen-1 and the Fc domain. The inset histogram shows the tail of the distribution.



Figure 3.10: The highest affinity configuration of nidogen-1 (red) and the human IgG2 Fc domain (blue) with a well depth of 23.5 kT.

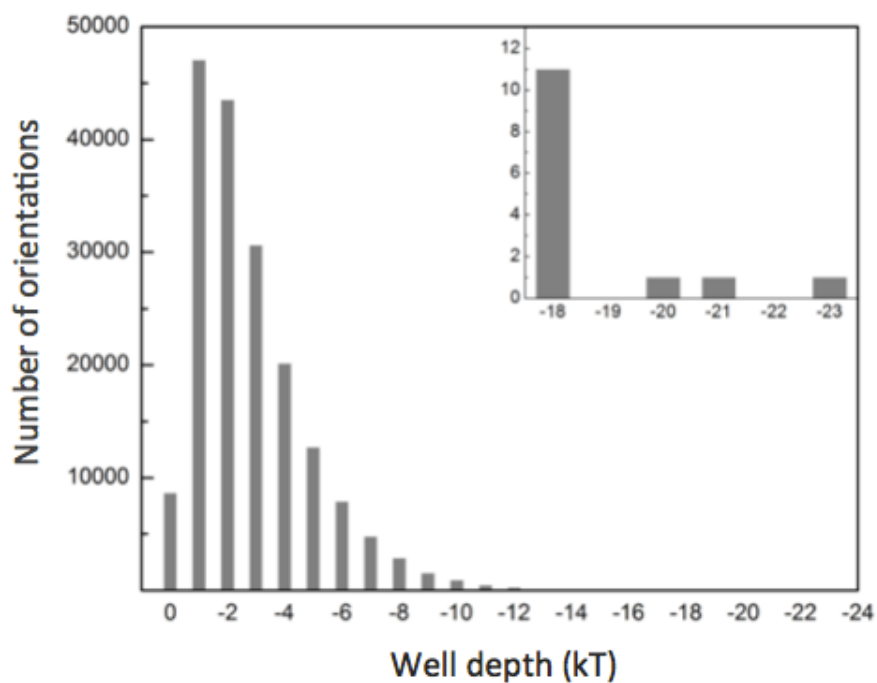


Figure 3.11: Histogram of the distribution of the non-electrostatic interaction well depths from 180,000 randomly sampled configurations of lipoprotein lipase and the Fc domain. The inset histogram shows the tail of the distribution.

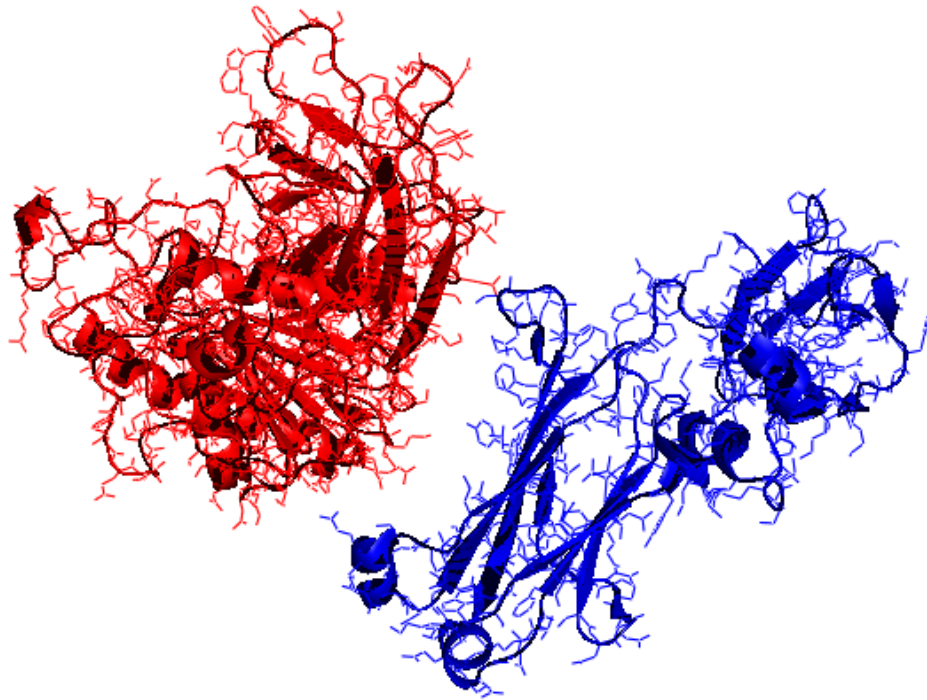


Figure 3.12: The highest-affinity configuration of lipoprotein lipase (red) and the human IgG2 Fc domain (blue), with a well depth of 33.5 kT.

### 3.6 Conclusions

This work demonstrates the importance of product association as a mechanism by which HCP impurities are retained in product fractions after a protein A purification. As was seen in previous work (Shukla and Hinckley, 2008; Tarrant et al., 2012), product association is as common as or more common than co-elution resulting from non-specific binding of HCP to chromatographic resins. This work shows that the total amount of product association varies significantly for different mAb products. These differences can make some mAbs considerably more difficult to purify to acceptable HCP levels. The results also demonstrate that small changes in the mAb

sequence can yield dramatic changes in HCP interactions; it is not reasonable to assume that related mAbs will interact only with the same population of HCP impurities.

The work also showed the difficulties of directly monitoring HCP impurity content using 2-DE of downstream process product fractions. The nature of the mAb purification process results in HCP and mAb concentrations that differ by orders of magnitude, even though the relatively low HCP content is still important and would be considered unacceptable by regulatory agencies.

The CIC method developed here provides insight into the mechanism of HCP impurity retention while avoiding the issues of product and impurity concentration differences. For example, CIC with mAbs and mAb fragments showed the specific domains with which some HCPs associate, such as the consistent binding of nidogen-1 via the Fc domain. Overall, the number of HCP that were found to bind to each mAb (10-15) and the number of HCP that were found to bind to at least 3 of the 4 mAbs tested (9) are small compared to the total population of HCP. A relatively small subpopulation of CHO HCP therefore appears responsible for giving rise to product-associated impurities. While some strongly binding proteins, such as insulin, may bind strongly at loading conditions but be relatively easy to remove in a wash step, this is not necessarily true for other proteins, which would require further investigation.

## Chapter 4

### HOST CELL PROTEIN IMPURITIES IN MONOCLONAL ANTIBODY PLATFORM PURIFICATION POLISHING STEPS

#### 4.1 Introduction

In typical mAb platform purification, the unit operations following the protein A affinity capture step consist of one or two non-affinity polishing columns (Curling and Gottschalk, 2007; Liu et al., 2010). The most commonly used non-affinity chromatographic resins are anion (AEX) or cation (CEX) exchange (Xu et al., 2012), hydrophobic interaction (HIC) (Chen et al., 2008), or multimodal (MMC) (Holstein et al., 2012; Morrison et al., 2010). The polishing columns are designed for removal of residual HCP, DNA, viruses, leached protein A ligand as well as product-related impurities, primarily mAb fragments and aggregates (Curling and Gottschalk, 2007).

In this chapter the behavior of HCP impurities in non-affinity polishing columns is described. Although the majority of HCP impurities are removed in the protein A capture step, there are often residual species that remain (Chen et al., 2010; Grzeskowiak et al., 2009). It has been proposed that replacing protein A chromatography with a non-affinity capture step would provide a significant cost savings for monoclonal antibody purification (Follman and Farner, 2004; Marichal-Gallardo and Álvarez, 2012; Miesegaes et al., 2012; Nfor et al., 2013; Pezzini et al., 2011). If the protein A capture step were replaced, understanding the behavior of the full set of HCPs on alternative, non-affinity, resins would be highly beneficial. Previous work analyzed complex mixtures of HCPs on different chromatographic resins and in non-affinity based platforms to determine the chromatographic behavior

of HCP impurities (Nfor et al., 2012; Nfor et al., 2013). The present study, although performed in the context of mAb platform processing, made use of a null CHO line for source material, so the resulting HCP chromatographic properties are relevant for any recombinant protein produced in CHO cells. Therefore, rather than studying the chromatographic behavior of the particular HCP impurities that clear protein A chromatography, this work is based on a ‘worst-case scenario’ approach by loading all HCPs to each polishing column.

The specific goal of the work was to identify difficult-to-remove HCP impurities in polishing columns and to determine why they are difficult to remove. Total product-association was measured and HCP-mAb cross-interaction chromatography was used to determine the importance of product-association in polishing columns. HCP fractionation and proteomic analyses were completed on four different resin types under typical operating conditions in order to identify potential co-eluting HCP species.

## **4.2 Binding Capacity of Polishing Resins**

HCP binding capacities of bind-and-elute polishing columns were determined to find the maximum concentration of co-eluting HCP impurities using standard methods and are reported in Table 4.1. The binding capacities were measured for CHO HCP (null CHO-K1 supernatant) at relevant column loading conditions, but without mAb present. The bind-and-elute column types for most mAb polishing steps are CEX, HIC and MMC (Shukla et al., 2007b).

At typical operating conditions, the capacity for mAb is between 10 and 80 mg/mL resin, according to resin manufacturers and previous studies (Chen et al., 2008; Fogle et al., 2012; Pabst et al., 2009; Senczuk et al., 2009; Stein and

Kiesewetter, 2007), approximately two orders of magnitude greater than the measured HCP binding capacity (Liu et al., 2011). In typical process conditions, the material loaded onto polishing columns has at least two orders of magnitude more product than HCP content (Hogwood et al., 2012). Although the binding capacity for HCP on all resins studied here appears low, it is sufficiently high to allow for retention of trace impurities and subsequent co-elution with the product molecule (Liu et al., 2011).

Table 4.1: Binding capacities of HCP on polishing columns.

<b>Resin</b>	<b>Condition</b>	<b>mg HCP/mL resin</b>
SP Sepharose FF	pH 4.5	1.21
SP Sepharose FF	pH 5.5	0.94
Butyl Sepharose FF	1 M AS, pH 7.0	0.95
Capto MMC	pH 4.5	0.81

### 4.3 Total Product Association in Polishing Columns

HCP-mAb product association in protein A affinity chromatography has been demonstrated previously (Levy et al., 2013; Shukla and Hinckley, 2008; Sisodiya et al., 2012; Tarrant et al., 2012). In order to determine the total extent and thus overall importance of product association in various non-affinity polishing columns, a series of similar purification procedures were carried out. Similar to previous work (Shukla and Hinckley, 2008) and protein A studies presented in Chapter 3, bind-and-elute purifications with and without HCP and mAb on SP Sepharose FF, Capto MMC and Butyl Sepharose FF were performed. The excess HCP in the elution fraction in the presence of mAb was calculated. This excess HCP content can be assumed to represent the total amount of HCP that associates to the mAb and is carried into the product fraction (Levy et al., 2013; Shukla and Hinckley, 2008; Sisodiya et al., 2012).

The results are presented in Figure 4.1. As discussed above, this method measures the total HCP that would be present if these non-affinity resins were used as a capture step. In an actual process environment the total HCP association in polishing columns is reduced because there is lower HCP content after protein A capture (Hogwood et al., 2012; Shukla et al., 2007b), but these results confirm that product-association is potentially a major route through which HCP can travel through polishing resins for the resins studied here.

The total extent of product association in SP Sepharose FF at pH 4.5 or 5.5, or Capto MMC at pH 4.5, is similar to association levels found in protein A affinity chromatography (Chapter 3) (Shukla and Hinckley, 2008; Sisodiya et al., 2012). Using the same experimental techniques, there was an unexpected decrease in total protein in the elution fraction for Butyl Sepharose FF when mAb and HCP were run together. It is possible that product-association was not significant, but it is also possible that mAb binding capacity was decreased due to displacement by adsorbed HCP impurities or HCP binding to mAbs at loading conditions (Brown et al., 2010). HCP-mAb CIC was carried out in HIC solution conditions to determine product-association characteristics and results are presented in the following section.

The variability of total HCP-mAb association in CEX and MMC columns is due largely to differences between mAb products and solution conditions rather than resin type. For instance, in SP Sepharose FF, an increase in pH from pH 4.5 to 5.5 results in a large increase in total HCP association in the presence of IDEC-152. MAb D<sub>M</sub> was found to have greater total product-association in protein A affinity chromatography than mAb D and IDEC-152, but on Capto MMC mAb D and IDEC-152 had considerably higher total product-association than mAb D<sub>M</sub>.

These results demonstrate the difficulty of predicting the overall HCP association of a new process for a new mAb. It is clear that significant product association in one step of a process does not imply that a product will have similar problems in a different part of the process. This also strongly suggests that if the correct solution conditions are chosen for any given mAb product, the extent of product-association could be minimized; if the associating HCPs are identified and isolated, CIC analysis (Tessier et al., 2004a) could be used to determine solution conditions where protein-protein interactions are weaker. However, this measurement does not indicate the source of differences in total association; differences could arise from the binding of a single HCP species or different binding characteristics of many HCP impurities.

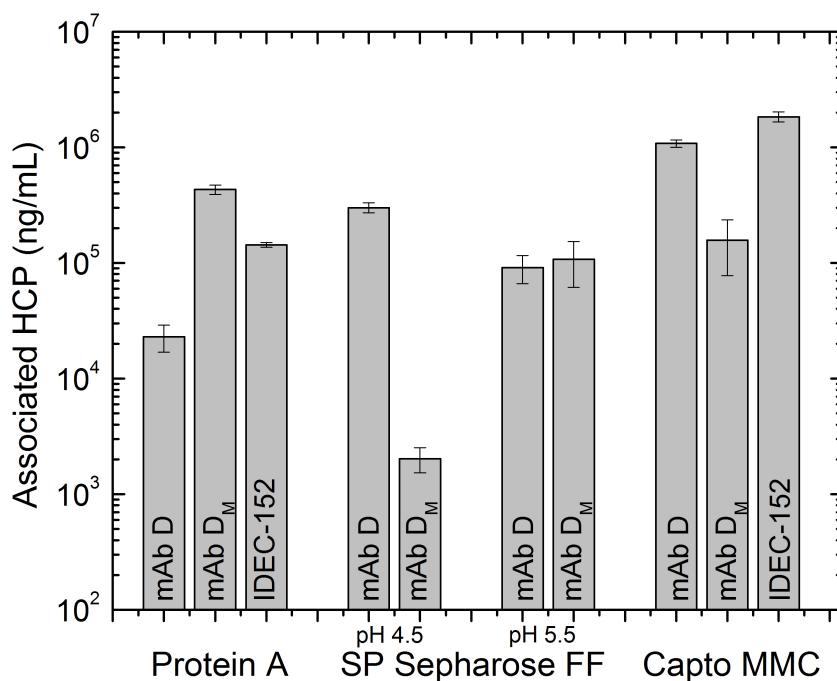


Figure 4.1: Excess HCP due to HCP-mAb product association in protein A, CEX and MMC columns for three mAbs.

#### 4.4 Cross-Interaction Chromatography: HCP-mAb Association in HIC

Although measurements of total product association in Butyl Sepharose FF, a hydrophobic interaction chromatographic resin, did not indicate significant product association, mAb-HCP CIC was run at HIC column loading conditions. Previously, HCP-CIC was run with the same mAbs (Chapter 3) for protein A loading conditions, namely 150 mM NaCl, pH 7.4, while the HIC loading conditions used here are 1.0 M ammonium sulfate, pH 7.0. Due to the different solution conditions it is expected that a different set of HCP impurities would tend to associate with mAbs.

Table 4.2 shows the CHO HCP impurities found to associate with mAb D or mAb D<sub>M</sub>. Overall, a smaller set of HCP impurities was identified as associated impurities compared with protein A loading solution conditions. Considering that total product association was not detectable by the methods used here, a smaller number of associating HCPs was expected. Five HCPs were found to associate with mAb D and seven were found to interact with mAb D<sub>M</sub>; four HCPs interacted with both mAbs. 2-DE image analysis can be found in Appendix B. Many of the associating HCP species in the HIC loading condition were also found to interact with mAbs D and D<sub>M</sub> in protein A solution conditions.

Chondroitin sulfate proteoglycan 4, sulfated glycoprotein, and cathepsin D were all found to associate with mAb D in protein A conditions and were found here to associate with both mAbs D and D<sub>M</sub> in HIC conditions. Nidogen-1 and SPARC were found to associate with both mAbs in protein A, but only with mAb D<sub>M</sub> in HIC processing. Actin was found to associate with both mAbs in protein A and HIC conditions. Nidogen-1 and actin were previously found in product fractions after various purification processes (Doneanu et al., 2012). Many of the associating HCPs identified here were previously identified as abundant HCPs in CHO supernatant.

Actin and SPARC account for 2.5 and 1.5 percent of total HCP, respectively, and chondroitin sulfate proteoglycan 4 and nidogen-1 each account for approximately 1 percent of all HCP content (Pezzini et al., 2011). As was found previously in Chapter 3 as well as mAb-mAb interaction studies in Chapters 6 and 7, the two-residue mutation from mAb D to mAb D<sub>M</sub> can have a considerable impact on protein-protein interactions. The self-interaction differences were especially pronounced at high concentrations of ammonium or lithium sulfate. The results here, which indicate that some HCP impurities bind to these mAbs at both protein A and HIC conditions and some bind differently to these very similar mAbs, are consistent with what has been previously observed with these mAbs.

The group of HCP impurities identified here as binding under both protein A and HIC conditions is of great interest. Due to attractive interactions with mAbs in both environments these impurities are anticipated to be among the most difficult HCPs to remove. The strong binding in different solution environments is also of practical interest for process design. Although neither solution would be used as a wash solution, for this group of HCP impurities product-association is not highly dependent on solution conditions. Designing a column wash to disrupt association might prove to be difficult based on these findings.

Dickkopf-related protein 3 was found to associate with mAbs D and D<sub>M</sub> in HIC but not in protein A conditions. These species are less troublesome because, in a typical platform purification scheme, there is a lower probability that these HCPs will be present in the HIC load because they do not bind to the mAb in the upstream capture step. However, if these species co-eluted through the capture step or if HIC is used as an alternative capture step, they would be difficult to remove.

A mechanistic basis for predicting binding would allow streamlining of the process of identifying candidates for product association. Figure 4.2 shows a scatter plot of calculated net charge at pH 7.0 versus molecular weight and of the radius of gyration for a sphere of equivalent volume versus estimated hydrophobicity for the HCP impurities found to associate in HIC columns. The estimated hydrophobicity was expressed as the grand average of hydropathicity (GRAVY) (Kyte and Doolittle, 1982). Negative values correspond to more hydrophilic and positive values to more hydrophobic proteins. The estimated protein parameters provide some insights into HCP-mAb association.

In HIC solution conditions there are a few highly positively-charged associating HCPs, but the most negatively-charged HCPs that product-associated in protein A affinity chromatography (Figure 3.7) appear not to associate here. MAbs are generally positively-charged at the solution pH used for HIC or protein A processes (Lehermayr et al., 2011). At low salt concentrations, such as in protein A loading, there are a number of HCP associations that can be attributed to charge-charge interactions. In the HIC solution conditions, the highly negatively-charged HCP no longer associate, likely due to screening out of charge-charge interactions because of the high salt concentration (Dumetz et al., 2007). The screening of electrostatic repulsion appears also to allow the association of a few positively-charged HCPs.

The associated HCPs in the HIC column are a subset of the more hydrophobic HCPs from the population of HCPs that product-associated in the protein A step. These correlations indicate that association in a HIC environment is more likely to occur with more hydrophobic protein impurities that generally have lower net charge. HCP molecular size and weight do not appear to have a significant correlation with

mAb interactions in HIC columns. Generally, the associating HCPs in HIC and protein A columns have similar molecular weights to the majority of secreted HCPs (Jin et al., 2010).

Many of the mAb-associating HCP impurities in the HIC solution environment also associated in protein A solution environments. There remains a baseline set of HCPs that bind to both mAbs, regardless of solution conditions. It is this subset of HCPs that should be closely monitored and new strategies for their removal should be considered. Also, estimates of protein properties indicate that some HCP associations in protein A chromatography are likely driven by charge-charge attraction, while the associations in HIC columns are due more to the hydrophobic nature of HCP impurities.

Table 4.2: CHO HCP impurities with attractive interactions to mAbs D and D<sub>M</sub> at pH 7.0, 1 M ammonium sulfate.

Protein ID	MAb D	MAb D <sub>M</sub>	Location
Chondroitin sulfate proteoglycan 4	+	+	Cell membrane, cell projection, membrane
Nidogen-1	-	+	Basement membrane, extracellular matrix
Actin	+	+	Cytoplasm
SPARC	-	+	Secreted
Cathepsin D	-	+	Lysosome, melanosome
Sulfated glycoprotein 1	+	+	Lysosome
Glucose regulated protein	+	-	ER
Dickkopf-related protein 3	+	+	Extracellular

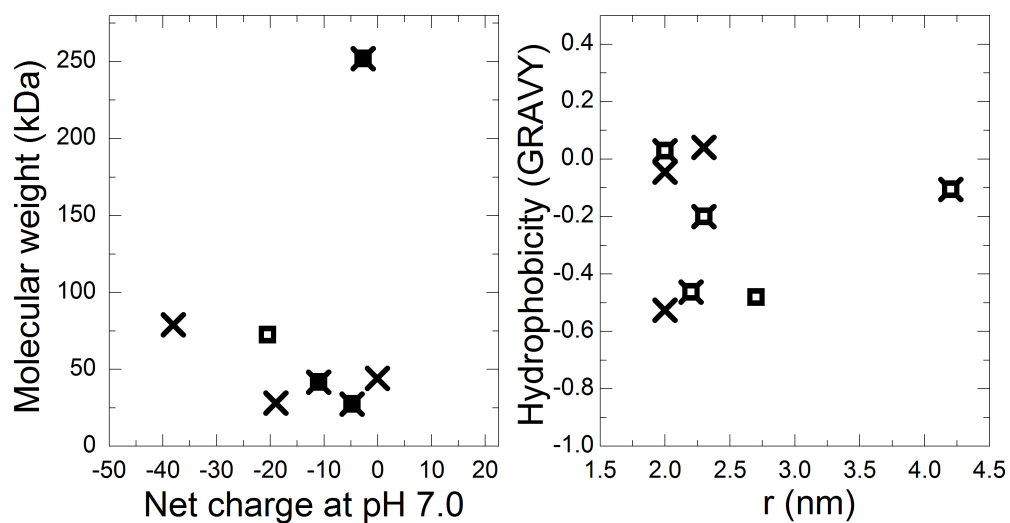


Figure 4.2: Estimated properties of HCP impurities found to associate to mAb D (□) and mAb D<sub>M</sub> (×) in HIC solution conditions.

#### **4.5 HCP Fractionation: Cation-Exchange Chromatography**

Null CHO supernatant was buffer exchanged, loaded and eluted with a linear salt gradient from SP Sepharose FF. As can be observed in the chromatogram in Figure 4.3, the majority of HCP impurities do not bind to the CEX resin at pH 4.5, 0 M NaCl. The chromatogram is similar to those in processes with HCP on CEX resins (Joucla et al., 2013; Nfor et al., 2012). Based on the A280 trace, the majority of HCP content is found in the flow-through fraction. The majority of secreted HCPs are acidic proteins (Jin et al., 2010), so it was expected that most HCPs would not bind to the resin. The acidic nature of HCP impurities generally makes CEX bind-and-elute an effective polishing method for reducing HCP concentration in mAb processes (Shukla et al., 2007b). The chromatogram (Figure 4.3) shows 3 main peaks across the gradient elution; however, the proteomic results do not neatly divide into 3 groups despite the A280 trace. Because the HCP impurities are low in concentration, A280 is not a reliable method to track chromatographic behavior of individual components.

The majority of identified HCP impurities in gradient elution on SP Sepharose FF are reasonably well resolved – found in no more than 2 fractions – with the exception of dickkopf-related protein 3. The largest population of impurities occurs in fraction C, which corresponds to a conductivity of ~50 mS/cm.

A total of 15 CHO HCPs that elute in at least one of the 4 fractions were identified using shotgun proteomics. Seven of the identified HCPs were previously found to product-associate with mAbs in either protein A affinity or HIC purification: chondroitin sulfate proteoglycan 4, clusterin, dickkopf-related protein 3, lipoprotein lipase, metalloproteinase inhibitor 1, nidogen-1 and SPARC. Of these proteins, clusterin and SPARC were found to bind to all four mAbs in the previous study of protein A product-association (Chapter 3) (Levy et al., 2013). In a mAb platform

process, these particular HCP impurities are more likely to be present in polishing columns due to their mAb-association characteristics. Cathepsin B, clusterin, legumain and metalloproteinase inhibitor 1 were identified in the CEX gradient elution here and they were previously identified in the elution fraction of a mAb capture process on Capto S (an alternative CEX resin); legumain was the most abundant co-eluting HCP impurity (Joucla et al., 2013).

In Figure 4.4 the estimated pI, net charge at pH 4.5, hydrophobicity (expressed as GRAVY index), and radius of gyration for a sphere of equivalent volume versus elution fraction are plotted for all identified co-eluting HCP. Protein properties were determined according to the procedures described in Section 2.11. The majority of the HCPs here have calculated isoelectric points above 5.0, and there is a significant population of basic HCPs found here as well. However, there is no obvious trend relating elution volume and pI. Previous studies of HCP gradient elution on CEX indicated a stronger correlation of elution volume and pI, but there were many outliers (Nfor et al., 2012). The estimated net charges at pH 4.5 become slightly more positive along the gradient elution, as would be expected based on theory, but there is considerable noise and there are many outliers. The inconsistencies are likely due to both uncertainties in the charge estimations and the anisotropy of HCP impurities. Surface charge distribution has previously been shown to play an important role in chromatographic retention (Chung et al., 2009; Yao and Lenhoff, 2004; Yao and Lenhoff, 2005). Unsurprisingly, there are no correlations with protein hydrophobicity and elution volume and protein size does not seem to play a role in retention.

Gel-based analysis was performed in addition to shotgun proteomics to get a clearer picture of the chromatographic behavior of the more abundant HCP impurities.

The method of analysis was adapted from previous work (Kröner et al., 2013; Nfor et al., 2013). An additional CEX gradient elution – identical to the gradient elution used for shotgun analysis and shown in Figure 4.3 – was completed here, but with 14 fractions collected across the gradient. The fractions were desalted, TCA-precipitated and run on SDS-PAGE, which was then stained with Sypro Ruby. Bands of interest were excised and identified using mass spectrometry. Chromatograms of individual HCP species were constructed based on densitometry measurements and are shown in Figure 4.5. The gel-based results are available for a more abundant subset of the proteins found by shotgun techniques, and some HCP species that were not identified by shotgun methods.

The chromatographic behavior of five CHO HCPs on SP Sepharose FF is shown in Figure 4.5. Insulin-like growth factor-binding protein 4, basement membrane specific heparan sulfate proteoglycan core protein and lactadherin were all identified in gel-based analysis but not identified in shotgun analysis. Insulin-like growth factor-binding protein 4 elutes late in the salt gradient compared to the majority of HCPs. Lactadherin is well-resolved and elutes at the start of the gradient elution, and basement membrane specific heparan sulfate proteoglycan core protein is found across the majority of the gradient elution.

SPARC and nidogen-1 were identified using both gel-based methods and shotgun analysis. Based on gel analysis (Figure 4.5) SPARC elutes in the middle 15 mL of the 30 mL linear salt gradient. In shotgun analysis SPARC was identified in the last 15 mL of the gradient elution. Nidogen-1 was present at a low level across the majority of the gradient elution. Shotgun analysis identified nidogen-1 only in the third fraction.

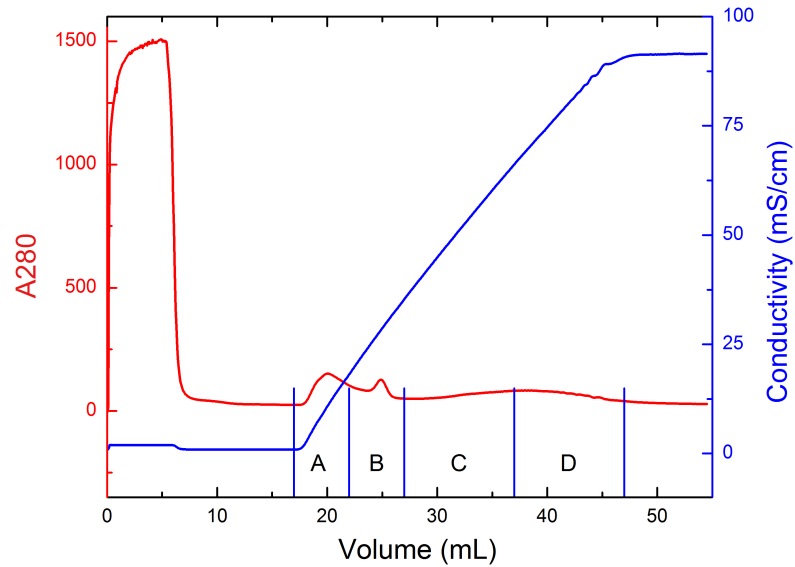


Figure 4.3: Null CHO supernatant chromatographic behavior on SP Sepharose FF at pH 4.5, eluted with 0-1 M NaCl linear gradient elution. Red trace is A280; blue trace is conductivity. Fractions A-D were collected for shotgun proteomic analysis.

Table 4.3: Shotgun proteomic results for fractions A-D of SP Sepharose FF gradient elution of CHO HCP impurities. Proteins in italics also associate with mAbs in protein A affinity chromatography.

Protein ID	pI	MW (kDa)	A	B	C	D
Alpha-N-acetylgalactosaminidase	8.0	47.2		+		
Cathepsin B	5.7	37.5	+			
<i>Chondroitin sulfate proteoglycan 4</i>	5.4	252.0			+	+
<i>Clusterin</i>	5.5	51.8			+	
Di-N-acetylchitobiase	5.4	33.0	+			
<i>Dickkopf-related protein 3</i>	4.4	38.4	+	+	+	+
dnaK-type molecular chaperone GRP78 precursor					+	
Glypican-1					+	
Legumain	6.1	49.6			+	
Leukemia inhibitory factor	9.1	17.4	+			
<i>Lipoprotein lipase</i>	8.0	50.5			+	
<i>Metalloproteinase inhibitor 1</i>	8.8	22.4			+	
<i>Nidogen-1</i>	4.8	79.0			+	
Nucleobindin-2	5.1	50.3			+	
<i>SPARC</i>	4.8	28.2			+	+

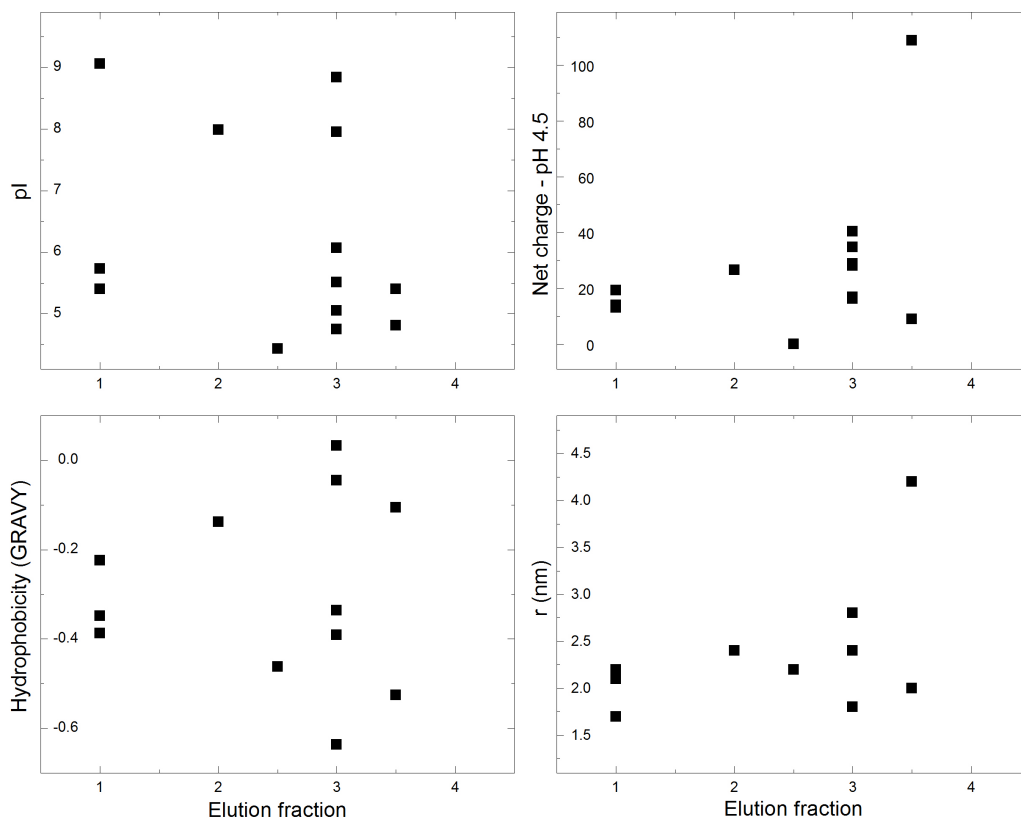


Figure 4.4: Estimated isoelectric point, net charge, hydrophobicity and size of identified HCP species from chromatographic fractions of SP Sepharose FF gradient elution.

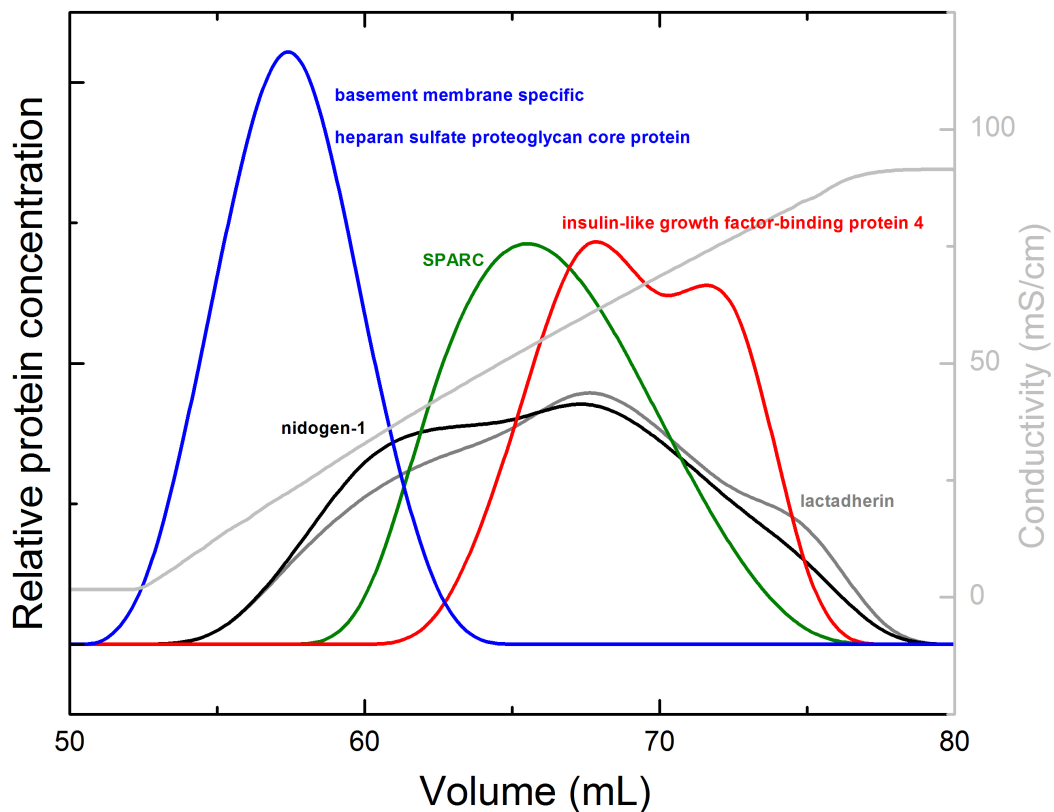


Figure 4.5: Gel-based chromatograms of identified CHO HCP impurities on SP Sepharose FF with linear gradient elution.

#### 4.6 HCP Fractionation: Anion-Exchange Chromatography

HCP retention on an anion-exchange resin, Q Sepharose FF, with linear gradient salt elution is investigated in this section. In a standard mAb platform process, AEX is normally operated in flow-through mode (Shukla et al., 2007b), so the gradient elution shown here is not relevant to most mAb platform processes. However, there could be non-mAb products produced in CHO cell culture – for example Fc-fusion proteins – for which AEX is an appropriate bind-and-elute process (Coffman et al., 2008).

Because the majority of HCP impurities are acidic proteins (Jin et al., 2010) there is much higher HCP binding on the AEX column than in CEX. The chromatogram shows what appear to be three major peaks across the salt gradient, all considerably larger than observed with other resins in this work. The HCP content in the elution fraction relative to the flow-through is higher than in previous studies using Mono Q (an alternative AEX resin), which had a larger portion of HCP in the flow-through (Nfor et al., 2012).

Shotgun proteomic analysis was able to identify 21 unique HCP impurities. Two of these proteins are found in the flow-through fraction, and the remaining 19 are found to elute along the linear salt gradient. The majority of proteins appear to be well resolved by AEX, as they were found in only one or two fractions. Seven of the identified HCPs were previously found to associate with mAbs in protein A affinity chromatography. One of the two impurities identified in the flow-through, metalloproteinase inhibitor 1, associates with IgG1 and IgG2 product molecules and is thus likely to be a problematic HCP in traditional mAb platform AEX flow-through processing. Legumain was identified in the third fraction here; legumain was found to elute at a similar point in the gradient here as in previous work, despite slightly modified solution conditions and a different AEX resin (Nfor et al., 2012). Many of the HCPs identified in AEX elution, such as actin and legumain, were also found to be among the most abundant CHO HCPs (Pezzini et al., 2011).

The HCPs identified that also product-associate in HIC or protein A are actin, chondroitin sulfate proteoglycan 4, dickkopf-related protein 3, lipoprotein lipase, metalloproteinase inhibitor 1, nidogen-1 and SPARC. Most of these HCPs were found to bind to all or most mAbs, and lipoprotein lipase, nidogen-1 and actin were all

identified as binding to the Fc domain of Mill04 in protein A affinity chromatography. For processes in which AEX is operated as a bind-and-elute step, e.g., for Fc-fusion products (Coffman et al., 2008), this set of HCP impurities would be likely to co-purify with the Fc-fusion species due to association with the Fc domain. Additionally, lipoprotein lipase can have potentially significant impact on product stability, as is discussed in Chapter 5.

Figure 4.7 shows the calculated pI, calculated net charge at pH 7, hydrophobicity and radius of gyration for the identified HCP impurities in each chromatographic fraction. As would be expected, the majority of pIs are below 7, with a few notable exceptions, similar to previous findings (Nfor et al., 2012). Histone H2A type 1, inter-alpha-trypsin inhibitor heavy chain H5, lipoprotein lipase, metalloproteinase inhibitor 1 and procollagen C-endopeptidase enhancer 1 all bind to the AEX column and are found in various fractions during gradient elution, despite being basic proteins. The calculated net charge on most of the HCP impurities is between -20 and +10. In general there is little correlation between net charge and elution order.

Many of the later eluting HCP species are not highly charged. It is possible that local charge clustering on the HCP surfaces drive chromatographic behavior in the absence of high net charge. There are, however, also a few highly-charged, late-eluting species. There is no clear trend regarding hydrophobicity of HCPs and elution order and although some of the late-eluting HCPs are much larger, protein size does not show a clear trend either.

To get a clearer picture of the chromatographic behavior of specific HCP impurities, gel-based analysis was performed in addition to shotgun proteomics. An

identical AEX gradient elution to that described above was completed, but with 14 fractions collected across the gradient. The analysis was performed as described in Section 4.5. Chromatograms of individual HCP species were constructed based on densitometry measurements and are shown in Figure 4.8. The gel results are available for a more abundant subset of the proteins found by shotgun techniques, and in most cases the chromatographic retention agrees in both analyses. Because of the nature of this technique, there is significant noise in the reconstructed chromatograms. The larger number of fractions in the gel-based analysis provides a better picture of how well resolved this set of impurities is and to what extent they are likely to co-elute with product molecules. For example, basement membrane-specific heparan sulfate proteoglycan core protein is confined to the end of the linear salt gradient, and glucose regulated protein is found only at the start of elution. In contrast, SPARC is found across the entire elution. This could be due to charge variants of this particular HCP. Many proteins have charge variants with different chromatographic properties (Ahrer and Jungbauer, 2006). Regardless of why it elutes across the entire gradient, it would be very difficult to remove in this process. Nidogen-1 and lipoprotein lipase, two HCP impurities that are frequently problematic and have been discussed here repeatedly, elute near the middle of the gradient in well-resolved peaks; nidogen-1 and lipoprotein lipase each account for greater than 1% of the total HCP population, which makes them some of the more abundant species (Pezzini et al., 2011).

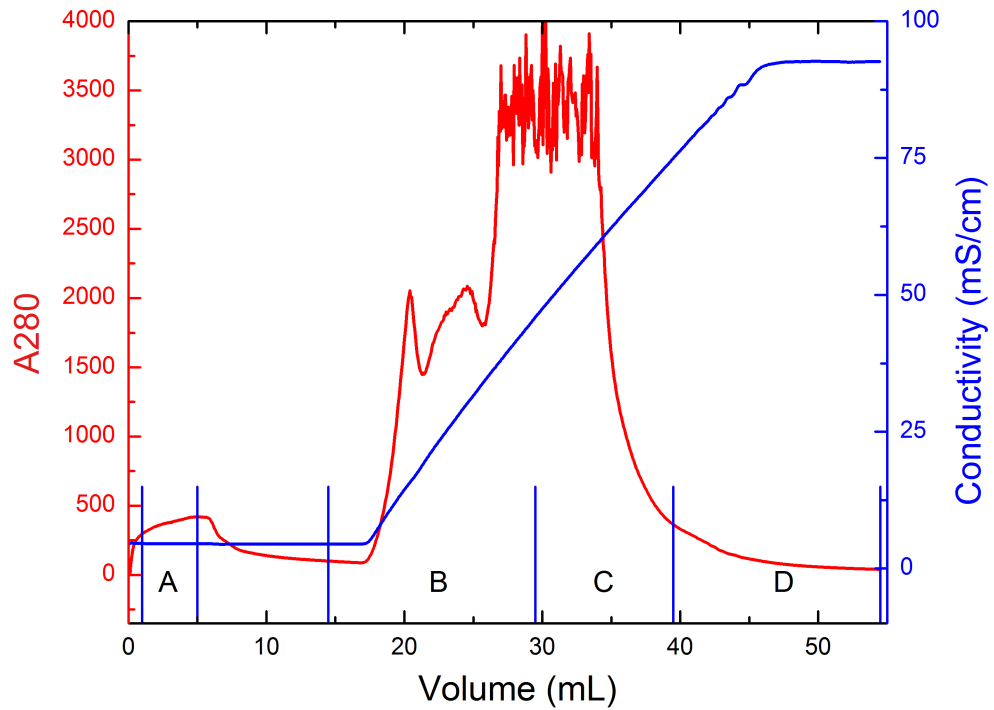


Figure 4.6: Null CHO supernatant chromatographic behavior on Q Sepharose FF, at pH 7.0 with 0-1 M NaCl linear gradient elution. Red trace is A280; blue trace is conductivity. Fractions A-D were collected for shotgun proteomic analysis.

Table 4.4: Shotgun proteomic results for fractions A-D of Q Sepharose FF gradient elution of CHO HCP impurities. Proteins in italics associate with mAbs in protein A affinity chromatography.

<b>Protein ID</b>	<b>pI</b>	<b>MW (kDa)</b>	<b>A</b>	<b>B</b>	<b>C</b>	<b>D</b>
<i>Actin</i>	5.2	41.7			+	
Basement membrane-specific heparan sulfate proteoglycan core protein	6.4	334.1			+	+
<i>Chondroitin sulfate proteoglycan 4</i>	5.4	252.0			+	+
<i>Dickkopf-related protein 3</i>	4.4	38.4		+		
Glypican-1					+	+
Histone H2A type 1	11.0	28.5			+	
Immunoglobulin superfamily member 8			+			
Inter-alpha-trypsin inhibitor heavy chain H5	8.5	107.9				+
Laminin subunit alpha-5	6.5	405.9				+
Laminin subunit beta-1	4.8	178.1				+
Laminin subunit gamma-1	5.0	172.1		+	+	+
Legumain	6.1	49.6			+	
<i>Lipoprotein lipase</i>	8.0	50.5				+
MAM domain-containing protein 2	4.6	25.2				+
Matrix metalloproteinase-9	5.6	78.9		+		
<i>Metalloproteinase inhibitor 1</i>	8.8	22.4	+	+		
<i>Nidogen-1</i>	4.8	79.0		+	+	+
Nucleobindin-2	5.1	50.3		+		
Procollagen C-endopeptidase enhancer 1	8.5	55.2		+		
<i>SPARC</i>	4.8	28.2		+	+	
Tubulointerstitial nephritis antigen-like	6.7	52.5				+

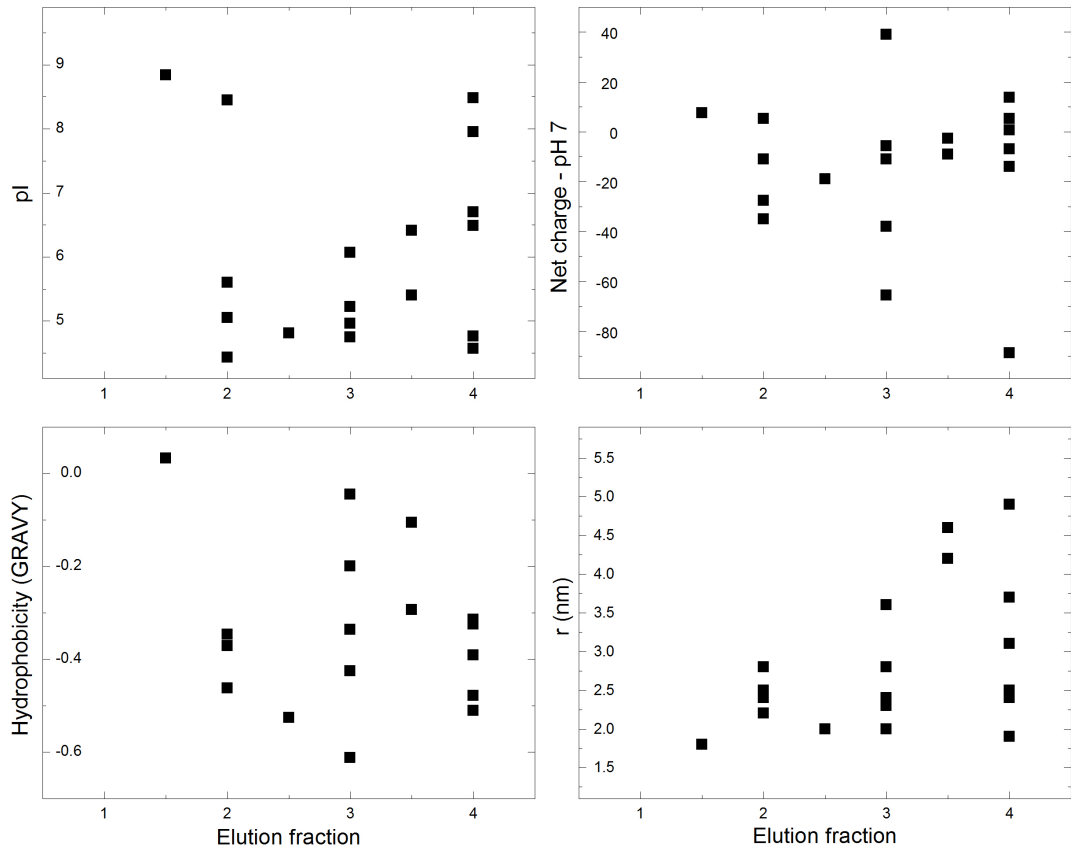


Figure 4.7: Estimated isoelectric point, net charge, hydrophobicity and size of HCP species from chromatographic fractions of Q Sepharose FF gradient elution.

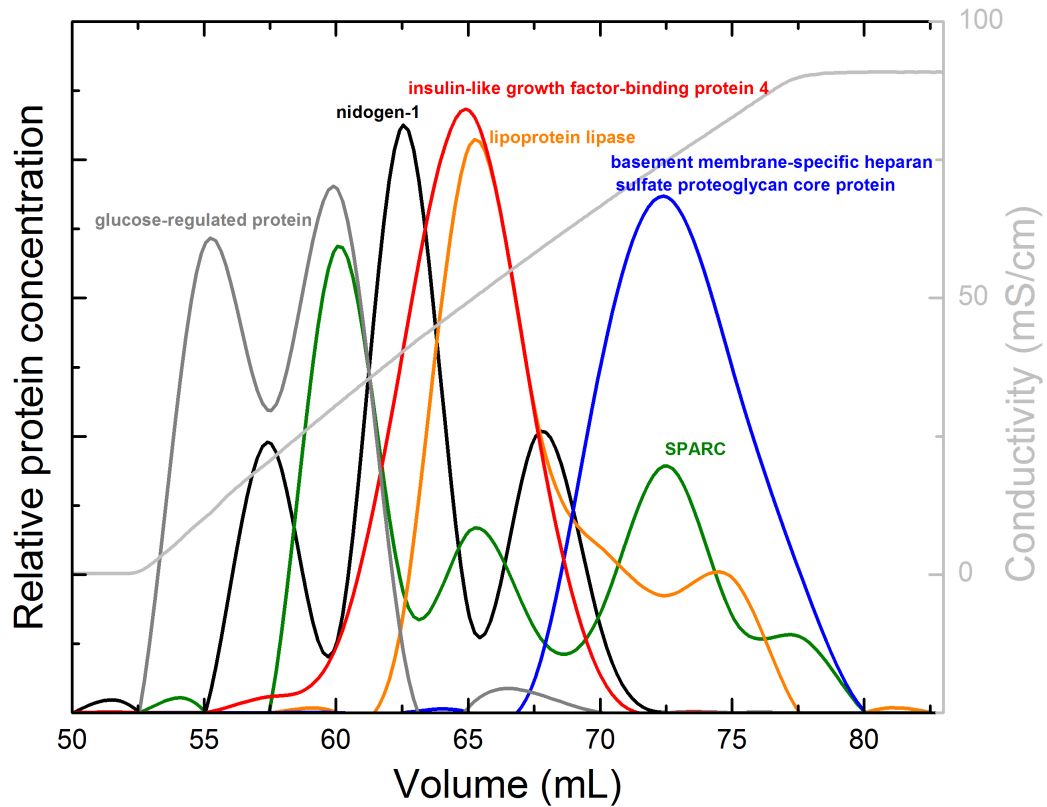


Figure 4.8: Gel-based chromatograms of identified CHO HCP impurities on Q Sepharose FF with linear gradient elution.

#### 4.7 HCP Fractionation: Hydrophobic Interaction Chromatography

HIC purification processes are commonly used in bind-and-elute mode for removal of mAb aggregates as well as other trace impurities (Chen et al., 2008). CHO HCP was loaded onto Butyl Sepharose FF at 1 M ammonium sulfate and was eluted using a linear salt gradient down to 0 M ammonium sulfate. The resulting chromatogram (Figure 4.9) shows two major peaks, the first and larger in fraction ‘A’ at the start of the ammonium sulfate gradient elution and the second in fraction ‘C’. The peaks are very well resolved on the chromatogram compared to the results on CEX or AEX resins shown earlier.

Shotgun proteomic analysis identified only 8 HCP impurities that elute at some point along the gradient. From the chromatogram it appeared that the majority of impurities would be contained in fractions 'A' and 'C', but fraction 'A' contains only three detectable HCPs. One of those three HCPs, SPARC, was previously identified as one of the 20 most abundant HCPs in CHO cell culture supernatant (Pezzini et al., 2011). Fraction 'C' contains the majority of HCP impurities.

Figure 4.10 shows how calculated pI, net charge at pH 7.0, hydrophobicity and molecular size of HCP impurities correlate with elution volume. There is a weak correlation of elution volume and pI, but net molecular charge calculations imply that electrostatic interactions are not important here. Although interactions with the resin are usually stated to be hydrophobic in nature, there is no correlation with the GRAVY index hydrophobicity. This could be due to the limitations of this metric for assessing hydrophobicity or because GRAVY estimates include the entire primary sequence rather than solvent-accessible residues. There is a weak correlation with protein size. Previous work found that larger proteins had longer elution times than smaller, similarly-flexible proteins on HIC resins with a Sepharose backbone (To and Lenhoff, 2007). The protein sizes reported here are based on primary amino acid sequences; it is possible that the identified late-eluting HCPs actually exist as larger oligomers or have significant posttranslational modifications. For example, lipoprotein lipase – found in fractions 'B' and 'C' – has been reported to form dimers (Zhang et al., 2005). However, it is difficult to make any overarching conclusions regarding HCP properties and HIC retention due to the small number of identified HCP species here.

Although the chromatogram indicates well-resolved elution volumes for HCPs, basement membrane-specific heparan sulfate proteoglycan core protein was found in

all 4 fractions and lactadherin and tubulointerstitial nephritis antigen-like were found in 3 out of 4 fractions. The shotgun proteomic analysis indicates that these individual species are not well resolved at all and would be difficult to remove if present in the column feed. None of these proteins have been previously identified as abundant in CHO cell culture (Pezzini et al., 2011).

Lipoprotein lipase, nidogen-1 and SPARC were all found to elute across the ammonium sulfate gradient and were previously found to associate with mAbs in protein A affinity chromatography. With the exception of lipoprotein lipase, this group of HCP impurities was also found to associate with mAbs in HIC solution conditions. Also, lipoprotein lipase, nidogen-1 and SPARC are three of the most abundant HCPs (Pezzini et al., 2011). These factors make this a particularly interesting group of HCPs. Due to the association in the upstream protein A column they are likely to present in polishing columns and there are multiple mechanisms that could cause this group of HCP impurities to be retained after HIC polishing.

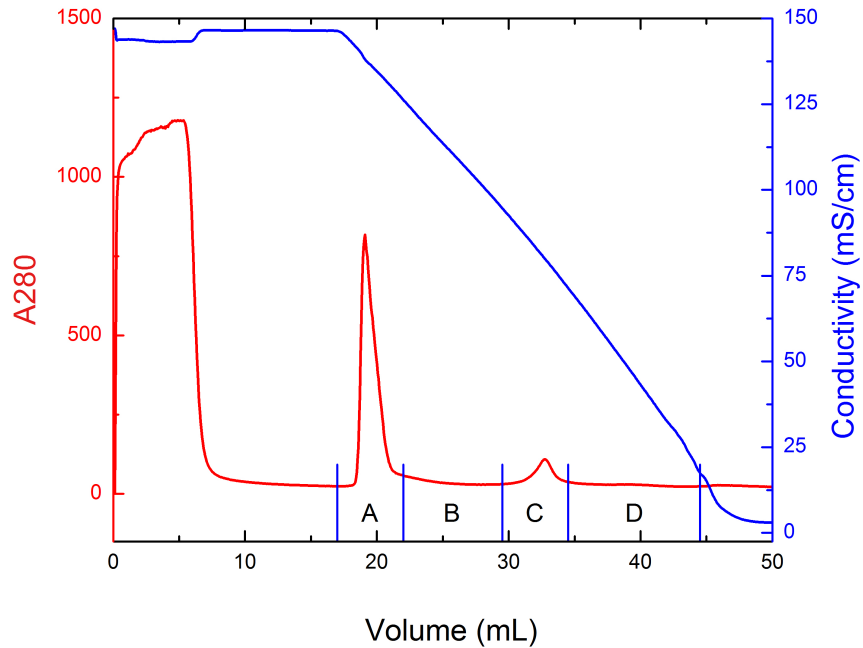


Figure 4.9: Null CHO supernatant chromatographic behavior on Butyl Sepharose FF, with loading at pH 7.0 and elution using a linear gradient from 1 M to 0 M ammonium sulfate. Red trace is A280; blue trace is conductivity. Fractions A-D were collected for shotgun proteomic analysis.

Table 4.5: Shotgun proteomic results for fractions A-D of Butyl Sepharose FF gradient elution of CHO HCP impurities. Proteins in italics associate with mAbs in protein A affinity chromatography.

<b>Protein ID</b>	<b>pI</b>	<b>MW (kDa)</b>	<b>A</b>	<b>B</b>	<b>C</b>	<b>D</b>
Basement membrane-specific heparan sulfate proteoglycan core protein	6.4	334.1	+	+	+	+
<i>Dickkopf-related protein 3</i>	4.4	38.4				+
Lactadherin	9.5	16.2	+	+	+	
Laminin subunit gamma-1	5.0	172.1			+	
<i>Lipoprotein lipase</i>	8.0	50.5		+	+	
<i>Nidogen-1</i>	4.8	79.0			+	+
<i>SPARC</i>	4.8	28.2	+			
Tubulointerstitial nephritis antigen-like	6.7	52.5		+	+	+

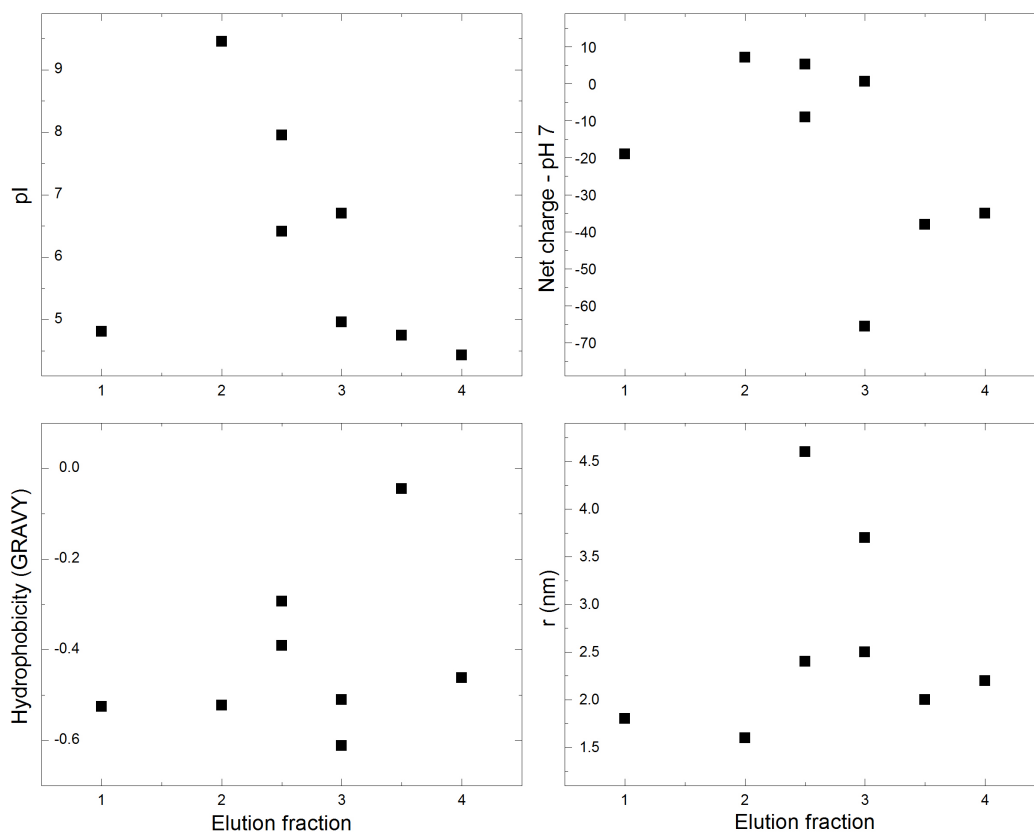


Figure 4.10: Estimated isoelectric point, net charge, hydrophobicity and size of HCP species from chromatographic fractions of Butyl Sepharose FF gradient elution.

#### 4.8 HCP Fractionation: Multimodal Chromatography

Capto MMC, a multimodal resin with cation-exchange and HIC properties, was used here in bind-and-elute mode. There are a number of different protocols for this particular resin and similar multimodal resins. The column was loaded at pH 4.5, identical loading conditions to those for SP Sepharose FF, and eluted using a simultaneous linear gradient to 1 M NaCl and non-linear gradient to pH 8.5. MAb

elution was difficult with only a pH or salt gradient; simultaneous gradients were found to be more effective. Simultaneous high-pH and high-salt concentrations previously were found to optimize mAb recovery from Capto MMC bind-and-elute processes, and only high-pH or high-salt elution resulted in low mAb yield (Joucla et al., 2013). As can be seen from the chromatogram in Figure 4.11, there is significant HCP content in the flow-through as well as during the gradient elution. The gradient elution is dominated by one well-resolved peak that was collected in fraction 'B'.

Shotgun proteomic analysis identified a total of 33 HCP impurities across the gradient elution. This was by far the largest set of HCP species identified for any of the 4 resins profiled here. As would be expected based on the chromatogram, the majority of HCP species were found in fractions 'B' and 'C'. There were 10 HCPs identified that had previously been found to associate with mAbs in protein A purification. Many of the same species that were identified in the other resins were found here as well, but the multi-modal ligand retained a number of HCP impurities that had not been identified in any other process examined. Cathepsin B, clusterin, laminin subunit beta, legmain, metalloproteinase inhibitor 1 and procollagen-lysine, 2-oxoglutarate 5-dioxygenase 1 were all identified here and in a previous study using Capto MMC as eluting in the product fraction (Joucla et al., 2013). Legumain was previously found to be the most abundant HCP impurity after mAb purification with Capto MMC (Joucla et al., 2013). The combination of CEX and HIC moieties did not result in a combination of HCPs from CEX and HIC resin types, indicating a cooperative binding effect.

Gel-based proteomics were used here to analyze more fractions across the gradient elution and to reconstruct individual chromatograms for individual HCP

impurities. However, only 3 HCP impurities had sufficient signal to retrieve reliable identification and complete analysis. Figure 4.12 shows nidogen-1, dickkopf-related protein 3 and chondroitin sulfate proteoglycan 4 chromatograms from gel-based methods eluting in that order. Nidogen-1 and chondroitin proteoglycan 4 were previously identified as highly abundant CHO HCPs (Pezzini et al., 2011). Previous studies of HCP behavior on Capto MMC also found a few highly abundant HCPs and a large number of low level HCPs (Joucla et al., 2013). All three proteins have been identified in previous analyses with different resins and here they all elute fairly early in the gradient. The order and position of elution from gel-based methods is more detailed due to the larger number of fractions, but confirms the identified elution order from shotgun methods.

As can be observed in Figure 4.13, the HCPs identified here all have pIs higher than the loading pH of 4.5, which is to be expected. The majority of HCPs found here are highly positively charged; this indicates that at loading the CEX mechanism is likely a driving force. There is not a good correlation of electrostatic properties and elution order, however. There are no highly charged proteins in early fractions, compared with a few very highly charged species in later fractions. Hydrophobicity is also not correlated with elution order, despite the hydrophobic character of the MMC ligand. Similar to HIC results, there is a slight dependence on molecular weight. Larger proteins tend to elute later in the gradient compared to smaller species. As discussed earlier, this could be related to higher affinity of larger proteins for HIC stationary phases (To and Lenhoff, 2007).

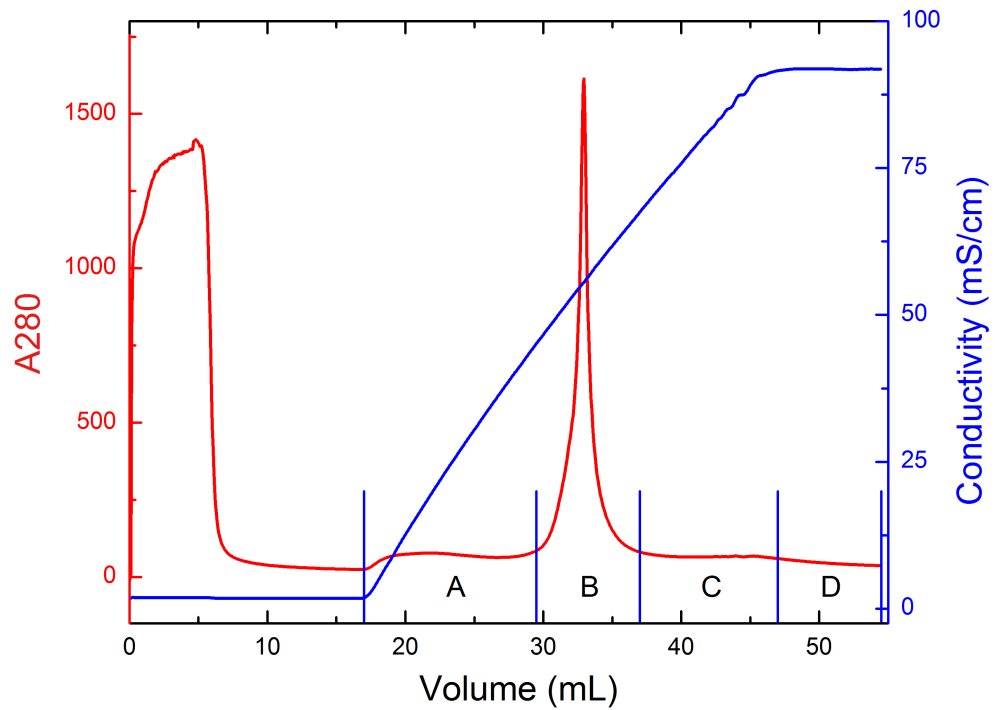


Figure 4.11: Null CHO supernatant chromatographic behavior on Capto MMC, with loading at pH 4.5 and elution using a linear gradient to 1 M NaCl, pH 8.5. Red trace is A280; blue trace is conductivity. Fractions A-D were collected for shotgun proteomic analysis.

Table 4.6: Shotgun proteomic results for fractions A-D of Capto MMC gradient elution of CHO HCP impurities. Proteins in italics associate with mAbs in protein A affinity chromatography.

Protein ID	pI	MW (kDa)	A	B	C	D
3-phosphoinositide-dependent protein kinase 1	5.7	89.6		+	+	
Alpha-galactosidase A	4.9	38.5	+			
Amyloid-like protein 2	5.0	78.3			+	
Basement membrane-specific heparan sulfate proteoglycan core protein	6.4	334.1		+	+	
Beta-actin	5.2	4.6		+	+	
Calcium-dependent serine proteinase	4.7	77.4		+		
Calsyntenin-1	4.7	92.3		+		
Cathepsin B	5.7	37.5		+		
<i>Chondroitin sulfate proteoglycan 4</i>	5.4	252.0		+	+	+
<i>Clusterin</i>	5.5	51.8		+	+	
<i>Complement C1r-A subcomponent</i>	5.7	80.1		+	+	
<i>Dickkopf-related protein 3</i>	4.4	38.4		+	+	
dnaK-type molecular chaperone GRP78 precursor				+	+	
<i>ERP57 protein</i>	6.0	56.8		+		
Follistatin-related protein 1	6.2	65.4		+		
<i>G-protein coupled receptor 56</i>	9.1	77.4		+		
<i>Galectin-3-binding protein</i>	5.1	63.8			+	
Glyceraldehyde-3-phosphate dehydrogenase	8.5	35.8		+		
Glypican-1	6.3	86.4		+	+	
Immunoglobulin superfamily member 8				+		
Inter-alpha-trypsin inhibitor heavy chain H5	8.5	107.9		+	+	
Lactadherin	9.5	16.2		+	+	
Laminin subunit beta-1	4.8	178.1		+		
Laminin subunit gamma-1	5.0	172.1			+	
Legumain	6.1	49.6		+		
<i>Lipoprotein lipase</i>	8.0	50.5			+	
Matrix metalloproteinase-9	5.6	78.9		+	+	
<i>Metalloproteinase inhibitor 1</i>	8.8	22.4		+	+	
N-acetylglucosamine-6-sulfatase	6.4	53.8	+			
N-sulphoglucosamine sulphohydrolase	6.0	56.5	+			
<i>Nidogen-1</i>	4.8	79.0	+	+	+	
Nucleobindin-2	5.1	50.3		+	+	
Peptidyl-glycine alpha-amidating monooxygenase B	6.1	94.8			+	
Procollagen C-endopeptidase enhancer 1	8.5	55.2			+	
Procollagen-lysine,2-oxoglutarate 5-Dioxygenase 1	5.8	76.0			+	
Ribonuclease T2	6.3	29.5		+		
Semaphorin-3C	7.0	55.6		+	+	
<i>SPARC</i>	4.8	28.2		+	+	
Syndecan-4			+	+		
Tissue alpha-L-fucosidase	6.0	53.4		+	+	
Tubulointerstitial nephritis antigen-like	6.7	52.5			+	

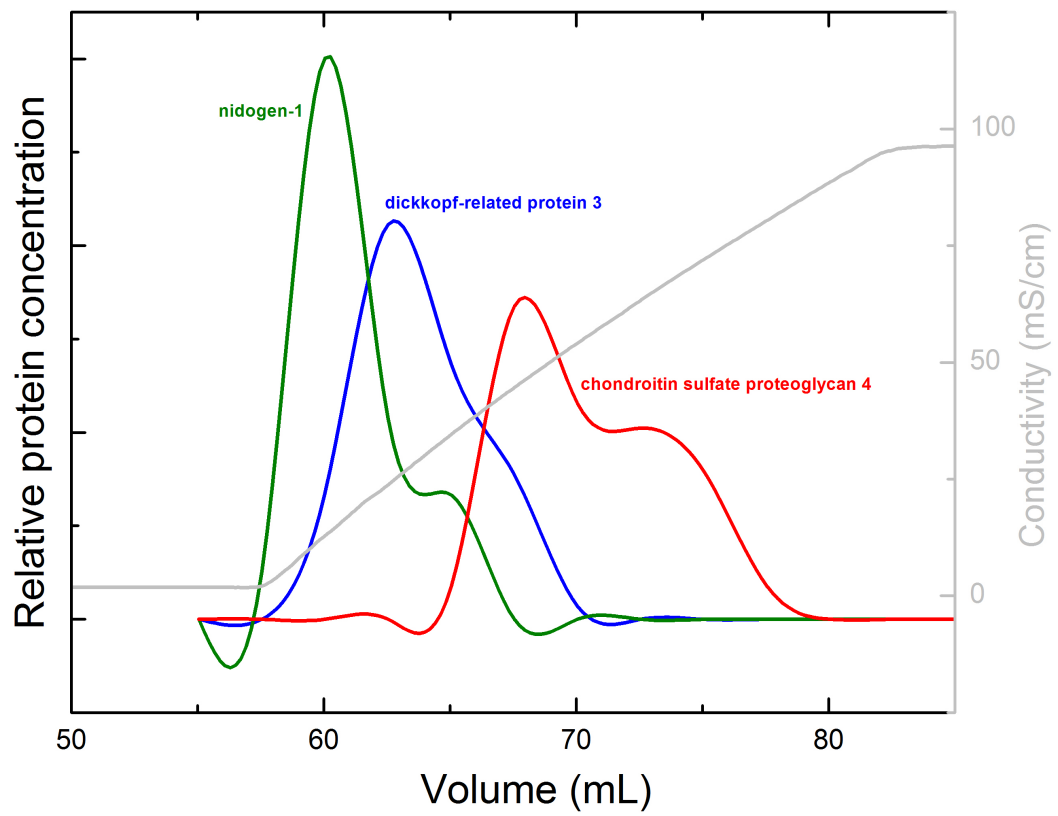


Figure 4.12: Gel-based chromatogram of HCP impurities on Capto MMC with simultaneous salt and pH gradient elution.

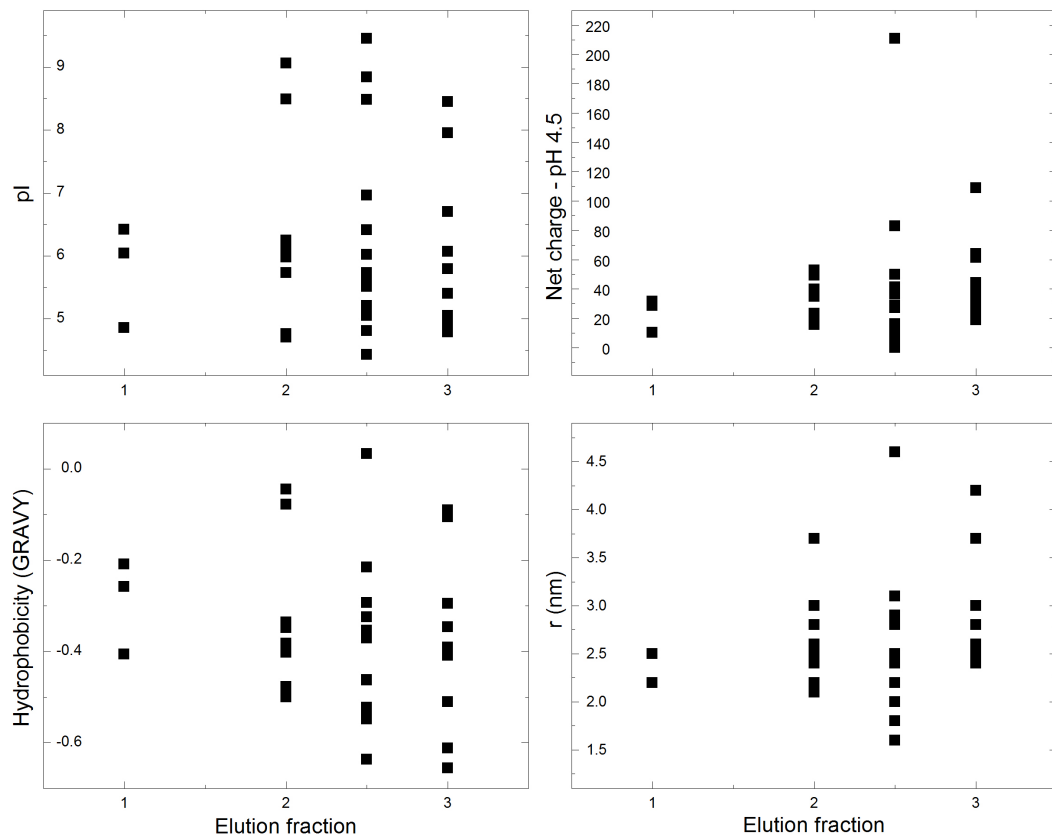


Figure 4.13: Estimated isoelectric point, net charge, hydrophobicity and size of HCP species from chromatographic fractions of Capto MMC gradient elution.

#### 4.9 HCP Homology Models

The shotgun and gel-based analyses of chromatographic fractions have resulted in valuable information for future process development efforts. The knowledge of specific HCP impurities that are difficult to remove, particularly those that are difficult to remove in multiple process schemes, can be implemented in various ways to improve downstream purification process performance. However, it is difficult to

develop mechanistic or predictive models for HCP retention from this data. The correlations of retention volume with various calculated molecular properties can shed some light on retention mechanisms and important variables, but are in no way predictive. In an effort to explain better some of the behavior of HCP impurities, homology models were developed for HCPs on the SWISS-MODEL workspace as described previously (Arnold et al., 2006). These models then allowed more detailed calculation of key molecular properties. Analysis of surface charge at relevant solution pH was completed using Poisson-Boltzmann electrostatics on the PDB2PQR server (Dolinsky et al., 2004). Solvent-accessible surface hydrophobicity was also assessed to help demonstrate the mechanism of retention for a few HCPs of interest.

One of the HCPs of interest with an available homology model was nidogen-1. This HCP impurity was found to associate with mAbs in protein A and HIC solution conditions and was also found in chromatographic fractions of all resin types studied here. It is also one of the more abundant HCP (Pezzini et al., 2011) and was previously found in the mAb product fraction of a protein A process (Doneanu et al., 2012). In Q Sepharose FF, which was run at pH 7.0, nidogen-1 was found to elute in the third fraction. The calculated charge of this HCP at pH 7.0 is -38, making it one of the more highly charged impurities and thus likely to be one of the more difficult to remove. Based on surface charges calculated from the homology model in Figure 4.14 it is clear that this protein has two oppositely charged patches. The negatively-charged patch likely controls adsorption on the AEX resin. Local charge clusters on protein surfaces can control surface adsorption, as shown previously (Hallgren et al., 2000).

The elution volume of nidogen-1 was similar to that of legumain, although legumain was one of the least charged HCP, with a net charge of -6. The homology

structure indicates that legumain also has a large negative patch on its surface that leads to larger-than-expected elution volumes (Figure 4.15). An even more dramatic example of protein surface characteristics outweighing net charge is tubulointerstitial nephritis antigen-like, which was found to elute at the end of the gradient in Q Sepharose FF but had a calculated net positive charge of +0.5. The surface charge also indicates a large negatively-charged patch that is likely responsible for the observed retention (Figure 4.16).

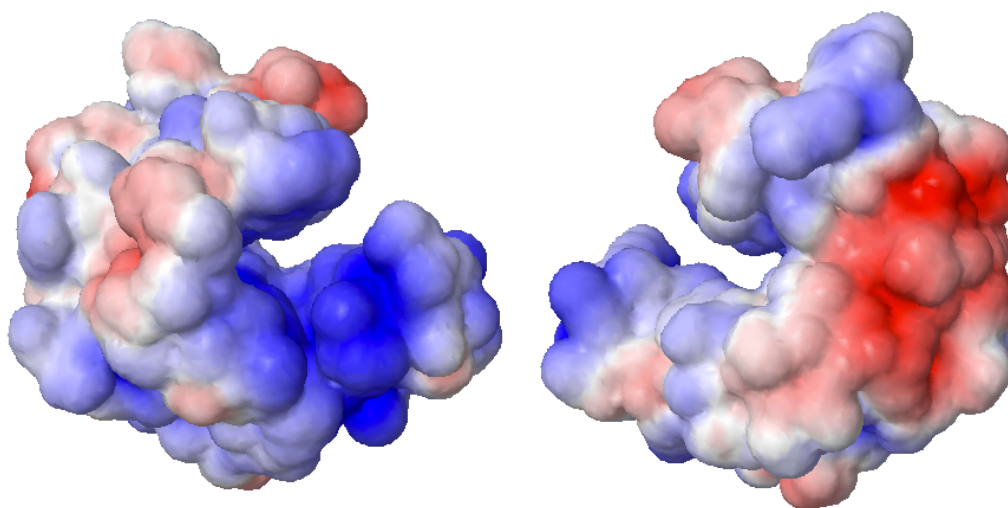


Figure 4.14: Nidogen-1 homology model with calculated surface charge at pH 7.0. Negative (red) and positive (blue) charges are indicated.

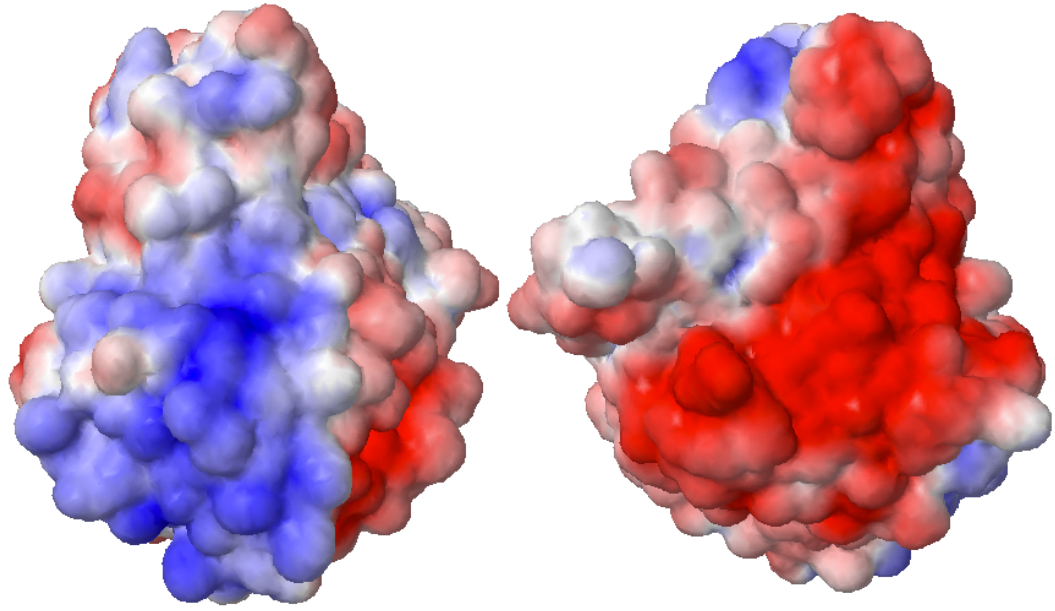


Figure 4.15: Legumain homology model with calculated surface charge at pH 7.0. Negative (red) and positive (blue) charges are indicated.

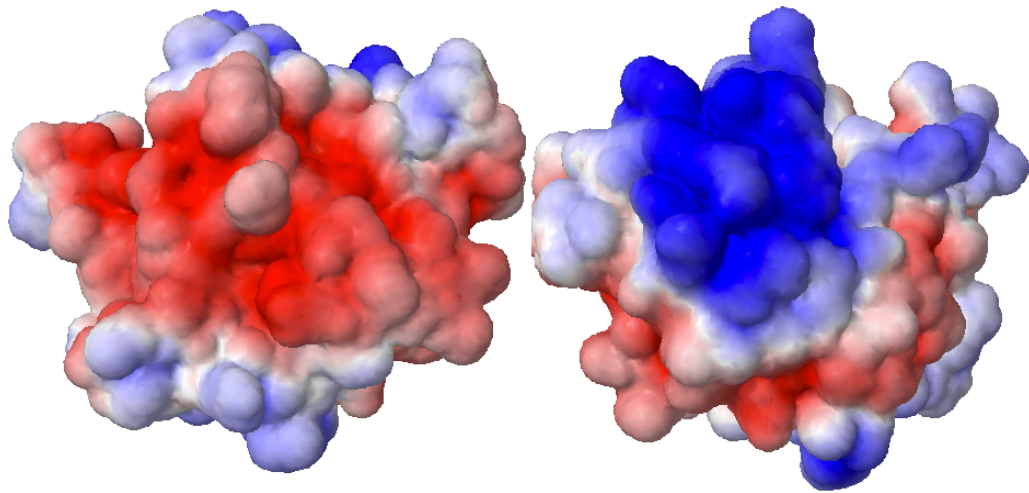


Figure 4.16: Tubulointerstitial nephritis antigen-like homology model with calculated surface charge at pH 7.0. Negative (red) and positive (blue) charges are indicated.

On Capto MMC as well as SP Sepharose FF it is expected that highly positively charged proteins will elute at larger volumes. At pH 4.5 nidogen-1 has an estimated charge of +17, which is a lower net charge than those of most of the HCPs identified as having similar elution volumes. Figure 4.17 shows the homology model with surface charges, and even though the net charge is lower, the majority of the molecular surface shows a positive potential.

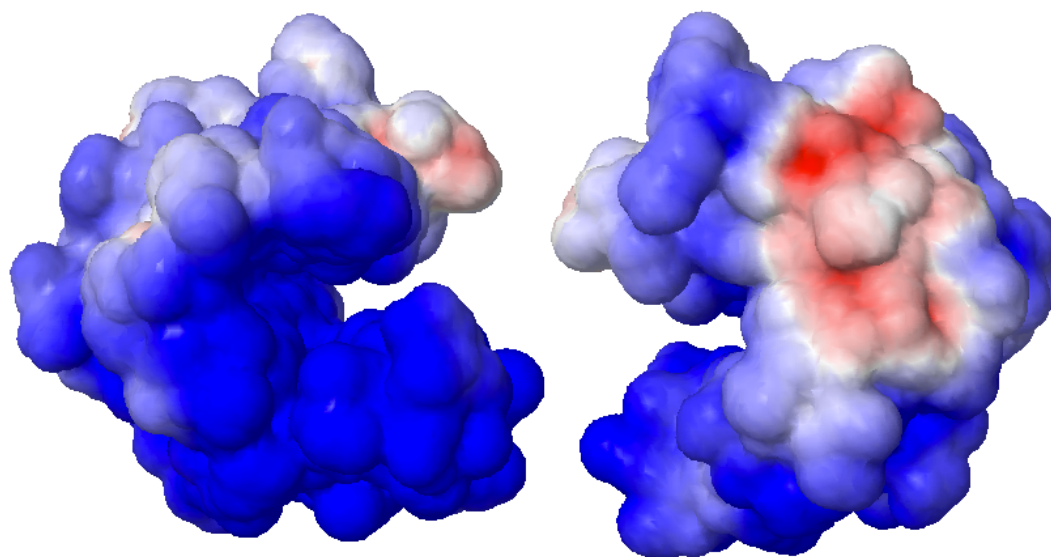


Figure 4.17: Homology model of nidogen-1 with surface charges indicated for pH 4.5. Negative (red) and positive (blue) charges are indicated.

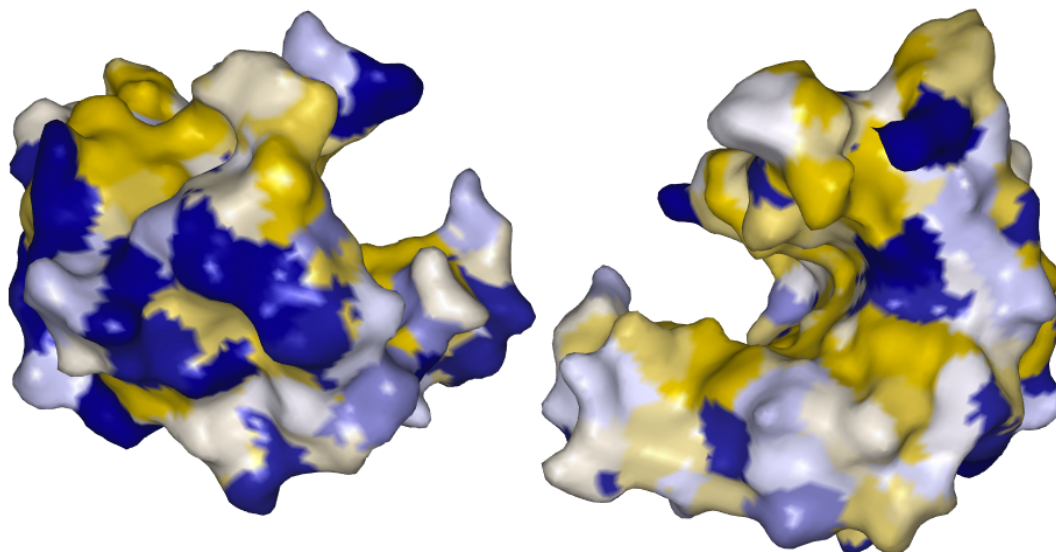


Figure 4.18: Homology model of nidogen-1 with surface hydrophobicity indicated. Hydrophobic (gold) and hydrophilic (blue) regions are indicated.

In HIC processing nidogen-1 was one of the later-eluting HCPs, although based on hydrophobicity calculations for the entire amino acid sequence it was not predicted to be one of the more hydrophobic impurities. Solvent-accessible hydrophobic residues were identified in the homology model (Figure 4.18) and similarly to previous analysis, this protein has a large hydrophobic patch on one side of the structure, which may be responsible for strong binding to the Butyl Sepharose FF resin.

These observations are qualitative and a more quantitative investigation of protein structure-retention relationships would be informative. Relationships of protein crystal structure and chromatographic retention have previously been performed (Buyel et al., 2013; Chen et al., 2007; Gill et al., 1994; Mazza et al., 2001; Roth et al., 1996; Yao and Lenhoff, 2004; Yao and Lenhoff, 2005), but there are no crystal structures available for the CHO proteins investigated here and there are only

available homology models for a small subset. A larger set of protein structures is necessary for more quantitative model predictions.

#### **4.10 Conclusions**

This work identified specific difficult-to-remove HCP impurities from non-affinity chromatographic polishing processes. As was previously shown for protein A purification, the importance of product-association was demonstrated for polishing columns. For the majority of cases, product-association occurs at a similar level in protein A and non-affinity columns. The biggest source of variability appears to be due to differences from mAb to mAb. CIC was able to identify HCP impurities that associate with two mAbs in a HIC process, and there was significant overlap with protein A results.

A relatively small population was found to co-elute in polishing columns. Efforts to develop predictive models and correlations based on estimated HCP isoelectric point, net charge and hydrophobicity were not successful. Evidence from available homology structures of a few HCPs of interest indicates that surface-accessible charge and hydrophobic patches are more important than overall molecular properties.

There are relatively few HCP impurities that co-elute or product-associate in platform downstream processing. An even smaller subset co-elutes or associates in multiple processes across a platform and is predicted to be the most difficult for removal. Table 4.7 indicates HCP impurities that associated with at least 3 of 4 mAbs in protein A processing and at least one additional purification step. These HCP impurities are of the most interest for future process development efforts. This work showed that it is hard to predict which HCP impurities will be difficult to remove and

why, but it has provided a list of impurities that should be monitored closely in mAb processes.

Table 4.7: HCP impurities found to associate with at least two mAbs in protein A purification and also difficult to remove in polishing steps.

<b>Protein ID</b>	<b>HIC ASSN</b>	<b>CEX</b>	<b>AEX</b>	<b>HIC</b>	<b>MMC</b>
Lipoprotein lipase		+		+	+
Chondroitin sulfate proteoglycan 4	+	+	+		+
Galectin-3-binding protein					+
G-protein coupled receptor 56					+
Nidogen-1	+	+	+	+	+
Actin	+		+		
SPARC	+	+	+	+	+
Clusterin		+			+

## Chapter 5

### EFFECTS OF LIPOPROTEIN LIPASE AS AN IMPURITY IN MONOCLONAL ANTIBODY DOWNSTREAM PROCESSING AND FORMULATIONS

#### 5.1 Introduction

Polysorbates are nonionic surfactants that are common additives in therapeutic mAb formulations. Of the 30 FDA approved mAbs as of 2012, 19 contained polysorbate 80 and 4 contained polysorbate 20 (Marichal-Gallardo and Álvarez, 2012). Polysorbates protect mAbs from degradation during purification, filtration, freeze-drying, storage and final delivery (Kerwin, 2008). They are thought to stabilize high-concentration mAb solutions by binding to the product molecules (Lee et al., 2011) or competing with mAbs for surface adsorption (Mahler et al., 2009). Polysorbate degradation has previously been studied and several different routes of polysorbate degradation in formulations have been identified (Ha et al., 2002; Khossravi et al., 2002; Kishore et al., 2010). Polysorbate degradation can lead to accelerated product degradation due to increased aggregation (Khossravi et al., 2002) or oxidation due to peroxide formation (Ha et al., 2002).

In Chapters 3 and 4, lipoprotein lipase (LPL) was identified as a difficult-to-remove HCP impurity in mAb downstream processing. The objectives of the present work are to determine if CHO LPL can enzymatically degrade polysorbates and to better characterize the interaction of CHO LPL with mAbs.

## 5.2 Lipase Catalysis

Lipases are a class of enzymes that hydrolyze ester bonds of substrates such as triglycerides, phospholipids and cholesteryl esters (Wong and Schotz, 2002). The lipase-catalyzed reaction scheme is indicated in Figure 5.1. LPL is a member of the lipase family, and it is distributed among a variety of tissues in animals. LPL tends to bind to capillary endothelium, where it supplies tissues with fatty acids derived from circulating triglycerides (Rojas et al., 1990).

The mechanism of LPL catalysis has been studied closely for both human and bovine species (Cheng et al., 1985; Kobayashi et al., 2002; MacPhee et al., 2000; McIlhargey, 2003; Posner et al., 1983; Shen, 2001; Shen et al., 2010; Shirai et al., 1983; Wong et al., 1994). Chinese hamster LPL is 88.6% identical to human LPL and 84.9% identical to bovine LPL. It has been proposed that three residues form the active catalytic triad in bovine and human LPL. Point mutations of Ser-132, Asp-156 and His-241 – the proposed triad – in human LPL lead to a complete loss of hydrolytic activity. These mutations did not affect the heparin affinity or lipid binding properties of LPL (Emmerich et al., 1992). The catalytic triad is conserved in Chinese hamster LPL.

The enzymatic activity of various lipases provides evidence that LPL could be active in formulation conditions. Apolipoprotein C-II (apoC-II) is known to enhance LPL activity against phospholipids, but has been shown to lower LPL hydrolysis rates of triacylglycerol (Shirai et al., 1983). LPL activity was identified using triacylglycerol as a substrate and without apoC-II at pH 7.4 and pH 8.0. Enzymatic activity was detected at various conditions between pH 7.0 and pH 9.0 (Shirai et al., 1983). The activity of *Candida regosa* lipase was maximal between pH 6.0 and 9.0 (Pereira et al., 2003). LPL from *Pseudomonas* is reported to maintain at least 50% of

maximum activity between pH 5.0 and 9.0 and becomes unstable at pH greater than 10 (Amano Enzyme, Inc.). By constructing chimeras of hepatic lipase and human LPL a two-domain structure of LPL has been proposed. The amino-terminal domain was shown to contain the catalytic triad and also to modulate the activation by apoC-II and inhibition by 1 M NaCl. The COOH-terminal domain was identified as a heparin-binding site (Davis et al., 1992). CHO cells have been shown previously to secrete LPL with enzymatic activity that is enhanced by the presence of apoC-II and inhibited by high NaCl concentration (Rojas et al., 1990). The degree of activation by apoC-II has been reported to range from two-fold (Posner et al., 1983) all the way to 100-fold (Schrecker and Greten, 1979). It has been shown that residues 39-62 in apoC-II are responsible for the activation of LPL (MacPhee et al., 2000). LPL enzymatic activity was still detectable without apoC-II (Posner et al., 1983). It was previously hypothesized that the active form of LPL is a dimer of identical monomer subunits that are associated in a non-covalent head-to-tail conformation (Kobayashi et al., 2002). Zhang et al. studied the folding of bovine LPL into active dimers and found that  $\text{Ca}^{2+}$  is necessary for proper folding and dimer formation (Zhang et al., 2005).

Christiansen et al. found that a mixture of lipases could have activity against non-ionic surfactants. This work showed significant hydrolysis of polysorbate 80 as well as Cr El and Cr RH 40 by pancreatic lipases at 37 °C and pH 6.8 in 90 minutes (Christiansen et al., 2010). The enzyme mixture used in this study was porcine pancreatin, which is a mixture of amylases, pancreatic lipases and proteases that have been extracted from porcine pancreas. While this previously measured activity against polysorbate is not specific to LPL or CHO proteins, due to the considerable homology between different lipase enzymes and lipases from different species, this result

provides strong evidence that CHO LPL could have enzymatic activity against polysorbates as well. The lipase activity against polysorbates is due to the similarity between polysorbates and triglycerides, with the ester linkage being the catalytic target. The structures of both polysorbates are shown in Figures 5.2a and 5.2b.

Prior studies using LPL and additional lipases suggest that CHO LPL could have enzymatic activity against polysorbates in the pH range of interest for typical mAb formulations (~ pH 5-7). Also, the presence of a co-factor – namely apoC-II – may not be necessary for hydrolysis to take place. However, it is possible that CHO apoC-II could be present due to purification difficulties and could contribute to increasing LPL activity.

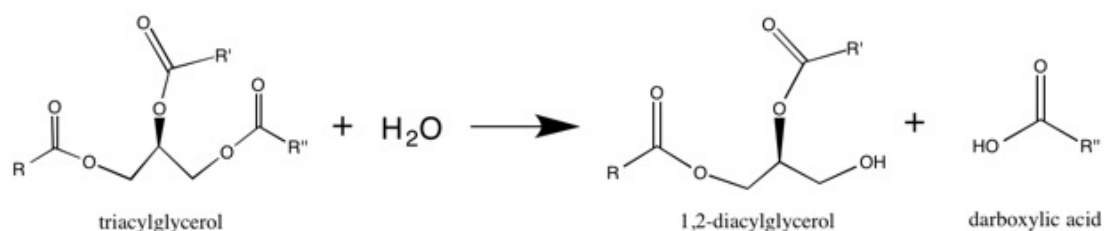


Figure 5.1: Catalytic hydrolysis by lipase of lipids into carboxylic acid and an alcohol.

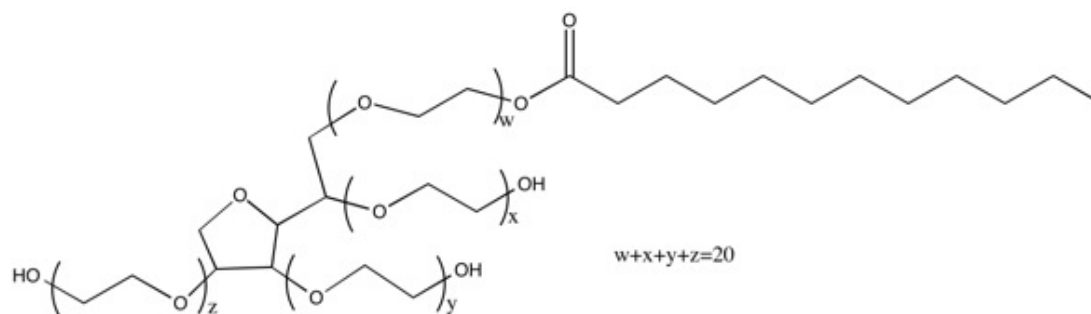


Figure 5.2a: Structure of polysorbate 20. Ester bond is a possible target for hydrolysis by lipases.

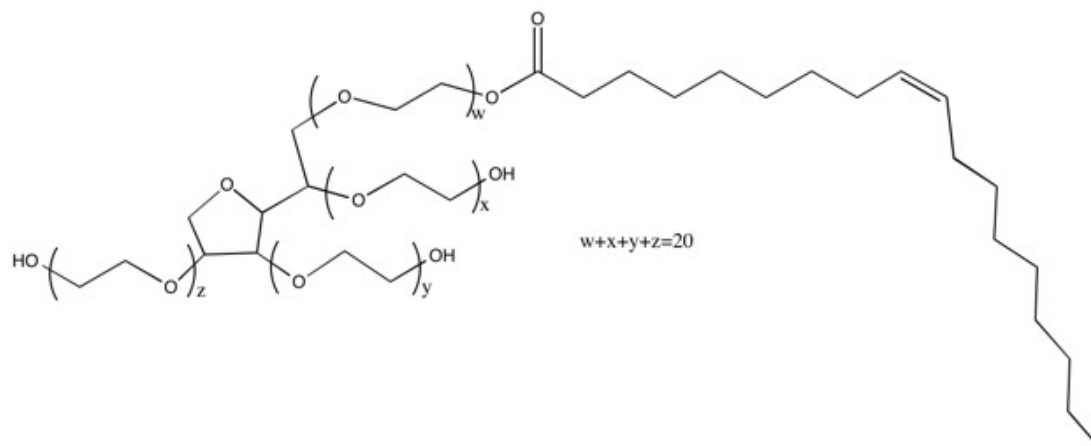


Figure 5.2b: Structure of polysorbate 80. Ester bond is a possible target for hydrolysis by lipases.

### 5.3 LPL Production

CHO LPL was expressed in *E. coli*, purified and refolded according to methods outlined in Section 2.14. Bacterial expression was used to produce large amounts of LPL rapidly.

#### 5.3.1 Expression in *E. coli*

As described in Section 2.14.1, an LPL-containing pET11a plasmid was transformed into BL21-competent cells in SOC broth and plated on ampicillin. Colonies were selected and cultures were grown overnight to seed the production culture.

To confirm LPL protein expression, two cultures were run in autoclaved 25 mg/mL LB broth with 100  $\mu$ g/mL ampicillin at 37 °C. The cultures were run with and without isopropyl  $\beta$ -D-1-thiogalactopyranoside (IPTG) induction. Cells were then pelleted, redissolved in PBS and heated to 100 °C after the addition of SDS loading buffer. The material was loaded and run on a 10% SDS PAGE gel to confirm the

expression of CHO LPL. The silver-stained gel is shown in Figure 5.3. The culture with IPTG induction has a band not present in the non-induced culture at slightly greater than 50 kDa, which is consistent with LPL.

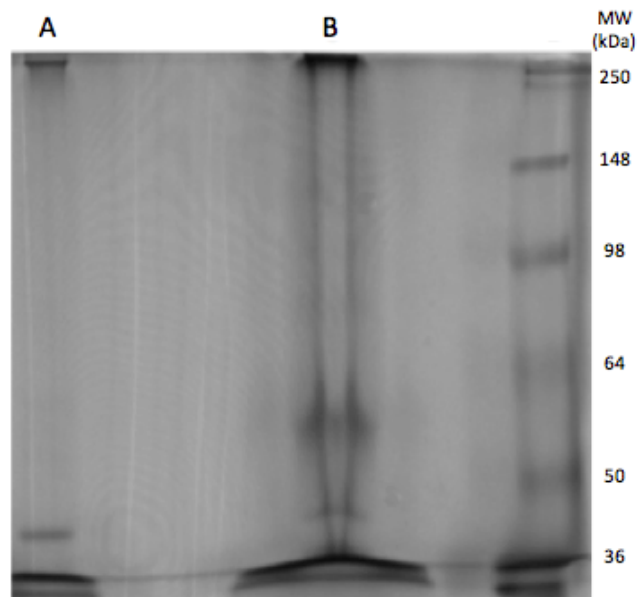


Figure 5.3: Silver-stained reducing SDS-PAGE of non-induced (A) and induced (B) LPL-producing *E. coli* cell cultures.

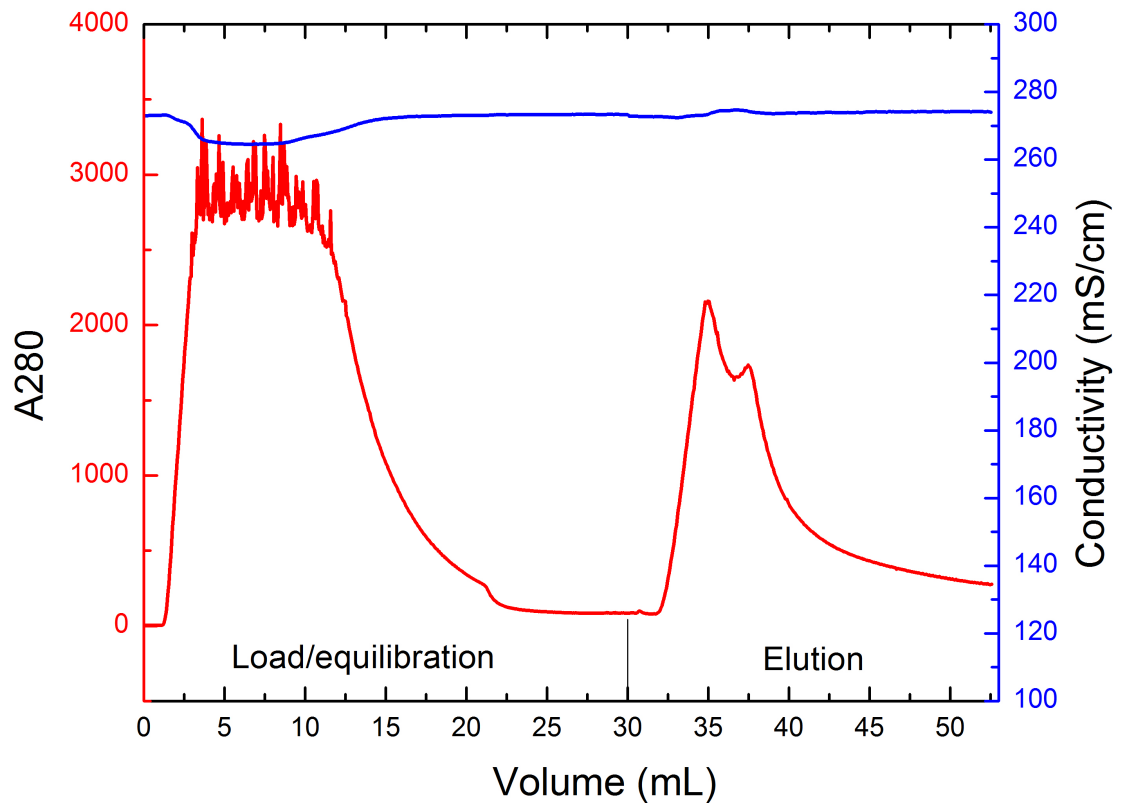


Figure 5.4: Ni-NTA affinity purification of recombinant CHO LPL with 250 mM imidazole step elution.

### 5.3.2 CHO LPL Purification

After confirmation of LPL expression (Figure 5.3), Ni-NTA affinity purification of LPL was completed as described in Section 2.14.2. A 750 mL cell culture harvest was homogenized and LPL inclusion bodies were resolubilized in 6 M guanidine HCl. The resulting chromatogram of Ni-NTA affinity purification is shown in Figure 5.4. The large A280 signal during loading is due to *E. coli* HCP impurities, cell debris and cell culture media additives flowing through the column. The step elution using 250 mM imidazole results in a large peak of eluting LPL with a

pronounced tail. Throughout the Ni-NTA purification the mobile phase was maintained at 6 M guanidine HCl.

SDS-PAGE was used to assess the purity of the Ni-NTA LPL elution pool. Samples were buffer-exchanged into PBS prior to loading the gel. The silver-stained reducing gel is shown in Figure 5.5a. This gel indicates a single band in both lanes A and B at approximately 50 kDa. The elution pool (lane B) contains no detectable impurities. The flow-through pool has a diffuse band at the same molecular weight as the band in the eluate. A western blot was run to confirm the presence of His-tagged LPL and is shown in Figure 5.5b. A mouse monoclonal anti-His tag antibody (G020, ABM, Richmond, BC, Canada) was used to detect His-tagged LPL. The anti-His western confirms that the ~50 kDa bands in the Ni-NTA flow-through and elution have a His-tag. The presence of LPL in the Ni-NTA flow-through is likely due to overloading the column. CHO LPL concentration was then determined using a Micro BCA™ assay (Thermo Scientific, Rockford, IL).

After confirming purification, LPL refolding was carried out as described in Section 2.14.3. Various refold procedures were attempted unsuccessfully. On-column refolding was attempted first. A linear gradient from 6 to 0 M guanidine HCl was run after loading solubilized inclusion bodies onto the Ni-NTA column. The gradient was followed by step elution with imidazole. The attempted on-column refold resulted in insoluble CHO LPL after elution. Rapid dilution at room temperature into 20 mM MES, pH 6.5 buffer also resulted in instantaneous precipitation. Gradual dilution using dialysis was also attempted. The guanidine HCl concentration was decreased in a stepwise fashion to 0 M at pH 6.5 and pH 8.5 at both room temperature and at 5 °C. In all cases the LPL precipitated. The rapid dilution with gentle stirring method described

in Section 2.14.3 was the most successful and resulted in only limited precipitate formation.

To confirm folding, reverse phase (RP)-HPLC was run with unfolded LPL (LPL solubilized in 6 M guanidine HCl) and refolded LPL. The LPL was injected into the C<sub>18</sub> column at 1 mL/min with a linear gradient from 0-100% acetonitrile in water over 45 minutes. The chromatograms are shown in Figure 5.6. The solubilized LPL has two main peaks and many smaller late-eluting peaks. The refolded LPL also has two main peaks. The majority of refolded LPL is contained in the early-eluting peak, likely due to less solvent exposure of the LPL hydrophobic core. The unfolded LPL interacts with the C<sub>18</sub> column with higher affinity, indicating that it has more hydrophobic character than the folded LPL. Unfortunately there is no CHO LPL standard to confirm correct folding. Without a proper standard this result cannot confirm proper LPL folding, but it does provide insight into the changes in LPL due to the refolding procedure. The enzymatic activity that was measured in subsequent sections is further evidence of proper folding of at least a subpopulation of the LPL.

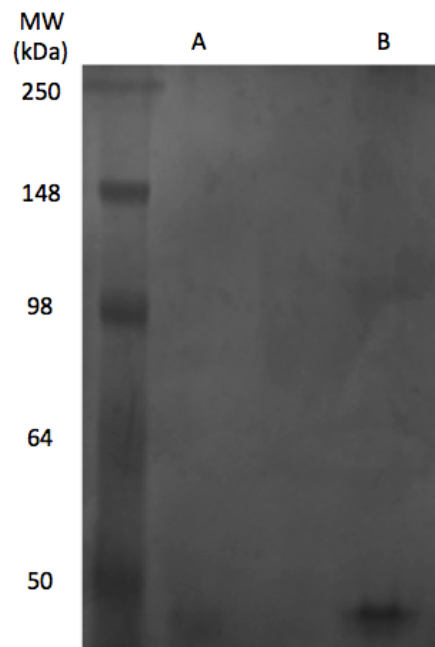


Figure 5.5a: The flow-through fraction (A) and elution fraction (B) of LPL Ni-NTA affinity purification on silver-stained reducing SDS-PAGE.



Figure 5.5b: Anti-His western blot of the LPL Ni-NTA affinity purification flow-through fraction (A) and elution fraction (B).

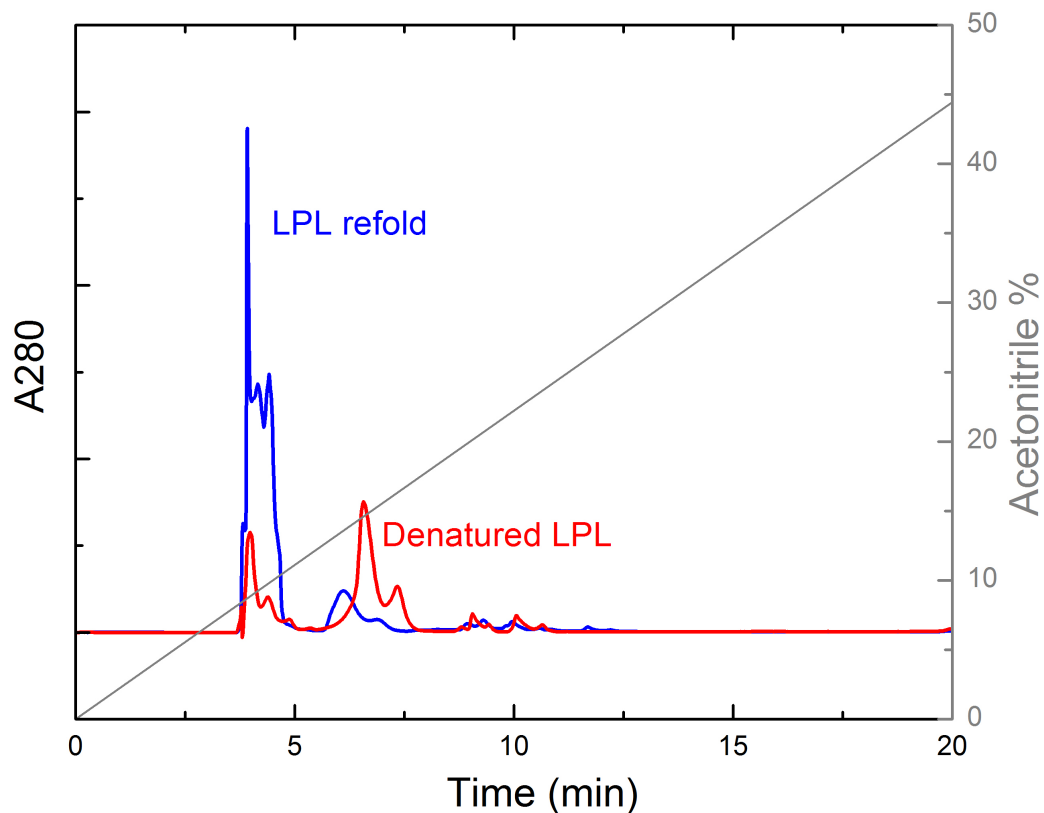


Figure 5.6: RP-HPLC gradient elution (45 min 0-100% acetonitrile linear gradient, C<sub>18</sub> column, 1 mL/min) of refolded LPL (blue) and LPL solubilized in 6 M guanidine HCl (red).

#### 5.4 Characterization of LPL Interaction with MAbs

The results in Chapter 3 indicate that CHO LPL associates with mAbs D, D<sub>M</sub> and IDEC-152 in protein A affinity purification. The LPL-mAb association was determined using mAb-HCP CIC and indicates the potential purification challenge of LPL in mAb processing. To understand better the mAb-LPL interaction, further studies were completed here.

#### 5.4.1 LPL-MAb CIC

Cross-interaction chromatography with immobilized mAb and free LPL (produced in *E. coli*) was used to measure the mAb-LPL osmotic second virial cross-coefficient ( $B_{23}$ ). The bacterially expressed LPL is identical in primary sequence to the native CHO protein, but the refolded protein may not have identical folding and is not glycosylated. MAb-LPL  $B_{23}$  values are shown in Figure 5.7. At protein A loading conditions (pH 7.4) with different concentrations of NaCl,  $B_{23}$  values for mAb C and mAb D with LPL are slightly positive. The non-attractive interactions found here do not agree with the previous results in Chapter 3.

There are a few possible explanations for the lack of attraction. This observation is most likely due to the lack of glycosylation or non-native folding. It is common for protein-protein interactions to be conformationally dependent (Eigenbrot et al., 2010; Sasamori et al., 2010; Zou et al., 2010). Additionally, the lack of glycosylation can change protein structure, stability and interactions (Jefferis et al., 1998). However, as is shown in subsequent sections, the refolded LPL used here does have enzymatic activity, which is evidence of at least appreciably correct folding. Another possibility is that only a small fraction of LPL is correctly folded and it remains irreversibly bound to the immobilized mAb in CIC experiments.

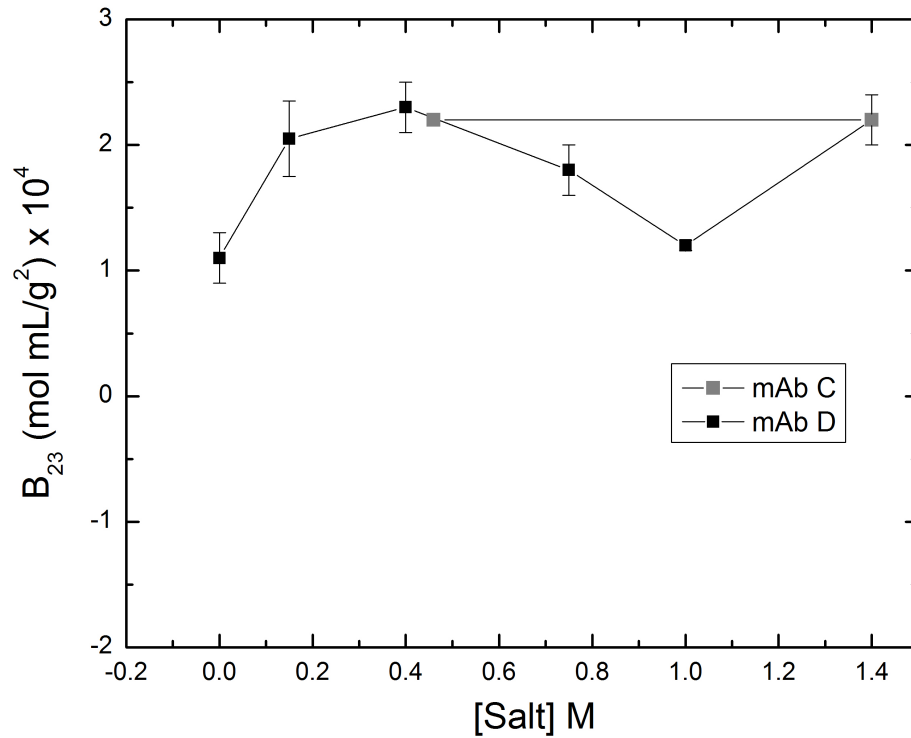


Figure 5.7: LPL-mAb osmotic second virial cross-coefficient ( $B_{23}$ ) at pH 7.4 as a function of sodium chloride concentration.

#### 5.4.2 LPL-MAb Yeast Surface Display

Yeast surface display (YSD) methods (Boder and Wittrup, 1997; Chao et al., 2006) were used as a second method to measure mAb-LPL interactions. Kyle Doolan (University of Delaware, Department of Chemical and Biomolecular Engineering) performed all YSD experiments described here using previously-established methods (Doolan and Colby, 2014). For this analysis, CHO LPL was fused to Aga2p and expressed in yeast cells, as described in Section 2.15. Yeast cells expressing LPL on their surface were then incubated for 45 minutes with fluorescently labeled mAb B, C, D,  $D_M$  or IDEC-152 in PBS with 10% BSA. The yeast cells were then washed and

analyzed using flow cytometry. Yeast cells expressing a non-immune scFv were also incubated with labeled mAb as a control.

LPL-mAb binding was measured in the presence of 500 nM of a fluorescently labeled mAb (Figure 5.8). MAbs B, C, D, D<sub>M</sub> and IDEC-152 were all found to have measurable attraction to LPL. However, the c-Myc tag on the c-terminal end of LPL on the yeast surface could not be detected. This could be due to a truncation of LPL or the c-Myc tag could be sterically hindered by LPL. Sequencing confirmed that there is not a genetic truncation. Non-specific binding to the nonimmune scFv control was minimal. MAbs D, D<sub>M</sub> and IDEC-152 were found in Chapter 3 to associate with LPL using HCP-mAb CIC analysis. The additional mAbs were not analyzed using HCP-mAb CIC.

Additionally, the Fc and Fab fragments of mAb B were analyzed here to determine domain specificity. Both Fc and Fab fragments were found to have attractive interactions to LPL (Figure 5.8); it appears that the Fc fragment has slightly higher affinity. Additional experiments are needed to confirm the higher affinity to the Fc domain but they could not be completed due to a limited fragment supply. It is possible that the papain cleavage of the mAb enables solvent access to attractive epitopes that are not accessible in the native mAb structure. Additional controls were run with peptides A and B (two small peptides that are unrelated to LPL or IgG) and an scFv, which is the antigen-binding domain of a mAb that targets an unrelated protein. These three additional controls indicate that the LPL-mAb binding is specific to mAbs; not all labeled mobile-phase proteins bind to LPL on yeast surface.

Table 5.1: Candidate protein A wash solutions adapted from previous work (Shukla and Hinckley, 2008).

Wash number	pH	Wash contents
1	4.4	50 mM citrate, 1% polysorbate 80
2	4.4	50 mM citrate, 1 M urea
3	9.0	25 mM tris, 10% isopropyl alcohol, 3 M urea
4	9.0	25 mM tris, 1% polysorbate 80, 10% isopropyl alcohol, 3 M urea

Wash solutions 1-4, specified in Table 5.1, were also studied here to determine their effect on mAb-LPL association. The four wash solutions were previously found to disrupt HCP-mAb associations while maintaining high mAb yield (Shukla and Hinckley, 2008). Yeast cells expressing LPL were incubated with fluorescently labeled mAb D as done previously. After flow cytometry to confirm mAb D-LPL binding, the cells were incubated in each of the four wash solutions. After an hour of incubation, flow cytometry was again used to measure the extent of mAb D-LPL binding. All 4 candidate washes were shown to be ineffective at removing the bound mAb. This further demonstrates the considerable difficulties with LPL removal.

In Figure 5.9 a full titration curve is presented for mAb D interacting with LPL, which allows a  $K_D$  for LPL-mAb binding to be estimated. The titration data were fit to a single binding-site model with no depletion, as described previously (Chao et al., 2006). In this case, the LPL-mAb D interaction has a  $K_D$  of approximately 400 nM. For comparison, affinities of this magnitude are on the lower end of typical antibody-antigen binding (Karush, 1978).

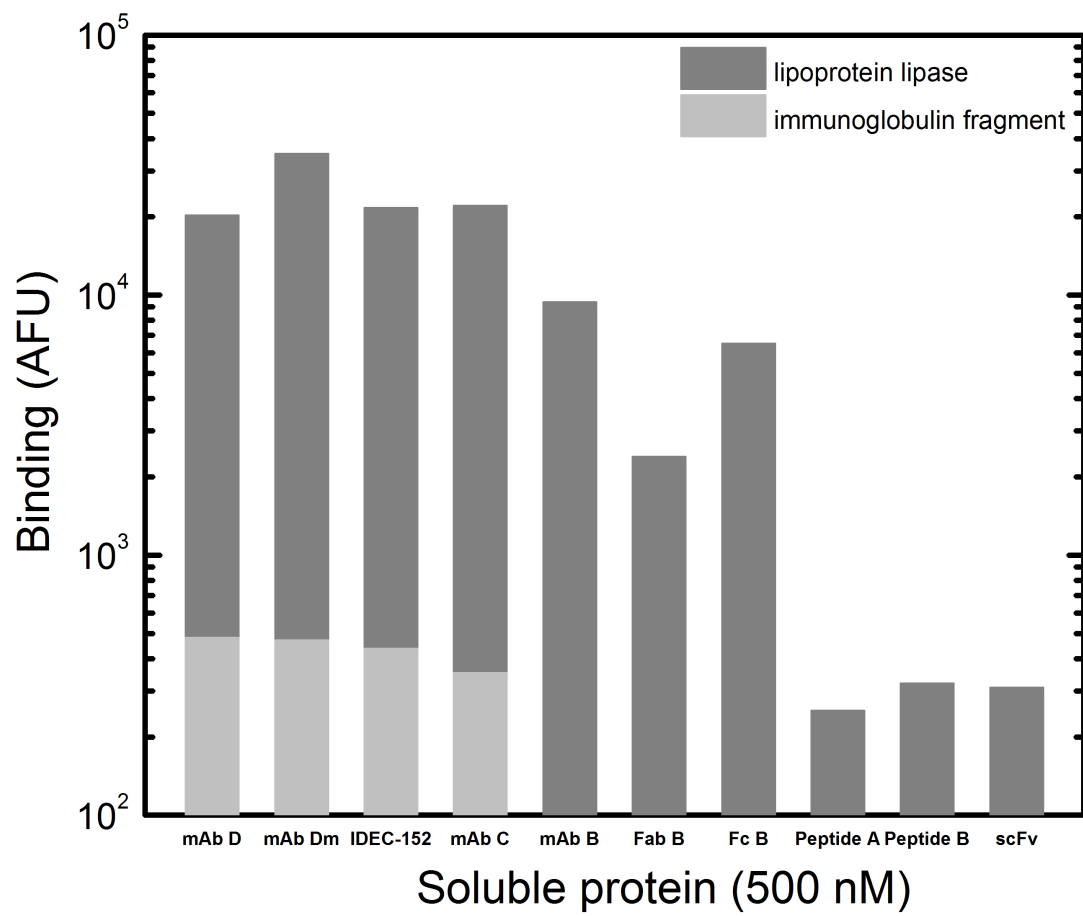


Figure 5.8: LPL-mAb binding measured using YSD of CHO LPL for 4 mAbs in PBS with a concentration of 500 nM mAb.

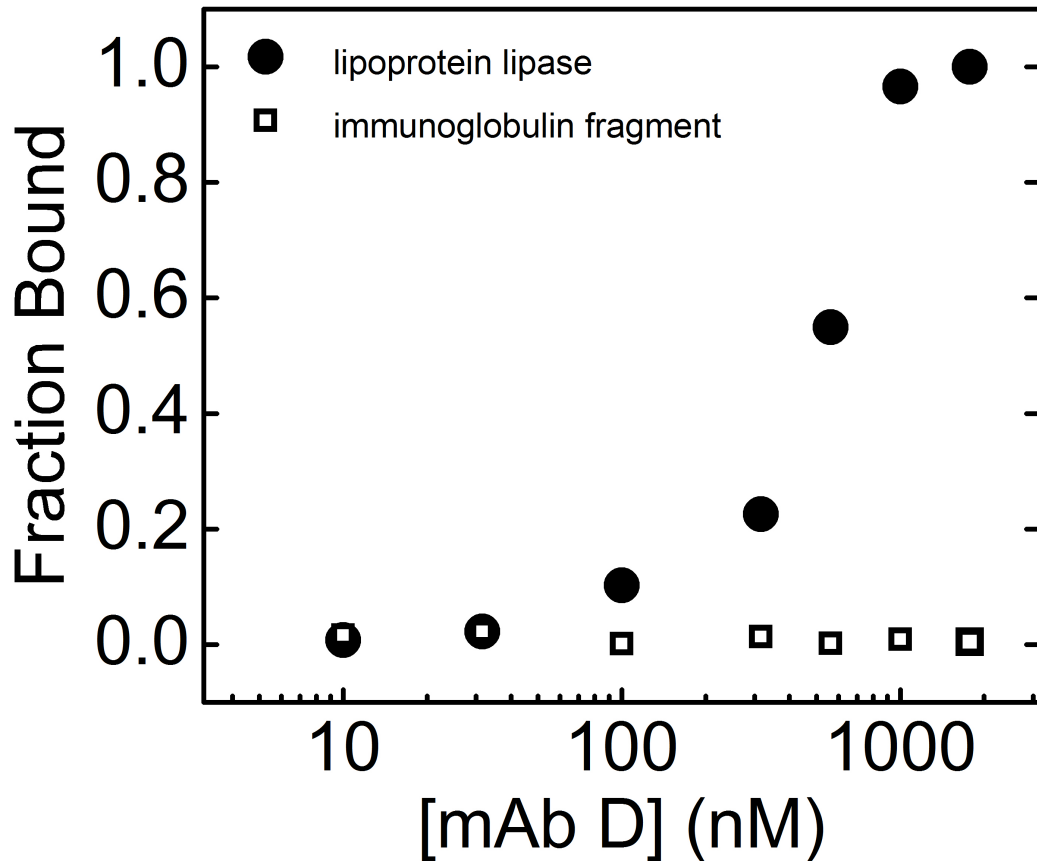


Figure 5.9: Titration of CHO LPL expressed on the yeast surface with mAb D to measure equilibrium binding constant  $K_D$ .

The LPL YSD results are consistent with the LPL-mAb association that was identified using HCP-mAb CIC. There are a few possible reasons that mAb-LPL interactions are detectable by YSD but not by mAb-LPL CIC. One possibility mentioned above is that glycosylation is important for this interaction. YSD will produce glycosylated LPL, but glycosylation structures will be different from those produced in mammalian host cells (Gai and Wittrop, 2007). Another possibility is that LPL folding is closer to the native structure on the yeast surface than in the recombinant LPL refold pool. The folding quality of LPL on the yeast surface is

unknown; enzymatic activity of surface-anchored LPL was not measured to confirm proper folding.

### 5.5 Enzymatic Activity of CHO LPL Expressed in *E. coli*

As discussed previously, polysorbates are frequent additives for maintaining mAb product quality and there is evidence that lipases have enzymatic activity against polysorbates (Christiansen et al., 2010). In this work, the CHO LPL produced in *E. coli* is tested for degradation of polysorbates.

Refolded LPL was buffer-exchanged into the buffer of interest, followed by the addition of 0.23 mM polysorbate 20 or 80 and then incubation at 37 °C for 24 hours. Polysorbate degradation was determined by measuring the concentration of released fatty acid using two methods described in Section 2.16. For the ADAM labeling-HPLC assay described in Section 2.16, a sample chromatogram comparing degraded and non-degraded polysorbate 80 is shown in Figure 5.10. The ADAM-labeled polysorbate degradation product has a characteristic peak at 7 minutes. Activity was measured at pH 5.0, 6.0 and 6.8 in the presence of either NaCl, CaCl<sub>2</sub> or no additional salt. These conditions were chosen as they are similar to FDA-approved mAb formulation conditions (Daugherty and Mrsny, 2006; Wang et al., 2006) and Ca<sup>2+</sup> was previously found to promote the formation of active LPL dimers (Kobayashi et al., 2002).

The experimentally measured degradation rates of polysorbate 80 are shown in Figure 5.11. Overall, there is measurable polysorbate 80 degradation in almost all of the conditions tested. Although these degradation rates were measured at an unrealistically high temperature for mAb storage, it is helpful to put the measured rates into context. For example, in a formulation containing 10 ppm LPL (0.2 μM

LPL), a degradation rate of 0.1  $\mu\text{M}$  polysorbate/ $\mu\text{M}$  LPL/hr translates to a polysorbate degradation of approximately 200  $\mu\text{M}$  per year. Polysorbate concentrations in mAb formulations are generally 0.1-1  $\mu\text{M}$  (Kishore et al., 2011). Degradation rates were found to increase with increasing pH, consistent with prior work on lipase catalysis that showed maximum rates at higher pH (Pereira et al., 2003; Shirai et al., 1983). The addition of the two salts has a minimal effect, contrary to previous findings (Kobayashi et al., 2002). The most extensive degradation was found at pH 6.8 with 10 mM  $\text{CaCl}_2$ , but similar rates were found with NaCl and no additional salt, so neither salt appears necessary for active LPL against polysorbate 80. The degradation rates measured here were similar to previous findings with pancreatin (Christiansen et al., 2010).

LPL degradation rates of polysorbate 20 are shown in Figure 5.12 for the same conditions as for polysorbate 80. Overall, LPL activity is much lower using polysorbate 20, which is less frequently added to formulations, but still commonly used (Daugherty and Mrsny, 2006; Wang et al., 2006). In contrast to the polysorbate 80 degradation results, most of the conditions with measurable degradation were at pH 5.0; polysorbate 20 at pH 6.8 with 10 mM  $\text{CaCl}_2$  was the only other condition where degradation was detected. Polysorbate 20 degradation rates at pH 5.0 increase significantly upon the addition of either NaCl or  $\text{CaCl}_2$ , consistent with observations in previous work (Kobayashi et al., 2002).

These findings demonstrate the possibility of polysorbate degradation due to CHO LPL presence in final formulations. HCPs with enzymatic activity have previously been observed to result in mAb degradation (Gao et al., 2010; Robert et al., 2009). The measured degradation rates show relative trends among different

conditions, but the implications of the nominal rates in a bioprocessing environment cannot readily be interpreted meaningfully due to a number of significant differences. In particular, the *E. coli*-produced LPL lacks glycosylation and is probably not completely folded. Also, these studies were completed at an elevated temperature. Rates of LPL degradation of polysorbate at typical storage temperatures were not measured.

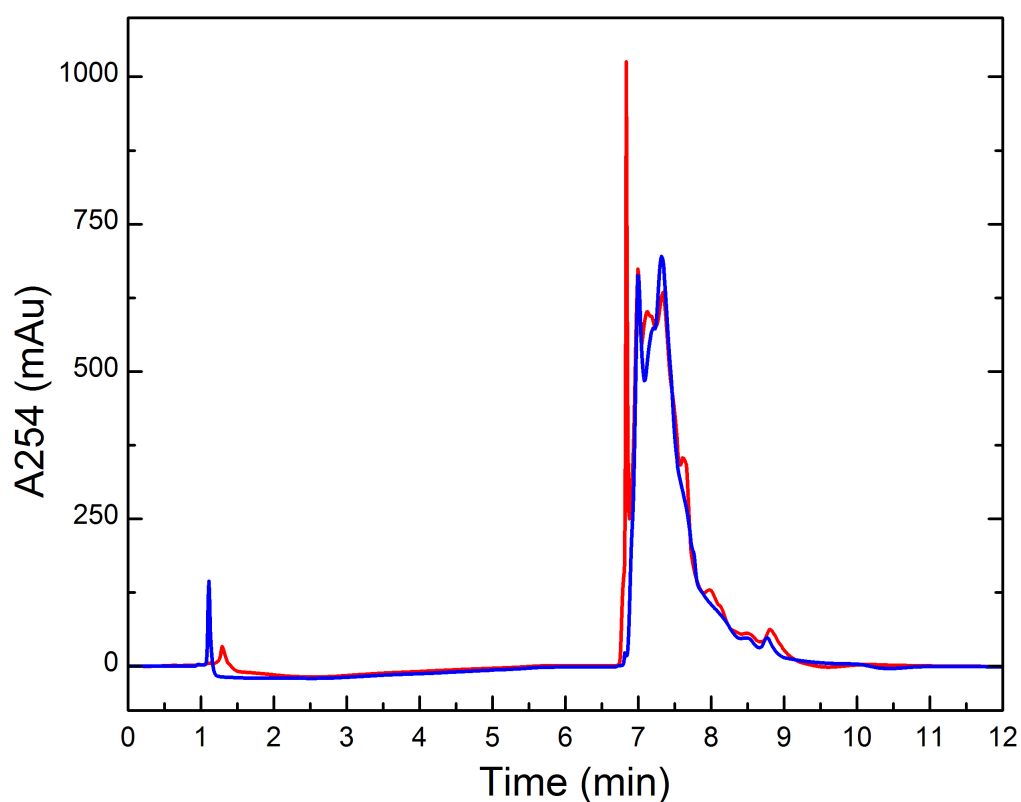


Figure 5.10: Representative chromatogram of ADAM-labeled degraded and non-degraded polysorbate 80.

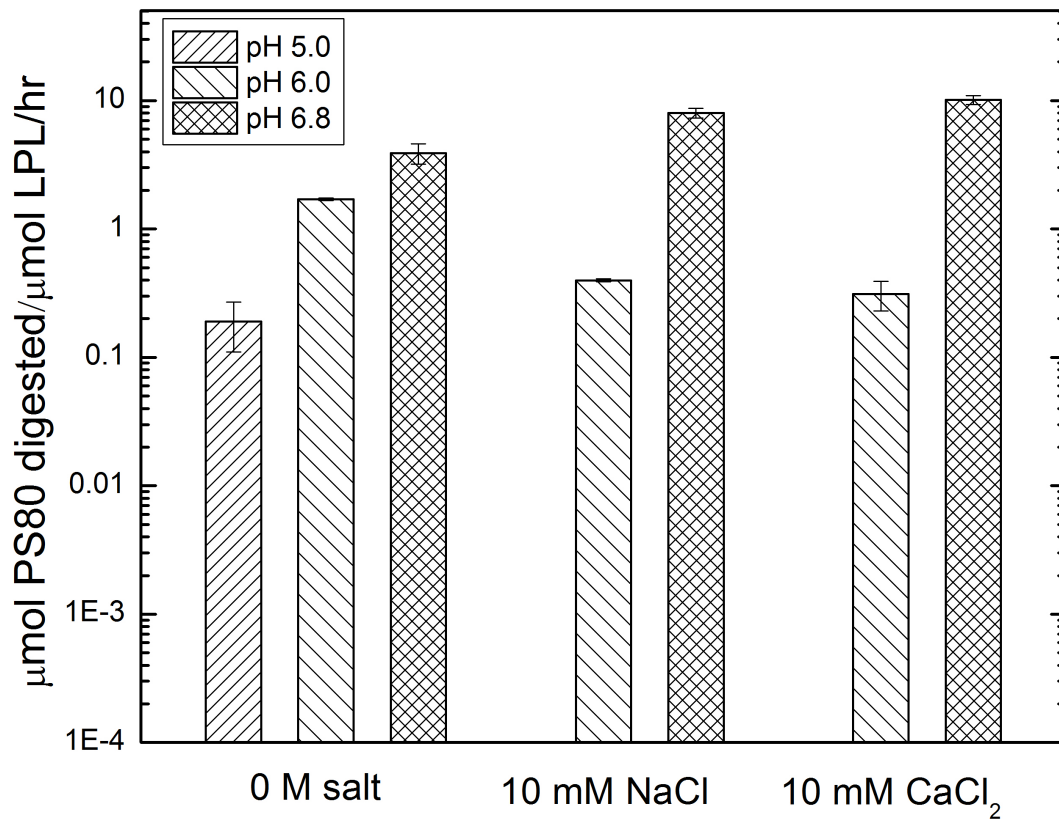


Figure 5.11: Digestion rate of polysorbate 80 by CHO LPL (produced in *E. coli*) in different solution conditions at 37 °C for 24 hours.

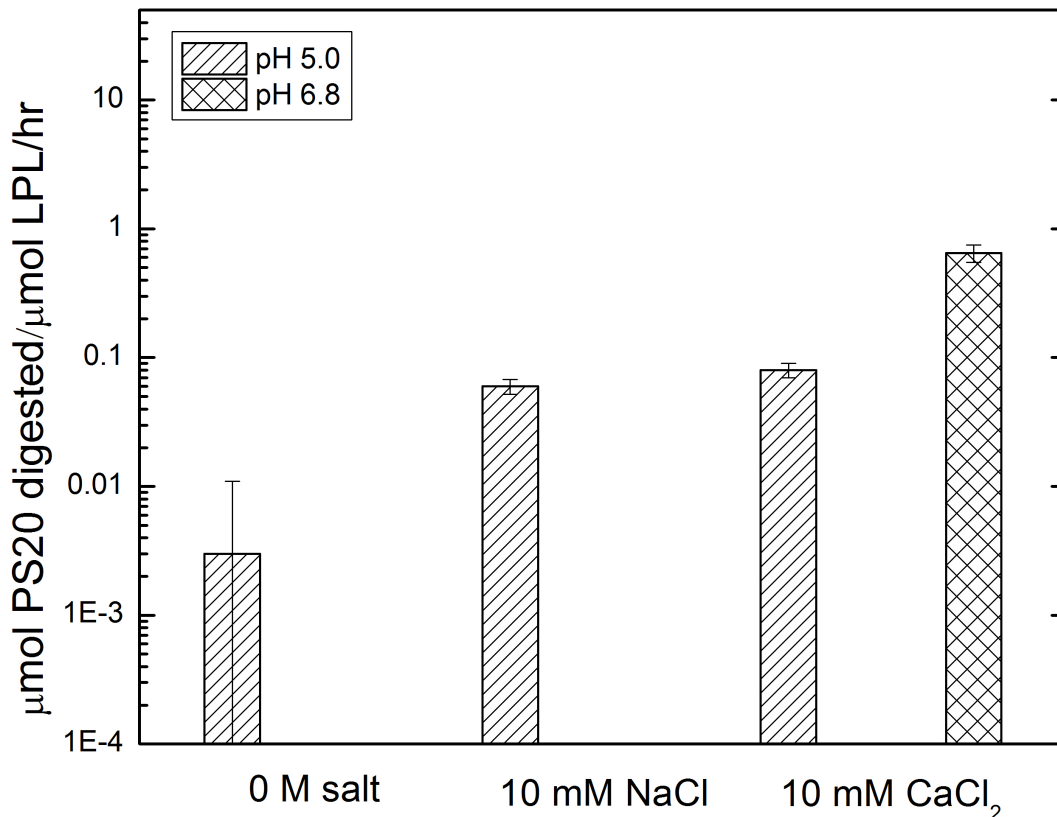


Figure 5.12: Digestion rate of polysorbate 20 by CHO LPL (produced in *E. coli*) in different solution conditions at 37 °C for 24 hours. No measurable digestion was found at pH 6.0.

## 5.6 Native CHO LPL Activity

In order to confirm enzymatic activity of native CHO LPL against polysorbates, a ‘knock-down’ CHO cell culture was prepared by Kristin Valente and Josephine Chiu (University of Delaware, Department of Chemical and Biomolecular Engineering) using previously established RNA interference methods (Hammond and Lee, 2011). The ‘knock-down’ culture is intended to have decreased expression levels of LPL. The supernatant from the ‘knock-down’ cell culture was buffer-exchanged into pH 6.8 with 10 mM CaCl<sub>2</sub> – the conditions with maximum polysorbate

degradation in Section 5.4 – and the null CHO supernatant was prepared identically. The two mixtures of HCP were then added to polysorbate 80 and incubated as done previously. Enzymatic degradation of polysorbate was measured using the free fatty acid detection kit described in Section 2.14. As can be seen in Figure 5.13, the ‘knock-down’ cell line has significantly less fatty acid released compared to the standard null CHO line; increased free fatty acid here is indicative of degraded polysorbate 80. Because the concentration of LPL is unknown in the null CHO line and there are additional HCPs present, it is not possible to calculate a specific enzymatic rate as with the bacterially produced LPL. Nevertheless, these results provide good evidence that the native CHO LPL can digest polysorbate 80, at least in certain conditions. The non-zero enzymatic degradation of polysorbate 80 by the ‘knock-down’ supernatant could be due to additional HCP impurities that also degrade polysorbate or to trace levels of LPL that persist despite the knock-down procedure.

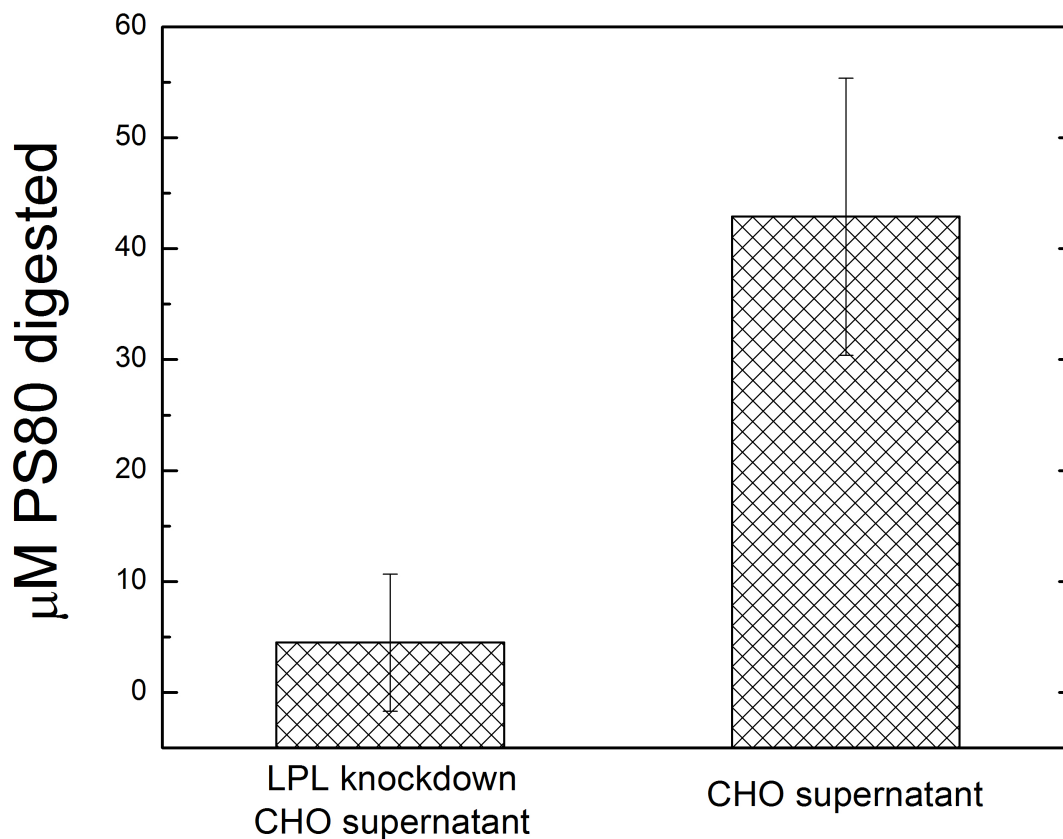


Figure 5.13: Polysorbate 80 degradation after 48 hours of incubation at 37 °C with CHO supernatant and LPL knockdown CHO supernatant.

## 5.7 Conclusions

The results of this chapter provide additional and more specific insights into the difficulties of removing LPL in mAb manufacturing processes and the potential impacts if LPL is not sufficiently removed. The implementation of YSD techniques for measuring LPL-mAb interactions provides an additional method from those previously developed for determining HCP-mAb interactions. It was utilized here specifically for LPL but could be used in future efforts for additional HCP impurities.

CHO LPL binds to a larger set of mAbs than previously shown, with reasonably high affinity ( $K_D \sim 400$  nM). Previously designed wash solutions for disrupting HCP-mAb association were shown to have no measurable effect on LPL-mAb association. This result highlights the difficulty of disrupting certain HCP-mAb interactions. The inability to break up the LPL-mAb association here is strong evidence that a 'knock-out' cell line may be the most efficient method of mitigating LPL purification difficulties. Alternative wash solutions could be developed, but based on these results, LPL-mAb complexes are exceedingly difficult to disrupt.

Finally, polysorbate degradation studies confirm that CHO LPL recombinantly produced in *E. coli* or natively produced by CHO cells can degrade either polysorbate 20 or 80 by ester hydrolysis in mAb formulation conditions. The optimal solution conditions for degradation of polysorbate 80 were consistent with previous findings for lipases (Pereira et al., 2003; Shirai et al., 1983). It was also found that for polysorbate 20, LPL had higher activity at pH 5.0 with either NaCl or CaCl<sub>2</sub> present at 10 mM.

These results demonstrate both the difficulty of removing LPL during mAb purification processes as well as the danger of not removing LPL. Degradation of polysorbate in formulations is a previously identified problem (Kishore et al., 2010) that should be avoided at all costs. At the very least LPL should be monitored through downstream purification and in final formulations; tracking LPL is not overly difficult and could provide insight into otherwise unexplained product degradation.

## Chapter 6

### MONOCLONAL ANTIBODY SELF-INTERACTIONS AND INSTANTANEOUS PHASE BEHAVIOR

#### 6.1 Introduction

Protein phase behavior is involved in numerous aspects of downstream processing, either by design as in crystallization (Smejkal et al., 2013; Trilisky et al., 2011; Zang et al., 2011) or precipitation processes (Capito et al., 2013; Oelmeier et al., 2013) or as an undesired effect, such as formation of large aggregates (Vázquez-Rey and Lang, 2011). Previous work has indicated a correlation between mAb-mAb interaction strength and phenomena such as aggregation and increased viscosity (Connolly et al., 2012; Saito et al., 2011). The present work compares the phase behavior and self-interaction strengths of a large set of mAbs that have been shown to exhibit liquid-liquid separation, aggregation, gelation, and crystallization (Lewus, 2011). The instantaneous phase behavior and self-interaction strengths were studied systematically as a function of a number of factors – including solution composition and pH – in order to explore the degree of variability among different antibodies.

The majority of the solution conditions explored here were adapted from previous work (Lewus, 2011; Lewus et al., 2011) in order to compare directly the phase behavior and interaction characteristics of mAbs with previous results. Most solution conditions were between pH 5.0 and 7.0 with different concentrations of ammonium or lithium sulfate. These are typical conditions for crystallization processes or hydrophobic interaction chromatography – a commonly used aggregate

removal step in mAb downstream processing that was discussed in Chapter 4 (Ghose et al., 2013; Nfor et al., 2011; To and Lenhoff, 2008). The mAbs compared here are all human IgG1 and IgG2 – as described in Chapter 2 – and are unrelated product molecules with the exception of mAbs D and D<sub>M</sub>. Some of the data for IDEC-152, mAb A and mAb B were collected previously (Lewus, 2011; Lewus et al., 2011).

## **6.2 MAb Instantaneous Phase Boundaries**

Instantaneous phase boundaries were identified for the full set of mAbs in different solution conditions. The batch method used for identifying phase boundary locations was described in Section 2.2. Instantaneous phase boundaries of mAbs were compared at pH 5.0 and pH 7.0 and in different concentrations of ammonium and lithium sulfate. Phase boundaries of mAbs D and D<sub>M</sub> were compared across a more extensive set of solution conditions, as discussed in Section 6.6. Instantaneous phase separation did not occur for the majority of mAbs in solutions of sodium chloride.

All mAbs compared here had relatively similar phase boundaries. In sulfate salt solutions it was found that at high salt concentrations – greater than 1.5 M lithium or ammonium sulfate – the solutions instantly phase-separated. As salt concentrations were incrementally decreased, mAbs became stable in solution, but only at low protein concentrations. For all mAbs the range of salt concentrations with experimentally observable phase boundaries was approximately 0.2 M. Identifying the phase boundary at lower salt concentrations was not possible due to the very high protein concentrations required to achieve phase separation. The shape and location of the instantaneous phase boundaries identified here are similar to those previously identified for mAbs (Ahamed et al., 2007; Lewus et al., 2011) and model proteins (Dumetz et al., 2008b).

Figure 6.1 shows the instantaneous phase boundaries for mAbs A-D, D<sub>M</sub>, IDEC-152 and Mill04 at pH 7.0 in solutions containing ammonium sulfate. As described above, the boundaries for each mAb had very similar overall properties, but they were shifted to different salt concentrations. IDEC-152, mAb B and mAb D<sub>M</sub> were all found to have similarly located phase boundaries.

MAb A and Mill04 were identified as outliers at pH 7.0 in ammonium sulfate, with phase boundaries at much lower salt concentrations than those for the other mAbs (Figure 6.1). MAbs C and D had phase boundaries shifted to higher concentrations of ammonium sulfate and appeared to be significantly more stable in solution than the majority of mAbs studied here. As is demonstrated in subsequent sections, this division of the set of mAbs into three groups applies more generally for all solution conditions tested; there is a group of less stable mAbs with phase boundaries at relatively low salt concentrations, a group of highly stable mAbs with phase boundaries at higher salt concentrations, and more typical mAbs with behavior between the two extremes.

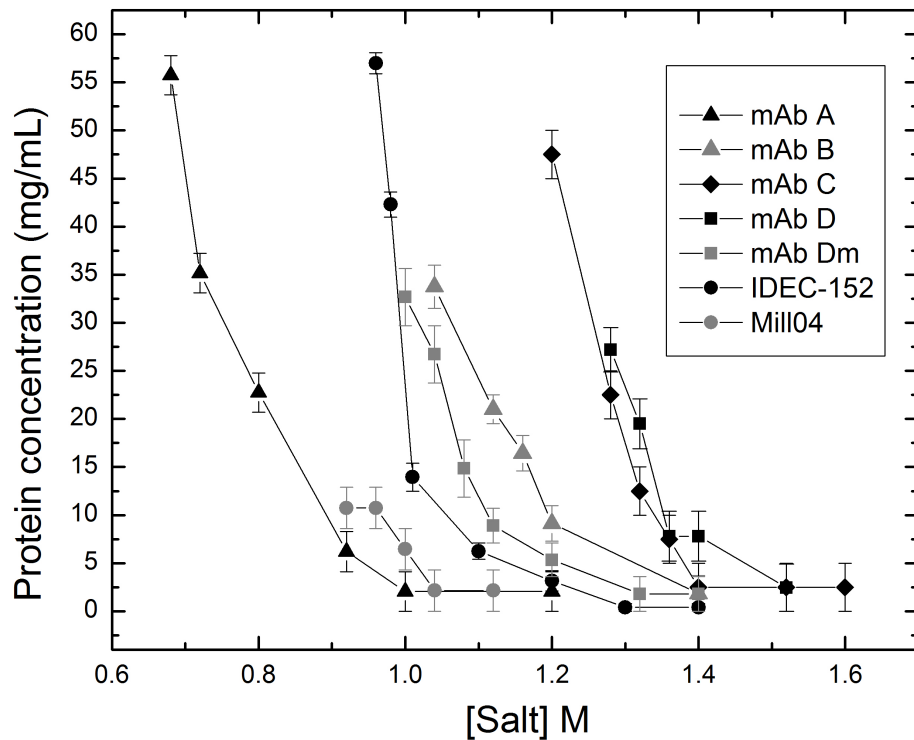


Figure 6.1: Instantaneous phase boundaries of mAbs at pH 7.0 in ammonium sulfate solutions.

### 6.2.1 Instantaneous Phase Boundaries in Different Salts

The instantaneous phase boundaries of the same set of mAbs at pH 7.0 in lithium sulfate (Figure 6.2) had similar properties. The largest difference between the boundaries in ammonium and lithium sulfate at pH 7.0 was a significant shift towards lower salt concentrations in lithium sulfate. This shift is consistent with the Hofmeister series (Collins, 2004; Hofmeister, 1888).

The relative positions of the instantaneous boundaries were maintained in solutions of both sulfate salts, with Mill04 as the single exception. In lithium sulfate solutions, the Mill04 boundary shifted to much lower salt concentrations than for any other mAb studied; it had observable phase separation in 0.4 M lithium sulfate,

compared with 0.7 M ammonium sulfate. Most of the phase boundaries measured were shifted approximately 0.1 M lower when switching from ammonium to lithium sulfate, consistent with the Hofmeister series (Hofmeister, 1888). Additionally, the boundaries were more varied with respect to salt concentration in lithium sulfate solutions. Although there were significant differences in instantaneous phase boundaries with different salt types, the mAbs can still be split into the same three groups described previously.

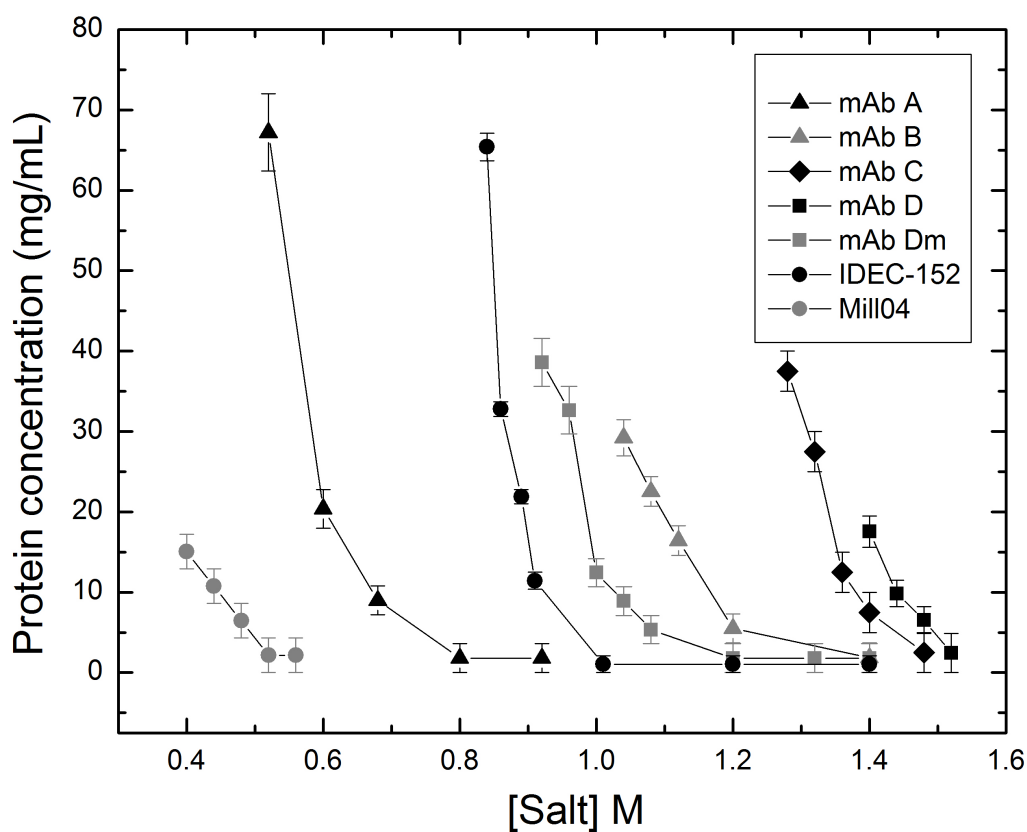


Figure 6.2: Instantaneous phase boundaries of mAbs at pH 7.0 in lithium sulfate solutions.

### 6.2.2 Instantaneous Phase Boundaries: Dependence on Solution pH

Phase boundaries for the majority of mAbs tested were also measured at pH 5.0 in ammonium and lithium sulfate solutions. Comparing Figures 6.1 and 6.3 or 6.2 and 6.4 shows the effect of lowering the pH from 7.0 to 5.0. The phase boundary for each mAb in ammonium sulfate shifted toward higher salt concentrations at lower pH, i.e., all of the mAbs were more stable in solution and less likely to phase-separate at lower pH. This was similar to previous findings of mAb solution stability with varying pH (Arzena et al., 2012; Chari et al., 2009). The set of mAbs shown here, and the majority of IgGs, have isoelectric points between 7.0 and 9.0. Lowering the pH from 7.0 to 5.0 results in a significant increase in net charge and a higher degree of mAb-mAb electrostatic repulsion, which can explain the higher solution stability (Lehermayr et al., 2011).

Each mAb was found to have increased solution stability at lower pH, but when comparing properties of different mAbs, net charge and isoelectric point were not good predictors of phase behavior; at lower salt concentrations these parameters are better indicators of mAb solution stability (Lehermayr et al., 2011). Although the effect of changing pH on net charge is understood, the distribution of charged residues in each mAb may vary significantly from protein to protein. Anisotropy appears to play a significant role and makes *a priori* prediction of pH effects difficult (Scherer et al., 2010; Yearley et al., 2013).

The degree to which phase boundaries shift with pH changes was similar for all mAbs and is similar to previous studies with model proteins (Dumetz et al., 2008a). For mAb A in ammonium sulfate solutions the change from pH 7.0 to 5.0 resulted in the phase boundary shifting from about 0.8 to 1.0 M ammonium sulfate and 0.6 to 0.9 M lithium sulfate. For IDEC-152 the phase boundaries shifted from 1.0 to 1.2 M

ammonium sulfate and 0.9 to 1.1 M lithium sulfate upon the same pH shift. The more stable mAbs also had similar shifts in their instantaneous boundaries: mAb C phase boundaries shifted from 1.3 to 1.4 M in ammonium sulfate solutions and 1.2 to 1.3 M in lithium sulfate solutions.

As was the case for the different salt types, the instantaneous phase boundaries of the mAbs studied here remained in the same order relative to each other with few exceptions as the solution pH was varied. The differences in instantaneous phase boundaries between mAb D and mAb D<sub>M</sub> are of particular interest due to the similarity of the two molecules. These mAbs differ only by 2 amino acids and mAb D was much more stable in high-salt solutions than mAb D<sub>M</sub>. The instantaneous phase boundary for mAb D was at much higher salt concentrations than the boundary for mAb D<sub>M</sub> at both pH 5.0 and 7.0 and in both ammonium and lithium sulfate.

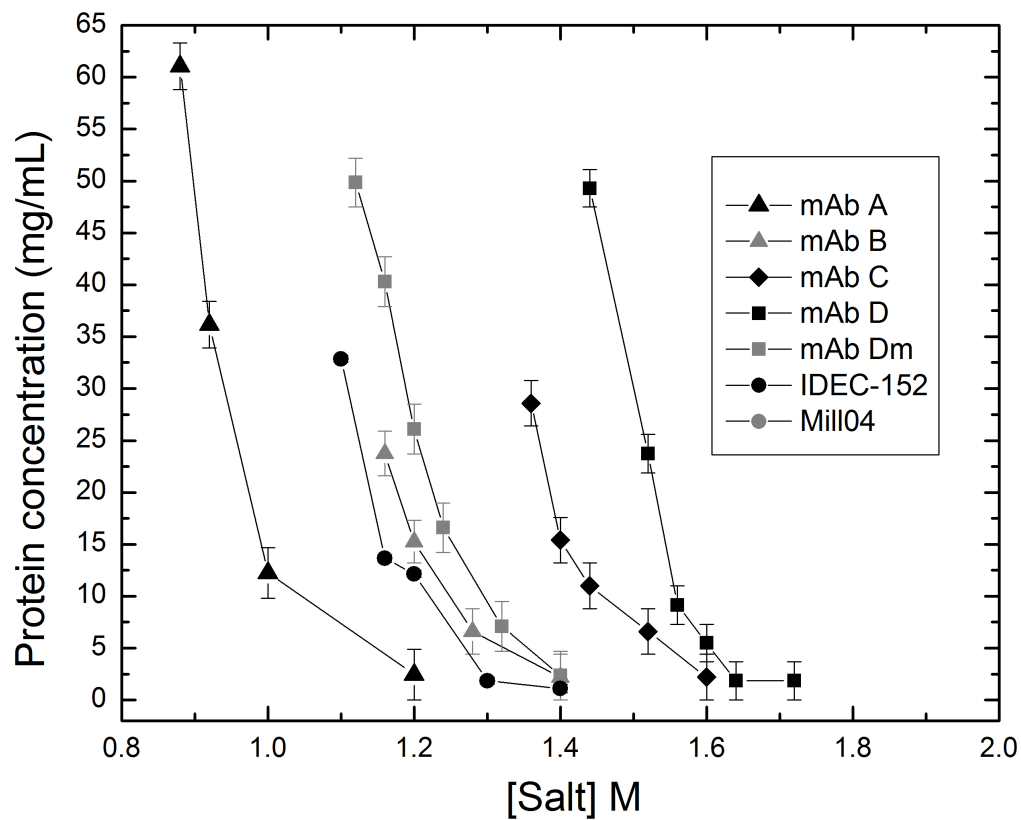


Figure 6.3: Instantaneous phase boundaries of mAbs at pH 5.0 in ammonium sulfate solutions.

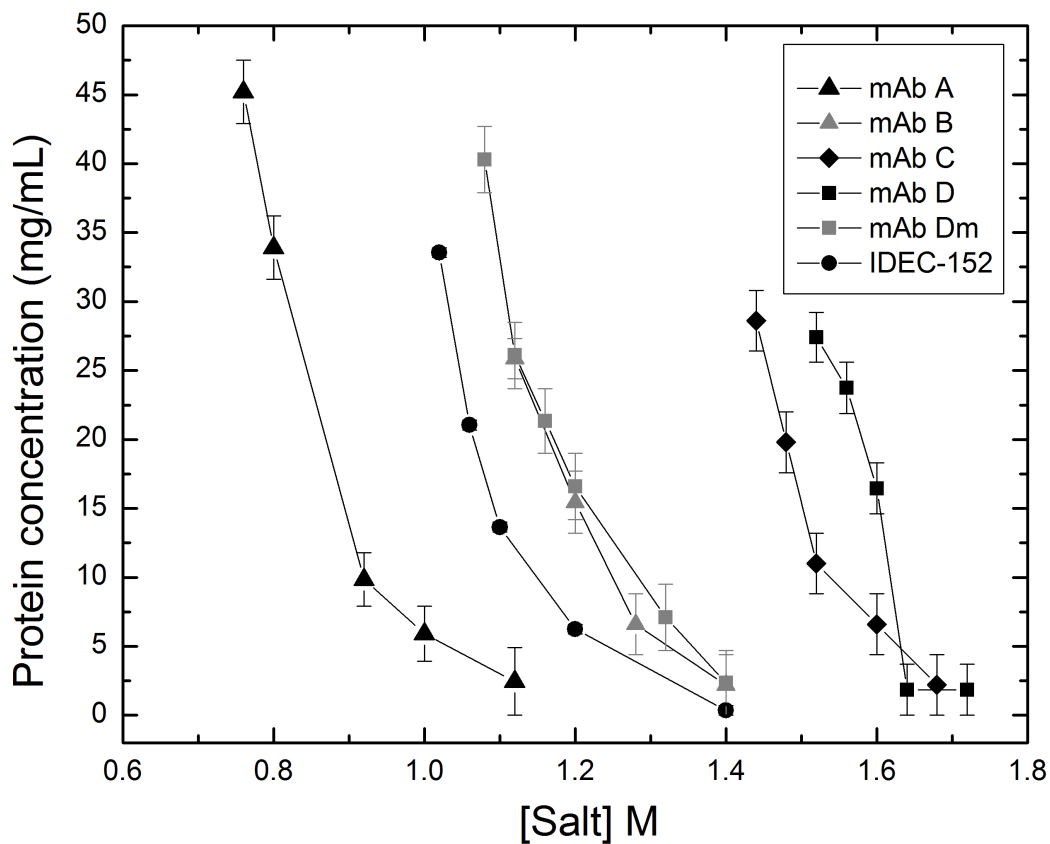


Figure 6.4: Instantaneous phase boundaries of mAbs at pH 5.0 in lithium sulfate solutions.

### 6.3 Co-Precipitation with HCP Product-Associated Impurity

In Chapter 3 the identification of HCP impurities that associate with different mAb products was described. The HCP impurities that associate with mAb molecules and are carried through downstream purification steps into formulations could potentially impact mAb stability or drug safety. Insulin was one of the HCP impurities found to have attractive interactions with the majority of mAbs (Levy et al., 2013). The instantaneous phase boundary of mAb D at pH 7.0 in ammonium sulfate was therefore measured in the presence of insulin to determine if insulin impacts mAb

phase behavior. Attractive cross-interaction strengths between two model proteins was previously shown to lead to co-precipitation (Cheng et al., 2008). Co-precipitation is frequently used to identify interacting proteins in biological systems (Howell et al., 2006).

The same batch method was used to identify phase boundaries here, but a constant concentration of insulin was added to each sample. As can be seen in Figure 6.5, at higher ammonium sulfate concentrations the addition of insulin had no measurable effect on the location of the instantaneous phase boundary. However, at lower salt concentrations – where the boundary starts to increase rapidly in mAb concentration – there was a significant difference in that the presence of insulin lowered the phase boundary by about 5 mg/mL. Identical solutions but with only one of the two proteins (mAb D or insulin) present did not phase-separate.

The experimental conditions used here represent a somewhat unrealistic concentration of insulin with respect to mAb for a typical manufacturing process. However, the results suggest that it would be possible for HCP impurities to have a measurable effect on product stability and possibly result in co-precipitation if they were not removed sufficiently.

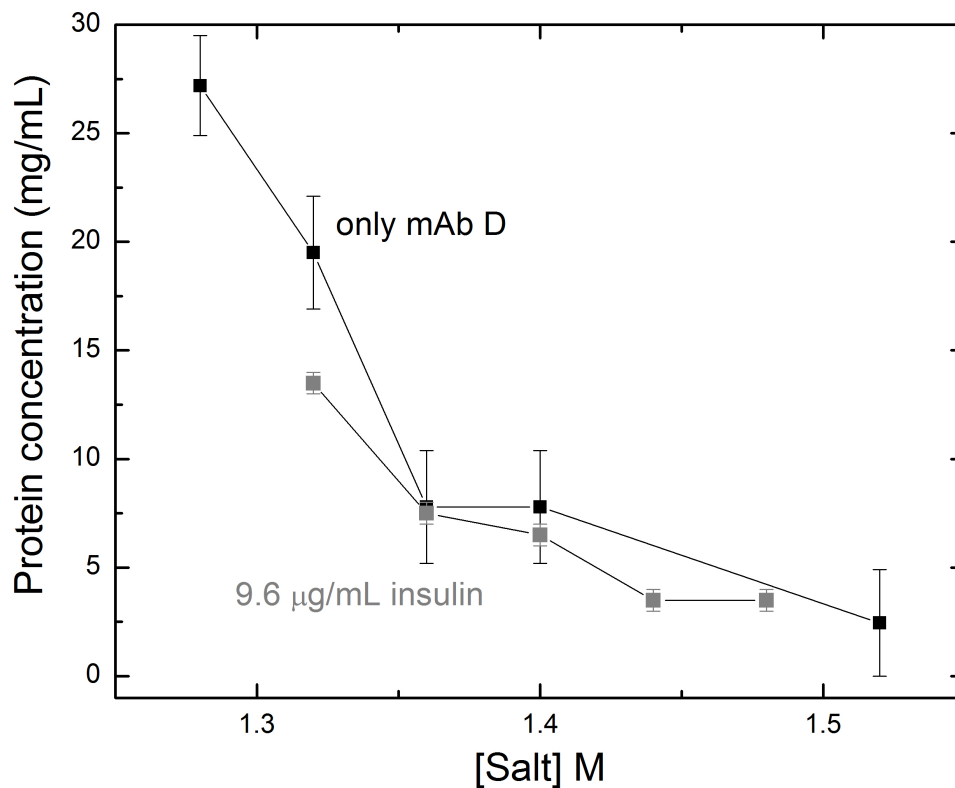


Figure 6.5: Instantaneous phase boundaries of mAb D with and without 9.6 µg/mL of insulin at pH 7.0 in various concentrations of ammonium sulfate.

#### 6.4 MAb Self-Interactions

Self-interactions of IgGs were measured using self-interaction chromatography (SIC) as described in Section 2.8 and similar to previous studies (Dumetz et al., 2008a; Lewus et al., 2011; Tessier et al., 2002a). The interaction strengths are expressed as second osmotic virial coefficients ( $B_{22}$ ). Positive values of  $B_{22}$  represent repulsive interactions, negative values correspond to attractive interactions and values close to zero represent no net attraction or repulsion.  $B_{22}$  values for protein solutions between -1 and  $-8 \times 10^{-4}$  mol mL/g<sup>2</sup> represent the ‘crystallization slot’, the range of moderately

attractive interactions likely to yield crystalline structures for proteins (George and Wilson, 1994).

SIC measurements were made at the same solution conditions used for instantaneous phase behavior experiments. Beyond the crystallization application noted above, self-interaction strength has important implications for mAb product stability, phase behavior, oligomerization and solution viscosity (Connolly et al., 2012; Yadav et al., 2011a; Yadav et al., 2012). This set of results shows the overall similarities from mAb to mAb as well as the behavior of a few outliers.

As was observed for instantaneous phase boundaries, this large set of IgG1 and IgG2 products had mostly similar interaction behavior, as can be seen in Figures 6.6-6.10, which are discussed in greater detail below. The self-interaction strengths for most mAbs at low salt concentration (0-0.2 M) was either slightly attractive or had no significant interactions –  $B_{22}$  values were close to zero. As salt concentrations were increased, the self-interactions gradually became more attractive and entered the ‘crystallization slot’ (George and Wilson, 1994) of moderate attraction. At a critical salt concentration – generally between 0.5 and 0.75 M – mAb-mAb self-interactions became highly attractive much more precipitously. While this form of the  $B_{22}$  dependence on salt was observed quite generally for mAbs, more specific comparisons are informative, and are presented in the subsections below.  $B_{22}$  dependence on salt concentration was similar to previous findings for mAbs (Lewus et al., 2011) and model proteins with salting-out behavior (Dumetz et al., 2008c; Tessier et al., 2002b).

Figure 6.6 shows the  $B_{22}$  values for mAbs at pH 7.0 in increasing concentrations of ammonium sulfate. As described above, each mAb shows an increase in self-attraction with higher ammonium sulfate concentrations. The highest

salt concentration recorded for each mAb was the strongest attraction that could be measured with SIC; at higher salt concentrations the mobile-phase mAb becomes essentially irreversibly bound to the column.

At the conditions in Figure 6.6 it is clear that the interaction behavior is consistent with instantaneous phase boundaries, and the mAbs can be divided into three groups that are similar to those in Section 6.2. Mill04 and mAb A have the strongest self-attraction by a considerable margin. The  $B_{22}$  values of both are somewhat negative at low ammonium sulfate concentrations, and around 0.4-0.5 M ammonium sulfate the slope becomes much steeper, with highly attractive interactions that are difficult to measure. It should be noted that the  $B_{22}$  values presented here were calculated assuming that all mAbs exist as monomers under measurement conditions, but it is shown in Chapter 7 that Mill04 – which shows by far the strongest self-association among the mAbs profiled – exists mostly as larger oligomers.

The next grouping of molecules includes mAb B, mAb C, mAb D<sub>M</sub> and IDEC-152. In ammonium sulfate at pH 7.0 these mAbs have nearly identical  $B_{22}$  trends as a function of salt concentration. With the exception of mAb C, this is the same set of mAbs identified with moderate salting-out behavior in the discussion of phase boundaries. Finally, mAb D is a non-interacting outlier, with highly attractive self-interactions not appearing until around 1.0 M ammonium sulfate.

There is a clear correlation between the location of the instantaneous phase boundary and the self-interaction strength for each mAb. The more highly attractive mAbs had phase boundaries shifted towards lower salt concentrations and the less attractive mAbs were much more stable in solution, requiring higher salt concentrations for phase separation. The correlation between  $B_{22}$  and instantaneous

phase boundaries found here for mAbs is similar to previous finding with globular model proteins (Dumetz et al., 2008b; Haas et al., 1999; Le Brun et al., 2009).

MAb  $B_{22}$  values, as expected, reflect stronger attraction in solutions of lithium sulfate compared to ammonium sulfate. This is consistent with the trends in phase boundaries discussed in Section 6.2 and previous studies of the Hofmeister series (Collins, 2004). For the mAbs with intermediate salting-out properties,  $B_{22}$  starts to become highly attractive at salt concentrations greater than 0.8 M at pH 7.0. In lithium sulfate at pH 7.0 (Figure 6.7), the same group of mAbs have  $B_{22}$  values that drop steeply at concentrations greater than 0.6 M, and  $B_{22}$  was not measurable at 0.8 M. Most of the mAbs have  $B_{22}$  profiles that are shifted between 0.1 and 0.2 M salt when switching from ammonium to lithium sulfate. This is similar to the observed shift in phase boundary location.

In solutions of sodium chloride at pH 7.0 only mAb A has instantaneous phase boundaries that were experimentally accessible. Previous work identified instantaneous phase separation of IDEC-152 in high concentrations of sodium chloride (Ahamed et al., 2007). However, a few mAbs had measurable attraction in sodium chloride solutions. The sodium chloride solutions are more likely to occur in a mAb platform manufacturing setting than ammonium and lithium sulfate solutions.

Mill04, the most self-attractive mAb in sulfate salt solutions, also showed the strongest self-attraction in sodium chloride. It appears that Mill04 displays electrostatic attraction at very low salt concentrations. As sodium chloride concentrations are increased those attractions are screened out and  $B_{22}$  increases slightly. At even higher salt concentrations Mill04 displays salting-out characteristics similar to those observed with sulfate salts, with increasingly attractive self-

interactions. This relationship between sodium chloride concentration and  $B_{22}$  is similar to previous studies with catalase (Dumetz et al., 2008a).

MAb A is the only other mAb studied here found to have strong self-interactions in sodium chloride solutions. The behavior is similar to that of Mill04 and consistent with that observed in ammonium and lithium sulfate solutions. IDEC-152 and mAb B self-interactions, which were measured at much higher salt concentrations, were of moderate strength in sulfate salts, and in sodium chloride they were significantly different from those of mAb A and Mill04. Attractive interactions were observed only at extremely high salt concentrations – between 1.0 and 4.0 M sodium chloride. Even at those high salt concentrations  $B_{22}$  values were only slightly negative. In solutions of sodium chloride, which would be more typical bioprocessing conditions than sulfate salts,  $B_{22}$  measurements indicate that only Mill04 and mAb A have strong self-interactions and thus a greater likelihood of stability, viscosity and oligomerization issues (Connolly et al., 2012; Saito et al., 2011; Vázquez-Rey and Lang, 2011).

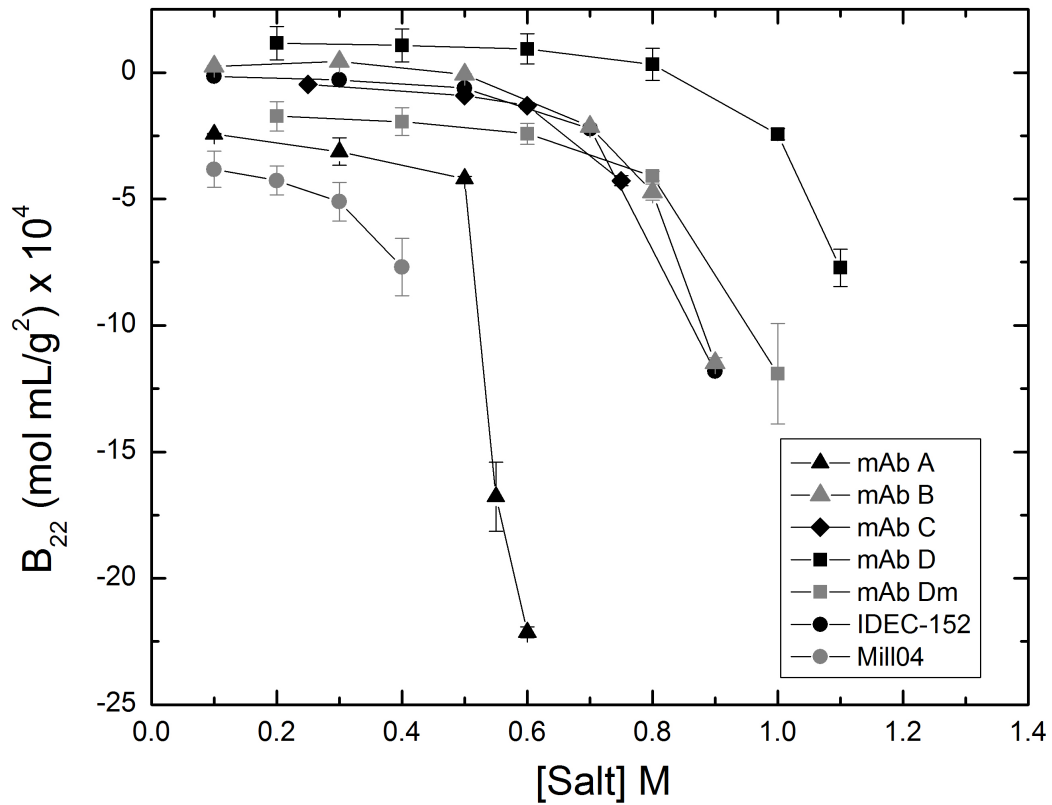


Figure 6.6: Osmotic second virial coefficients of mAbs at pH 7.0 in ammonium sulfate solutions, measured using self-interaction chromatography.

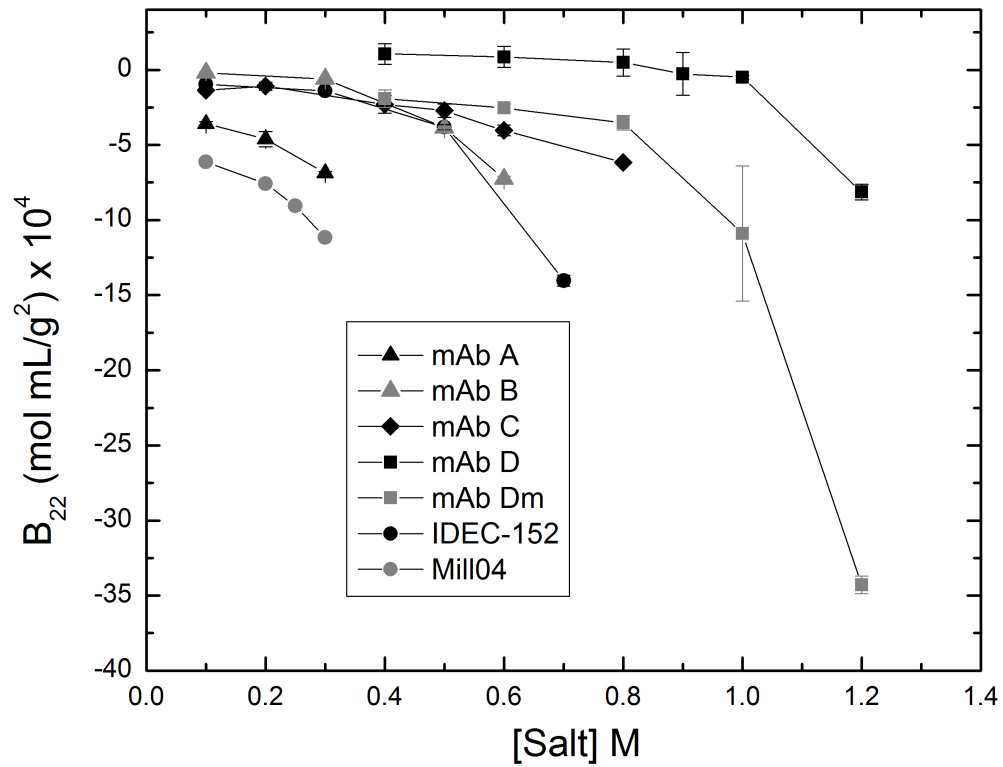


Figure 6.7: Osmotic second virial coefficients of mAbs at pH 7.0 in lithium sulfate solutions, measured using self-interaction chromatography.

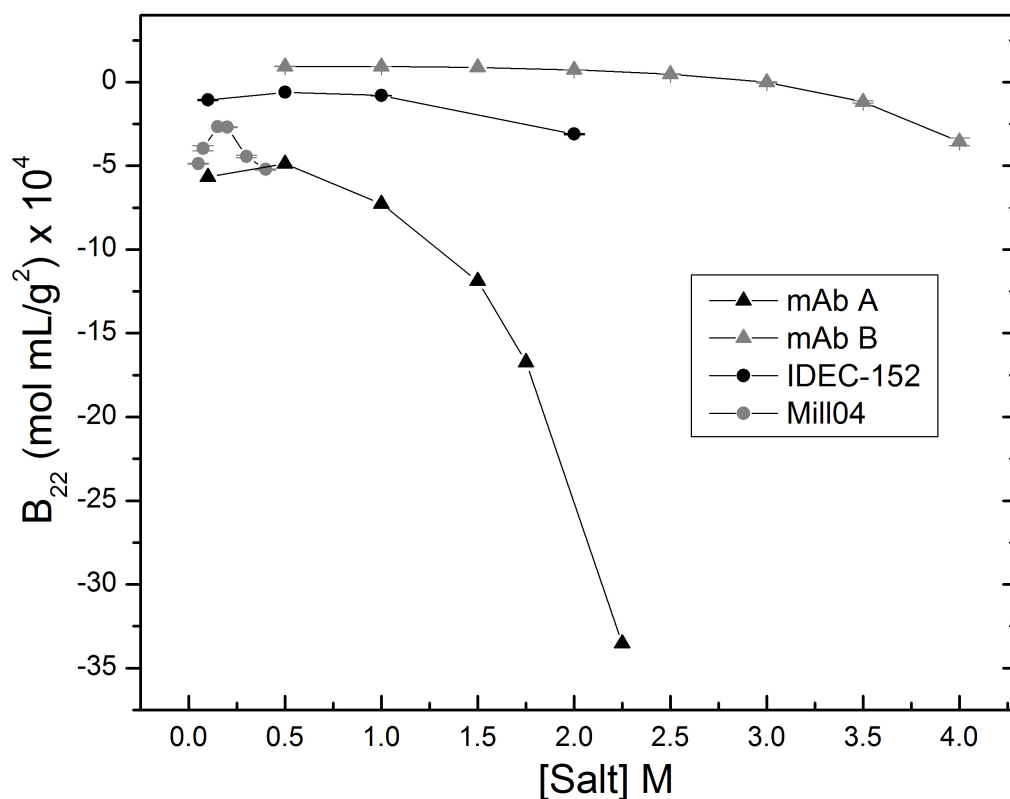


Figure 6.8: Osmotic second virial coefficients of mAbs at pH 7.0 in sodium chloride solutions, measured using self-interaction chromatography.

#### 6.4.1 $B_{22}$ Values as a Function of Solution pH

Figures 6.9 and 6.10 show mAb  $B_{22}$  values in solutions of ammonium and lithium sulfate at pH 5.0. Due to insufficient supplies of materials, not all mAbs were included in these pH studies. At pH 5.0 the mAbs generally did not have highly attractive two-body interactions until sulfate salt concentrations were close to 1.0 M. Such lower self-attraction at lower solution pH is consistent with previous results (Arzena et al., 2012; Saito et al., 2011; Sule et al., 2012). At pH 5.0 the location of the steep drop in  $B_{22}$  for most mAbs is shifted approximately 0.2 M from that at pH 7.0. Also, although a smaller set of mAbs was used at pH 5.0, it appears that there is less

variability from mAb to mAb at the lower pH, with the exception of mAb D. As in the various data sets presented previously, mAb D shows the least attractive protein-protein interactions at all solution conditions examined.

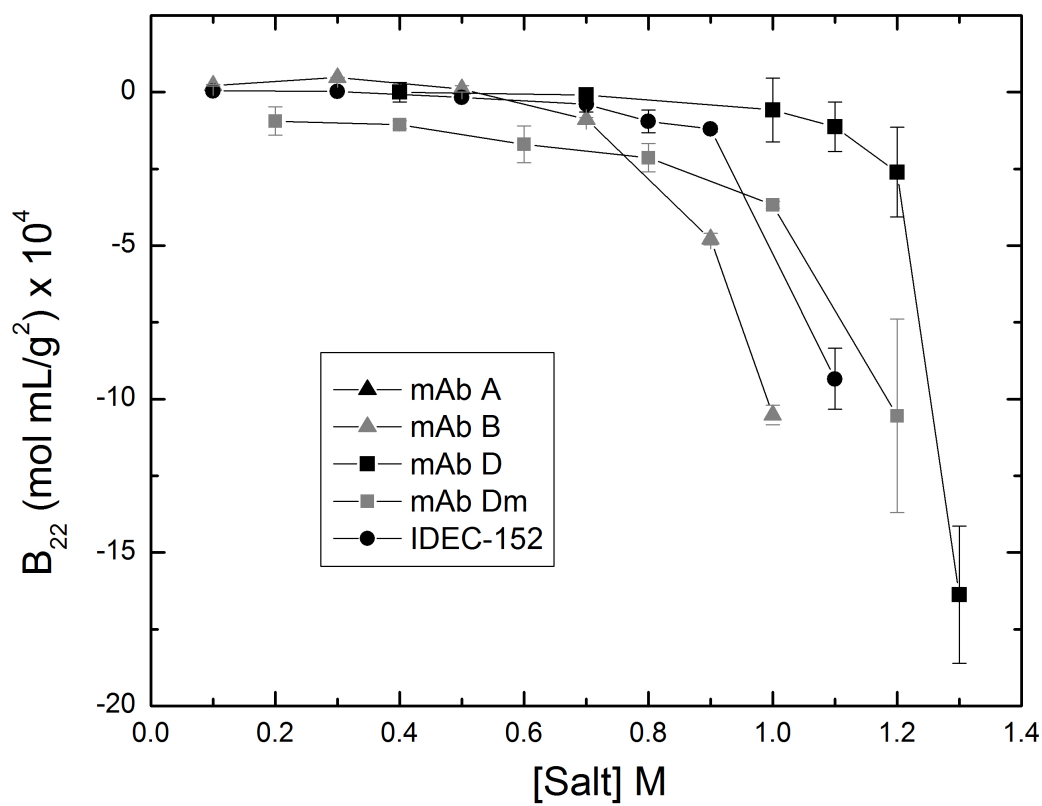


Figure 6.9: Osmotic second virial coefficients of mAbs at pH 5.0 in ammonium sulfate solutions, measured using self-interaction chromatography.

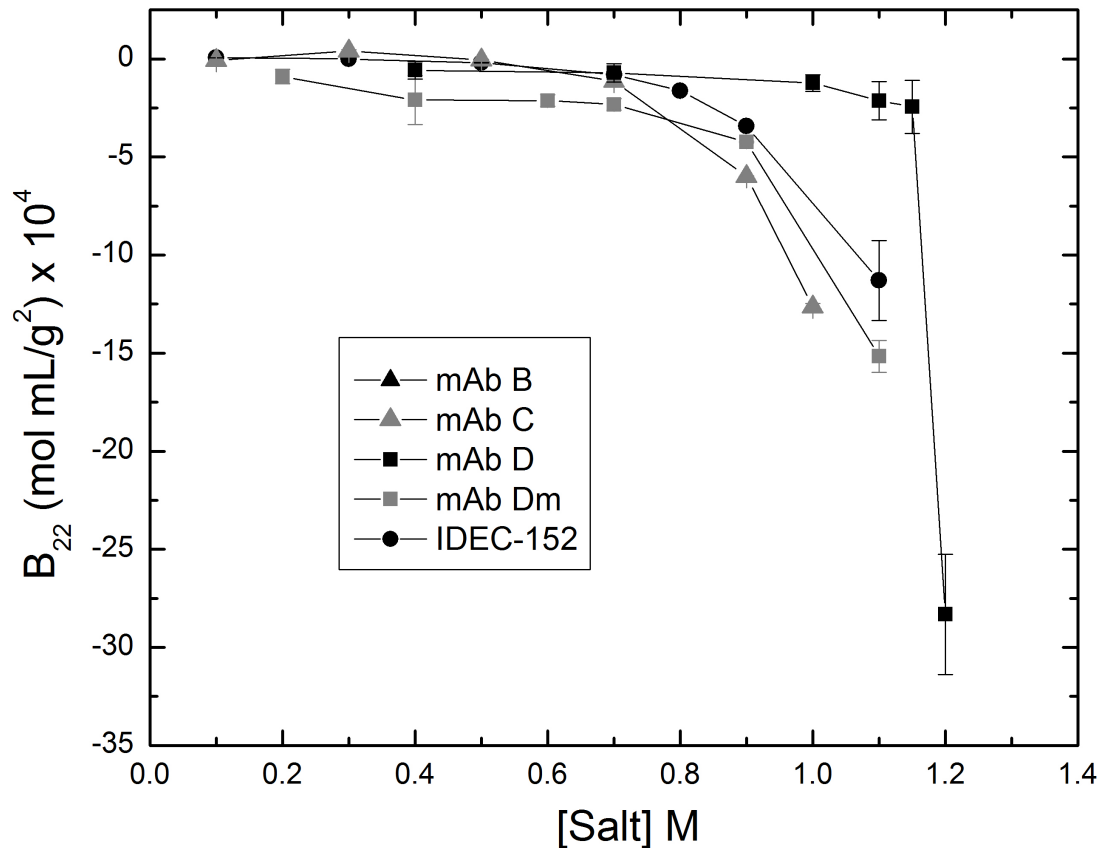


Figure 6.10: Osmotic second virial coefficients of mAbs at pH 5.0 in lithium sulfate solutions, measured using self-interaction chromatography.

### 6.5 ANS Fluorescence

In order to investigate further the driving forces for self-interaction and instantaneous phase separation at the high salt concentrations used here, 8-anilinoanthracene-1-sulfonic acid (ANS) fluorescence was used (Rubin et al., 2012) as a reporter. ANS is a fluorescent molecule with much higher fluorescent signal in non-aqueous environments. In protein solutions, ANS has much higher fluorescence emission when it is bound to hydrophobic residues in partially unfolded protein intermediates (Arosio et al., 2012; Semisotnov et al., 1991). At low salt concentrations

it can also interact with charged amino acids, but at the high salt concentrations of interest, charge-charge interactions are expected to be screened out. Therefore if the conventional interpretation is accurate, ANS fluorescence serves as a probe of hydrophobic interactions.

Results for ANS fluorescence of mAbs B, C, D and D<sub>M</sub> are presented in Figures 6.11-6.14. For all four mAbs, the ANS signal increases monotonically as the ammonium or lithium sulfate concentration is increased from 0 M to 1.7 M. Previous work with salting-out mAbs had similar findings (Rubin et al., 2012). The ANS fluorescence is higher for lithium sulfate than for ammonium sulfate at all salt concentrations. The ANS signal increases gradually and roughly linearly as the salt concentration is increased from 0 to around 0.8 M. This region corresponds to moderately attractive interactions, as measured by  $B_{22}$ . As the salt concentration is increased beyond the critical salt concentration at which  $B_{22}$  becomes highly negative, ANS fluorescence increases rapidly. At even higher concentrations, beyond the indicated instantaneous phase boundaries, phase separation occurs and the fluorescence intensity is considerably higher. Previous studies have measured large increases in ANS fluorescence upon formation of large protein aggregates (Carver et al., 1995) and shown a strong correlation of ANS fluorescence and protein precipitation (Hayakawa and Nakai, 1985; Kenig et al., 2004).

These results may imply that the attractive mAb-mAb interactions at high salt concentration are due largely to hydrophobic interactions. These hydrophobic interactions could be due to partial unfolding and exposure of buried hydrophobic residues (Semisotnov et al., 1991), or to greater solvent accessibility of surface hydrophobic patches (Arosio et al., 2012; Young et al., 1994). However, an alternative

interpretation is that the increase in ANS fluorescence results from loss of solvent accessibility due to ANS sequestration within the protein dense phase.

Figure 6.15 shows  $B_{22}$  values for the four mAbs at different salt concentrations, plotted against the measured ANS fluorescence at the same conditions. The data shown here are from the slightly attractive region. All four mAbs show a qualitatively similar relationship between  $B_{22}$  and ANS fluorescence, with ANS fluorescence increasing monotonically as  $B_{22}$  decreases.

As before, the comparison of mAbs D and  $D_M$  can be informative, which here is expressed directly in terms of ANS fluorescence. MAb D, which shows weaker self-attraction, gives rise to a much lower ANS fluorescence intensity across the salt concentration range explored here. The two-residue mutation of mAb  $D_M$  gives rise to a much higher ANS fluorescence intensity. It is possible that removal of two charged residues near the CDR of mAb  $D_M$  resulted in poor solvation and local hydrophobic patches became more solvent accessible or that structural differences due to the mutation resulted in greater exposure of hydrophobic residues. The increase in ANS fluorescence in response to the two-residue mutation of mAb D is similar to previous findings with single amino acid mutations of proteins (Andley et al., 2008; Andrésen et al., 2010; Kenig et al., 2004)

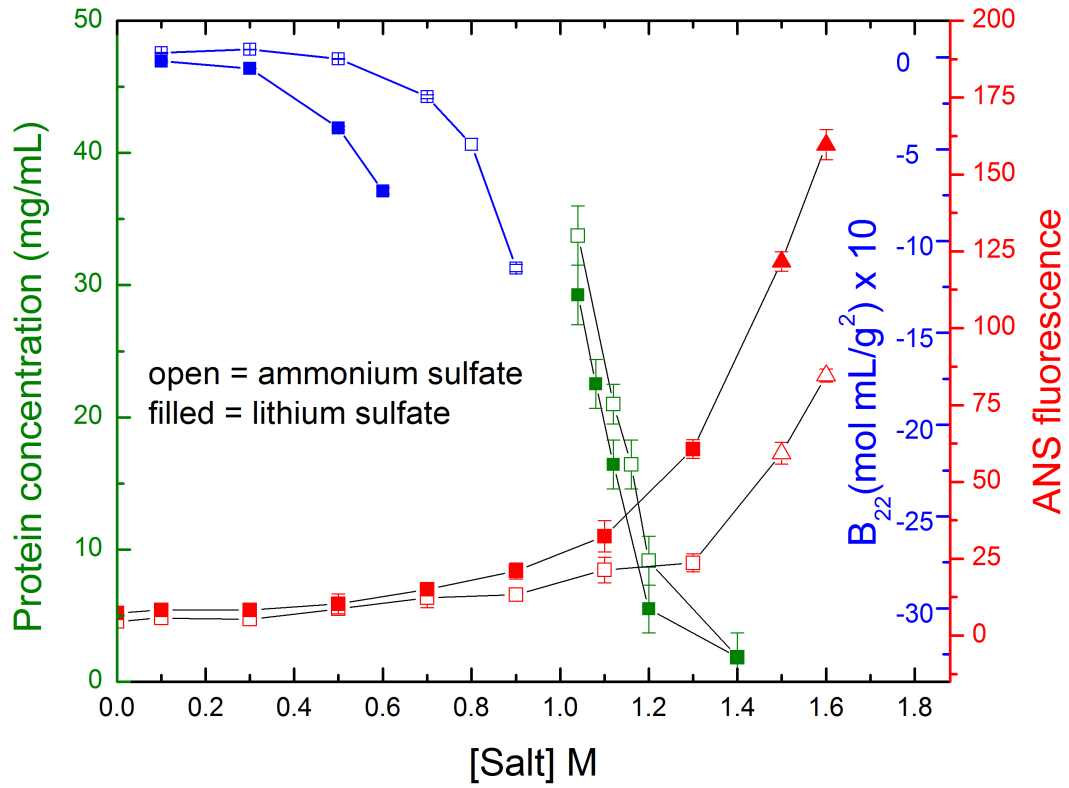


Figure 6.11: ANS fluorescence in solutions of mAb B, plotted together with the instantaneous phase boundary and  $B_{22}$  at pH 7.0 for ammonium sulfate (open symbols) and lithium sulfate (filled symbols) solutions. MAb samples with visible phase separation during ANS fluorescence measurements are indicated ( $\Delta$ ).

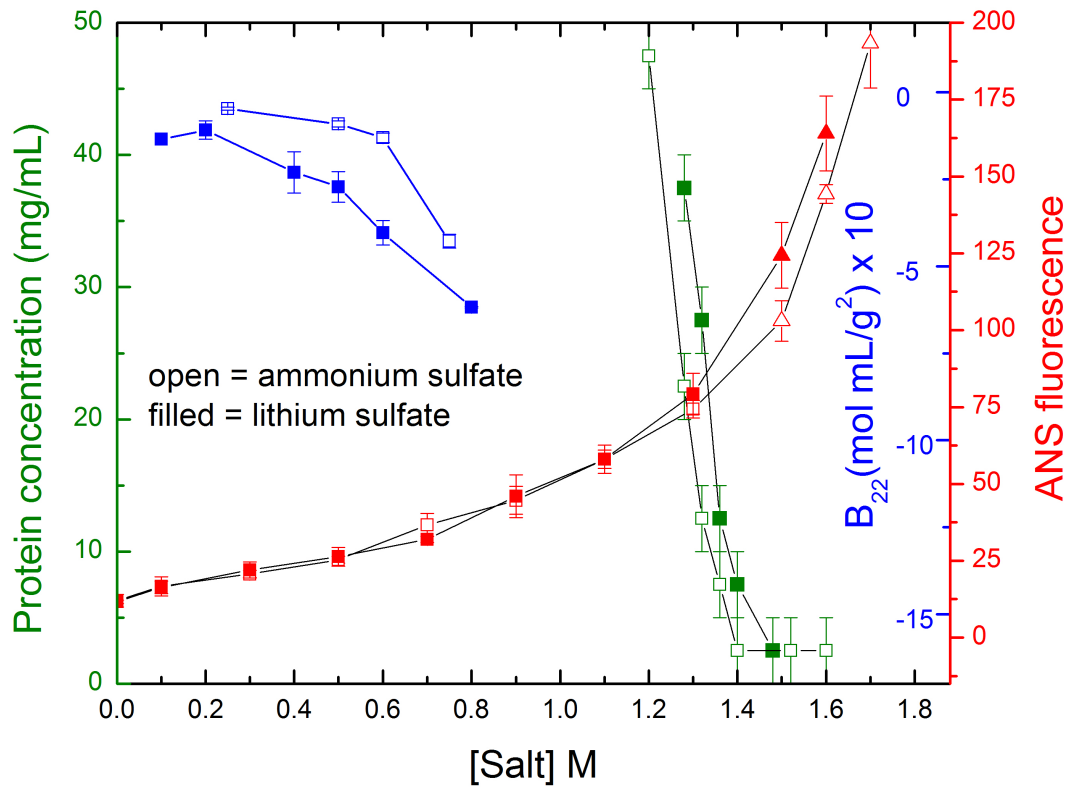


Figure 6.12: MAb C ANS fluorescence, instantaneous phase boundary and  $B_{22}$  at pH 7.0 with ammonium sulfate (open symbols) and lithium sulfate (filled symbols). MAb samples with visible phase separation during ANS fluorescence measurements are indicated ( $\Delta$ ).

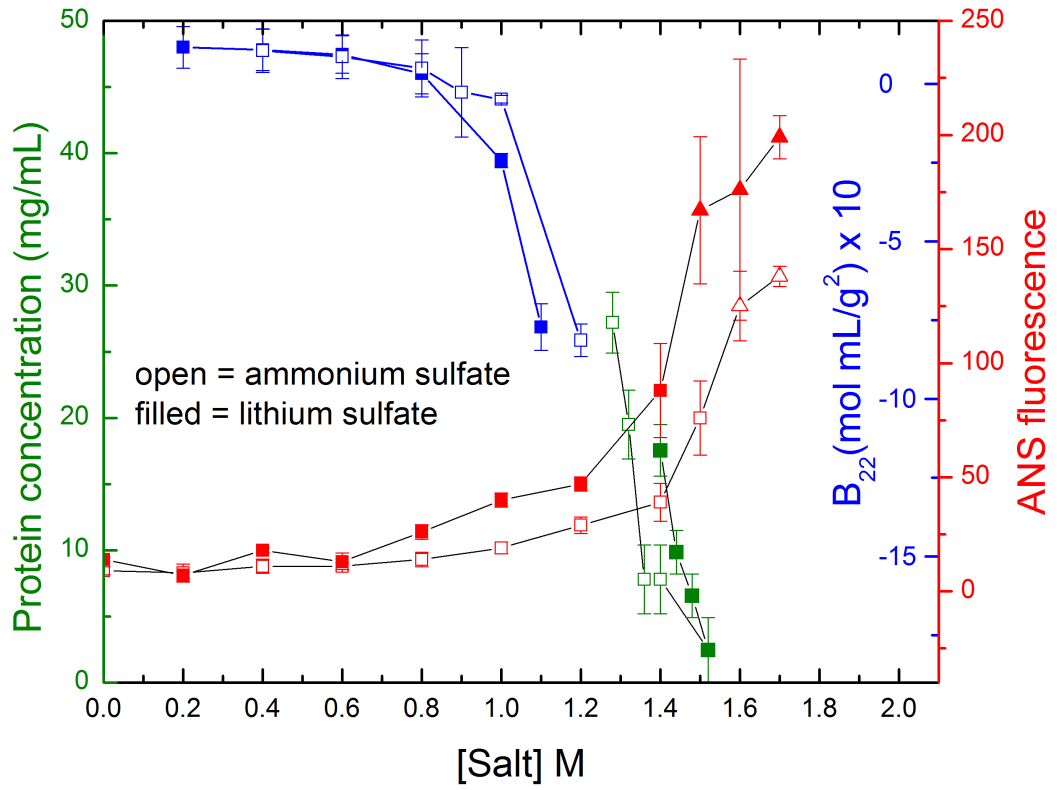


Figure 6.13: MAb D ANS fluorescence, instantaneous phase boundary and  $B_{22}$  at pH 7.0 with ammonium sulfate (open symbols) and lithium sulfate (filled symbols). MAb samples with visible phase separation during ANS fluorescence measurements are indicated ( $\Delta$ ).

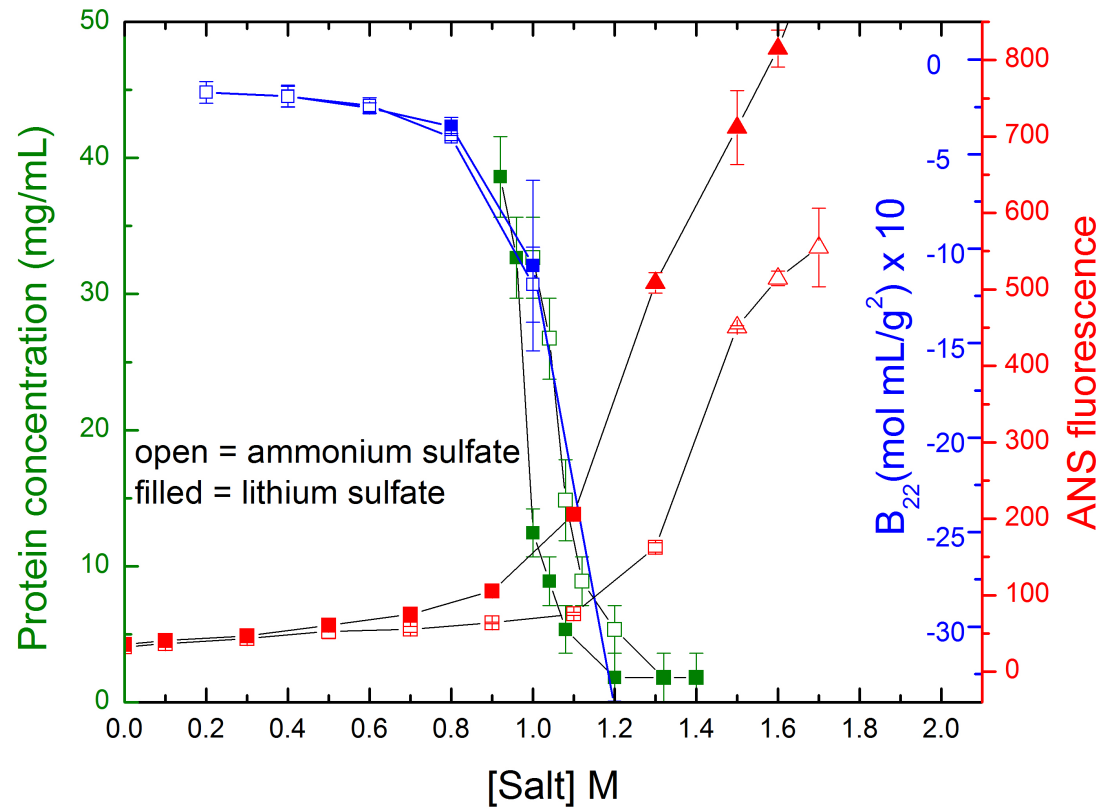


Figure 6.14: MAb D<sub>M</sub> ANS fluorescence, instantaneous phase boundary and  $B_{22}$  at pH 7.0 with ammonium sulfate (open symbols) and lithium sulfate (filled symbols). MAb samples with visible phase separation during ANS fluorescence measurements are indicated ( $\Delta$ ).

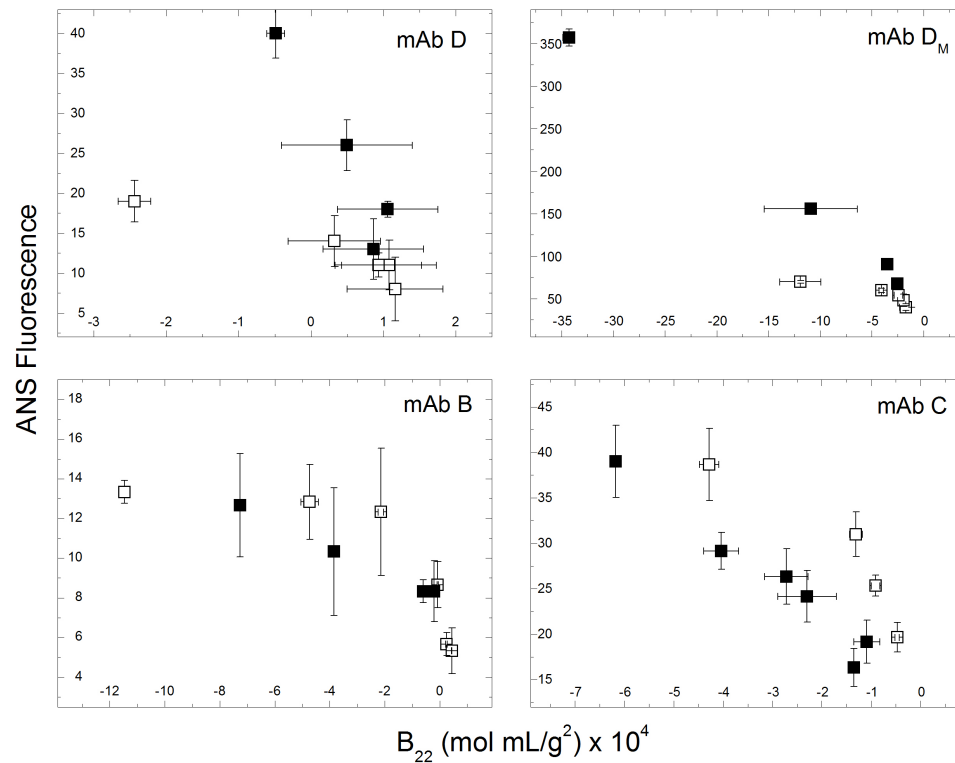


Figure 6.15: ANS fluorescence vs.  $B_{22}$  for mAbs D, D<sub>M</sub>, B and C in ammonium sulfate (open symbols) and lithium sulfate (filled symbols) at pH 7.0.

### 6.6 MAb D and MAb D<sub>M</sub> Instantaneous Phase Boundary and $B_{22}$ Comparison

As discussed earlier, mAbs D and D<sub>M</sub> differ only in two charged residues near the CDR and have estimated isoelectric points of 8.1 and 7.9, respectively. Based on homology structures of mAbs D and D<sub>M</sub> (not shown) it is clear that the mutated residues are solvent-accessible. The comparison of  $B_{22}$  values as well as instantaneous phase boundaries in previous sections highlighted some of the functional differences between the two mAbs as a result of the mutations. In this section, those properties are explored further. Solvent-exposed charged residues near the CDR have previously been found to be important in mAb-mAb interactions and aggregation (Perchiacca et al., 2014; Yadav et al., 2011b; Yearley et al., 2013).

First, Figures 6.16 and 6.17 show the instantaneous phase boundaries of mAbs D and  $D_M$  in ammonium and lithium sulfate solutions across a wider range of solution pH values. The general findings discussed previously still hold: mAb  $D_M$  has a phase boundary shifted to lower salt concentrations than for mAb D for solutions at all pH values. For both mAbs, as the pH is lowered the boundary shifts to a higher salt concentration. This trend applies for both mAbs from pH 7.0 to pH 4.0, but at pH 3.0 the mAb phase boundary shifts back to lower salt concentration. It is likely that this is due to loss of structural stability at low pH, which has been observed for mAbs in previous studies (Calmettes et al., 1991; Ejima et al., 2006; Vázquez-Rey and Lang, 2011; Vermeer and Norde, 2000; Welfle et al., 1999). This significant change in properties during the shift from pH 4.0 to pH 3.0 could potentially impact bioprocessing. During protein A elution and low-pH viral inactivation processes, the solution pH is typically reduced to between 3.0 and 4.0 and, based on these results, this could cause phase separation or aggregation. The phase boundaries and interaction strengths of MAb D and  $D_M$  are consistent with the net charge on each mAb: the more highly charged mAb D has less negative  $B_{22}$  values than the lesser-charged mAb  $D_M$ .

Figure 6.18 shows the  $B_{22}$  values for both mAbs D and  $D_M$  at pH 7.0 in ammonium and lithium sulfate as well as the  $B_{23}$  values – the two-body interaction strength of mAb D interacting with mAb  $D_M$  – at the same conditions. In solutions of both salts the  $B_{23}$  values lie between the  $B_{22}$  values for each mAb. This result implies that the mutated domain on one molecule of mAb  $D_M$  does not interact directly with the mutated domain on the second molecule to yield increased attraction. The mutated domain interacts with a different part of the molecular surface on the second molecule. Another observation of this system is that at high concentrations of ammonium

sulfate, the mAb D- $D_M B_{23}$  values are similar to  $B_{22}$  values for mAb D and in high concentrations of lithium sulfate the interactions were similar to mAb  $D_M$  self-interactions.

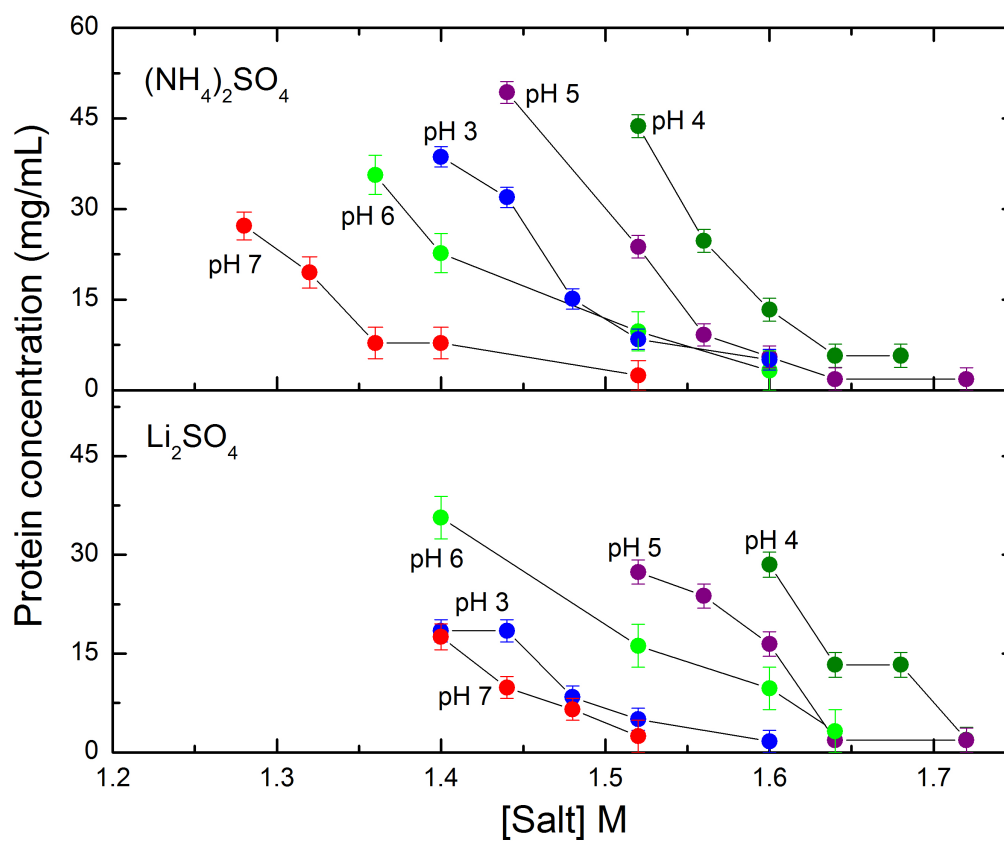


Figure 6.16: Instantaneous phase boundaries of mAb D as a function of pH with different concentrations of ammonium or lithium sulfate.

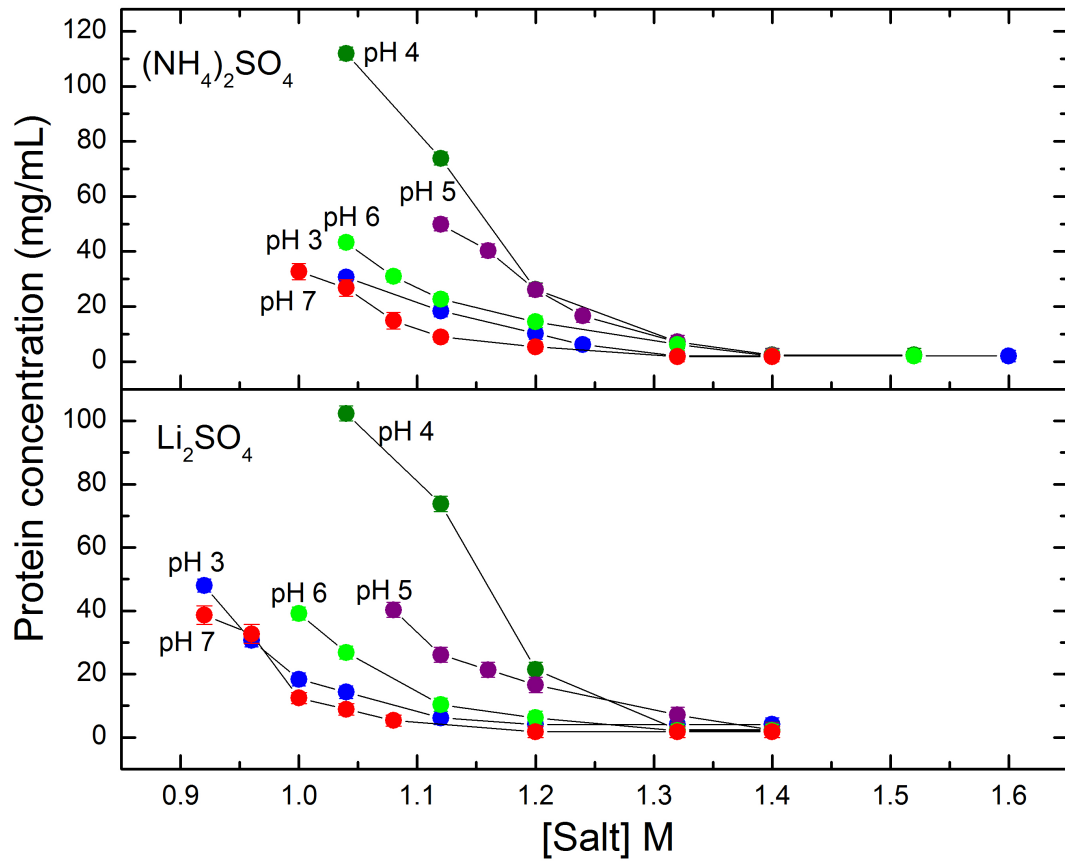


Figure 6.17: Instantaneous phase boundaries of mAb  $D_M$  as a function of pH with different concentrations of ammonium or lithium sulfate.

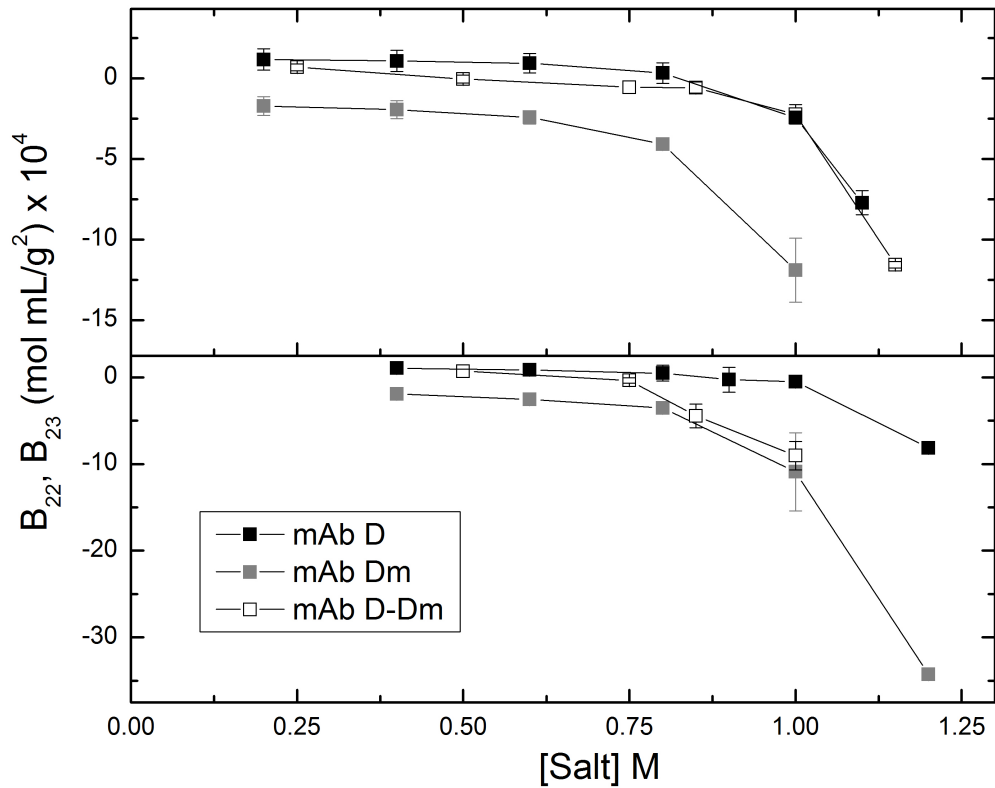


Figure 6.18:  $B_{22}$  values of mAbs D and  $D_M$  and the cross-interaction of mAbs D and  $D_M$  at pH 7.0 in ammonium and lithium sulfate solutions.

## 6.7 Conclusions

The antibodies studied here are salted-out by sulfate salts, and follow the Hofmeister series in their response to changes in salt type. The behavior of IDEC-152, mAb B, mAb C and mAb  $D_M$  were similar, while mAb A and Mill04 exhibited stronger self-attraction and a higher tendency to phase-separate, and mAb D showed much weaker self-attractions. The hypervariable region may be responsible for these differences, or the subclass of mAb A and Mill04 may play a role. Charged residues near the CDR play a major role in interactions, as evidenced by the behavior of mAb

D and mAb D<sub>M</sub> and previous studies (Perchiacca et al., 2014; Yadav et al., 2012; Yearley et al., 2013).

Correlations between interaction measurements, in terms of  $B_{22}$ , and phase boundaries for salt type and protein type suggest that the qualitative behavior of mAbs can be predicted based on a small amount of information. Given the  $B_{22}$  value and phase boundary of a mAb in a single salt, the phase behavior for that mAb in a different salt solution can be reasonably estimated from only the measured  $B_{22}$  values, or vice versa. Similar relationships of  $B_{22}$  and phase boundaries of proteins have been identified previously (Dumetz et al., 2008b; Lewus et al., 2011).

Although this work compares a large set of mAbs and has identified a number of trends, there were not a sufficient number of products here to draw specific conclusions about different IgG subtypes. MAb B has the lowest net charge and should have weaker repulsive electrostatic forces – at least at low salt concentrations – and should thus be much more self-attractive than mAbs A, C, D or D<sub>M</sub>, but that is not the case. MAb B actually had weaker self-interactions than other mAbs in low salt concentrations (Figure 6.8). At the higher salt concentrations studied here, electrostatics are not the major driving force. ANS results highlighted the important role that solvent accessibility plays in mAb-mAb salting-out. The findings in this chapter highlight the difficulties of making quantitative predictions of phase boundaries and  $B_{22}$  due to the anisotropy of antibodies.

## Chapter 7

### MONOCLONAL ANTIBODY OLIGOMERIZATION AND FRAGMENT INTERACTION STRENGTH

#### 7.1 Introduction

Oligomerization, aggregation, phase behavior and increased viscosity are all frequent challenges that are related to highly attractive mAb-mAb interactions (Roberts et al., 2011; Sahin et al., 2010; Saito et al., 2011; Scherer et al., 2010). In Chapter 6, a number of IgG1 and IgG2 products were compared based on self-interaction strength and instantaneous phase boundaries in different solution conditions (pH, salt type, salt concentration). The first goal of this chapter is to assess the oligomerization characteristics and tendencies of this set of mAbs and to compare them to the overall mAb-mAb interaction strengths, as expressed in terms of the osmotic second virial coefficient. Oligomerization was monitored using dynamic light scattering (DLS) and analytical ultracentrifugation (AUC) (Lebowitz et al., 2009) for a subset of mAbs at solution conditions explored in Chapter 6. The solutions tested were at neutral pH with various concentrations of ammonium or lithium sulfate.

Oligomerization and aggregation studies of mAbs frequently assess mAb stability in formulation conditions (Sahin et al., 2010; Scherer et al., 2010), but this work was focused on understanding crystallization processes as well as stability in purification process steps such as hydrophobic interaction chromatographic polishing.

The second goal of this work was to determine experimentally mAb fragment interaction strengths and hence to probe the contributions of individual fragments to

mAb self-association. Highly self-attractive mAbs and mAbs with typical interaction behavior from Chapter 6 were selected for this set of experiments.

Previous work with different IgG products has found highly attractive mAb self-interactions and oligomerization to have different origins. Highly solvent-exposed charged residues near the CDR were found to be crucial for self-association and aggregation in one study (Yadav et al., 2011b); it was also demonstrated that negative charge patches on Fab fragments lead to decreased electrostatic repulsion and increased self-assembly (Yadav et al., 2012). In Chapter 6 charged residues near the CDR were identified as important to interaction strength for mAbs D and D<sub>M</sub>. Fab-Fab interactions were found to drive crystallization of an IgG1 (Yagi et al., 2004), and the high viscosity of a mAb solution was found to be due to strong Fab-Fab attraction (Kanai et al., 2008). Another study found liquid-liquid separation of a mAb to be driven by attractive Fc-Fc interactions (Nishi et al., 2011). Based on the different conclusions of previous studies it is likely that these properties differ for different mAbs. The goal of this work was therefore to understand better the origin of attraction for the highly self-attractive mAbs in comparison with less attractive molecules that are less likely to form oligomers. Two simple models were developed to provide insight into the role of fragment interactions in determining the overall mAb-mAb interaction strength.

## **7.2 MAb Oligomerization Tendencies**

The oligomerization properties of a subset of the mAbs from Chapter 6 were examined here. This analysis was an extension of previous efforts to understand mAb oligomerization tendencies and characteristics (Lewus, 2011). First, DLS was used to determine the relationship between different solution conditions and the average

hydrodynamic radius of each mAb. Those results were then compared to the  $B_{22}$  values for the mAb at the same conditions. This technique and the analysis completed here do not give detailed information about the nature of the oligomeric complexes, or the precise number of mAb molecules per unit, but it does give information about conditions that lead to aggregate formation.

Figure 7.1 shows the hydrodynamic diameter measured by DLS for mAbs B-D,  $D_M$ , IDEC-152 and Mill04. All results here were collected at pH 7.0 after 24 hours of incubation at room temperature. All mAbs shown were found to increase in hydrodynamic diameter as the sulfate salt concentration was increased. At low salt concentrations the mAbs were generally stable, with a hydrodynamic diameter of around 12 nm. The notable exception was Mill04, for which the hydrodynamic diameter at 20 mM sodium phosphate and 0 M additional salt was 21 nm. Based on the results here it is unlikely Mill04 exists as a stable monomer, but only as larger oligomers. The measured hydrodynamic diameter is much larger than for previously-studied mAbs at similar solution conditions (Mahler et al., 2005; Mosbæk et al., 2012; Nobbmann et al., 2007). The onset of increasing oligomer size is consistent with the highly attractive self-interactions at low salt concentrations that were measured for Mill04, but the lack of stable monomers could not be predicted from  $B_{22}$  alone.  $B_{22}$  has previously been correlated to oligomerization and aggregate formation (Cheng et al., 2008; Dumetz et al., 2008b; Le Brun et al., 2009; Lewus, 2011). The measured hydrodynamic diameters here cannot be readily interpreted in terms of the distribution of oligomers in the solution, except to conclude that Mill04 exists as larger oligomers than do any of the other mAbs at low salt.

Mill04 was also analyzed in solutions of sodium chloride at pH 7.0. It was found previously that Mill04 had attractive self-interactions in sodium chloride solutions, but not to the same extent as in sulfate salts (Section 6.4). As expected, the measured hydrodynamic diameter in solutions of sodium chloride is much smaller. As the sodium chloride concentration was increased the diameter remained relatively constant, around 20 nm. This is much larger than expected for a mAb monomer, indicating that Mill04 does not exist as stable monomers.

The other mAbs in Figure 7.1 exhibit gradual increases in hydrodynamic diameter with increasing salt concentrations. Going back to the results in Chapter 6, this gradual increase in diameter, and formation of small oligomers, correlates well with the increased mAb-mAb attraction in the same solutions. The relative order of mAb self-interaction strength is retained here as well. For example, mAb D was found to be more stable in solution than the mutated mAb  $D_M$ . MAb  $D_M$  shows a steady increase in hydrodynamic diameter between 0.3 and 0.7 M salt. MAb D, however, has almost no increase in diameter until the salt concentration is greater than 0.7 M, similar to the solution conditions necessary for mAb-mAb attraction. IDEC-152 had similar self-interaction strengths as mAb  $D_M$  and they were found here to have similar oligomerization properties. The correlation of  $B_{22}$  and aggregation propensity is consistent with previous findings (Lewus, 2011; Saito et al., 2011).

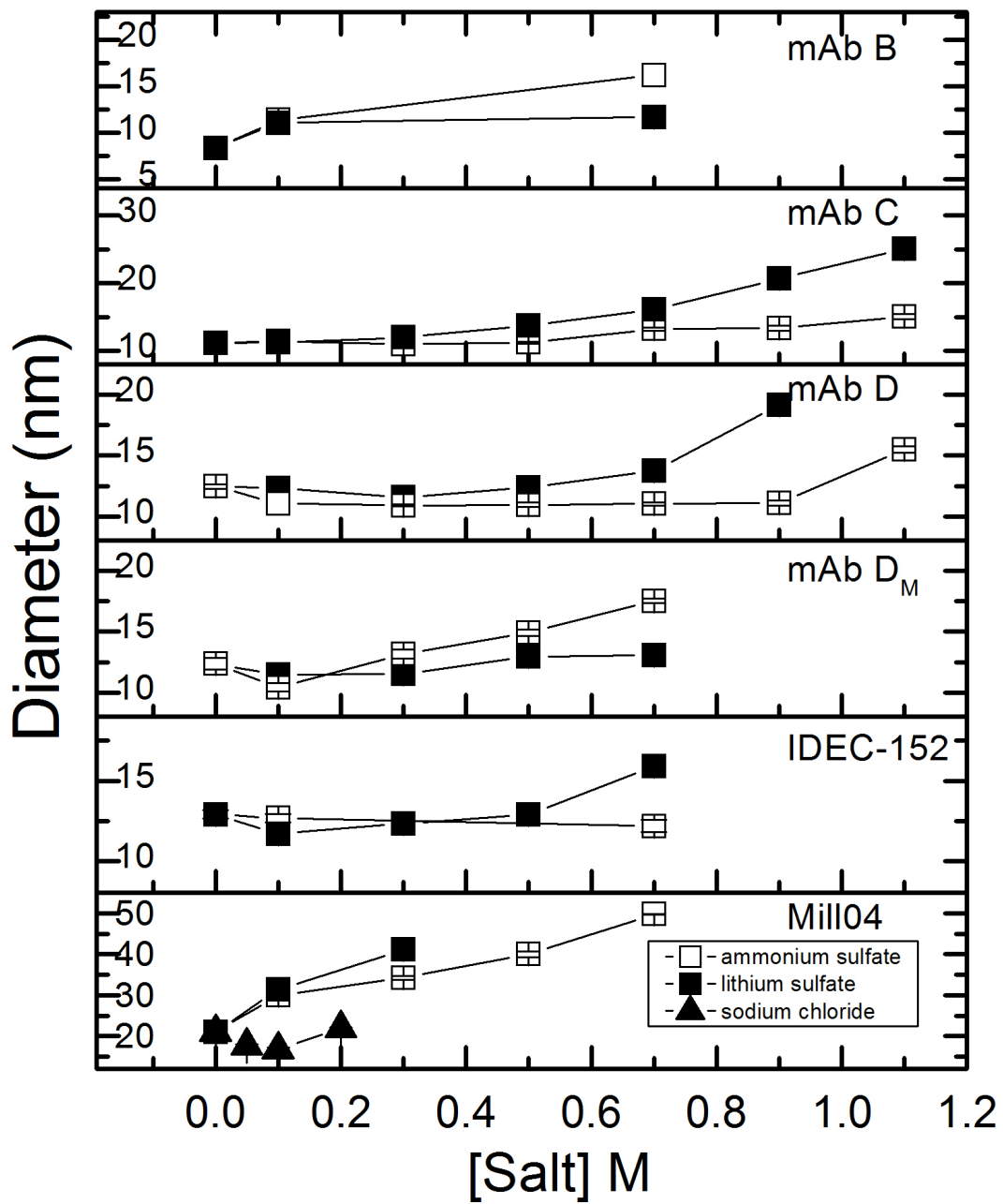


Figure 7.1: Dynamic light scattering results for six different mAbs in solutions of ammonium and lithium sulfate and sodium chloride at pH 7.0 after 24 hours of incubation at room temperature.

AUC was used also used to study mAb oligomerization tendencies as described in Section 2.4.2. AUC results were analyzed using SEDFIT version 12.52 to determine a continuous distribution of sedimentation coefficients (continuous c(S) model) (Brown and Schuck, 2006) and density and viscosity of all solvents were interpolated from values in International Critical Tables (Washburn, 1926). Reported sedimentation coefficients were all normalized to standard conditions of 20 °C in water ( $S_{20,w}$ ). Figure 7.2 shows the AUC results for mAb B in ammonium and lithium sulfate solutions as well as for IDEC-152 in lithium sulfate solution. Both mAbs have been identified as being relatively stable in solution, with moderate protein-protein self-interaction strength. The AUC result for mAb B in 0.7 M ammonium sulfate is typical of that for stable mAbs in that the majority of the mAb B population has a normalized sedimentation coefficient of approximately  $S_{20,w} = 6$  S, which is typical of a mAb monomer (Arthur et al., 2009; Gabrielson et al., 2007; Shire et al., 2009). The only other significant population is a trace dimer content, with a sedimentation coefficient of approximately 8.5 S. MAb dimers usually have sedimentation coefficients between 9 and 10 S (Arthur et al., 2009; Ejima et al., 2006), but it is possible that the solution viscosity was underestimated, resulting in a slight decrease in  $S_{20,w}$ . In lithium sulfate solution, mAb B shows much more pronounced dimerization and although the data are difficult to resolve here, there are two relatively equal populations of monomer and dimer. The stronger salting-out properties of the lithium ion compared with ammonium were enough to shift the monomer-dimer balance for mAb B appreciably

IDEC-152 has similar  $B_{22}$  and phase boundary trends to those of mAb B, but different oligomerization tendencies based on AUC. DLS results at 0.7 M salt are

similar for both mAbs, but AUC here indicates that IDEC-152, rather than forming a large population of dimers, forms smaller subgroups of dimers and trimers with  $S_{20,w} \sim 12$  S, which is consistent with previously identified mAb trimers (Arthur et al., 2012; Gabrielson et al., 2007). Up to this point, the two mAbs were difficult to distinguish from each other based on interaction strength and phase behavior.  $B_{22}$  was found to be a good predictor of oligomerization, but it was not found to predict the size of the resulting oligomers.

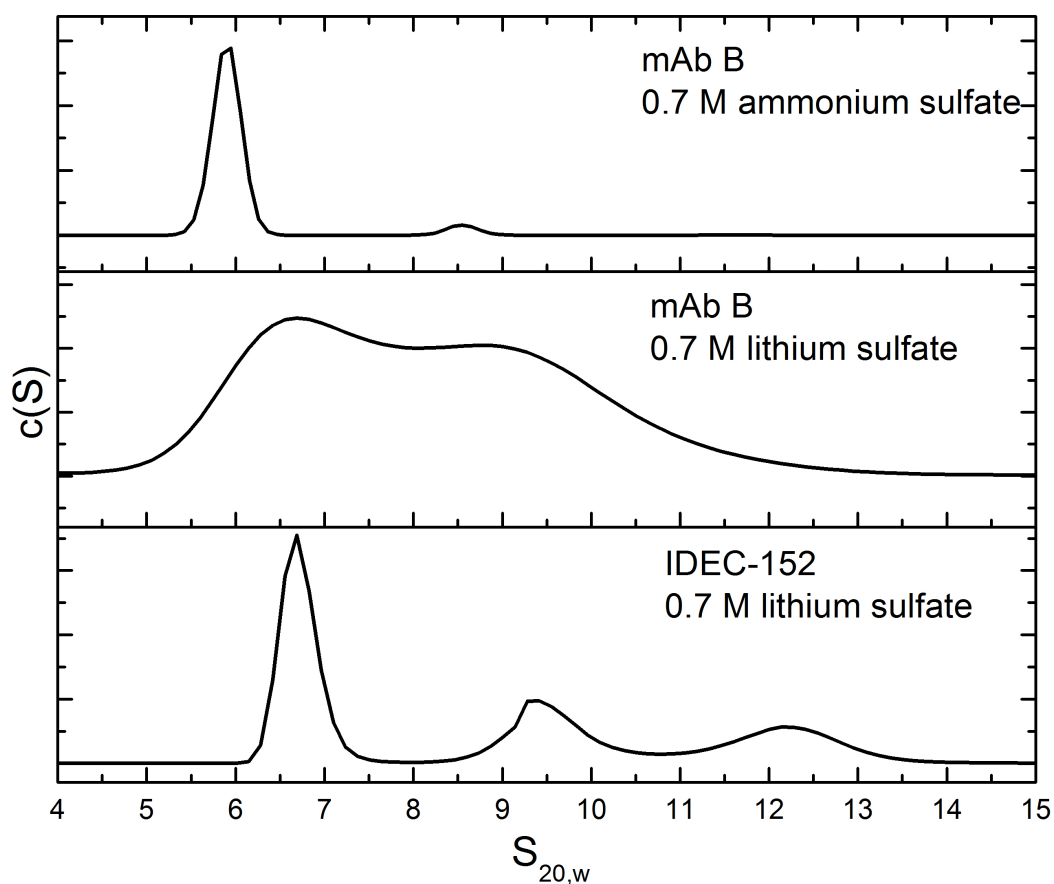


Figure 7.2: Analytical ultracentrifugation of 5 mg/mL mAb B and 5 mg/mL IDEC-152 in ammonium and lithium sulfate at pH 7.0.

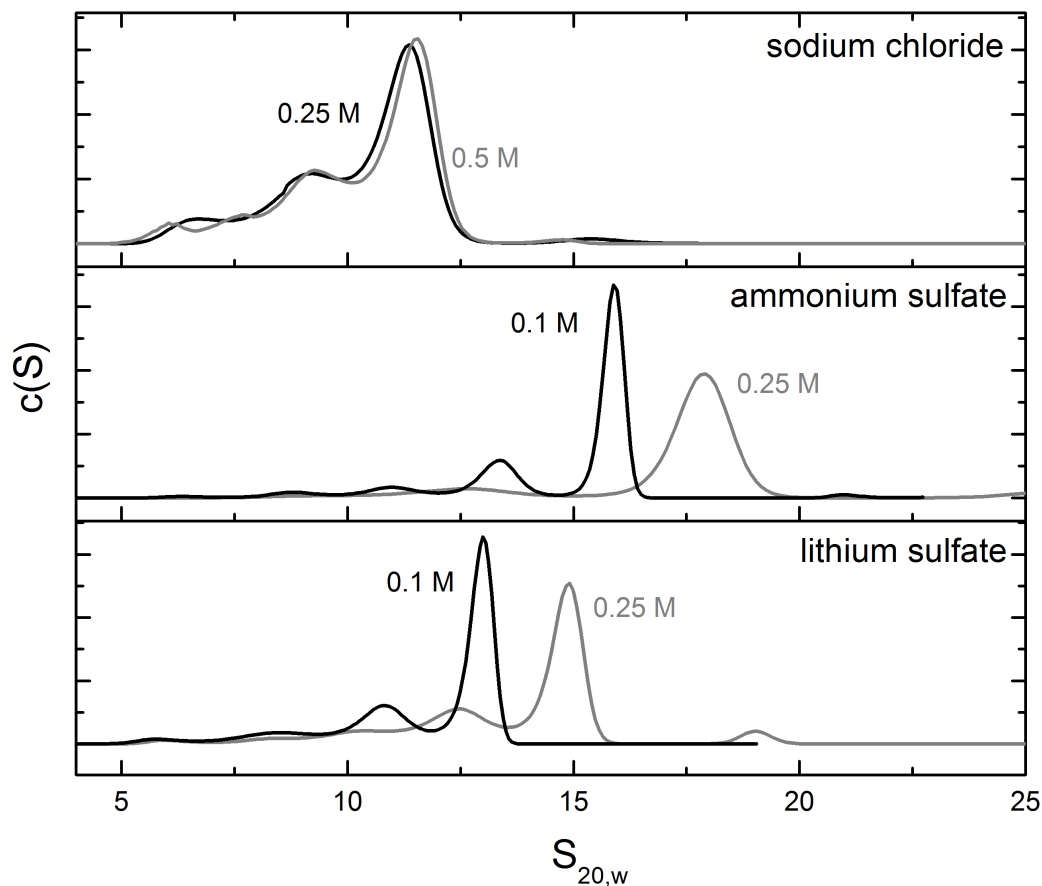


Figure 7.3: Analytical ultracentrifugation of 5 mg/mL Mill04 in ammonium and lithium sulfate and sodium chloride solutions at pH 7.0.

Figure 7.3 shows the AUC results for Mill04 in solutions of three different salts, which elucidate the DLS results presented above and  $B_{22}$  values presented in Chapter 6. Mill04 differs appreciably in oligomerization behavior from the IDEC-152 and mAb B results, which are mostly monomeric –  $S_{20,w} \sim 6$  S – under the solution conditions studied. The only monomer population is found in solutions of sodium

chloride, and even there it is a very minor component of the solution. The Mill04 oligomerization state does not change significantly with increasing sodium chloride concentration. The main peak in sodium chloride solution appears to be a dimer or trimer based on previous mAb AUC results (Arthur et al., 2009; Arthur et al., 2012; Gabrielson et al., 2007; Shire et al., 2009). There is only a minor population of larger oligomers present at these conditions.

The anomalous behavior of Mill04 is also seen in ammonium and lithium sulfate solutions, in that an increase from 0.1 to 0.25 M of either salt results in an almost complete shift to larger Mill04 oligomers. This appears to confirm the DLS results showing a steep increase in hydrodynamic diameter with increasing salt concentration. At 0.1 M of either sulfate salt there are still low concentrations of monomer and dimer and slightly higher concentrations of apparent trimers ( $S_{20,w} \sim 11$  S), based on previous mAb AUC studies (Arthur et al., 2009; Arthur et al., 2012; Gabrielson et al., 2007; Shire et al., 2009). In 0.1 M lithium sulfate the majority of Mill04 is in the form of larger oligomeric species ( $S_{20,w} \sim 13$  S). Solutions with low concentrations of ammonium sulfate (0.1 M) lead to a majority of mAb in oligomers with  $S_{20,w} \sim 16$  S. Contrary to previous results (Lewus, 2011), larger oligomer species are formed in ammonium sulfate than in lithium sulfate solutions. Increasing the concentrations of both salts to 0.25 M results in most of the Mill04 being in the form of larger oligomers in ammonium sulfate ( $S_{20,w} \sim 18$  S) and lithium sulfate ( $S_{20,w} \sim 15$  S). Mill04 is not stable as a monomer at any condition studied here and as a result, the  $B_{22}$  values measured in Chapter 6 may be misleading, as the analysis there was premised on the presence of monomers only.

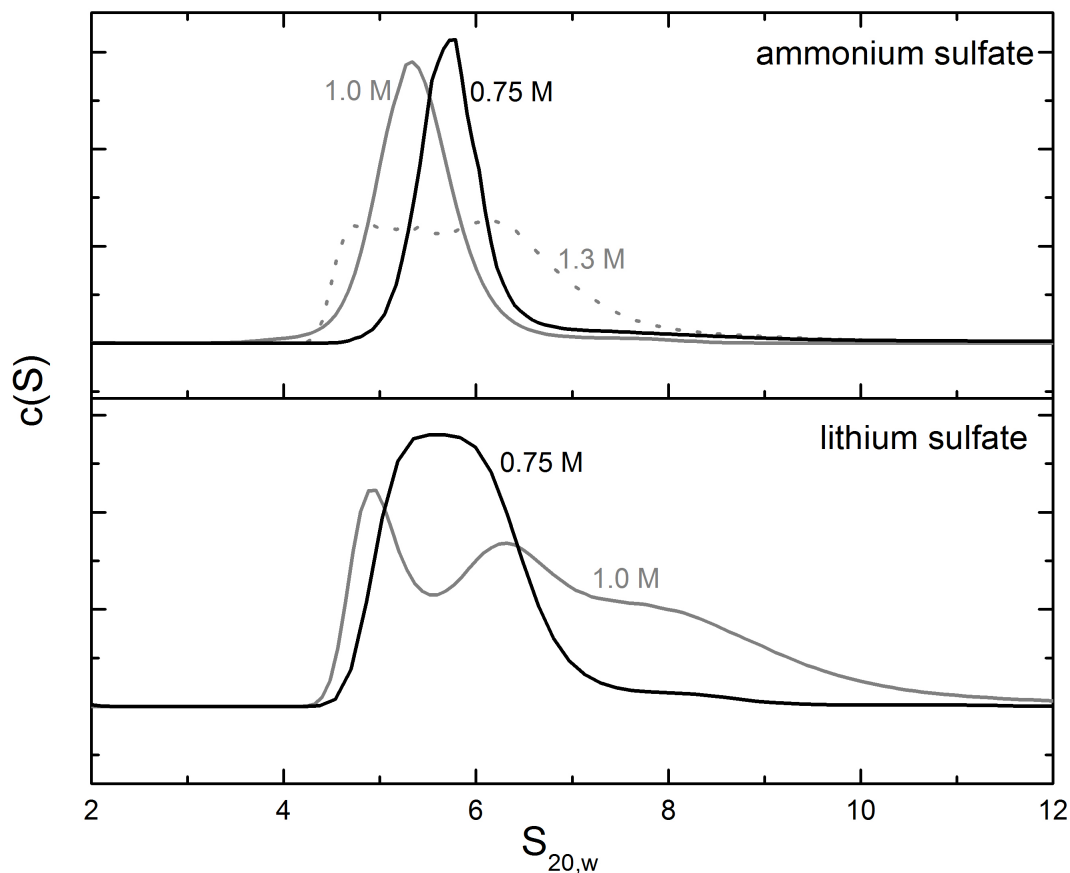


Figure 7.4: Analytical ultracentrifugation of 5 mg/mL mAb C in ammonium and lithium sulfate solutions at pH 7.0.

Figure 7.4 shows the AUC results for mAb C, one of the more stable mAbs profiled in Chapter 6. In concentrations of 0.75 M or 1 M ammonium sulfate or 1 M lithium sulfate, mAb C is stable as a monomer. In these conditions the majority of the mAb population has a sedimentation coefficient of  $S_{20,w} \sim 6$  S, and a trace amount of dimer is present as well. At larger concentrations, of 1.3 M ammonium sulfate and 1 M lithium sulfate, oligomerization is more apparent. Although the fit is not smooth for these conditions, multiple peaks are forming at values of the sedimentation coefficient that would be expected for dimers (Arthur et al., 2009; Arthur et al., 2012; Gabrielson

et al., 2007; Shire et al., 2009). The mAb C AUC results at 1.3 M ammonium sulfate and 1 M lithium sulfate are similar to those in sedimentation velocity simulations of rapidly reversible monomer-dimer systems (Howlett et al., 2006). MAb C oligomerization is sensitive to salt type, which is observed here as well as in the DLS results, with oligomers forming at much lower salt concentrations for lithium sulfate.

Together, the AUC and DLS measurements indicate the oligomerization tendencies of the mAbs studied here. The relative tendencies discussed above are consistent with the overall mAb interaction strengths and phase boundaries measured in Chapter 6. Mill04 shows the strongest self-attraction and has the most prevalent oligomerization. MAbs B, D<sub>M</sub> and IDEC-152 all have moderate self-interaction strengths and were shown here to exhibit some oligomerization, but to remain mostly monomeric. Finally, mAbs C and D are two of the least self-attractive mAbs and here were the most stable as monomers, by a considerable margin. As shown by previous work, B<sub>22</sub> is a good qualitative predictor of oligomerization (Lewus, 2011), but it is unable to predict the nature of the oligomerization, as each mAb has different characteristics even with similar B<sub>22</sub> values. This is presumably a reflection of the orientationally averaged nature of B<sub>22</sub>, compared to the likely strong and local orientation dependence that is intrinsic to the formation of oligomers.

### **7.3 Fragment Interactions**

Osmotic second virial coefficients for fragments of four of the previously studied mAbs were measured here. As described in Section 2.5, fragment interactions were measured by enzymatically cleaving mAbs and purifying the resulting Fc and Fab fragments, followed by CIC to measure the osmotic virial coefficients for each combination of fragments.

IDEC-152 and mAb B were chosen for this work because they represent mAbs with moderate self-interactions and stability on par with the majority of mAbs studied previously. Mill04 was chosen due to its highly self-attractive nature and anomalous oligomerization behavior, discussed previously in this chapter. Finally, mAb C represents the most stable molecule, which has highly attractive self-interactions only at high salt concentration. Additionally, due to challenges with papain digestion, only IgG1 molecules could be studied here. Due to that limitation, mAbs D and D<sub>M</sub> were excluded.

### 7.3.1 IDEC-152 Fragment Interactions

IDEC-152 was found to have similar self-interaction strengths to the majority of stable mAbs profiled. At pH 7.0, in solutions of sulfate salts, the B<sub>22</sub> value did not start to become highly negative, indicating strong attraction, until the salt concentrations exceeded 0.5-0.6 M. In solutions of sodium chloride, also at pH 7.0, the mAb-mAb interactions were slightly attractive at high salt concentrations, but interactions were generally weak.

Figure 7.5 shows the B<sub>22</sub> and B<sub>23</sub> values measured for IDEC-152 fragment interactions. The interaction strength follows similar trends for Fab-Fab, Fc-Fc and Fc-Fab interactions. In all cases the interactions are slightly attractive until salt concentrations greater than 0.8 M, beyond which interactions become highly attractive. The fragment interactions are qualitatively similar to model protein interactions (Dumetz et al., 2007; Tessier et al., 2002b). The only noticeable difference among the three interaction pairs is that the Fc-Fab interaction is more attractive than the others at the conditions profiled here. Coarse-grained mAb-mAb modeling has previously demonstrated the importance of Fc-Fab interactions for some mAb self-

interactions (Chaudhri et al., 2012). Fab-Fab interactions (Chaudhri et al., 2012; Chaudhuri et al., 2013; Kanai et al., 2008; Yadav et al., 2009; Yadav et al., 2010) as well as Fc-Fc interactions (Nishi et al., 2011) have previously been found to drive mAb-mAb association. These interactions are all considerably weaker than the mAb-mAb interactions and are measurable to much higher salt concentrations. In sodium chloride solutions, the three fragment interaction measurements showed no attraction and slight repulsion.

The full mAb had strong self-attraction at salt concentrations even around 0.5 M salt, but none of the fragment interactions are particularly attractive there. To determine if there are cooperative or simultaneous interactions with multiple fragments, Fab-mAb CIC was performed. In this case, the intact mAb was immobilized and purified Fab was injected into the mobile phase. As can be seen in Figure 7.5, Fab-mAb  $B_{23}$  values follow similar trends to the mAb-mAb behavior. There are two possible explanations for this. The first possibility is that the enzymatic cleavage resulted in altered interactions, presumably by removing the attractive interaction site, particularly if the attractive interactions occur in the hinge region of the IgG. The second possibility is that there are simultaneous interactions with Fc and Fab domains when a full mAb interacts with a second full mAb.

There is a similar result in sodium chloride solutions. Even though the fragment interactions were all either repulsive or non-attractive, at low salt concentrations the Fab-mAb interaction is relatively attractive. The decrease in attraction with additional salt suggests that this is an electrostatic interaction. In the case of sodium chloride it is likely that IgG cleavage has removed part of the molecule

contributing to this interaction. Overall, therefore, this largely stable mAb displays slightly attractive contributions from all fragment interactions.

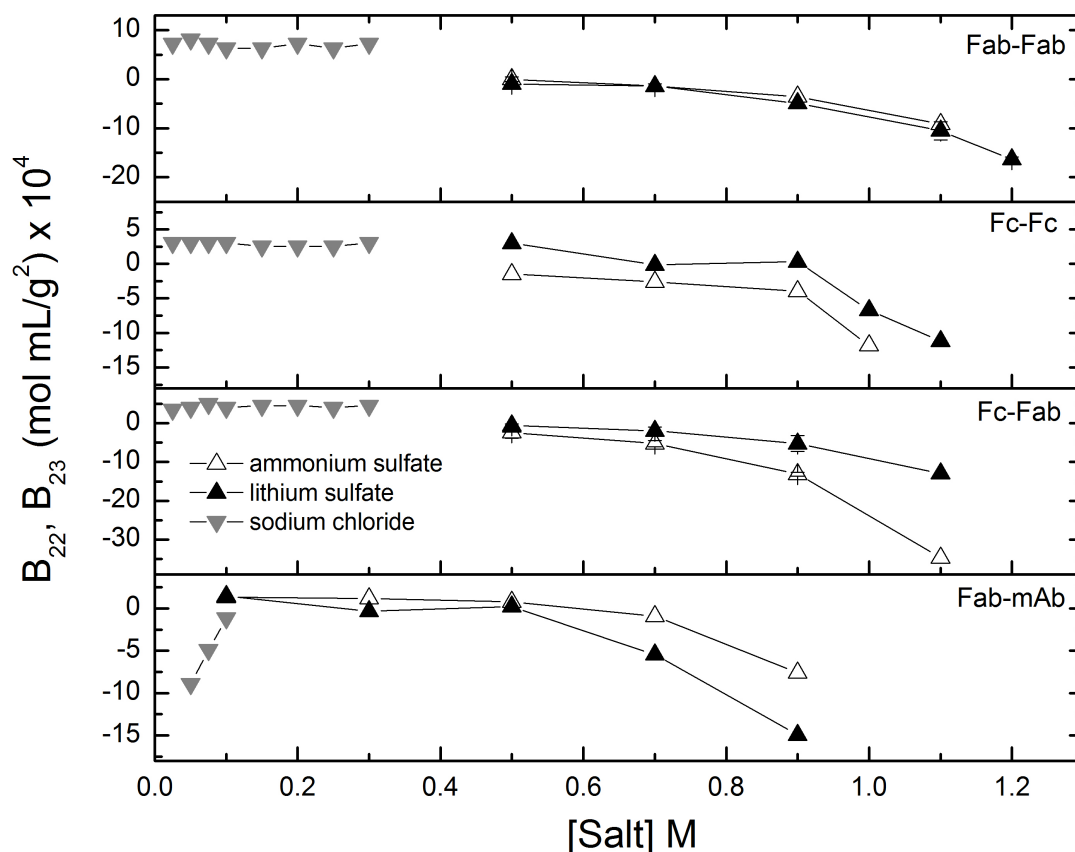


Figure 7.5: IDEC-152 fragment interaction strengths in sodium chloride, ammonium and lithium sulfate salts at pH 7.0.

### 7.3.2 Mill04 Fragment Interactions

Fragment interactions for Mill04 were desirable for elucidating the highly self-attractive nature of Mill04. Figure 7.6 shows the  $B_{22}$  and  $B_{23}$  values of the fragment interactions at pH 7.0 in ammonium and lithium sulfate solutions. The full mAb had highly attractive self-interactions even at low concentrations of sulfate salts.

The Fc-Fc and Fc-Fab fragment interactions are repulsive or non-attractive at a wide range of salt concentrations. Measurements were made at concentrations as high as 0.9 M, much higher than experimentally possible for the full mAb interactions. In contrast, the Fab-Fab interactions show almost identical trends to the results for the intact mAb B<sub>22</sub>. These results indicate that the highly self-attractive nature of Mill04 is due predominantly to Fab-Fab interactions, similar to previous findings that identified Fab-Fab interactions as the most attractive (Chaudhri et al., 2012; Chaudhuri et al., 2013; Kanai et al., 2008; Yadav et al., 2010; Yadav et al., 2012); there is no significant contribution from the Fc domain.

Understanding the origin of the highly attractive interactions could provide clues as to the oligomerization pattern. Based on these results Fab-Fab contacts will mediate oligomer growth of Mill04. There is also the possibility, due to the self-attractive nature and IgG structure, that two mAbs interact with both Fab domains simultaneously. To understand better the potential impact of Mill04 fragment interactions, a relatively simple model is developed later in this chapter.

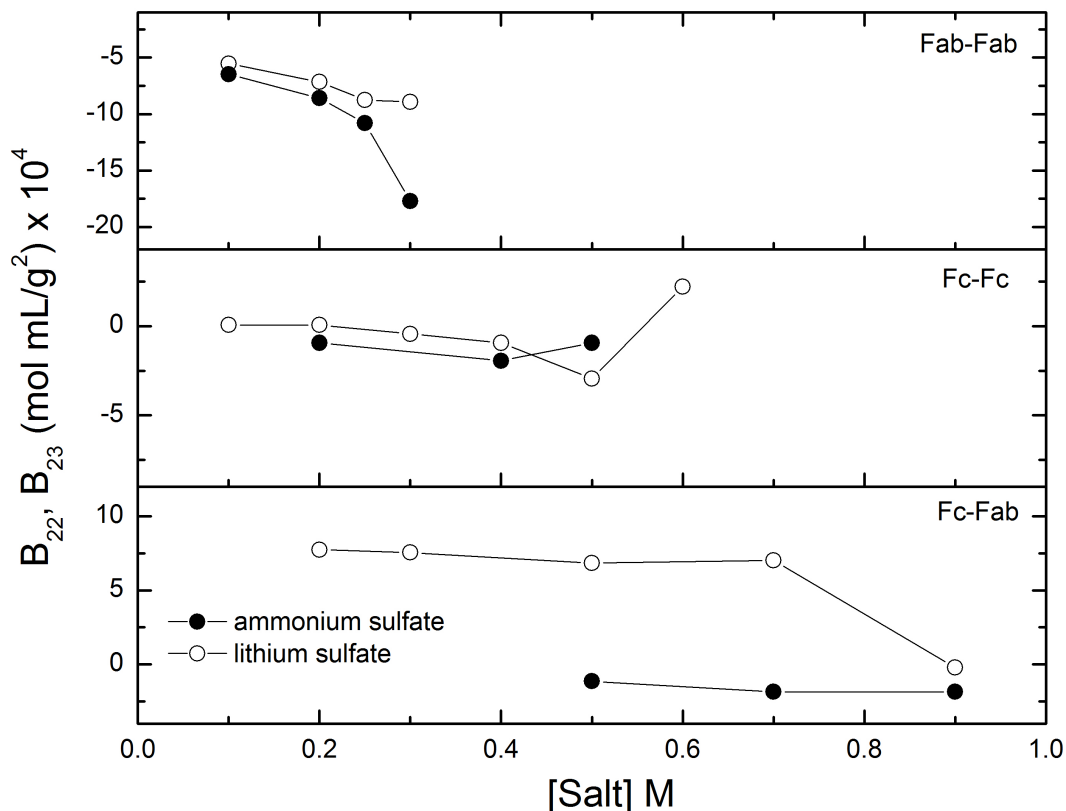


Figure 7.6: Mill04 fragment interaction strengths in ammonium and lithium sulfate solutions at pH 7.0.

### 7.3.3 MAb B Fragment Interactions

MAb B was similar in overall self-interaction behavior to IDEC-152. It was found to be relatively stable in solutions of ammonium and lithium sulfate and had almost identical interaction strength to the set of stable mAbs identified in Chapter 6. The IDEC-152 fragment interactions indicated weakly attractive contributions from all fragments. MAb B and IDEC-152 also have similar oligomerization behavior, with a small population of dimers appearing as  $B_{22}$  starts to become highly negative. The major difference between the two species is that IDEC-152 also forms some higher-order oligomers.

In Chapter 6, mAb B in ammonium and lithium sulfate at pH 7.0 was found to display weakly attractive self-interactions for salt concentrations up to around 0.6-0.7 M. Beyond that concentration, self-interactions become highly attractive. Fragment interaction strengths for mAb B are shown in Figure 7.7. The Fab-Fab and Fab-Fc interactions display almost no attractive features, even at considerably higher salt concentrations than those that resulted in strong mAb-mAb attraction. Fc-Fc interactions have some salting-out characteristics, but become highly attractive only at considerably higher salt concentrations than seen for the intact mAb. Fc-Fc interactions drive mAb-mAb interactions for some previously studied mAbs (Nishi et al., 2011). Similarly to IDEC-152, it was hypothesized that attractive interactions might involve residues within the hinge region of mAb B. The Fc-mAb interaction trends shown in Figure 7.7 appear to confirm that the hinge region is likely driving mAb B self-association. It is possible that IDEC-152, with strong Fab-mAb interactions, formed a small fraction of trimers because an individual IgG can interact with two different molecules through its two Fab domains. MAb B, for which oligomerization appears to be driven by Fc-mAb interactions, was found to form only dimers.

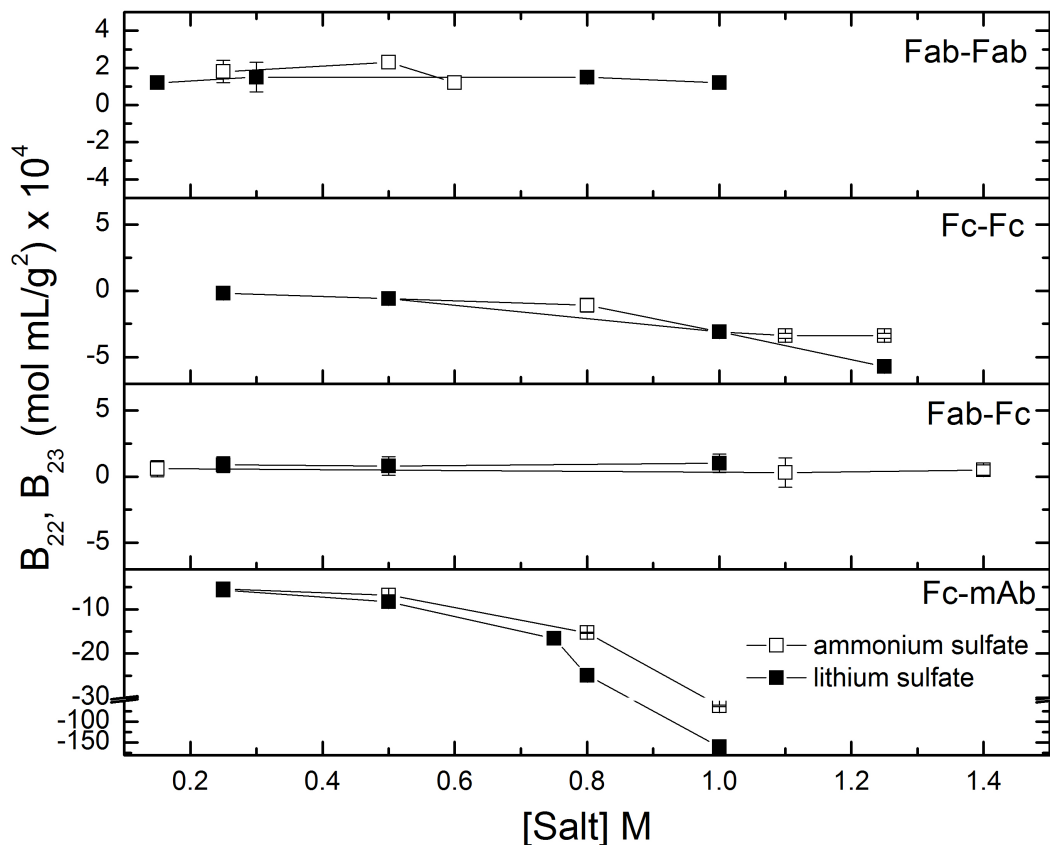


Figure 7.7: MAb B fragment interaction strengths in ammonium and lithium sulfate solutions at pH 7.0.

### 7.3.4 MAb C Fragment Interactions

MAb C was identified earlier (Figures 6.6-6.10) as being similar to IDEC-152 and the stable mAbs. It was found that greater than 0.5-0.6 M salt resulted in highly attractive interactions and large negative  $B_{22}$  values. MAb C oligomerization tendencies were also similar to those of previously identified stable mAbs. At solution conditions with highly attractive self-interactions there was a significant population of dimers.

Figure 7.8 shows the fragment interactions for mAb C. All fragment interactions were found to be attractive if the salt concentration was sufficiently high. However, Fab-Fab interactions do not become attractive until salt concentrations considerably higher than observed for mAb-mAb interactions. Fc-Fc and Fab-Fc interactions were both found to be highly attractive, with Fc-Fc becoming attractive at slightly lower salt concentrations and driving mAb-mAb self-attraction. Fc-Fc interactions have been found to drive self-interactions previously (Nishi et al., 2011) and Fab-Fc electrostatic interactions were important for a different mAb (Chaudhri et al., 2012; Chaudhuri et al., 2013). Oligomerization did not start until conditions at which Fab-Fc interactions were found to be highly attractive. Strong Fc-Fc interactions therefore seem insufficient to result in oligomerization.

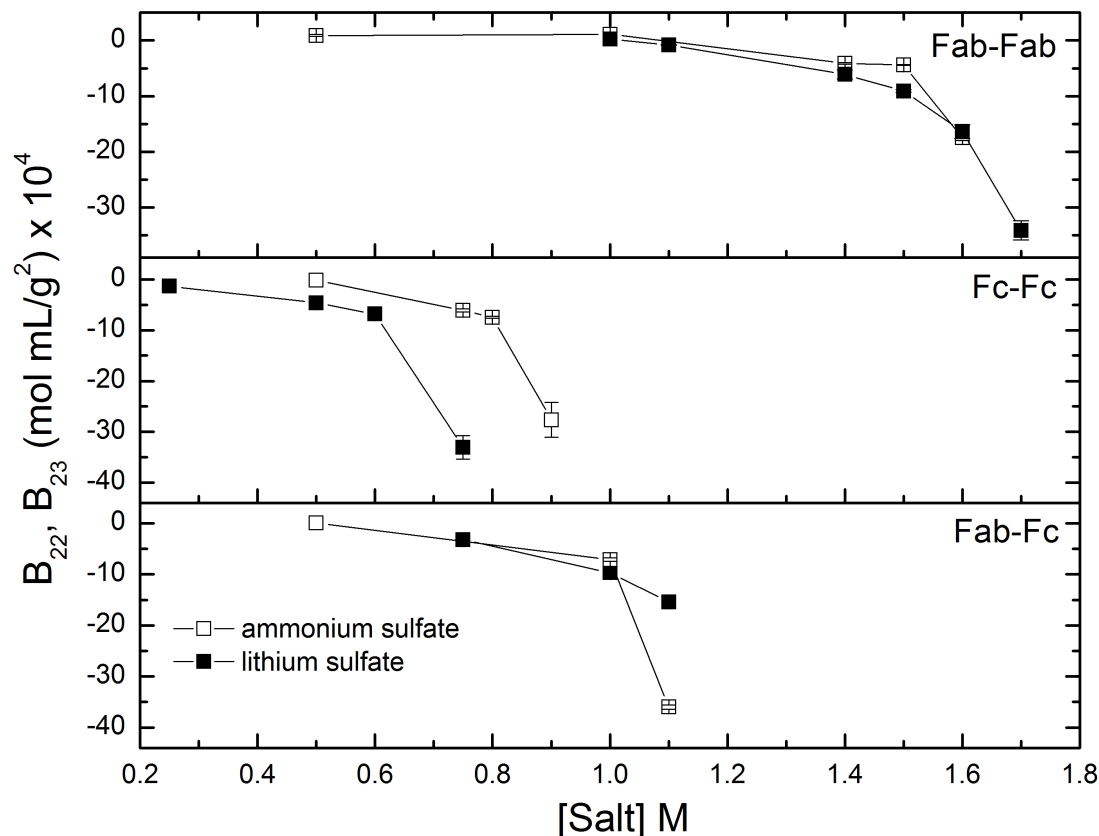


Figure 7.8: MAb C fragment interaction strengths in various concentrations of ammonium and lithium sulfate at pH 7.0.

## 7.4 Calculation of Full MAb Interaction from Fragments

### 7.4.1 Stoichiometric Mixing-Rule Model

To understand better the contribution of fragment interactions to the full mAb-mAb interaction strength, a few simple models were developed here. The first is based on a stoichiometric gas mixing rule (Sandler, 2011). For this model, it was assumed that a mAb solution can be represented as a 2:1 mixture of Fab:Fc molecules. It is also assumed that the fragments in the mixture experience only two-body interactions. The  $B_{22}$  of the mixture (the full mAb) is then calculated from

$$B_{2,mix} = \sum_{i=1}^C \sum_{j=1}^C x_i x_j B_{2,ij}$$

where  $C$  is the number of components (2 in this case),  $x$  is the mole fraction of each component and  $B_{2,ij}$  is the second osmotic virial coefficient for the interaction of components  $i$  and  $j$ .

As can be seen in Figure 7.9, this model does a good job of predicting the full mAb  $B_{22}$  for IDEC-152. The relative success of this model supports the idea that the moderate attraction and relative stability of IDEC-152 could be partially due to two-body interactions of different fragments, rather than multivalent interactions. In contrast, when the same model is applied to Mill04, the mAb-mAb attraction is underpredicted by a large margin. Mill04 has very strong mAb-mAb attraction, but among the fragments strong attraction only for Fab-Fab. The assumption of two-body interactions in this model is therefore unrealistic for Mill04. It is possible that multiple Fab-Fab contacts are made simultaneously, resulting in the observed behavior as hypothesized previously (Kanai et al., 2008). Similarly, the stoichiometric model predicts much weaker attraction than measured for mAbs B and C. For mAb B, this is due to the strongest attraction being reflected in Fc-mAb interactions, which are not included in the model. MAb C interactions appear driven by Fc-Fc interactions, the interaction that contributes the least in this model, and the mixing rule does not predict highly attractive interactions until Fc-Fab interactions start to contribute as well.

#### 7.4.2 Three-Sphere Model

A second model was developed to take into account the possibility of more than one fragment interaction simultaneously contributing to the overall mAb self-attraction, as is expected for Mill04. An idealized model of a mAb was built from

three spheres (two Fabs, one Fc) of equivalent volume to each of the mAb fragments. The two Fab spheres were placed touching the surface of the Fc sphere and separated by an angle of 115°, a typical Fab-Fab separation angle in IgG structures (Sandin et al., 2004; Saphire et al., 2002). Similar coarse-grained mAb-mAb models have been developed previously (Chaudhri et al., 2012; Chaudhuri et al., 2013).

The measured second osmotic virial coefficients for each fragment interaction pair (Fc-Fc, Fc-Fab, Fab-Fab) were translated to interaction potentials. This procedure treated the fragment interactions as isotropic interactions of two spheres. The Yukawa potential was used as the attractive potential:

$$u(r) = \infty, \text{ for } 0 \leq r \leq \sigma; u(r) = -\frac{\sigma\epsilon}{r} e^{-b(r-\sigma)} \text{ for } r > \sigma$$

where  $\sigma$  is the radius of the sphere of equivalent volume of each fragment,  $\epsilon$  is the well depth and  $b$  is a parameter characterizing the well width. It has previously been shown that the Lennard-Jones 140-35 potential is a good model of short-range, non-electrostatic interactions between protein molecules of moderate size (Hloucha et al., 2001), which is an appropriate assumption here. The  $b$  parameter in the Yukawa potential was selected in order to minimize the total error between the Yukawa and the 140-35 Lennard-Jones potentials with identical well depths.

Well depths were calculated for each experimentally measured fragment interaction strength ( $B_{22}$  or  $B_{23}$ ) using the Yukawa potential described above. Spherical particles with isotropic interactions were assumed. The second virial coefficient between isotropic spheres has been determined previously as (McQuarrie, 2000)

$$B_{22} = -\frac{2\pi N_A}{MW^2} \int_0^\infty \left[ \left( e^{-\frac{u(r)}{kT}} \right) - 1 \right] r^2 dr$$

where  $N_A$  is Avogadro's number, MW is the protein molecular weight,  $u(r)$  is the Yukawa potential,  $k$  is Boltzmann's constant,  $T$  is temperature and  $r$  is the center-to-center distance of the two protein molecules. The well depths calculated from experimentally measured  $B_{22}$  and assuming mAb fragments are isotropic and spherical were used in the construction of three-sphere mAb models. The constructed three-sphere model is not isotropic or spherical. The  $B_{22}$  of anisotropic molecules is given as (McQuarrie, 2000; Neal et al., 1998)

$$B_{22} = -\frac{1}{16MW^2\pi^2} \int_0^{2\pi} \int_0^{\pi} \int_0^{2\pi} \int_0^{2\pi} \int_0^{\pi} \int_0^{\infty} [e^{-W/kT} - 1] \times r_{12}^2 dr_{12} \sin\theta d\theta d\phi d\alpha \sin\beta d\beta d\gamma$$

where  $W$  is the potential of mean force,  $r_{12}$  is the center-to-center distance between the two protein molecules,  $\phi$  and  $\theta$  are the spherical angles representing the translation of the second protein molecule relative to the first, and  $\alpha$ ,  $\beta$  and  $\gamma$  are the Euler angles describing the rotation of the second molecule. The  $B_{22}$  values were calculated from the three-sphere model using Monte Carlo integration (Press et al., 1986), as done previously (Asthagiri et al., 1999; Neal et al., 1998; Quang et al., 2014). The Monte Carlo integral is computed as

$$B_{22} = -\frac{1}{16MW^2\pi^2} \frac{V}{N} \left[ \sum_{i=1}^N \left( \frac{1}{3} r_c^3 \right)_i - \sum_{i=1}^N (I_{in})_i \right]$$

$$I_{in} = \int_{r_c}^{\infty} \left( e^{-\frac{W}{kT}} - 1 \right) r^2 dr$$

where  $N$  is the number of randomly sampled orientations and  $V$  is the hypervolume of the configurational space. The potential of mean force ( $W$ ), which appears in the inner integral ( $I_{in}$ ), is represented by the Yukawa potential, using the parameters described

above. In this integration scheme the first model mAb is held stationary with all three sphere centers in the x-y plane and its center of mass at the origin. A second identical model mAb is then rotated randomly in the three Euler angles and then translated far enough away from the first molecule in a random direction such that there are no significant interactions. The second molecule is then iteratively moved towards the origin – closer to the first mAb – as the radial inner integral is calculated. The radial integration is terminated when the molecules touch and the corresponding center-to-center distance is reported as  $r_C$ .

The  $B_{22}$  values predicted by the three-sphere model are compared to the experimentally determined  $B_{22}$  values and those predicted using the stoichiometric mixing rule in Figure 7.9. The  $B_{22}$  values predicted by the three-sphere model are close to experimentally determined values for Mill04. For IDEC-152, this model has a similar trend compared to the experimental findings, with slightly less negative  $B_{22}$ . For mAb C the three-sphere model predicts  $B_{22}$  values that are shifted to a higher salt concentration by approximately 0.2 M compared to  $B_{22}$  measured with SIC. Finally, for mAb B, this model does not predict any significant mAb-mAb attraction. Overall, the three-sphere model is an improvement over the mixing-rule model for Mill04, but not significantly more successful for the other three mAbs here.

This model provides a simplistic representation of mAb-mAb interactions, but it provides more accurate predictions of Mill04  $B_{22}$  values than does the mixing rule. The improved accuracy here is presumably due to inclusion of multi-body interactions. As has been shown before,  $B_{22}$  values can be dominated by a few highly attractive molecular orientations (Neal et al., 1998). For the three-sphere model, the most attractive orientations are ones in which two molecules are oriented so as to

enable two simultaneous Fab-Fab interactions. This model supports the hypothesis that multipoint interactions are driving the outlier behavior of Mill04, although the model is certainly an idealized one.

For mAbs B and C, the model predictions are not as successful. Both models use individual fragment interaction strengths as inputs, and mAb B does not fit either model well. Both models were unsuccessful for mAb B because neither model incorporates Fc-mAb interaction strengths, which were the main contribution to mAb B self-interactions. MAb C has similar results for the three-sphere model as for the stoichiometric model, with both models underpredicting the total mAb attraction. Because the driving force of interaction for mAb C appears to be Fc-Fc attraction, the three-sphere model does not add any attraction – each mAb only has one Fc, making multipoint interactions impossible. It is possible that, similar to mAb B and IDEC-152, there are important interactions with the hinge region that are missing from this analysis but that drive the stronger than anticipated mAb-mAb attraction.

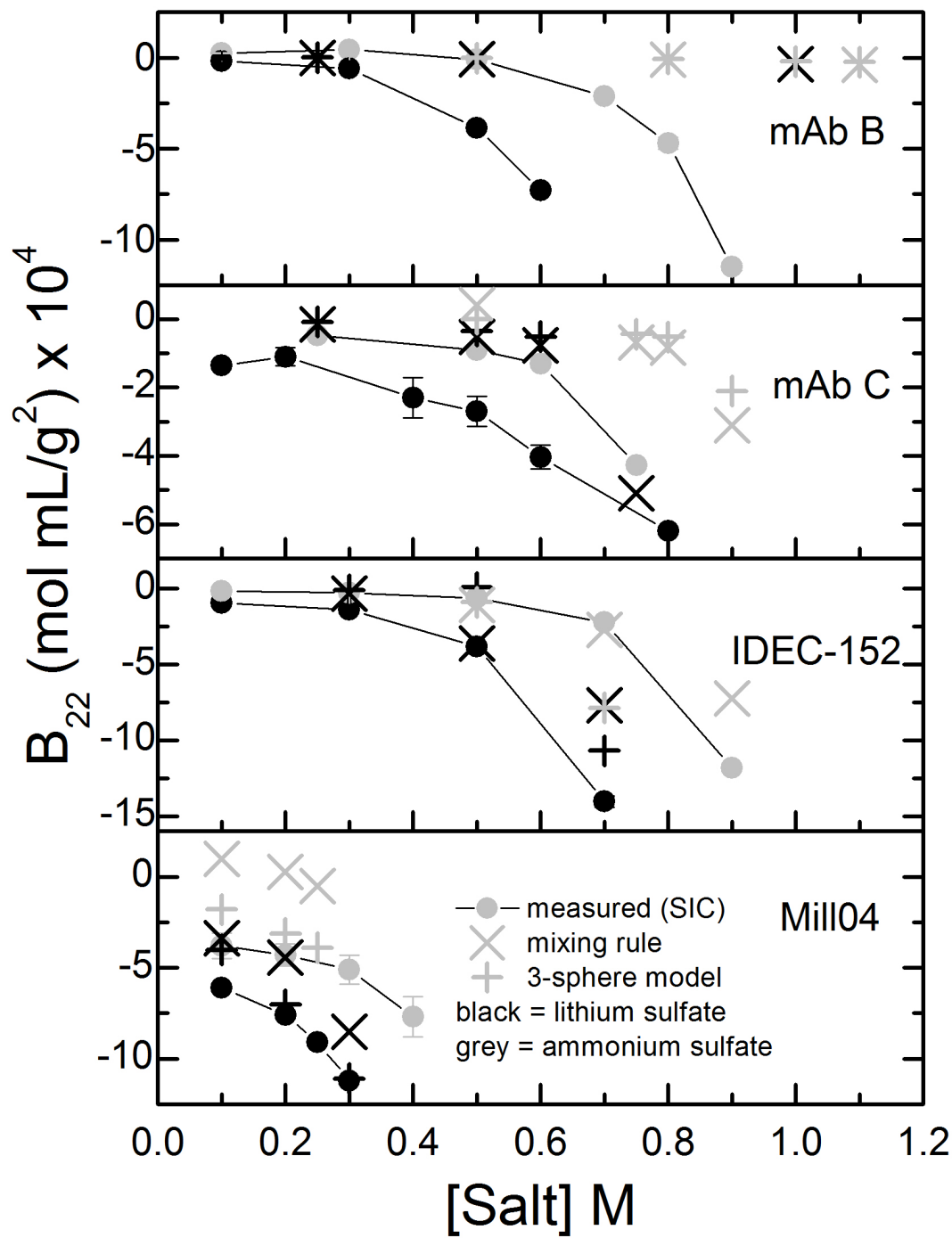


Figure 7.9: Second osmotic virial coefficients measured by SIC for mAbs B, C, IDEC-152 and Mill04 at pH 7.0 in ammonium and lithium sulfate, and calculated  $B_{22}$  values from two different fragment interaction models.

## 7.5 Conclusions

This work provides connections between mAb-mAb interaction strength ( $B_{22}$ ), oligomerization state – determined by AUC and DLS – and mAb fragment interaction strengths. First, the correlation between  $B_{22}$  and oligomerization tendency is clear – stronger mAb-mAb attraction results in increased hydrodynamic radius and thus oligomerization. However,  $B_{22}$  is a poor predictor of the oligomerization state. AUC results show that each mAb has different oligomerization patterns and species even if the overall interaction strengths are similar. Second osmotic virial coefficients are orientationally averaged measures of interaction and mAbs are highly anisotropic molecules. The oligomer species are driven by specific interactions, rather than overall attraction.

Fragment interactions were measured between Fc and Fab fragments to understand better the origin of attractive interactions that may lead to oligomerization and phase separation. As indicated by previous results (Kanai et al., 2008; Nishi et al., 2011; Yadav et al., 2011b; Yadav et al., 2012; Yagi et al., 2004), each mAb has different origins of attraction. Fab-Fab, Fc-Fc, Fc-Fab and Fc-mAb interactions were all found to be highly attractive interactions for different mAbs.

The development of two simple models provided some insight into how the fragment interactions might apply in the full mAb-mAb interactions. Fab-Fab and Fc-Fab interactions tend to have more influence on mAb behavior due to stoichiometric factors. Although the three-sphere model is highly idealized, Mill04 interactions are described well by multivalent interactions.

There are limitations and possible artifacts with this analysis as well. It appears that for at least two mAbs, hinge region interactions drive overall behavior. A finer-grained and detailed model would provide better insight into these interactions.

Analysis of fragment interaction strengths can give insights into the origin of highly attractive mAb-mAb interactions, such as in the case of Mill04, and the resulting oligomerization patterns. Although the  $B_{22}$  values for mAb-mAb interactions were similar for some of the mAbs studied here, the fragment interactions were very different. Domain-level interaction analysis demonstrates the significant differences between mAb products, despite highly conserved amino acid sequences. The sample size here is small, but it appears that the consequences of highly attractive Fab-Fab interactions are very different than Fc-Fc interactions. Investigation of a larger set of mAb fragments would be highly informative.

## **Chapter 8**

### **CONCLUSIONS AND RECOMMENDATIONS FOR FUTURE WORK**

#### **8.1 Conclusions**

The primary goal of this work was to identify and characterize difficult-to-remove HCP impurities in downstream platform purification of mAbs. The second goal was to measure self-interaction strengths and identify instantaneous phase boundaries for a diverse set of mAb products in different solution environments. Completion of these objectives has resulted in a number of insights that have practical implications for future mAb bioprocessing.

##### **8.1.1 HCP Impurities in MAb Bioprocessing**

The importance of HCP-mAb interactions in downstream purification was demonstrated in Chapters 3 and 4, which showed that attractive HCP-mAb interactions result in HCP impurities that are particularly difficult to remove. Building on previous work (Shukla and Hinckley, 2008), the total extent of HCP-mAb association was found to depend on individual mAb products more than the resin type or the solution environment. HCP-mAb product-association therefore appears to be a major mechanism through which HCP impurities co-purify with mAb products in different chromatographic processes.

The development of HCP-mAb CIC coupled with proteomic analysis allowed the identification of specific HCP impurities that associate with different mAbs in protein A and HIC columns. A subset of CHO HCP impurities that associate with all or most IgG products was identified with this method. The considerable sequence

homology between different mAbs results in a consistent group of associating HCPs. However, a unique set of HCP impurities that bind to each mAb was identified in addition to the HCPs that bind to all mAbs. Even minor changes to the primary sequence of mAbs were found to impact significantly the population of associating HCPs.

The identification of specific HCP impurities that product-associate is useful information. A variety of improvements to process development strategies can be made based on the identification of HCP impurities that were found to bind to all or most mAbs in both protein A affinity chromatography and HIC. However, the associating HCPs that are unique to each mAb still need to be dealt with on a case-by-case basis.

HCP impurities that have similar chromatographic properties to mAb products were identified in Chapter 4. In many cases the HCP species identified here will have been removed in the protein A affinity step, but a number of HCP impurities were identified that product-associate to mAbs in protein A columns and co-elute with mAbs in polishing columns. This work has provided a more detailed picture than previously available of how specific HCP impurities travel through downstream processes by both associating with mAbs and co-eluting.

The results in Chapter 4 can be applied beyond traditional mAb platform processing. The chromatographic properties of HCP impurities in four different columns could be applied for developing an alternative capture step. Also, because null CHO supernatant was used, the results are not specific to a particular mAb process. The HCP retentions determined here are relevant to the purification of any recombinant protein produced in CHO cell culture.

The study of LPL interactions with mAbs and activity against polysorbates in Chapter 5 serves as a specific example of the impact HCP impurities can have. LPL is an example of an HCP that causes indirect product degradation. Rather than directly affecting patients or product molecules, our results indicate that it can degrade additives in formulations that could then result in product degradation. Not only is LPL problematic if present in formulations, but it is also a member of the HCP subpopulation that binds to most mAb products.

There are a number of potential implementations of this work that could have significant positive impact on mAb platform manufacturing processes. The development of ‘knock-out’ cell lines for the specific HCP impurities identified as difficult to remove and harmful to product quality is one potential application of this work. This would completely eliminate the purification challenge of particular HCP impurities. However, there are a large number of HCPs that associate with most mAbs and it is unlikely that all of them are unnecessary for host-cell proliferation.

For HCP species that cannot be ‘knocked-out’ of production cell lines there are additional actions that can be taken. The list of HCPs generated in this work allows for more specific monitoring than traditional ELISA methods. In addition to measuring total HCP content with ELISA, specific HCP impurities can be monitored. Without the identity of HCP impurities that are frequently problematic, monitoring specific HCP impurities at process intermediates can be a difficult task. With the HCP identities provided here, antibodies against specific HCPs can be used to monitor clearance of associating HCPs throughout downstream processes. This would provide much more valuable information than only an ELISA for making process-development decisions based on HCP clearance.

### 8.1.2 MAb-MAb Interactions and Phase Boundaries

Instantaneous phase boundaries and self-interactions of a large set of mAbs were studied in Chapters 6 and 7. This work builds on previous results for mAb-mAb interactions and phase boundaries (Lewus, 2011; Lewus et al., 2011) and similar work with model proteins (Dumetz et al., 2008b). Overall, it was found that self-interactions and phase boundaries are similar for most IgG products. In solutions of sulfate salts most of the mAbs studied had nearly identical  $B_{22}$  trends and instantaneous phase boundaries. The relationship between  $B_{22}$  and phase-boundary location was qualitatively similar for all mAbs as well. Most mAbs have nearly identical salting-out behavior, although there are highly stable mAbs as well as unstable mAbs with outlying behavior that were also identified. The divergent behavior of mAbs D and  $D_M$  shows the considerable impact of minor structural changes on product molecules. These results are consistent with previous work indicating the impact of charged residues near the CDR (Yadav et al., 2011b).

$B_{22}$  is an effective measure of overall interaction strength and a good predictor of phase-boundary location as well as oligomerization. However, as was found here,  $B_{22}$  is not a good predictor of oligomer species formed. MAbs with similarly negative  $B_{22}$  values were found to form very different oligomer species as salt concentrations were increased. This is largely due to the anisotropy of mAbs and their interactions.

The interaction patterns of different mAb fragments indicated the origin of some highly attractive mAb interactions as well as more stable mAb behavior in solution. These results showed that strong self-attraction is often due to specific fragment interactions. The fragment interactions were measured for four mAbs and all four had different origins of attraction. Fc-Fc, Fab-Fab, Fab-mAb and Fc-mAb were all found to be highly attractive in different molecules. Although mAbs are highly

similar molecules, small differences in structure can lead to large differences in how they interact and their solution stability.  $B_{22}$  measurements of mAb-mAb interactions are useful for predicting phase-boundary locations and conditions conducive to oligomerization. Because mAbs are large, anisotropic molecules that are sensitive to minor structural changes, more detailed domain-based analysis can provide much greater insight into oligomerization mechanisms and potentially allow engineering of more stable mAbs.

## **8.2 Future Work**

The work completed here has contributed significantly to the understanding of HCP and mAb behavior in downstream purification of mAbs. The findings can be applied in a number of ways to improve platform purification processes.

### **8.2.1 Improved Upstream Technology**

This work was focused on various aspects of downstream purification, but applying the results here to upstream processes can be highly beneficial as well. HCP impurities that were found to cause purification difficulties could be eliminated completely by engineering ‘knock-out’ cell lines. Specifically, ‘knock-outs’ would be valuable for the HCP impurities that were found to associate to multiple mAbs across multiple column-types. CHO HCP species such as chondroitin sulfate proteoglycan 4, nidogen-1, SPARC and clusterin are examples of such impurities.

For many of these CHO HCPs there is limited prior research, so it is unclear if they are necessary for mAb-producing cell lines. It is unlikely that all of the problematic HCPs identified in this work could be eliminated from cell lines without negatively impacting upstream productivity. The payoff of removing difficult HCPs

from production cell lines – even only a few that bind to most products – could have a significant impact on downstream purification efforts.

### **8.2.2 Yeast-Surface Display Technology Development**

The LPL-mAb interaction measurements using YSD methods in Chapter 5 provide a proof-of-concept for future work. The results of Chapter 5 showed that HCP-mAb interactions that result in product-association in downstream processes are measurable using YSD. Starting with the population of difficult-to-remove CHO HCPs identified in this work, these results can be expanded significantly.

First, the analysis completed for LPL can be completed for the rest of the identified HCP impurities. Each HCP impurity of interest can be individually expressed on the yeast surface. The  $K_D$  of each HCP with different mAbs and mAb fragments could be measured in a variety of solution conditions. The mAb-HCP interaction strength could also be measured in potential wash solutions in order to design washes to remove specific product-associated HCPs. Established epitope-mapping techniques could also be used to identify the residues on the HCP responsible for mAb association (Chao et al., 2004).

The second major part of this work would be to express mAbs or individual mAb domains on the yeast surface. The HCP impurities of interest would then be expressed in CHO cells, purified and fluorescently labeled. The same mAb-HCP interaction measurements could then be made as described above. More interestingly, the epitope mapping analysis could be applied the mAb. Specific residues on the mAb responsible for association to various HCPs could be identified and mutated to prevent HCP-mAb associations. Specifically for HCP impurities that cannot be knocked out, this could be a powerful strategy to improve downstream process efficiencies.

It is also possible to analyze mAb-mAb interactions using this method. Labeled mAb could be added to yeast cells expressing mAbs or mAb fragments on the surface and mAb-mAb interaction strengths could be measured. The same epitope mapping strategy can then be applied and mutations on the mAb that lead to decreased binding could be identified. This will provide additional mechanistic insight to the mAb-mAb interactions measured in Chapters 6 and 7. Similar work has been done previously for antibody fragments (Traxlmayr et al., 2013).

### **8.2.3 High-Throughput Product-Association Method Development**

The HCP-CIC method developed in Chapter 3 to identify product-associated HCP was implemented at the 1 mL column scale. It would be of great value to the biopharmaceutical industry to have a more high-throughput CIC method.

A high-throughput CIC method could be accomplished with minimal changes to the procedure. MAb could be immobilized onto activated particles according to the current method. The immobilized-mAb resin then would be dispensed into a 96-well plate rather than a single column. The resin would be equilibrated with protein A loading buffer, followed by filtration to remove the equilibration buffer and the addition of null CHO supernatant. After equilibration with the HCP mixture the resin would again be washed with equilibration buffer. Then, potential column washes can be assessed in each well. Test washes would be added to wells, followed by filtration to collect the wash fractions.

The analysis from this procedure could take a few forms that would provide different information. The simplest analysis would be to measure the total protein content in each collected fraction by total protein assay (such as BCA or Bradford) or ELISA. The more valuable information would come from identifying specific HCP

impurities cleared by different wash solutions. Antibodies against the HCPs of interest (those identified in Chapters 3 and 4) could be used to choose the most appropriate wash solution.

If more detail is desired, the same 96-well plate could be run, but a more comprehensive proteomic technique could be used. LC/LC/MS could be run for each wash fraction to have a more global analysis of specific HCP impurities removed by each candidate column-wash solution.

#### **8.2.4 MAb-HCP Interaction Calculations**

LPL-Fc and nidogen-1-Fc interaction orientation calculations were started in the present work. The limited results presented here revealed a number of attractive orientations. It would be interesting and informative to expand this set of results. There are additional homology models available for HCP impurities of interest and there are different Fc and Fab crystal structures available as well.

This method could be run in parallel to the YSD epitope mapping. Identified interaction sites based on these calculations could be verified using YSD and vice versa. Mutations to mAbs could be made to disrupt the identified HCP interactions. Such analysis, along with YSD analysis, can provide clear molecular-level insights into mAb-HCP interactions that can have an impact on mAb processing and antibody engineering and design.

#### **8.2.5 HCP Analysis for Alternative Cell Lines**

This work focused specifically on CHO HCP impurities because mAbs are a large portion of biopharmaceutical pipelines and they are almost exclusively produced in CHO cells. Antibody fragments such as single-chain variable fragments (scFv) as

well as Fc fusion proteins are becoming more popular as potential therapeutics (Beck and Reichert, 2011; Holt et al., 2003; Nelson, 2010). These product molecules are commonly produced in *E. coli* cell culture rather than CHO (Huang et al., 2012; Kudou et al., 2011; Padiolleau-Lefevre et al., 2007). Bacterial cell culture processes require a lysis step because products are not secreted as they are with mammalian cells. Cell lysis results in the release of a large amount of HCP into the harvest. Many antibody fragment therapeutics do not have well-established platform purification processes, which could make insights into HCP behavior even more useful. A better understanding of HCP impurities in bacterial cell-culture processing of non-mAb therapeutics could be valuable, especially if these classes of therapeutics continue to grow in popularity.

## REFERENCES

- Adams ET Jr, Wan PJ, Crawford EF. 1978. Membrane and vapor pressure osmometry. *Methods in enzymology* **48**:69.
- Aggarwal S. 2014. What's fueling the biotech engine-2012 to 2013. *Nature Biotechnology*.
- Ahamed T, Esteban BNA, Ottens M, van Dedem GWK, van der Wielen LAM, Bisschops MAT, Lee A, Pham C, Thommes J. 2007. Phase behavior of an intact monoclonal antibody. *Biophysical Journal* **93**:610–619.
- Ahamed T, Ottens M, van Dedem GWK, van der Wielen LAM. 2005. Design of self-interaction chromatography as an analytical tool for predicting protein phase behavior. *Journal of Chromatography A* **1089**:111–124.
- Ahrer K, Jungbauer A. 2006. Chromatographic and electrophoretic characterization of protein variants. *Journal of Chromatography B* **841**:110–122.
- Andley UP, Hamilton PD, Ravi N. 2008. Mechanism of insolubilization by a single-point mutation in  $\alpha$ A-crystallin linked with hereditary human cataracts. *Biochemistry* **47**:9697–9706.
- Andrésen C, Jalal S, Aili D, Wang Y, Islam S, Jarl A, Liedberg B, Wretling B, Mårtensson L-G, Sunnerhagen M. 2010. Critical biophysical properties in the *Pseudomonas aeruginosa* efflux gene regulator MexR are targeted by mutations conferring multidrug resistance. *Protein Science* **19**:680–692.
- Arnold K, Bordoli L, Kopp J, Schwede T. 2006. The SWISS-MODEL workspace: a web-based environment for protein structure homology modelling. *Bioinformatics* **22**:195–201.
- Arosio P, Barolo G, Müller-Späh T, Wu H, Morbidelli M. 2011. Aggregation stability of a monoclonal antibody during downstream processing. *Pharmaceutical research* **28**:1884–1894.
- Arosio P, Jaquet B, Wu H, Morbidelli M. 2012. Biophysical Chemistry. *Biophysical Chemistry* **168-169**:19–27.
- Arthur KK, Gabrielson JP, Hawkins N, Anafi D, Wypych J, Nagi A, Sullivan JK, Bondarenko PV. 2012. In vitro stoichiometry of complexes between the soluble

- RANK ligand and the monoclonal antibody Denosumab. *Biochemistry* **51**:795–806.
- Arthur KK, Gabrielson JP, Kendrick BS, Stoner MR. 2009. Detection of protein aggregates by sedimentation velocity analytical ultracentrifugation (SV-AUC): Sources of variability and their relative importance. *Journal of Pharmaceutical Sciences* **98**:3522–3539.
- Arzena D, Kuzman D, Podgornik R. 2012. Colloidal interactions between monoclonal antibodies in aqueous solutions. *Journal of Colloid And Interface Science* **384**:207–216.
- Asthagiri D, Neal BL, Lenhoff AM. 1999. Calculation of short-range interactions between proteins. *Biophysical Chemistry* **78**:219–231.
- Asthagiri D, Paliwal A, Abras D, Lenhoff AM, Paulaitis ME. 2005. A consistent experimental and modeling approach to light-scattering studies of protein-protein interactions in solution. *Biophysical Journal* **88**:3300–3309.
- Beck A, Reichert JM. 2011. Therapeutic Fc-fusion proteins and peptides as successful alternatives to antibodies. *mabs* **3**:415–416.
- Bjellqvist B, Hughes GJ, Pasquali C, Paquet N, Ravier F, Sanchez JC, Frutiger S, Hochstrasser DF. 1993. The focusing positions of polypeptides in immobilized pH gradients can be predicted from their amino acid sequences. *Electrophoresis* **14**:1023–1031.
- Boder ET, Wittrup KD. 1997. Yeast surface display for screening combinatorial polypeptide libraries. *Nature Biotechnology* **15**:553–557.
- Bomans K, Lang A, Roedl V, Adolf L, Kyriosoglou K, Diepold K, Eberl G, Mølhøj M, Strauss U, Schmalz C, Vogel R, Reusch D, Wegele H, Wiedmann M, Bulau P. 2013. Identification and monitoring of host cell proteins by mass spectrometry combined with high performance immunochemistry testing. Ed. William R Abrams. *PLoS ONE* **8**.
- Brown A, Bill J, Tully T, Radhamohan A, Dowd C. 2010. Overloading ion-exchange membranes as a purification step for monoclonal antibodies. *Biotechnology and Applied Biochemistry* **56**:59–70.
- Brown PH, Schuck P. 2006. Macromolecular Size-and-Shape Distributions by Sedimentation Velocity Analytical Ultracentrifugation. *Biophysical Journal* **90**:4651–4661.
- Butler M, Meneses-Acosta A. 2012. Recent advances in technology supporting biopharmaceutical production from mammalian cells. *Applied Microbiology and Biotechnology* **96**:885–894.
- Buyel JF, Woo JA, Cramer SM, Fischer R. 2013. The use of quantitative structure-activity relationship models to develop optimized processes for the removal of

- tobacco host cell proteins during biopharmaceutical production. *Journal of Chromatography A* **1322**:18–28.
- Calmettes P, Cser L, Rajnavölgyi É. 1991. Temperature and pH dependence of immunoglobulin G conformation. *Archives of Biochemistry and Biophysics* **291**:277–283.
- Capito F, Bauer J, Rapp A, Schroeter C, Kolmar H, Stanislawski B. 2013. Feasibility study of semi-selective protein precipitation with salt-tolerant copolymers for industrial purification of therapeutic antibodies. *Biotechnology and bioengineering* **110**:2915–2927.
- Carver JA, Guerreiro N, Nicholls KA, Truscott RJ. 1995. On the interaction of  $\alpha$ -crystallin with unfolded proteins. *Biochimica et Biophysica Acta (BBA)-Protein Structure and Molecular Enzymology* **1252**:251–260.
- Champion K, Madden H, Dougherty J, Shacter E. 2005. Defining your product profile and maintaining control over it, part 2. *BioProcess International* **5**:52–57.
- Chao G, Cochran JR, Dane Wittrup K. 2004. Fine epitope mapping of anti-epidermal growth factor receptor antibodies through random mutagenesis and yeast surface display. *Journal of Molecular Biology* **342**:539–550.
- Chao G, Lau WL, Hackel BJ, Sazinsky SL, Lippow SM, Wittrup KD. 2006. Isolating and engineering human antibodies using yeast surface display. *Nature Protocols* **1**:755–768.
- Chari R, Jerath K, Badkar AV, Kalonia DS. 2009. Long- and short-range electrostatic interactions affect the rheology of highly concentrated antibody solutions. *Pharmaceutical research* **26**:2607–2618.
- Chaudhri A, Zarraga IE, Kamerzell TJ, Brandt JP, Patapoff TW, Shire SJ, Voth GA. 2012. Coarse-grained modeling of the self-association of therapeutic monoclonal antibodies. *The Journal of Physical Chemistry B* **116**:8045–8057.
- Chaudhuri R, Cheng Y, Middaugh CR, Volkin DB. 2013. High-throughput biophysical analysis of protein therapeutics to examine interrelationships between aggregate formation and conformational stability. *AAPS J* **16**:48–64.
- Chen J, Tetrault J, Zhang Y, Wasserman A, Conley G, DiLeo M, Haines E, Nixon AE, Ley A. 2010. The distinctive separation attributes of mixed-mode resins and their application in monoclonal antibody downstream purification process. *Journal of Chromatography A* **1217**:216–224.
- Chen J, Tetrault J, Ley A. 2008. Comparison of standard and new generation hydrophobic interaction chromatography resins in the monoclonal antibody purification process. *Journal of Chromatography A* **1177**:272–281.
- Chen J, Yang T, Luo Q, Breneman CM, Cramer SM. 2007. Investigation of protein retention in hydrophobic interaction chromatographic (HIC) systems using the

- preferential interaction theory and quantitative structure property relationship models. *Reactive and Functional Polymers* **67**:1561–1569.
- Cheng CF, Bensadoun A, Bersot T, Hsu JS, Melford KH. 1985. Purification and characterization of human lipoprotein lipase and hepatic triglyceride lipase. Reactivity with monoclonal antibodies to hepatic triglyceride lipase. *Journal of Biological Chemistry* **260**:10720–10727.
- Cheng Y-C, Bianco CL, Sandler SI, Lenhoff AM. 2008. Salting-out of lysozyme and ovalbumin from mixtures: predicting precipitation performance from protein–protein Interactions. *Industrial & Engineering Chemistry Research* **47**:5203–5213.
- Chick H, Martin CJ. 1913. The precipitation of egg-albumin by ammonium sulphate. A contribution to the theory of the “salting-out” of proteins. *Biochemical Journal* **7**:380–398.
- Christiansen A, Backensfeld T, Weitschies W. 2010. Effects of non-ionic surfactants on in vitro triglyceride digestion and their susceptibility to digestion by pancreatic enzymes. *European Journal of Pharmaceutical Sciences* **41**:376–382.
- Chung WK, Hou Y, Freed A, Holstein M, Makhatadze GI, Cramer SM. 2009. Investigation of protein binding affinity and preferred orientations in ion exchange systems using a homologous protein library. *Biotechnology and bioengineering* **102**:869–881.
- Coffman JL, Kramarczyk JF, D Kelley B. 2008. High-throughput screening of chromatographic separations: I. Method development and column modeling. *Biotechnology and bioengineering* **100**:605–618.
- Cohn EJ, Strong LE, Hughes W, Mulford DJ, Ashworth JN, Melin ME, Taylor HL. 1946. Preparation and properties of serum and plasma proteins. IV. A system for the separation into fractions of the protein and lipoprotein components of biological tissues and fluids. *Journal of the American Chemical Society* **68**:459–475.
- Collins KD. 2004. Ions from the Hofmeister series and osmolytes: effects on proteins in solution and in the crystallization process. *Methods* **34**:300–311.
- Connell-Crowley L, Nguyen T, Bach J, Chinniah S, Bashiri H, Gillespie R, Moscariello J, Hinckley P, Dehghani H, Vunnum S, Vedantham G. 2011. Cation exchange chromatography provides effective retrovirus clearance for antibody purification processes. *Biotechnology and bioengineering* **109**:157–165.
- Connolly BD, Petry C, Yadav S, Demeule B, Ciaccio N, Moore JMR, Shire SJ, Gokarn YR. 2012. Weak interactions govern the viscosity of concentrated

- antibody solutions: high-throughput analysis using the diffusion interaction parameter. *Biophysical Journal* **103**:69–78.
- Curling J, Gottschalk U. 2007. Process chromatography: five decades of innovation. *BioPharm International* **20**:70–83.
- Curtis RA, Montaser A, Prausnitz JM, Blanch HW. 1998. Protein-protein and protein-salt interactions in aqueous protein solutions containing concentrated electrolytes (vol 57, pg 11, 1997). *Biotechnology and bioengineering* **58**:451–451.
- Curtis RA, Prausnitz JM, Blanch HW. 2000. Protein-protein and protein-salt interactions in aqueous protein solutions containing concentrated electrolytes. *Biotechnology and bioengineering* **57**:11–21.
- Daugherty AL, Mersny RJ. 2006. Formulation and delivery issues for monoclonal antibody therapeutics. *Advanced Drug Delivery Reviews* **58**:686–706.
- Davis RC, Wong H, Nikazy J, Wang K, Han Q, Schotz MC. 1992. Chimeras of hepatic lipase and lipoprotein lipase. Domain localization of enzyme-specific properties. *Journal of Biological Chemistry* **267**:21499–21504.
- De Jesus M, Wurm FM. 2011. Manufacturing recombinant proteins in kg-ton quantities using animal cells in bioreactors. *European Journal of Pharmaceutics and Biopharmaceutics* **78**:184–188.
- Deisenhofer J. 1981. Crystallographic refinement and atomic models of a human Fc fragment and its complex with fragment B of protein A from *Staphylococcus aureus* at 2.9- and 2.8-Å resolution. *Biochemistry* **20**:2361–2370.
- DePhillips P, Lenhoff AM. 2000. Pore size distributions of cation-exchange adsorbents determined by inverse size-exclusion chromatography. *Journal of Chromatography A* **883**:39–54.
- Dolinsky TJ, Nielsen JE, McCammon JA, Baker NA. 2004. PDB2PQR: an automated pipeline for the setup of Poisson-Boltzmann electrostatics calculations. *Nucleic Acids Research* **32**:W665–W667.
- Doneanu C, Xenopoulos A, Fadgen K, Murphy J, Skilton SJ, Prentice H, Stapels M, Chen W. 2012. Analysis of host-cell proteins in biotherapeutic proteins by comprehensive online two-dimensional liquid chromatography/mass spectrometry. *mabs* **4**:24–44.
- Doolan KM, Colby DW. 2014. Conformation dependent epitopes of prion protein antibodies probed by mutational scanning and deep sequencing (Submitted).
- Dumetz AC, Chockla AM, Kaler EW. 2008a. Effects of pH on protein-protein interactions and implications for protein phase behavior. *Biochimica et Biophysica Acta*.
- Dumetz AC, Chockla AM, Kaler EW, Lenhoff AM. 2008b. Protein phase behavior in

- aqueous solutions: crystallization, liquid-liquid phase separation, gels, and aggregates. *Biophysical Journal* **94**:570–583.
- Dumetz AC, Lewus RA, Lenhoff AM, Kaler EW. 2008c. Effects of ammonium sulfate and sodium chloride concentration on PEG/protein liquid–liquid phase separation. *Langmuir* **24**:10345–10351.
- Dumetz AC, Snellinger-O'Brien AM, Kaler EW, Lenhoff AM. 2007. Patterns of protein-protein interactions in salt solutions and implications for protein crystallization. *Protein Science* **16**:1867–1877.
- Eigenbrot C, Ultsch M, Dubnovitsky A, Abrahmsen L, Hard T. 2010. Structural basis for high-affinity HER2 receptor binding by an engineered protein. *Proceedings of the National Academy of Sciences* **107**:15039–15044.
- Ejima D, Tsumoto K, Fukada H, Yumioka R, Nagase K, Arakawa T, Philo JS. 2006. Effects of acid exposure on the conformation, stability, and aggregation of monoclonal antibodies. *Proteins* **66**:954–962.
- Elcock AH, McCammon JA. 2001. Calculation of weak protein-protein interactions: The pH dependence of the second virial coefficient. *Biophysical Journal* **80**:613–625.
- Emmerich J, Beg OU, Peterson J, Previato L, Brunzell JD, Brewer HB, Santamarina-Fojo S. 1992. Human lipoprotein lipase. Analysis of the catalytic triad by site-directed mutagenesis of Ser-132, Asp-156, and His-241. *Journal of Biological Chemistry* **267**:4161–4165.
- FDA. 1999. Guidance for Industry. Food and Drug Administration.
- Feher G, Kam Z. 1984. Nucleation and growth of protein crystals: general principles and assays. *Methods in enzymology* **114**:77–112.
- Fogle J, Mohan N, Cheung E, Persson J. 2012. Effects of resin ligand density on yield and impurity clearance in preparative cation exchange chromatography. I. Mechanistic evaluation. *Journal of Chromatography A* **1225**:62–69.
- Fogle J, Persson J. 2012. Effects of resin ligand density on yield and impurity clearance in preparative cation exchange chromatography. II. Process characterization. *Journal of Chromatography A* **1225**:70–78.
- Follman D, Farner R. 2004. Factorial screening of antibody purification processes using three chromatography steps without protein A. *Journal of Chromatography A* **1024**:79–85.
- Gabrielson JP, Randolph TW, Kendrick BS, Stoner MR. 2007. Sedimentation velocity analytical ultracentrifugation and SEDFIT/c(s): Limits of quantitation for a monoclonal antibody system. *Analytical Biochemistry* **361**:24–30.
- Gai SA, Wittrup KD. 2007. Yeast surface display for protein engineering and

- characterization. *Current Opinion in Structural Biology* **17**:467–473.
- Galkin O, Vekilov PG. 2001. Nucleation of protein crystals: critical nuclei, phase behavior, and control pathways. *Journal of crystal growth* **232**:63–76.
- Gao SX, Zhang Y, Stansberry-Perkins K, Buko A, Bai S, Nguyen V, Brader ML. 2010. Fragmentation of a highly purified monoclonal antibody attributed to residual CHO cell protease activity. *Biotechnology and bioengineering* **108**:977–982.
- Gasteiger E, Hoogland C, Gattiker A, Duvaud S, Wilkins MR, Appel RD, Bairoch A. 2005. Protein identification and analysis tools on the ExPASy server. In: Walker, JM, editor. *The Proteomics Protocols Handbook*. Humana Press, pp. 571–607.
- George A, Wilson WW. 1994. Predicting protein crystallization from a dilute solution property. *Acta Crystallographica Section D Biological Crystallography* **50**:361–365.
- Gerba CP, Hou K. 1985. Endotoxin removal by charge-modified filters. *Applied and environmental microbiology* **50**:1375–1377.
- Ghose S, Hubbard B, Cramer SM. 2007. Binding capacity differences for antibodies and Fc-fusion proteins on protein A chromatographic materials. *Biotechnology and bioengineering* **96**:768–779.
- Ghose S, Tao Y, Conley L, Cecchini D. 2013. Purification of monoclonal antibodies by hydrophobic interaction chromatography under no-salt conditions. *mabs* **5**:795–800.
- Gill DS, Roush DJ, Willson RC. 1994. Adsorption heterogeneity and thermodynamic driving forces in anion exchange equilibria of cytochrome b<sub>5</sub>. *Journal of Colloid And Interface Science* **167**:1–7.
- Gillespie CM, Asthagiri D, Lenhoff AM. 2014. Polymorphic protein crystal growth: influence of hydration and ions in glucose isomerase. *Crystal Growth & Design* **14**:46–57.
- Goldsby RA. 2003. Immunology. Macmillan.
- Grzeskowiak JK, Tscheliessnig A, Toh PC, Chusainow J, Lee YY, Wong N, Jungbauer A. 2009. 2-D DIGE to expedite downstream process development for human monoclonal antibody purification. *Protein Expression and Purification* **66**:58–65.
- Guiochon G, Beaver LA. 2011. Separation science is the key to successful biopharmaceuticals. *Journal of Chromatography A* **1218**:8836–8858.
- Gutiérrez AH, Moise L, De Groot AS. 2012. Of [hamsters] and men: A new perspective on host cell proteins. *Human vaccines & immunotherapeutics* **8**:1172.
- Ha E, Wang W, Wang YJ. 2002. Peroxide formation in polysorbate 80 and protein

- stability. *Journal of Pharmaceutical Sciences* **91**:2252–2264.
- Haas C, Drenth J, Wilson WW. 1999. Relation between the solubility of proteins in aqueous solutions and the second virial coefficient of the solution. *The Journal of Physical Chemistry B* **103**:2808–2811.
- Hallgren E, Kálmán F, Farnan D, Horváth C, Ståhlberg J. 2000. Protein retention in ion-exchange chromatography: effect of net charge and charge distribution. *Journal of Chromatography A* **877**:13–24.
- Hamilton RG. 2001. The human IgG subclasses. Ed. Chandra Mohan. Calbiochem-Novabiochem Corporation.
- Hammond S, Lee KH. 2011. RNA interference of cofilin in Chinese hamster ovary cells improves recombinant protein productivity. *Biotechnology and bioengineering* **109**:528–535.
- Hari SB, Lau H, Razinkov VI, Chen S, Latypov RF. 2010. Acid-induced aggregation of human monoclonal IgG1 and IgG2: molecular mechanism and the effect of solution composition. *Biochemistry* **49**:9328–9338.
- Harris LJ, Skaletsky E, McPherson A. 1995. Crystallization of intact monoclonal antibodies. *Proteins* **23**:285–289.
- Hayakawa S, Nakai S. 1985. Relationships of hydrophobicity and net charge to the solubility of milk and soy proteins. *Journal of Food Science* **50**:486–491.
- Hayduk E, Choe L, Lee K. 2004. A two-dimensional electrophoresis map of Chinese hamster ovary cell proteins based on fluorescence staining. *Electrophoresis* **25**:2545–2556.
- Hloucha M, Lodge J, Lenhoff AM, Sandler SI. 2001. A patch–antipatch representation of specific protein Interactions. *Journal of crystal growth* **232**:195–203.
- Hofmeister F. 1888. Zur lehre der wirkung der salze. Zweite mittheilung. *Arch Exp Pathol Pharmacol* **24**:247–260.
- Hogwood CEM, Tait AS, Koloteva Levine N, Bracewell DG, Smales CM. 2012. The dynamics of the CHO host cell protein profile during clarification and protein A capture in a platform antibody purification process. *Biotechnology and bioengineering*.
- Holstein MA, Nikfetrat AAM, Gage M, Hirsh AG, Cramer SM. 2012. Improving selectivity in multimodal chromatography using controlled pH gradient elution. *Journal of Chromatography A* **1233**:152–155.
- Holt LJ, Herring C, Jaspers LS, Woolven BP, Tomlinson IM. 2003. Domain antibodies: proteins for therapy. *Trends In Biotechnology* **21**:484–490.

- Howell JM, Winstone TL, Coorssen JR, Turner RJ. 2006. An evaluation of in vitro protein–protein interaction techniques: Assessing contaminating background proteins. *Proteomics* **6**:2050–2069.
- Howlett G, Minton A, Rivas G. 2006. Analytical ultracentrifugation for the study of protein association and assembly. *Current Opinion in Chemical Biology* **10**:430–436.
- Huang C-J, Lin H, Yang X. 2012. Industrial production of recombinant therapeutics in *Escherichia coli* and its recent advancements. *Journal of Industrial Microbiology & Biotechnology* **39**:383–399.
- Hunter AK, Wang X, Suda EJ, Herberg JT, Shell RE, Thomas KE, Dufield RL, Gustafson ME, Mozier NM, Ho SV. 2009. Separation of product associating *E. coli* host cell proteins OppA and DppA from recombinant apolipoprotein A-I<sub>milano</sub> in an industrial HIC unit operation. *Biotechnology Progress* **25**:446–453.
- Jayapal KP, Wlaschin KF, Hu W, Yap MG. 2007. Recombinant protein therapeutics from CHO cells-20 years and counting. *Chemical Engineering Progress* **103**:40.
- Jefferis R, Lund J, Pound JD. 1998. IgG-Fc-mediated effector functions: molecular definition of interaction sites for effector ligands and the role of glycosylation. *Immunological reviews* **163**:59–76.
- Jin M, Szapiel N, Zhang J, Hickey J, Ghose S. 2010. Profiling of host cell proteins by two-dimensional difference gel electrophoresis (2D-DIGE): Implications for downstream process development. *Biotechnology and bioengineering* **105**:306–316.
- Jorgensen WL, Tirado-Rives J. 1988. The OPLS [optimized potentials for liquid simulations] potential functions for proteins, energy minimizations for crystals of cyclic peptides and crambin. *Journal of the American Chemical Society* **110**:1657–1666.
- Joucla G, Le Sénéchal C, Bégorre M, Garbay B, Santarelli X, Cabanne C. 2013. Cation exchange versus multimodal cation exchange resins for antibody capture from CHO supernatants: identification of contaminating host cell proteins by mass spectrometry. *Journal of Chromatography B* **942-943**:126–133.
- Judge RA, Johns MR, White CA. 1995. Protein-purification by bulk crystallization - the recovery of ovalbumin. *Biotechnology and bioengineering* **48**:316–323.
- Kallberg K, Johansson HO, Bulow L. 2012. Multimodal chromatography: An efficient tool in downstream processing of proteins. *Biotechnology Journal* **7**:1485–1495.
- Kanai S, Liu J, Patapoff TW, Shire SJ. 2008. Reversible self-association of a concentrated monoclonal antibody solution mediated by Fab-Fab interaction that impacts solution viscosity. *Journal of Pharmaceutical Sciences* **97**:4219–4227.

- Karush F. 1978. The affinity of antibody: range, variability, and the role of multivalence:85–116.
- Kayser V, Chennamsetty N, Voynov V, Helk B, Trout BL. 2011. Conformational stability and aggregation of therapeutic monoclonal antibodies studied with ANS and Thioflavin T binding. *mabs* **3**:408–411.
- Kenig M, Berbic S, Krijestorac A, Kroon-Zitko L, Tusek M, Pompe-Novak M, Zerovnik E. 2004. Differences in aggregation properties of three site-specific mutants of recombinant human stefin B. *Protein Science* **13**:63–70.
- Kerwin BA. 2008. Polysorbates 20 and 80 used in the formulation of protein biotherapeutics: Structure and degradation pathways. *Journal of Pharmaceutical Sciences* **97**:2924–2935.
- Khosravi M, Kao Y-H, Mrsny RJ, Sweeney TD. 2002. Analysis methods of polysorbate 20: a new method to assess the stability of polysorbate 20 and established methods that may overlook degraded polysorbate 20. *Pharmaceutical research* **19**:634–639.
- Kiese S, Pappenger A, Friess W, Mahler H-C. 2008. Shaken, not stirred: mechanical stress testing of an IgG1 antibody. *Journal of Pharmaceutical Sciences* **97**:4347–4366.
- Kishore RSK, Kiese S, Fischer S, Pappenger A, Grauschopf U, Mahler H-C. 2011. The degradation of polysorbates 20 and 80 and its potential impact on the stability of biotherapeutics. *Pharmaceutical research* **28**:1194–1210.
- Kishore RSK, Pappenger A, Dauphin IB, Ross A, Buergi B, Staempfli A, Mahler H-C. 2010. Degradation of polysorbates 20 and 80: studies on thermal autoxidation and hydrolysis. *Journal of Pharmaceutical Sciences* **100**:721–731.
- Kobayashi Y, Nakajima T, Inoue I. 2002. Molecular modeling of the dimeric structure of human lipoprotein lipase and functional studies of the carboxyl-terminal domain. *European journal of biochemistry* **269**:4701–4710.
- Kramarczyk JF, Kelley BD, Coffman JL. 2008. High-throughput screening of chromatographic separations: II. Hydrophobic interaction. *Biotechnology and bioengineering* **100**:707–720.
- Krawitz D, Forrest W, Moreno G, Kittleson J, Champion K. 2006. Proteomic studies support the use of multi-product immunoassays to monitor host cell protein impurities. *Proteomics* **6**:94–110.
- Kröner F, Hanke AT, Nfor BK, Pinkse MWH, Verhaert PDEM, Ottens M, Hubbuch J. 2013. Analytical characterization of complex, biotechnological feedstocks by pH gradient ion exchange chromatography for purification process development. *Journal of Chromatography A* **1311**:55–64.

- Kudou M, Ejima D, Sato H, Yumioka R, Arakawa T, Tsumoto K. 2011. Refolding single-chain antibody (scFv) using lauroyl-L-glutamate as a solubilization detergent and arginine as a refolding additive. *Protein Expression and Purification* **77**:68–74.
- Kunz W, Henle J, Ninham BW. 2004. “Zur Lehre von der Wirkung der Salze” (about the science of the effect of salts): Franz Hofmeister's historical papers. *Current Opinion in Colloid & Interface Science* **9**:19–37.
- Kupke DW. 1960. Osmotic Pressure. In: Anfinsen, CB, editor. *Advances in protein chemistry*. Academic Press Inc., Vol. 15, pp. 57–130.
- Kyte J, Doolittle RF. 1982. A simple method for displaying the hydropathic character of a protein. *Journal of Molecular Biology* **157**:105–132.
- Le Brun V, Friess W, Schultz-Fademrecht T, Muehlau S, Garidel P. 2009. Lysozyme-lysozyme self-interactions as assessed by the osmotic second virial coefficient: Impact for physical protein stabilization. *Biotechnology Journal* **4**:1305–1319.
- Lebowitz J, Lewis MS, Schuck P. 2009. Modern analytical ultracentrifugation in protein science: A tutorial review. *Protein Science* **11**:2067–2079.
- Lee HJ, McAuley A, Schilke KF, McGuire J. 2011. Molecular origins of surfactant-mediated stabilization of protein drugs. *Advanced Drug Delivery Reviews* **63**:1160–1171.
- Lehermayr C, Mahler H-C, Mäder K, Fischer S. 2011. Assessment of net charge and protein-protein interactions of different monoclonal antibodies. *Journal of Pharmaceutical Sciences* **100**:2551–2562.
- Levy NE, Valente KN, Choe LH, Lee KH, Lenhoff AM. 2013. Identification and characterization of host cell protein product-associated impurities in monoclonal antibody bioprocessing. *Biotechnology and bioengineering*.
- Lewis RA. 2011. Monoclonal antibody interactions and phase behavior; University of Delaware.
- Lewis RA, Darcy PA, Lenhoff AM, Sandler SI. 2011. Interactions and phase behavior of a monoclonal antibody. *Biotechnology Progress* **27**:280–289.
- Li J, Zhu Z. 2010. Research and development of next generation of antibody-based therapeutics. *Nature Publishing Group* **31**:1198–1207.
- Lim Y, Wong NSC, Lee YY, Ku SCY, Wong DCF, Yap MGS. 2010. Engineering mammalian cells in bioprocessing – current achievements and future perspectives. *Biotechnology and Applied Biochemistry* **55**:175–189.
- Liu HF, Ma J, Winter C, Bayer R. 2010. Recovery and purification process development for monoclonal antibody production. *mabs* **2**:480–499.

- Liu HF, McCooley B, Duarte T, Myers DE, Hudson T, Amanullah A, van Reis R, Kelley BD. 2011. Exploration of overloaded cation exchange chromatography for monoclonal antibody purification. *Journal of Chromatography A* **1218**:6943–6952.
- Luhrs KA, Harris DA, Summers S, Parseghian MH. 2009. Evicting hitchhiker antigens from purified antibodies. *Journal of Chromatography B* **877**:1543–1552.
- MacPhee CE, Hatters DM, Sawyer WH, Howlett GJ. 2000. Apolipoprotein C-II 39-62 activates lipoprotein lipase by direct lipid-independent binding. *Biochemistry* **39**:3433–3440.
- Mahler H-C, Müller R, Frieß W, Delille A, Matheus S. 2005. Induction and analysis of aggregates in a liquid IgG1-antibody formulation. *European Journal of Pharmaceutics and Biopharmaceutics* **59**:407–417.
- Mahler H-C, Senner F, Maeder K, Mueller R. 2009. Surface activity of a monoclonal antibody. *Journal of Pharmaceutical Sciences* **98**:4525–4533.
- Manning MC, Chou DK, Murphy BM, Payne RW, Katayama DS. 2010. Stability of protein pharmaceuticals: an update. *Pharmaceutical research* **27**:544–575.
- Marichal-Gallardo PA, Álvarez MM. 2012. State-of-the-art in downstream processing of monoclonal antibodies: process trends in design and validation. *Biotechnology Progress* **28**:899–916.
- Mazza CB, Sukumar N, Breneman CM, Cramer SM. 2001. Prediction of protein retention in ion-exchange systems using molecular descriptors obtained from crystal structure. *Analytical Chemistry* **73**:5457–5461.
- McIlhargey TL. 2003. Identification of a lipoprotein lipase cofactor-binding site by chemical cross-linking and transfer of apolipoprotein C-II-responsive lipolysis from lipoprotein lipase to hepatic lipase. *Journal of Biological Chemistry* **278**:23027–23035.
- McPherson A. 1982. Preparation and analysis of protein crystals. Wiley.
- McPherson A. 2004. Introduction to protein crystallization. *Methods* **34**:254–265.
- McQuarrie DA. 2000. Statistical Mechanics. University Science Books.
- Miesegeaes GR, Lute S, Strauss DM, Read EK, Venkiteshwaran A, Kreuzman A, Shah R, Shamlou P, Chen D, Brorson K. 2012. Monoclonal antibody capture and viral clearance by cation exchange chromatography. *Biotechnology and bioengineering*.
- Miesegeaes G, Lute S, Brorson K. 2010. Analysis of viral clearance unit operations for monoclonal antibodies. *Biotechnology and bioengineering* **106**:238–246.
- Morrison CJ, Gagnon P, Cramer SM. 2010. Purification of monomeric mAb from associated aggregates using selective desorption chromatography in hydroxyapatite systems. *Biotechnology and bioengineering* **108**:813–821.

- Mosbæk CR, Konarev PV, Svergun DI, Rischel C, Vestergaard B. 2012. High concentration formulation studies of an IgG2 antibody using small angle x-ray scattering. *Pharmaceutical research* **29**:2225–2235.
- Neal BL, Asthagiri D, Lenhoff AM. 1998. Molecular origins of osmotic second virial coefficients of proteins. *Biophysical Journal* **75**:2469–2477.
- Neal BL, Lenhoff AM. 1995. Excluded volume contribution to the osmotic second virial coefficient for proteins. *AIChE J.* **41**:1010–1014.
- Nelson AL. 2010. Antibody fragments. *mabs* **2**:77–83.
- Nfor BK, Ahamed T, Pinkse MW, van der Wielen LA, Verhaert PD, van Dedem GW, Eppink MH, van de Sandt EJ, Ottens M. 2012. Multi-dimensional fractionation and characterization of crude protein mixtures: Toward establishment of a database of protein purification process development parameters. *Biotechnology and bioengineering* **109**:3070–3083.
- Nfor BK, Ahamed T, van Dedem GWK, Verhaert PDEM, van der Wielen LAM, Eppink MHM, van de Sandt EJAX, Ottens M. 2013. Model-based rational methodology for protein purification process synthesis. *Chemical Engineering Science* **89**:185–195.
- Nfor BK, Hylkema NN, Wiedhaup KR, Verhaert PDEM, van der Wielen LAM, Ottens M. 2011. High-throughput protein precipitation and hydrophobic interaction chromatography: salt effects and thermodynamic interrelation. *Journal of Chromatography A* **1218**:8958–8973.
- Nishi H, Miyajima M, Wakiyama N, Kubota K, Hasegawa J, Uchiyama S, Fukui K. 2011. Fc domain mediated self-association of an IgG1 monoclonal antibody under a low ionic strength condition. *Journal of Bioscience and Bioengineering* **112**:326–332.
- Nobmann U, Connah M, Fish B, Varley P, Gee C, Mulot S, Chen J, Zhou L, Lu Y, Sheng F, Yi J, Harding SE. 2007. Dynamic light scattering as a relative tool for assessing the molecular integrity and stability of monoclonal antibodies. *Biotechnology and Genetic Engineering Reviews* **24**:117–128.
- Oelmeier SA, Ladd-Effio C, Hubbuch J. 2013. Journal of Chromatography A. *Journal of Chromatography A* **1319**:118–126.
- Pabst TM, Suda EJ, Thomas KE, Mensah P, Ramasubramanyan N, Gustafson ME, Hunter AK. 2009. Binding and elution behavior of proteins on strong cation exchangers. *Journal of Chromatography A* **1216**:7950–7956.

- Padiolleau-Lefevre S, Alexandrenne C, Dkhissi F, Clement G, Essono S, Blache C, Couraud J-Y, Wijkhuisen A, Boquet D. 2007. Expression and detection strategies for an scFv fragment retaining the same high affinity than Fab and whole antibody: Implications for therapeutic use in prion diseases. *Molecular Immunology* **44**:1888–1896.
- Paliwal A, Asthagiri D, Abras D, Lenhoff AM, Paulaitis ME. 2005. Light-scattering studies of protein solutions: role of hydration in weak protein-protein interactions. *Biophysical Journal* **89**:1564–1573.
- Perchiacca JM, Lee CC, Tessier PM. 2014. Optimal charged mutations in the complementarity-determining regions that prevent domain antibody aggregation are dependent on the antibody scaffold. *Protein Engineering Design and Selection* **27**:29–39.
- Pereira EB, Zanin GM, Castro HF. 2003. Immobilization and catalytic properties of lipase on chitosan for hydrolysis and esterification reactions. *Brazilian Journal of Chemical Engineering* **20**:343–355.
- Pezzini J, Joucla G, Gantier R, Toueille M, Lomenech A-M, Le Sénéchal C, Garbay B, Santarelli X, Cabanne C. 2011. Antibody capture by mixed-mode chromatography: A comprehensive study from determination of optimal purification conditions to identification of contaminating host cell proteins. *Journal of Chromatography A* **1218**:8197–8208.
- Posner I, Wang CS, McConathy WJ. 1983. Kinetics of bovine milk lipoprotein lipase and the mechanism of enzyme activation by apolipoprotein C-II. *Biochemistry* **22**:4041–4047.
- Press WH, Teukolsky SA, Vetterling WT, Flannery BP. 1986. Numerical recipes: the art of scientific computing. Cambridge: Cambridge University Press.
- Quang LJ, Sandler SI, Lenhoff AM. 2014. Anisotropic contributions to protein–protein interactions. *Journal of Chemical Theory and Computation* **10**:835–845.
- Rathore AS, Kumar V, Tugcu N, Godavarti R. 2013. Evolution of the monoclonal antibody purification platform. *BioPharm International* **26**:32–48.
- Reichert JM. 2012. Marketed therapeutic antibodies compendium. *mabs* **4**:310–312.
- Robert F, Bierau H, Rossi M, Agugiaro D, Soranzo T, Broly H, Mitchell-Logean C. 2009. Degradation of an Fc-fusion recombinant protein by host cell proteases: Identification of a CHO cathepsin D protease. *Biotechnology and bioengineering* **104**:1132–1141.
- Roberts CJ, Das TK, Sahin E. 2011. Predicting solution aggregation rates for therapeutic proteins: Approaches and challenges. *International Journal of Pharmaceutics* **418**:318–333.

- Rojas C, Enerbäck S, Bengtsson-Olivecrona G. 1990. Synthesis and secretion of active lipoprotein lipase in Chinese-hamster ovary (CHO) cells. *Biochemical Journal* **271**:11.
- Roth CM, Unger KK, Lenhoff AM. 1996. Mechanistic model of retention in protein ion-exchange chromatography. *Journal of Chromatography A* **726**:45–56.
- Roussel A. 1999. The structure of an entire noncovalent immunoglobulin kappa light-chain dimer (Bence-Jones protein) reveals a weak and unusual constant domain association. *European journal of biochemistry* **260**:192–199.
- Rubin J, Linden L, Coco WM, Bommarius AS, Behrens SH. 2012. Salt-induced aggregation of a monoclonal human immunoglobulin G1. *Journal of Pharmaceutical Sciences* **102**:377–386.
- Sahin E, Grillo AO, Perkins MD, Roberts CJ. 2010. Comparative effects of pH and ionic strength on protein-protein interactions, unfolding, and aggregation for IgG1 antibodies. *Journal of Pharmaceutical Sciences* **99**:4830–4848.
- Saito S, Hasegawa J, Kobayashi N, Kishi N, Uchiyama S, Fukui K. 2011. Behavior of monoclonal antibodies: relation between the second virial coefficient ( $B_2$ ) at low concentrations and aggregation propensity and viscosity at high concentrations. *Pharmaceutical research* **29**:397–410.
- Sandin S, Öfverstedt L-G, Wikström A-C, Wrange Ö, Skoglund U. 2004. Structure and flexibility of individual immunoglobulin G molecules in solution. *Structure* **12**:409–415.
- Sandler SI. 2011. An introduction to applied statistical thermodynamics. John Wiley & Sons, Ltd.
- Saphire EO, Stanfield RL, Max Crispin MD, Parren PWHI, Rudd PM, Dwek RA, Burton DR, Wilson IA. 2002. Contrasting IgG structures reveal extreme asymmetry and flexibility. *Journal of Molecular Biology* **319**:9–18.
- Sasamori E, Suzuki S, Kato M, Tagawa Y, Hanyu Y. 2010. Characterization of discontinuous epitope of prion protein recognized by the monoclonal antibody T2. *Archives of Biochemistry and Biophysics* **501**:232–238.
- Schenauer MR, Flynn GC, Goetze AM. 2012. Analytical Biochemistry. *Analytical Biochemistry* **428**:150–157.
- Scherer TM, Liu J, Shire SJ, Minton AP. 2010. Intermolecular interactions of IgG1 monoclonal antibodies at high concentrations characterized by light scattering. *The Journal of Physical Chemistry B* **114**:12948–12957.
- Schrecker O, Greten H. 1979. Activation and inhibition of lipoprotein lipase studies with artificial lipoproteins. *biochimica et biophysica acta (BBA)-Lipids and Lipid Metabolism* **572**:244–256.

- Schwertner D, Kirchner M. 2010. Are generic HCP assays outdated. *BioProcess International*:56–61.
- Sear RP. 1999. Phase behavior of a simple model of globular proteins. *Journal of Chemical Physics* **111**:4800.
- Semisotnov GV, Rodionova NA, Razgulyaev OI, Uversky VN, Gripas AF, Gilmanshin RI. 1991. Study of the molten globule intermediate state in protein folding by a hydrophobic fluorescent-probe. *Biopolymers* **31**:119–128.
- Senczuk AM, Klinke R, Arakawa T, Vedantham G, Yigzaw Y. 2009. Hydrophobic interaction chromatography in dual salt system increases protein binding capacity. *Biotechnology and bioengineering* **103**:930–935.
- Shen Y. 2001. Functional Analyses of Human Apolipoprotein CII by site-directed mutagenesis. *Journal of Biological Chemistry* **277**:4334–4342.
- Shen Y, Lookene A, Zhang L, Olivecrona G. 2010. Site-directed mutagenesis of apolipoprotein CII to probe the role of its secondary structure for activation of lipoprotein lipase. *Journal of Biological Chemistry* **285**:7484–7492.
- Shih YC, Prausnitz JM, Blanch HW. 1992. Some Characteristics of Protein Precipitation by Salts. *Biotechnology and bioengineering* **40**:1155–1164.
- Shirai K, Fitzharris TJ, Shinomiya M, Muntz HG, Harmony JA, Jackson RL, Quinn DM. 1983. Lipoprotein lipase-catalyzed hydrolysis of phosphatidylcholine of guinea pig very low density lipoproteins and discoidal complexes of phospholipid and apolipoprotein: effect of apolipoprotein C-II on the catalytic mechanism. *Journal of lipid research* **24**:721–730.
- Shire SJ, Gombotz W, Bechtold-Peters K, Andya J. 2009. Current trends in monoclonal antibody development and manufacturing. Springer.
- Shire SJ, Shahrokh Z, Liu J. 2004. Challenges in the development of high protein concentration formulations. *Journal of Pharmaceutical Sciences* **93**:1390–1402.
- Shukla AA, Hinckley P. 2008. Host cell protein clearance during Protein A chromatography: development of an improved column wash step. *Biotechnology Progress* **24**:1115–1121.
- Shukla AA, Gupta P, Han X. 2007a. Protein aggregation kinetics during Protein A chromatography. *Journal of Chromatography A* **1171**:22–28.
- Shukla AA, Hubbard B, Tressel T, Guhan S, Low D. 2007b. Downstream processing of monoclonal antibodies - application of platform approaches. *Journal of Chromatography B* **848**:28–39.
- Singh SK, Cousens LP, Alvarez D, Mahajan PB. 2012. Determinants of immunogenic response to protein therapeutics. *Biologicals* **40**:364–368.

- Sisodiya VN, Lequieu J, Rodriguez M, McDonald P, Lazzareschi KP. 2012. Studying host cell protein interactions with monoclonal antibodies using high throughput protein A chromatography. *Biotechnology Journal* **7**:1233–1241.
- Smejkal B, Agrawal NJ, Helk B, Schulz H, Giffard M, Mechelke M, Ortner F, Heckmeier P, Trout BL, Hekmat D. 2013. Fast and scalable purification of a therapeutic full-length antibody based on process crystallization. *Biotechnology and bioengineering* **110**:2452–2461.
- Stein A, Kiesewetter A. 2007. Cation exchange chromatography in antibody purification: pH screening for optimised binding and HCP removal. *Journal of Chromatography B* **848**:151–158.
- Steward MW. 1984. *Antibodies, Their Structure and Function*. Taylor & Francis 1 pp.
- Sule SV, Cheung JK, Antochshuk V, Bhalla AS, Narasimhan C, Blaisdell S, Shameem M, Tessier PM. 2012. Solution pH that minimizes self-association of three monoclonal antibodies is strongly dependent on ionic strength. *Molecular Pharmaceutics* **9**:744–751.
- Swinnen K, Krul A, Van Goidsenhoven I, Van Tichelt N, Roosen A, Van Houdt K. 2007. Performance comparison of protein A affinity resins for the purification of monoclonal antibodies. *Journal of Chromatography B* **848**:97–107.
- Tait AS, Hogwood CEM, Smales CM, Bracewell DG. 2011. Host cell protein dynamics in the supernatant of a mAb producing CHO cell line. *Biotechnology and bioengineering* **109**:971–982.
- Tarrant RDR, Velez-Suberbie ML, Tait AS, Smales CM, Bracewell DG. 2012. Host cell protein adsorption characteristics during protein a chromatography. *Biotechnology Progress* **28**:1037–1044.
- Teplyakov A, Zhao Y, Malia TJ, Obmolova G, Gilliland GL. 2013. IgG2 Fc structure and the dynamic features of the IgG CH<sub>2</sub>–CH<sub>3</sub> interface. *Molecular Immunology* **56**:131–139.
- Teske C, Blanch H, Prausnitz J. 2004. Chromatographic measurement of interactions between unlike proteins. *Fluid Phase Equilibria* **219**:139–148.
- Tessier PM, Lenhoff AM, Sandler SI. 2002a. Rapid measurement of protein osmotic second virial coefficients by self-interaction chromatography. *Biophysical Journal* **82**:1620–1631.
- Tessier PM, Vandrey SD, Berger BW, Pazhianur R, Sandler SI, Lenhoff AM. 2002b. Self-interaction chromatography: a novel screening method for rational protein crystallization. *Acta Crystallographica Section D Biological Crystallography* **D58**:1531–1535.

- Tessier PM, Sandler SI, Lenhoff AM. 2004a. Direct measurement of protein osmotic second virial cross coefficients by cross-interaction chromatography. *Protein Science* **13**:1379–1390.
- Tessier P, Verruto V, Sandler S, Lenhoff A. 2004b. Correlation of diafiltration sieving behavior of lysozyme-BSA mixtures with osmotic second virial cross-coefficients. *Biotechnology and bioengineering* **87**:303–310.
- The UniProt Consortium. 2011. Reorganizing the protein space at the Universal Protein Resource (UniProt). *Nucleic Acids Research* **40**:D71–D75.
- Thompson JH, Chung WK, Zhu M, Tie L, Lu Y, Aboulaich N, Strouse R, Mo WD. 2014. Improved detection of host cell proteins (HCPs) in a mammalian cell-derived antibody drug using liquid chromatography/mass spectrometry in conjunction with an HCP-enrichment strategy. *Rapid Communications in Mass Spectrometry* **28**:855–860.
- To BCS, Lenhoff AM. 2007. Hydrophobic interaction chromatography of proteins I. The effects of protein and adsorbent properties on retention and recovery. *Journal of Chromatography A* **1141**:191–205.
- To BCS, Lenhoff AM. 2008. Hydrophobic interaction chromatography of proteins III. Transport and kinetic parameters in isocratic elution. *Journal of Chromatography A* **1205**:46–59.
- Touelle M, Uzel A, Depoisier J-F, Gantier R. 2011. Designing new monoclonal antibody purification processes using mixed-mode chromatography sorbents. *Journal of Chromatography B* **879**:836–843.
- Traxlmayr MW, Lobner E, Antes B, Kainer M, Wiederkum S, Hasenhindl C, Stadlmayr G, Ruker F, Woisetschlager M, Moulder K, Obinger C. 2013. Directed evolution of Her2/neu-binding IgG1-Fc for improved stability and resistance to aggregation by using yeast surface display. *Protein Engineering Design and Selection* **26**:255–265.
- Trilisky E, Gillespie R, Osslund TD, Vunnum S. 2011. Crystallization and liquid-liquid phase separation of monoclonal antibodies and fc-fusion proteins: Screening results. *Biotechnology Progress* **27**:1054–1067.
- Tscheliessnig AL, Konrath J, Bates R, Jungbauer A. 2013. Host cell protein analysis in therapeutic protein bioprocessing—methods and applications. *Biotechnology Journal*.
- Tugcu N, Roush DJ, Göklen KE. 2007. Maximizing productivity of chromatography steps for purification of monoclonal antibodies. *Biotechnology and bioengineering* **99**:599–613.

- Valente JJ, Verma KS, Manning MC, William Wilson W, Henry CS. 2005. Second virial coefficient studies of cosolvent-induced protein self-interaction. *Biophysical Journal* **89**:4211–4218.
- Valente KN, Choe LH, Lenhoff AM, Lee KH. 2012. Optimization of protein sample preparation for two-dimensional electrophoresis. *Electrophoresis* **33**:1947–1957.
- Vázquez-Rey M, Lang DA. 2011. Aggregates in monoclonal antibody manufacturing processes. *Biotechnology and bioengineering* **108**:1494–1508.
- Vermeer AW, Norde W. 2000. The thermal stability of immunoglobulin: unfolding and aggregation of a multi-domain protein. *Biophysical Journal* **78**:394–404.
- Wang C, Soice NP, Ramaswamy S, Gagnon BA, Umana J, Cotoni KA, Bian N, Cheng K-SC. 2007. Cored anion-exchange chromatography media for antibody flow-through purification. *Journal of Chromatography A* **1155**:74–84.
- Wang W, Singh S, Zeng DL, King K, Nema S. 2006. Antibody structure, instability, and formulation. *Journal of Pharmaceutical Sciences* **96**:1–26.
- Wang W, Wang YJ, Wang DQ. 2008. Dual effects of Tween 80 on protein stability. *International Journal of Pharmaceutics* **347**:31–38.
- Wang X, Hunter AK, Mozier NM. 2009. Host cell proteins in biologics development: identification, quantitation and risk assessment. *Biotechnology and bioengineering* **103**:446–458.
- Washburn EW. 1926. International Critical Tables of Numerical Data, Physics, Chemistry and Technology. National Academies.
- Weaver J, Husson SM, Murphy L, Wickramasinghe SR. 2013. Anion exchange membrane adsorbers for flow-through polishing steps: Part II. Virus, host cell protein, DNA clearance, and antibody recovery. *Biotechnology and bioengineering* **110**:500–510.
- Welfle K, Misselwitz R, Hausdorf G, Höhne W, Welfle H. 1999. Conformation, pH-induced conformational changes, and thermal unfolding of anti-p24 (HIV-1) monoclonal antibody CB4-1 and its Fab and Fc fragments. *Biochimica et Biophysica Acta (BBA)-Protein Structure and Molecular Enzymology* **1431**:120–131.
- Wilson MR, Easterbrook-Smith SB. 1992. Clusterin binds by a multivalent mechanism to the Fc and Fab regions of IgG. *Biochimica et Biophysica Acta (BBA)-Protein Structure and Molecular Enzymology* **1159**:319–326.
- Wolfe LS, Barringer CP, Mostafa SS, Shukla AA. 2014. Multimodal chromatography: Characterization of protein binding and selectivity enhancement through mobile phase modulators. *Journal of Chromatography A* **1340**:151–156.

- Wong H, Davis RC, Thuren T, Goers JW, Nikazy J, Waite M, Schotz MC. 1994. Lipoprotein lipase domain function. *Journal of Biological Chemistry* **269**:10319–10323.
- Wong H, Schotz MC. 2002. The lipase gene family. *Journal of lipid research* **43**:993–999.
- Xu X, Nagarajan H, Lewis NE, Pan S, Cai Z, Liu X, Chen W, Xie M, Wang W, Hammond S, Andersen MR, Neff N, Passarelli B, Koh W, Fan HC, Wang J, Gui Y, Lee KH, Betenbaugh MJ, Quake SR, Famili I, Palsson BO, Wang J. 2011. The genomic sequence of the Chinese hamster ovary (CHO)-K1 cell line. *Nature Biotechnology*:1–8.
- Xu Z, Li J, Zhou JX. 2012. Process development for robust removal of aggregates using cation exchange chromatography in monoclonal antibody purification with implementation of quality by design. *Preparative Biochemistry and Biotechnology* **42**:183–202.
- Yadav S, Laue TM, Kalonia DS, Singh SN, Shire SJ. 2012. The influence of charge distribution on self-association and viscosity behavior of monoclonal antibody solutions. *Molecular Pharmaceutics* **9**:791–802.
- Yadav S, Liu J, Shire SJ, Kalonia DS. 2009. Specific interactions in high concentration antibody solutions resulting in high viscosity. *Journal of Pharmaceutical Sciences* **99**:1152–1168.
- Yadav S, Shire SJ, Kalonia DS. 2010. Factors affecting the viscosity in high concentration solutions of different monoclonal antibodies. *Journal of Pharmaceutical Sciences* **99**:4812–4829.
- Yadav S, Shire SJ, Kalonia DS. 2011a. Viscosity behavior of high-concentration monoclonal antibody solutions: Correlation with interaction parameter and electroviscous effects. *Journal of Pharmaceutical Sciences* **101**:998–1011.
- Yadav S, Sreedhara A, Kanai S, Liu J, Lien S, Lowman H, Kalonia DS, Shire SJ. 2011b. Establishing a link between amino acid sequences and self-associating and viscoelastic behavior of two closely related monoclonal antibodies. *Pharmaceutical research* **28**:1750–1764.
- Yagi H, Takahashi N, Yamaguchi Y, Kato K. 2004. Temperature-dependent isologous Fab–Fab interaction that mediates cryocrystallization of a monoclonal immunoglobulin G. *Molecular Immunology* **41**:1211–1215.
- Yao Y, Lenhoff AM. 2004. Electrostatic contributions to protein retention in ion-exchange chromatography. 1. Cytochrome c variants. *Analytical Chemistry* **76**:6743–6752.

- Yao Y, Lenhoff AM. 2005. Electrostatic contributions to protein retention in ion-exchange chromatography. 2. Proteins with various degrees of structural differences. *Analytical Chemistry* **77**:2157–2165.
- Yearley EJ, Zarraga IE, Shire SJ, Scherer TM, Gokarn Y, Wagner NJ, Liu Y. 2013. Small-angle neutron scattering characterization of monoclonal antibody conformations and interactions at high concentrations. *Biophysical Journal* **105**:720–731.
- Young L, Jernigan RL, Covell DG. 1994. A role for surface hydrophobicity in protein-protein recognition. *Protein Science* **3**:717–729.
- Zang Y, Kammerer B, Eisenkolb M, Lohr K, Kiefer H. 2011. Towards protein crystallization as a process step in downstream processing of therapeutic antibodies: screening and optimization at microbatch scale. Ed. Sue Cotterill. *PLoS ONE* **6**:1–8.
- Zhang L, Lookene A, Wu G, Olivecrona G. 2005. Calcium triggers folding of lipoprotein lipase into active dimers. *Journal of Biological Chemistry* **280**:42580–42591
- Zhu G, Sun L, Wojcik R, Kernaghan D, McGivney JB, Dovichi NJ. 2012. A rapid cIEF–ESI–MS/MS method for host cell protein analysis of a recombinant human monoclonal antibody. *Talanta* **98**:253–256.
- Zou WQ, Langeveld J, Xiao X, Chen S, McGeer PL, Yuan J, Payne MC, Kang HE, McGeehan J, Sy MS, Greenspan NS, Kaplan D, Wang GX, Parchi P, Hoover E, Kneale G, Telling G, Surewicz WK, Kong Q, Guo JP. 2010. PrP conformational transitions alter species preference of a PrP-specific antibody. *Journal of Biological Chemistry* **285**:13874–13884.

## **Appendix A**

### **IDENTIFIED 2-DE SPOTS FOR PROTEIN A PRODUCT ASSOCIATION**

#### **A.1 Quantification of Missing Spots from 2-DE Images**

As described in the Section 2.10, ‘flow-through’ gels were compared to ‘load’ gels using Image Master 5 software. Spots that were found on the ‘load’ gel and missing from the ‘flow-through’ gel were identified as CHO HCPs associated with the immobilized mAb or mAb fragment. Using Image Master 5, the spots were integrated. The values in the table below reflect percent volume in flow-through divided by percent volume in load for spots of interest. A 50% reduction in spot volume was considered indicative of an associated HCP. For a few cases, due to either an obstructing artifact or very low total protein content in the flow-through gel, spot quantification did not indicate a 50% reduction in spot volume even though there was a qualitative change based on visual inspection. Enlarged images of ‘load’ and ‘flow-through’ spots of interest can be found below.

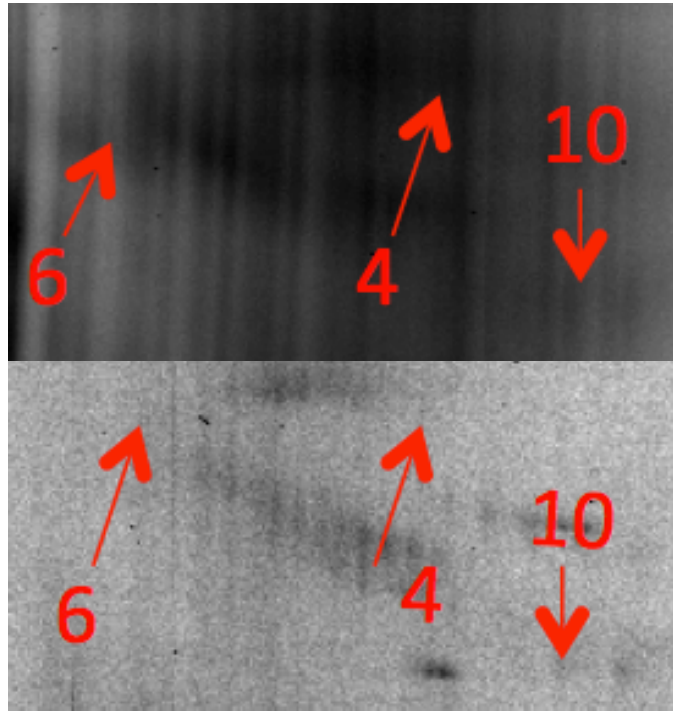
Table A.1: Integrated HCP spot volume in ‘flow-through’ gel divided by integrated HCP spot volume in ‘load’ gel for protein A loading conditions.

Protein ID	MAB D	MAB D <sub>M</sub>	IDEC-152	Mill04	Mill04 Fab	Mill04 Fc
1. Neural cell adhesion molecule	-	*	0.14	0.32	-	-
2. Renin receptor	-	*	-	0.08	0.07	-
3. Lipoprotein lipase	0.38	0.09	0.45	-	-	0.34
4. Chondroitin sulfate protoglycan 4	*	-	0.48	0.31	0.48	-
5. Alpha-enolase	-	0.31	-	-	-	-
6. Galectin-3-binding protein	0.20	-	-	0.21	-	0.26
7. G-protein coupled receptor 56	*	-	0.32	0.24	-	0.25
8. V-type proton ATPase subunit S1	-	0.32	-	-	-	-
9. Nidogen-1	0.40	0.10	0.18	0.29	-	0.13
10. ATP synthase subunit beta, mitochondrial	0.20	0.29	-	-	-	0.26
11. Vimentin	*	0.51	-	-	-	-
12. Heat shock protein	0.16	0.45	-	-	-	-
13. Actin	0.10	0.27	-	0.35	-	0.35
14. Peroxiredoxin 1	-	-	-	-	-	0.17
15.a,b SPARC	0.16	0.36	0.25	0.27	*	-
16.a,b Clusterin	*	*	0.38	0.27	*	-
17. Complement C1r-a sub-component	0.37	-	-	-	-	-
18. Metalloproteinase inhibitor 1	0.33	-	-	-	-	-
19. Insulin	0.21	0.38	0.16	0.17	-	-
20. Cathepsin D	-	*	-	-	-	-
21. Sulfated glycoprotein 1	0.16	-	-	-	-	-
22. Lysosomal protective protein	-	-	-	-	-	0.38

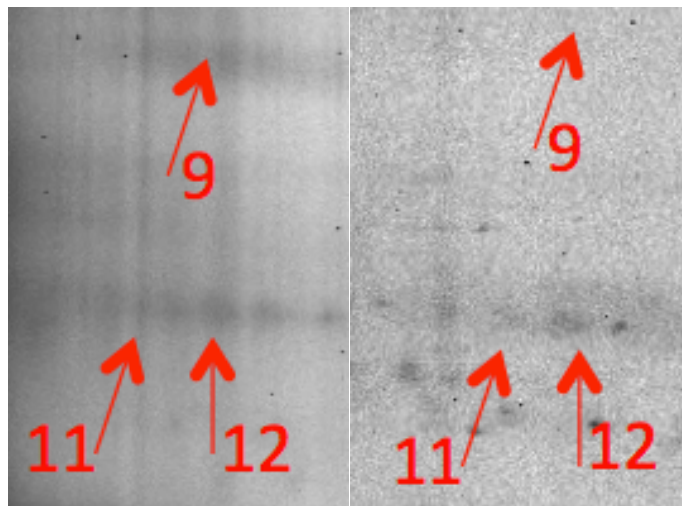
\* Cases for which spot integration did not confirm spots identified as missing based on visual inspection

### A.1.1 MAb D HCP-CIC 2-DE Analysis: Protein A Solution Conditions

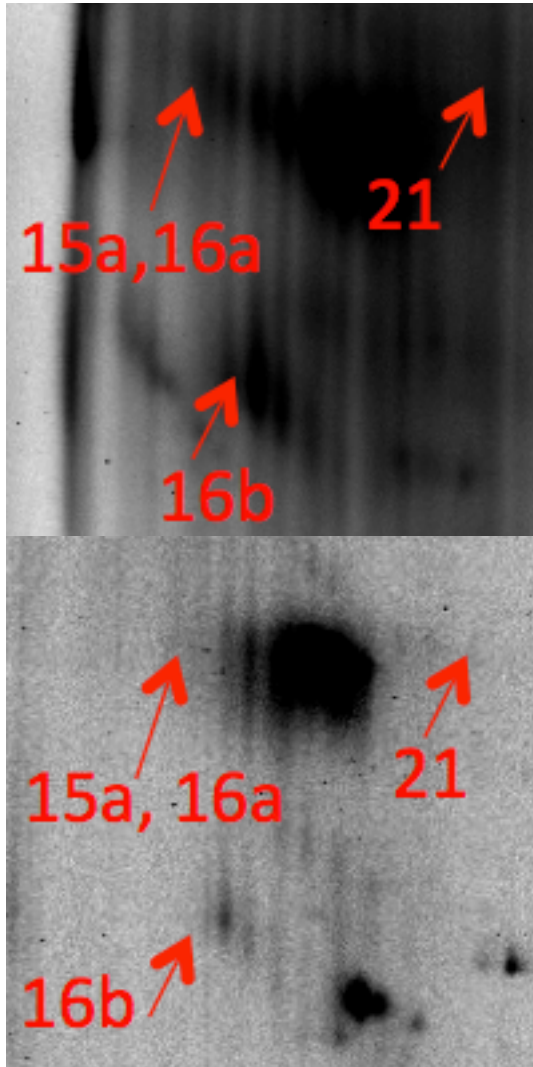
Numbers on 'load' and 'flow-through' gels refer to Table A.1.



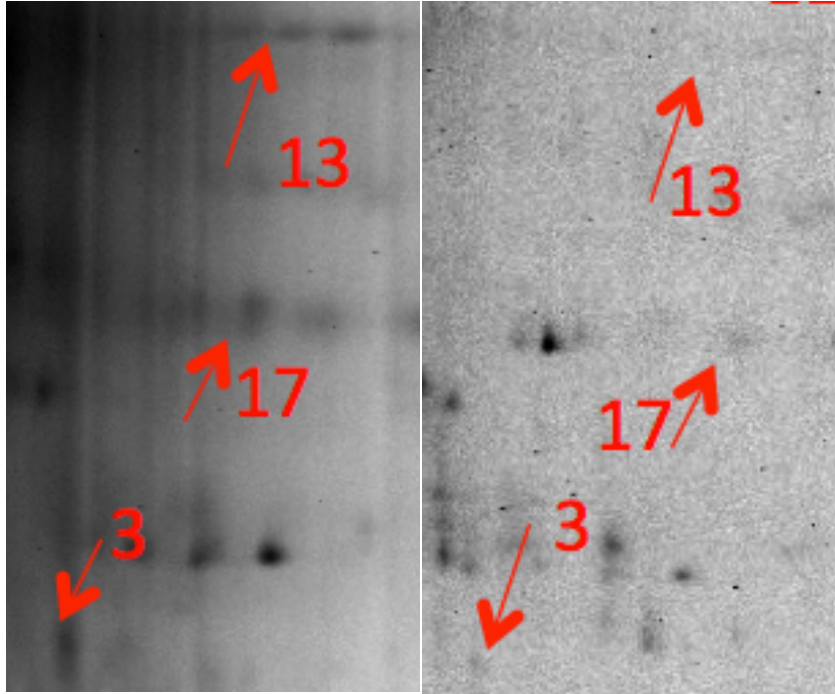
Load (above) and flow-through (below)



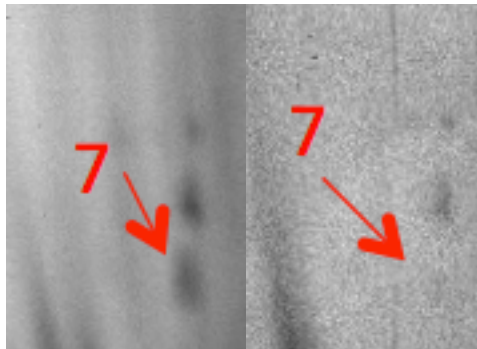
Load (left) and flow-through (right)



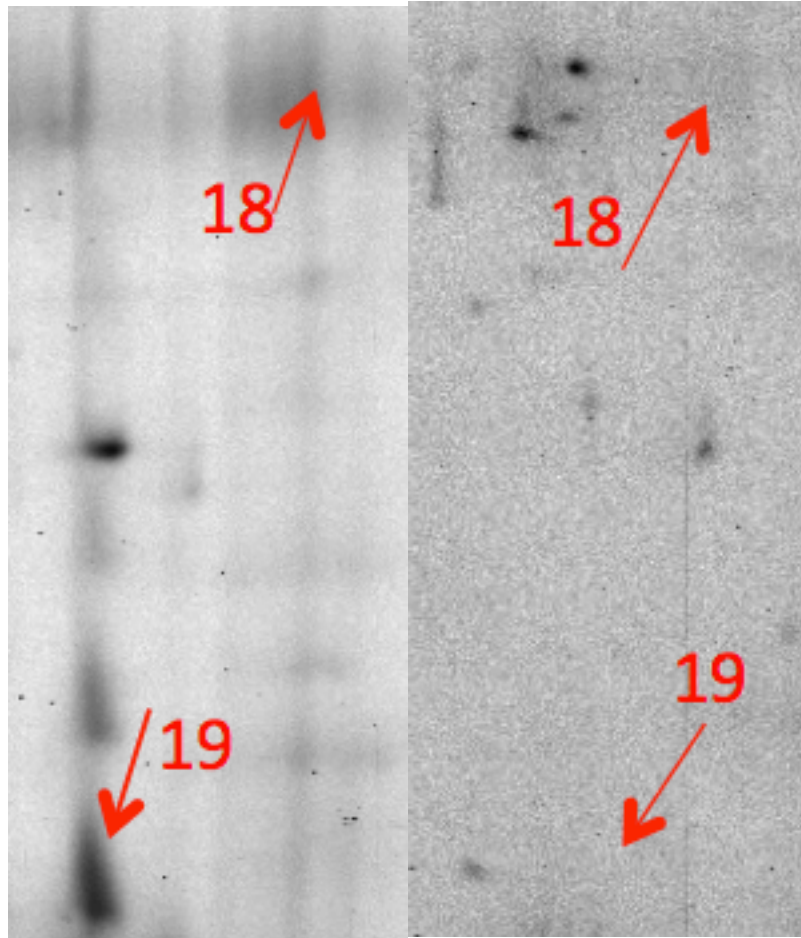
Load (above) and flow-through (below)



Load (left) and flow-through (right)



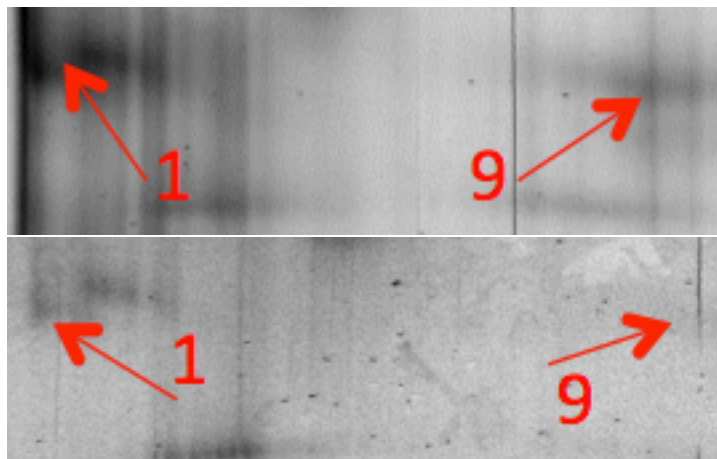
Load (left) and flow-through (right)



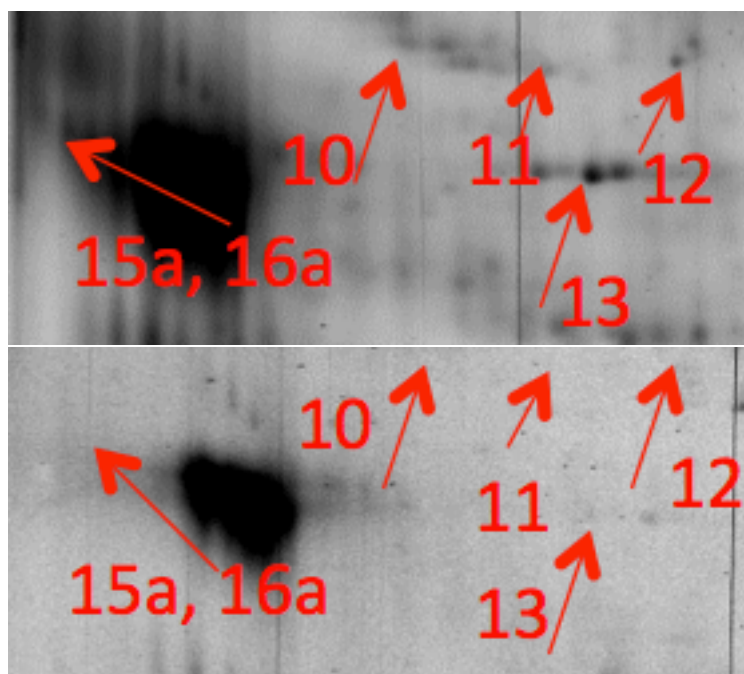
Load (left) and flow-through (right)

### A.1.2 MAb D<sub>M</sub> HCP-CIC 2-DE Analysis: Protein A Solution Conditions

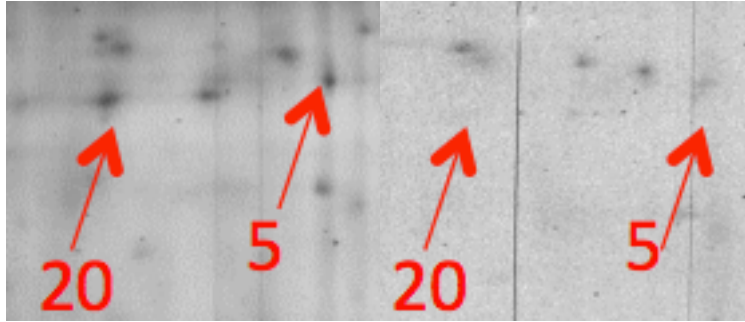
Numbers on 'load' and 'flow-through' gels refer to Table A.1.



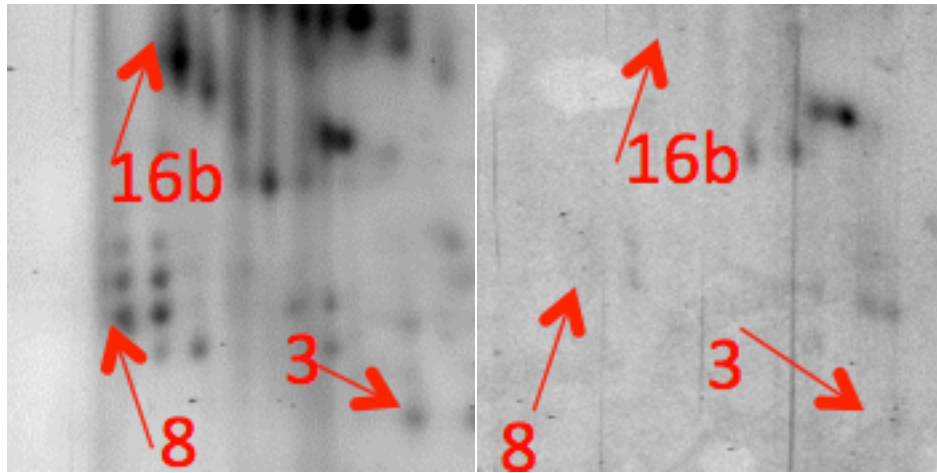
Load (above) and flow-through (below)



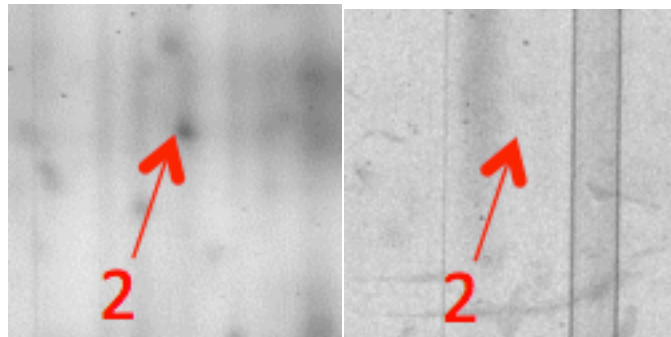
Load (above) and flow-through (below)



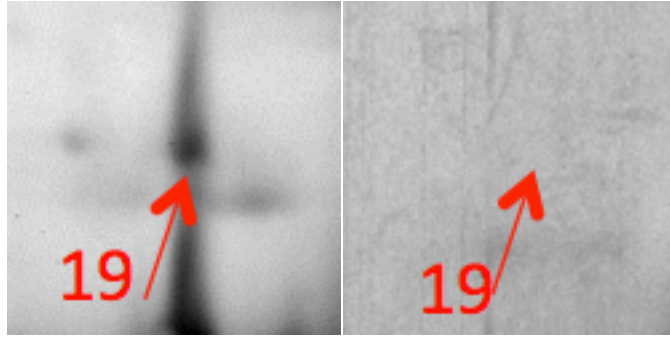
Load (left) and flow-through (right)



Load (left) and flow-through (right)



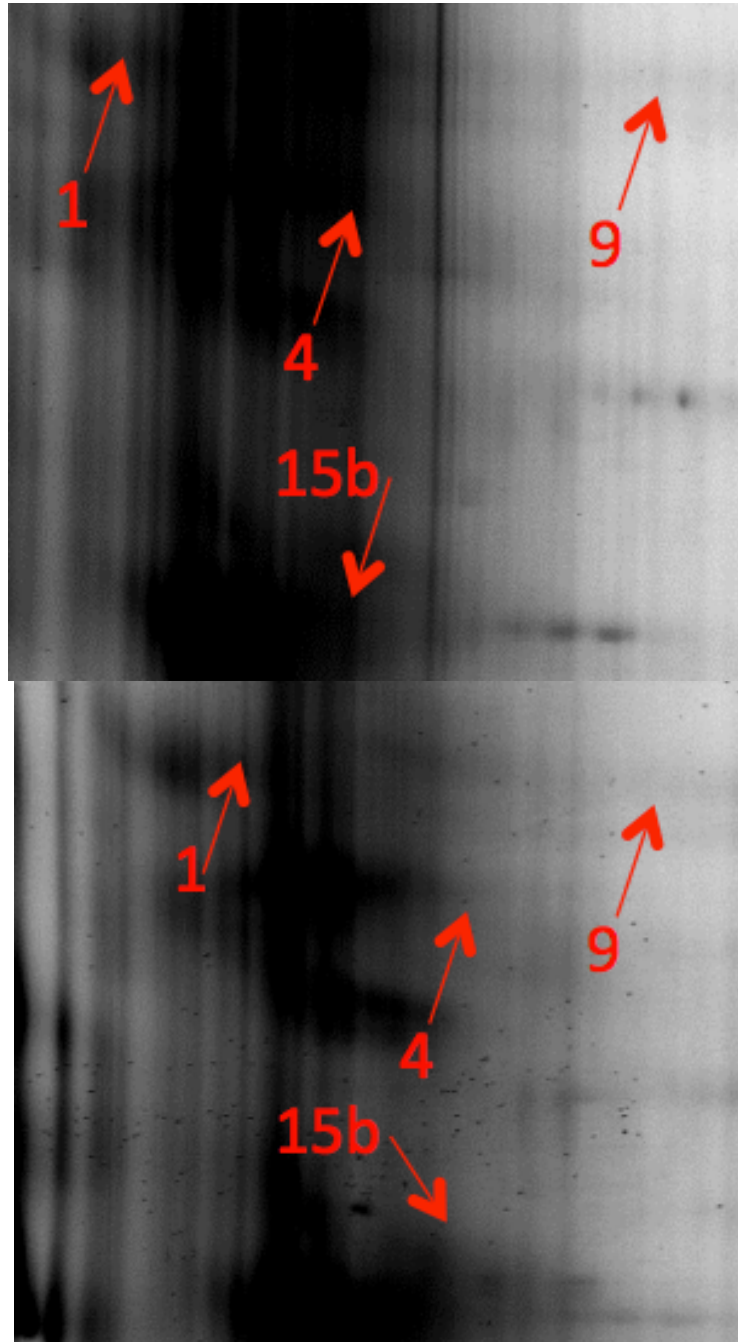
Load (left) and flow-through (right)



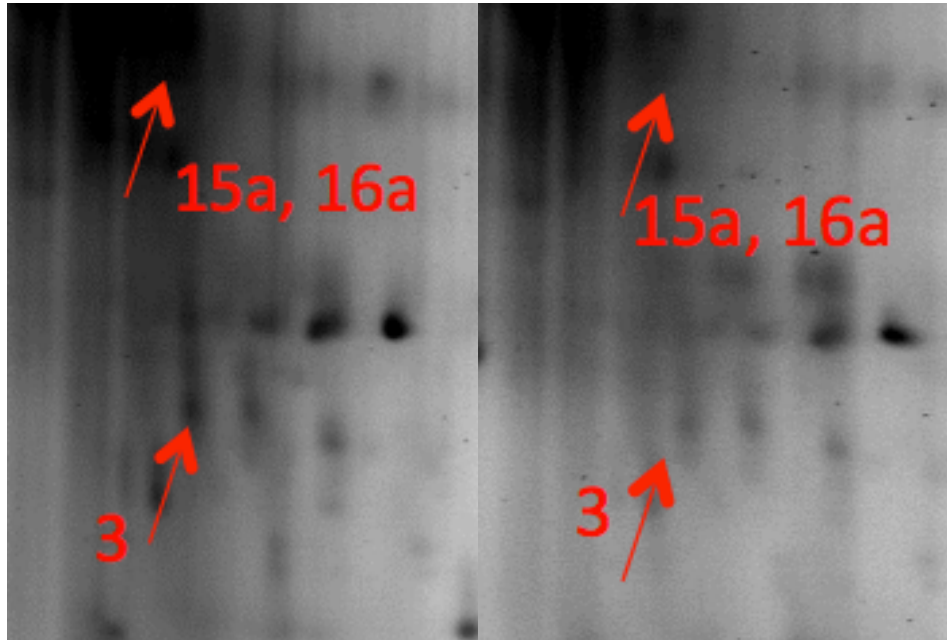
Load (left) and flow-through (right)

### A.1.3 IDEC-152 HCP-CIC 2-DE Analysis: Protein A Solution Conditions

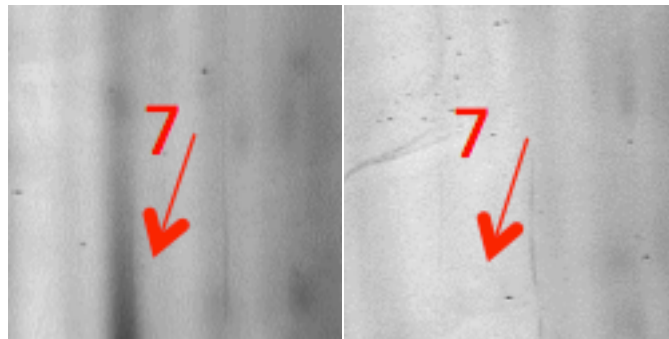
Numbers on 'load' and 'flow-through' gels refer to Table A.1.



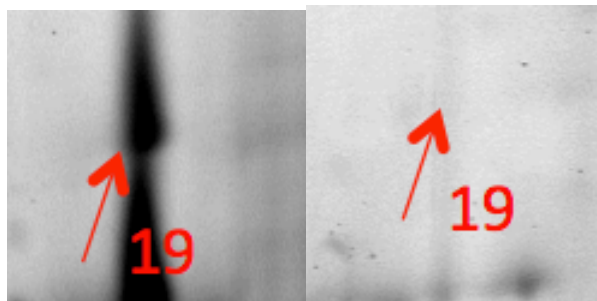
Load (above) and flow-through (below)



Load (left) and flow-through (right)



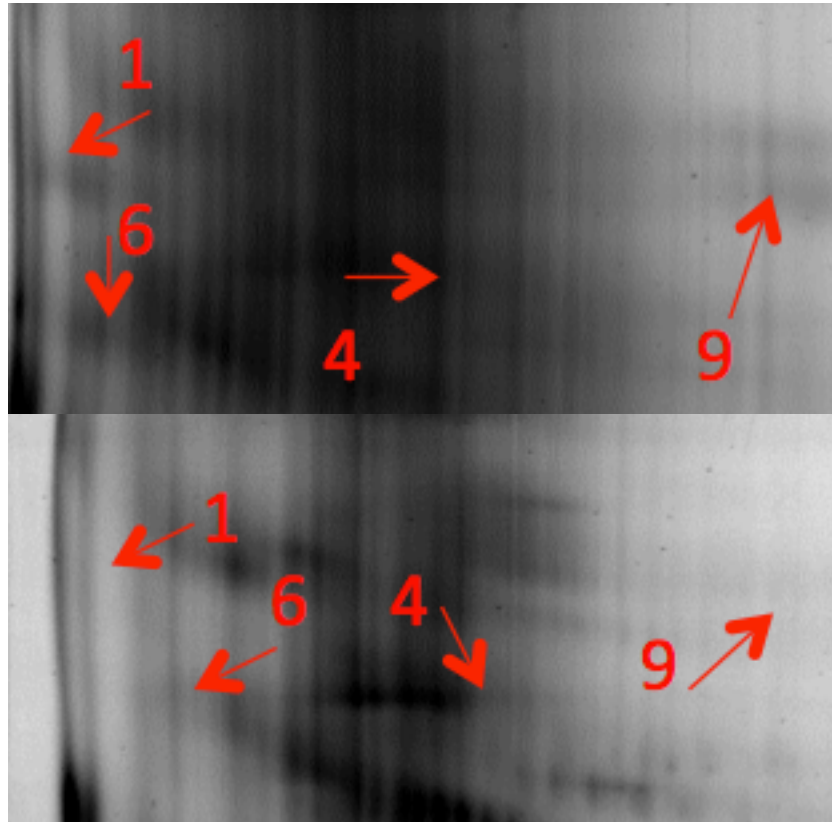
Load (left) and flow-through (right)



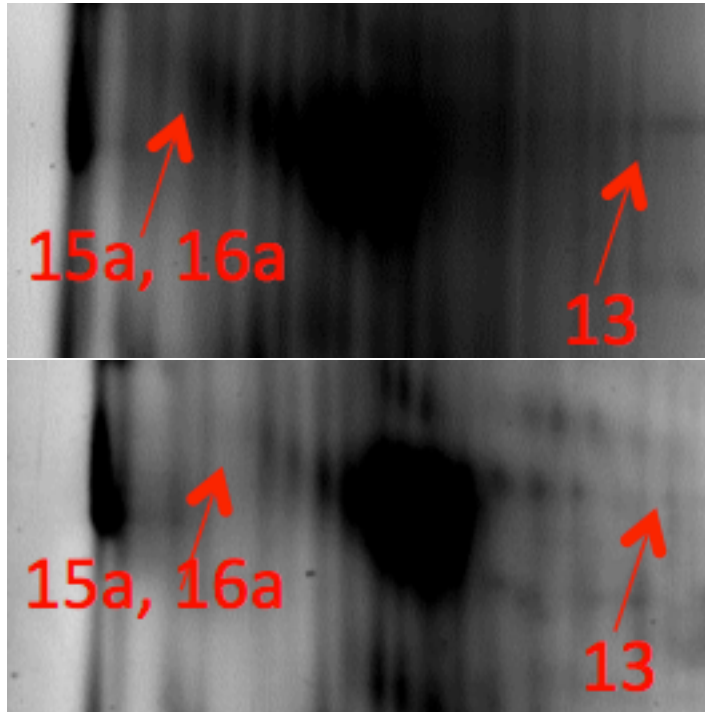
Load (left) and flow-through (right)

#### A.1.4 Mill04 HCP-CIC 2-DE Analysis: Protein A Solution Conditions

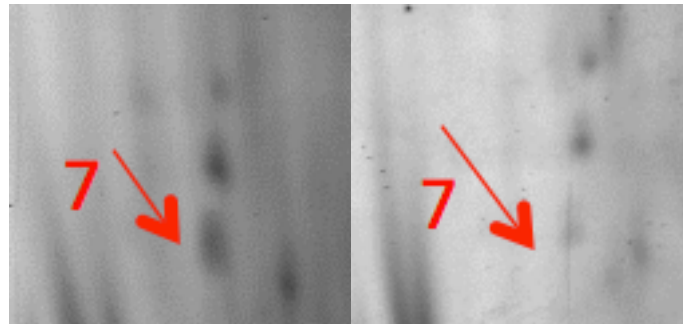
Numbers on 'load' and 'flow-through' gels refer to Table A.1.



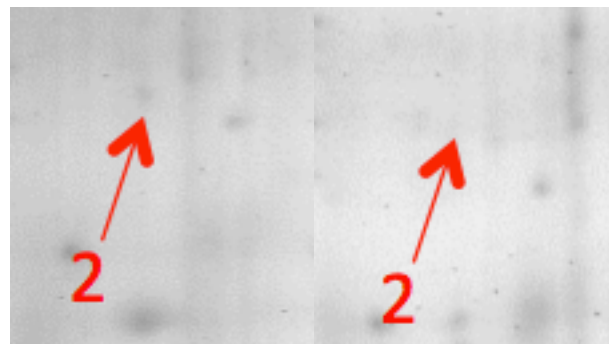
Load (above) and flow-through (below)



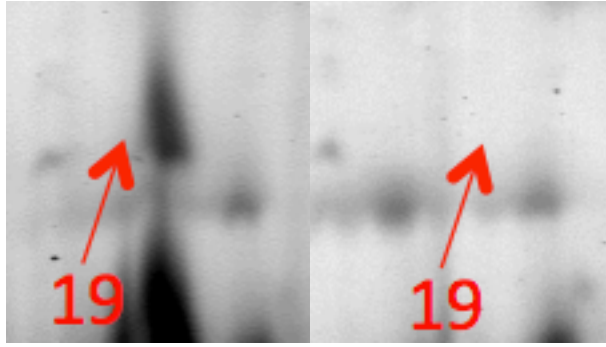
Load (above) and flow-through (below)



Load (left) and flow-through (right)



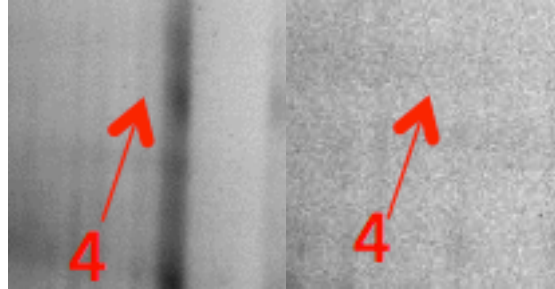
Load (left) and flow-through (below)



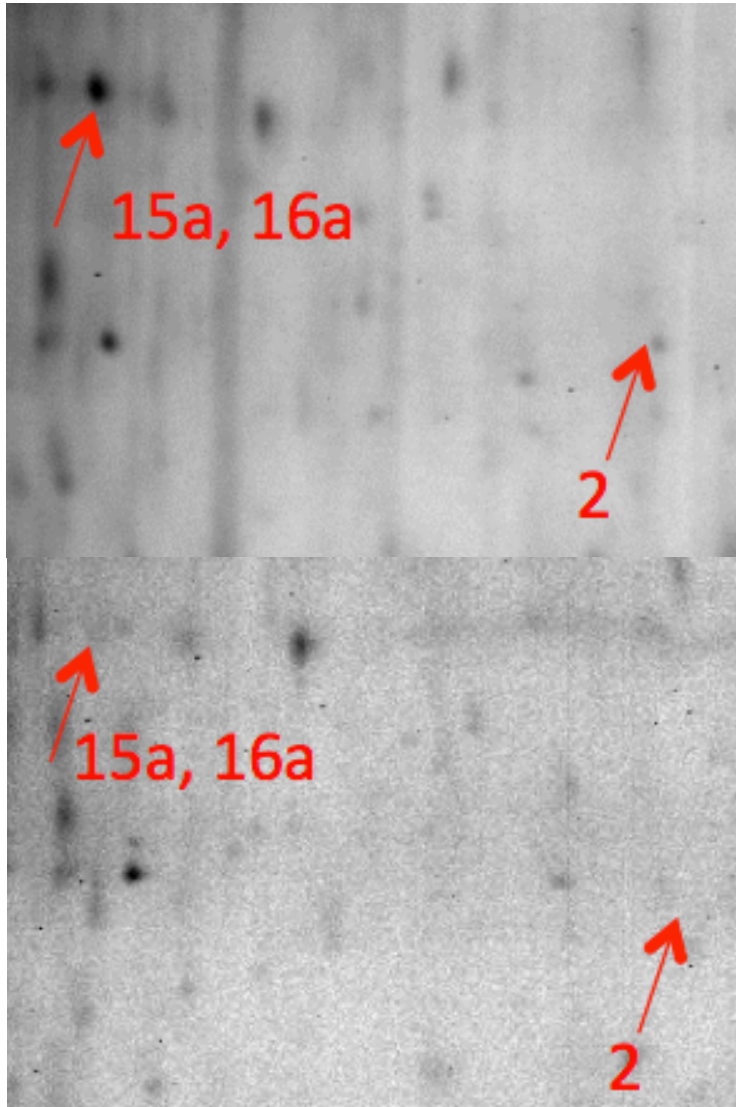
Load (left) and flow-through (below)

### A.1.5 Mill04 Fab HCP-CIC 2-DE Analysis: Protein A Solution Conditions

Numbers on 'load' and 'flow-through' gels refer to Table A.1.



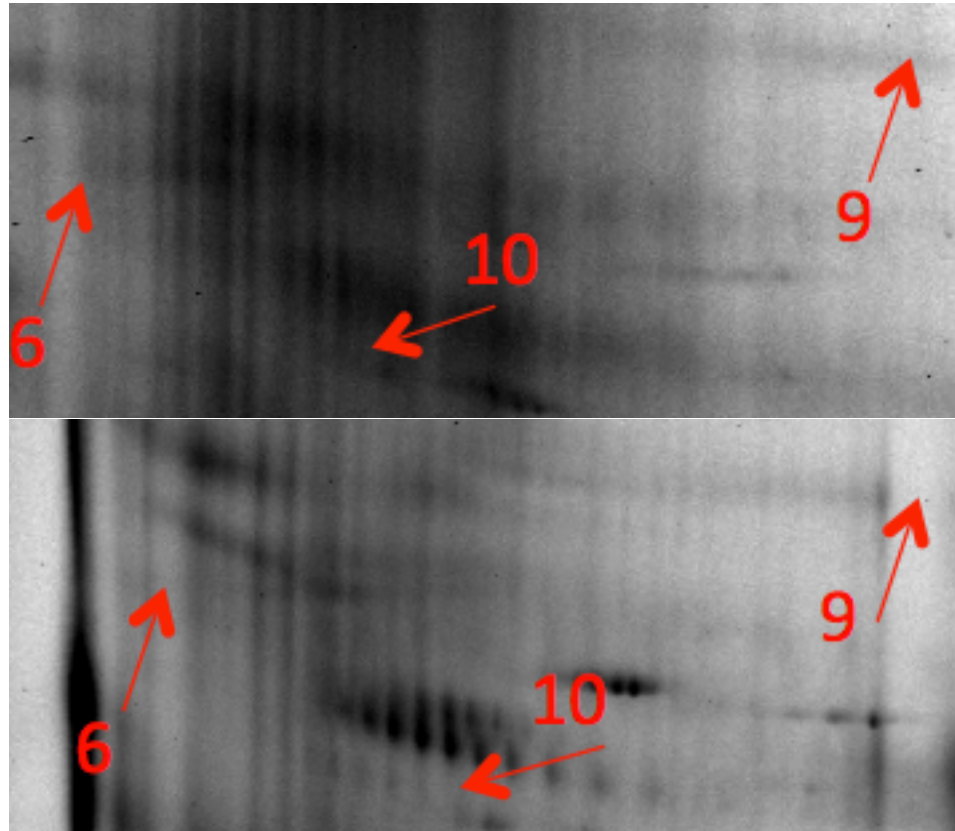
Load (left) and flow-through (right)



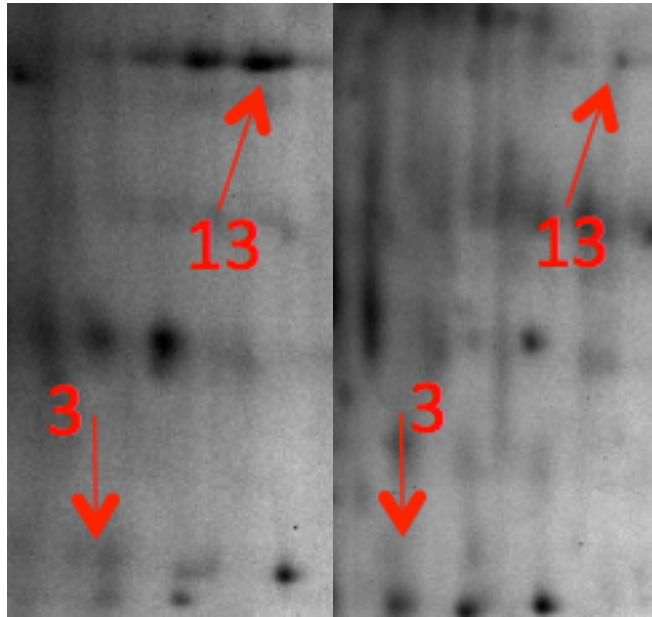
Load (above) and flow-through (below)

### A.1.6 Mill04 Fc HCP-CIC 2-DE Analysis: Protein A Solution Conditions

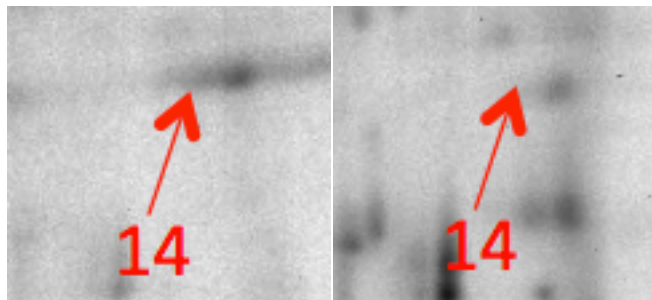
Numbers on 'load' and 'flow-through' gels refer to Table A.1.



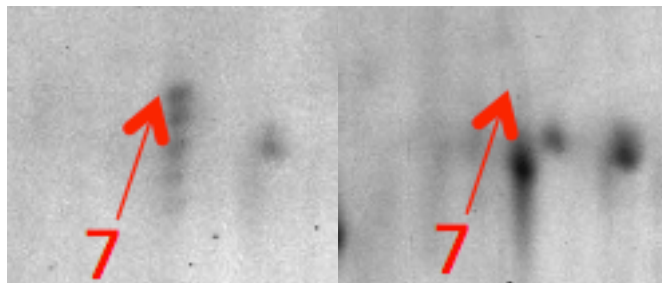
Load (above) and flow-through (below)



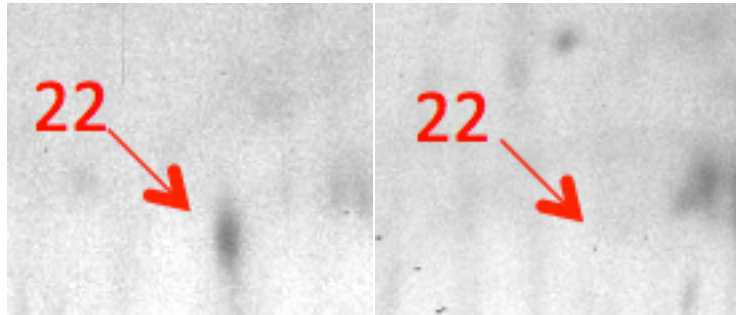
Load (left) and flow-through (right)



Load (left) and flow-through (right)



Load (left) and flow-through (right)



Load (left) and flow-through (right)

## Appendix B

### IDENTIFIED 2-DE SPOTS FOR HIC PRODUCT ASSOCIATION

#### B.1 Quantification of Missing Spots from 2-DE Images

As described in the Section 2.10, ‘flow-through’ gels were compared to ‘load’ gels using Image Master 5 software. Spots that were found on the ‘load’ gel and missing from the ‘flow-through’ gel were identified as CHO HCPs associated with the immobilized mAb or mAb fragment. The ‘load’ and ‘flow-through’ gels for HIC CIC are in Figure B.1. Using Image Master 5, the spots were integrated. The values in Table B.1 reflect percent volume in flow-through divided by percent volume in load for spots of interest. A 50% reduction in spot volume was considered indicative of an associated HCP. Enlarged images of ‘load’ and ‘flow-through’ spots of interest can be found in the following sections.

Table B.1: Integrated HCP spot volume in ‘flow-through’ gel divided by integrated HCP spot volume in ‘load’ gel for HIC loading conditions.

<b>Protein ID</b>	<b>MAb D</b>	<b>MAb D<sub>M</sub></b>
1. Chondroitin sulfate protoglycan 4	0.46	0.11
2. Nidogen-1	-	0.05
3. Actin	0.12	0.41
4. SPARC	-	0.36
5. Cathepsin D	-	0.41
6. Sulfated glycoprotein 1	0.14	0.18
7. Glucose regulated protein	0.14	-
8. Dickkopf-related protein 3	0.09	0.24

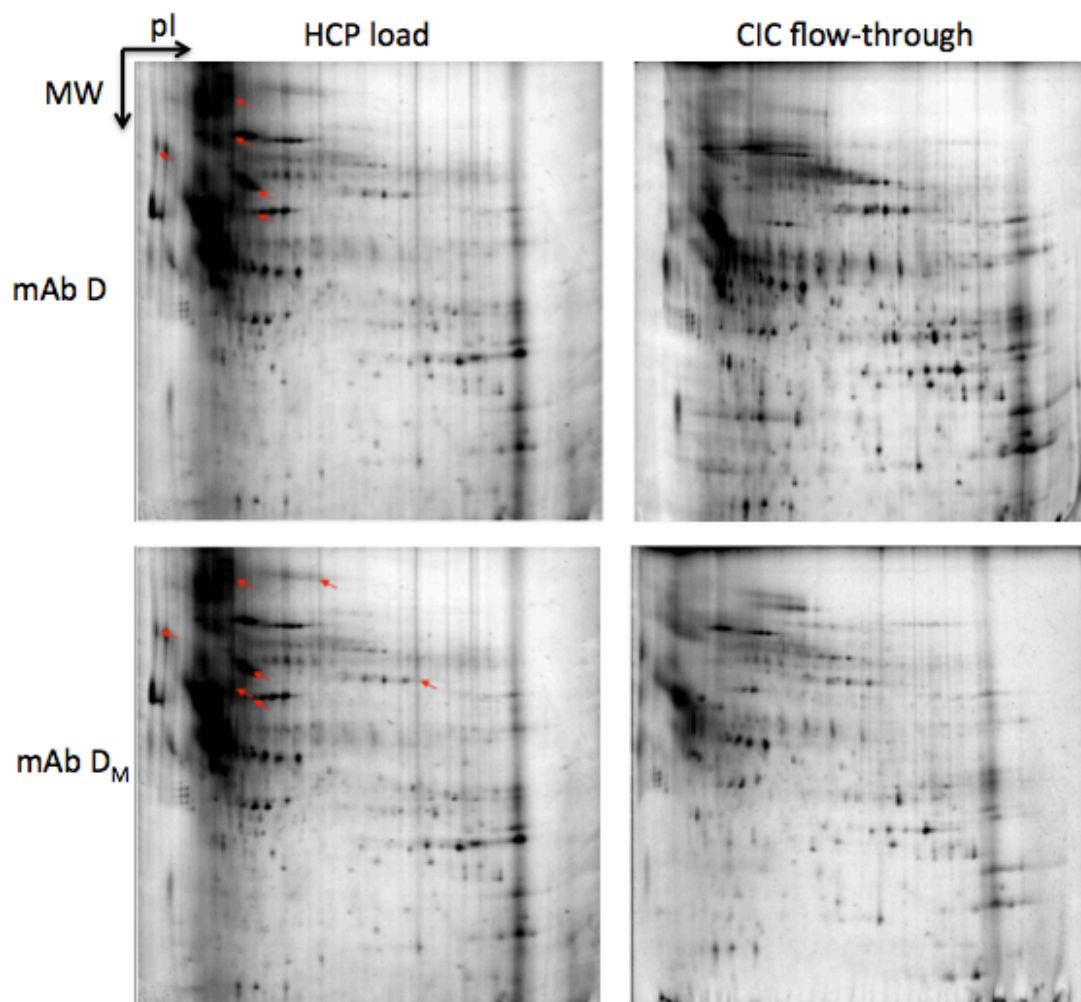
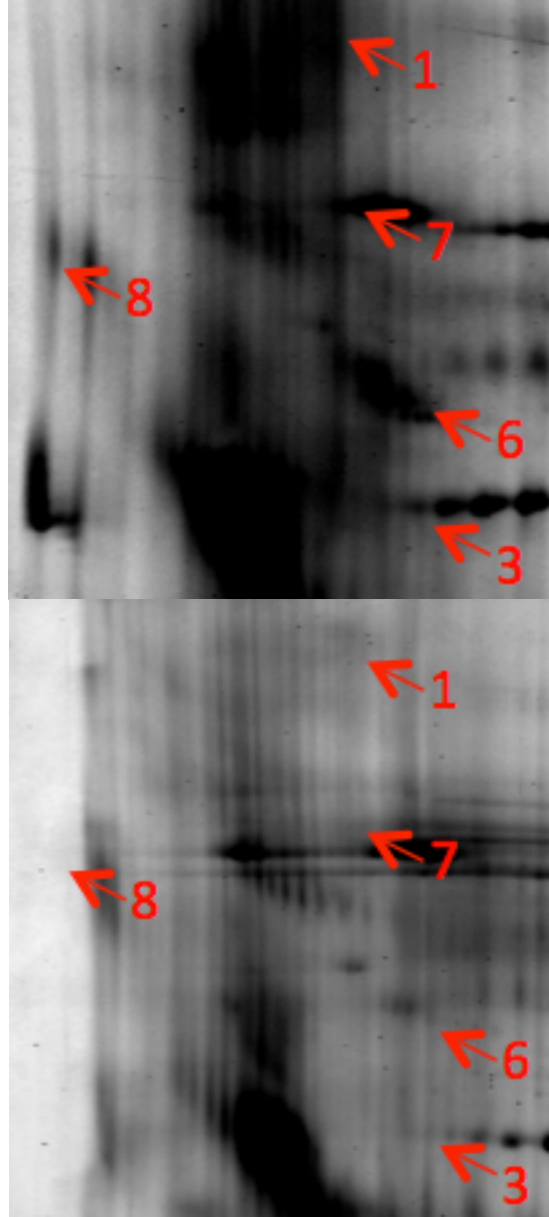


Figure B.1: Analyzed 2-DE ‘load’ (left column) and ‘flow-through’ (right column) gels for HCP CIC of mAb D and mAb D<sub>M</sub> in HIC loading conditions. Indicated spots on ‘load’ gels are absent from corresponding ‘flow-through’ gels and represent strongly interacting HCPs.

### B.1.1 MAb D HCP-CIC 2-DE Analysis: HIC Conditions

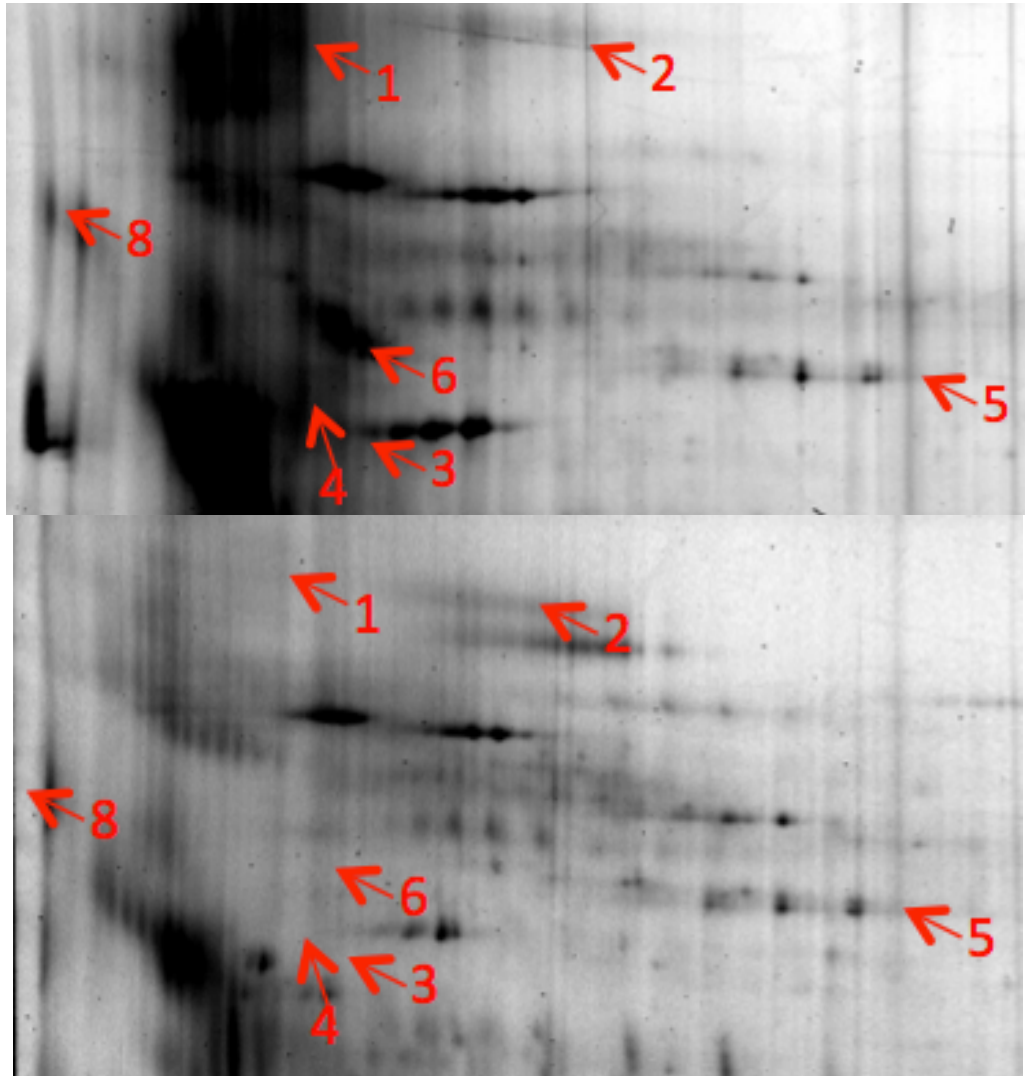
Numbers on 'load' and 'flow-through' gels refer to Table B.1.



Load (above) and flow-through (below)

### B.1.2 MAb D<sub>M</sub> HCP-CIC 2-DE Analysis: HIC Conditions

Numbers on 'load' and 'flow-through' gels refer to Table B.1.



Load (above) and flow-through (below)

## **Appendix C**

### **MAB FRAGMENT PURIFICATION**

MAB B, mAb C, IDEC-152 and Mill04 were digested by papain and purified using a two-column scheme described in Section 2.5. The two-column process consists of protein A affinity purification followed by a second chromatographic purification to separate Fc from undigested and partially digested mAb. The second column was different for each mAb (Table 2.2). The chromatographic results for the second column in each process are described here.

#### **C.1 MAb B Fc Chromatographic Purification**

Eluate from the protein A affinity purification of papain-digested mAb B was loaded onto SP Sepharose FF at pH 4.5 followed by a 25 CV linear salt gradient from 0 to 0.5 M NaCl. The chromatogram is in Figure C.1. There is a small amount of material that does not bind to the column. This is likely due to overloading of the CEX column. There are two major peaks across the linear salt gradient elution. The earlier eluting peak is the purified Fc domain. The later eluting peak contains undigested mAb, partially digested mAb and mAb aggregate. The relative size of the two main peaks is indicative of the low efficiency of papain cleavage of mAb B. The majority of material here is full mAb rather than Fc.

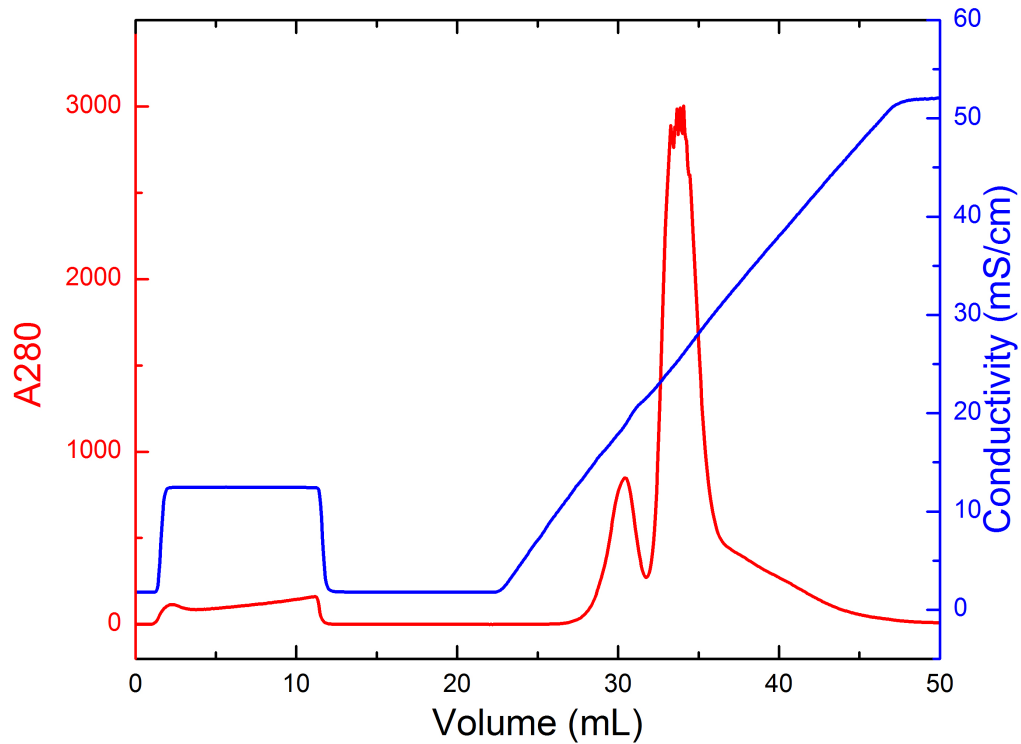


Figure C.1: Chromatographic purification of mAb B Fc on SP Sepharose FF at pH 4.5 with a 25 CV linear gradient from 0 to 0.5 M NaCl. The first peak is the Fc domain and the second peak is undigested mAb.

## C.2 MAb C Fc Chromatographic Purification

MAb C Fc fragments were purified similarly to mAb B. Linear salt gradient elution on SP Sepharose FF at pH 4.5 was used to separate mAb C Fc fragments from undigested mAb in the protein A affinity column eluate. The chromatogram is in Figure C.2. Similarly to mAb B fragment purification, there are two main peaks eluting across the linear salt gradient. The peaks are similar in size, indicating slightly improved papain digestion efficiency compared to mAb B. However, the chromatographic separation is worse. The first peak is mAb C Fc and the second peak is undigested mAb. Subsequent mAb C Fc purifications used a more gradual linear

salt gradient to allow for collection of pure Fc in early fractions. Chromatographic fractions collected at the start of the first peak were sufficiently pure for cross-interaction chromatographic applications.

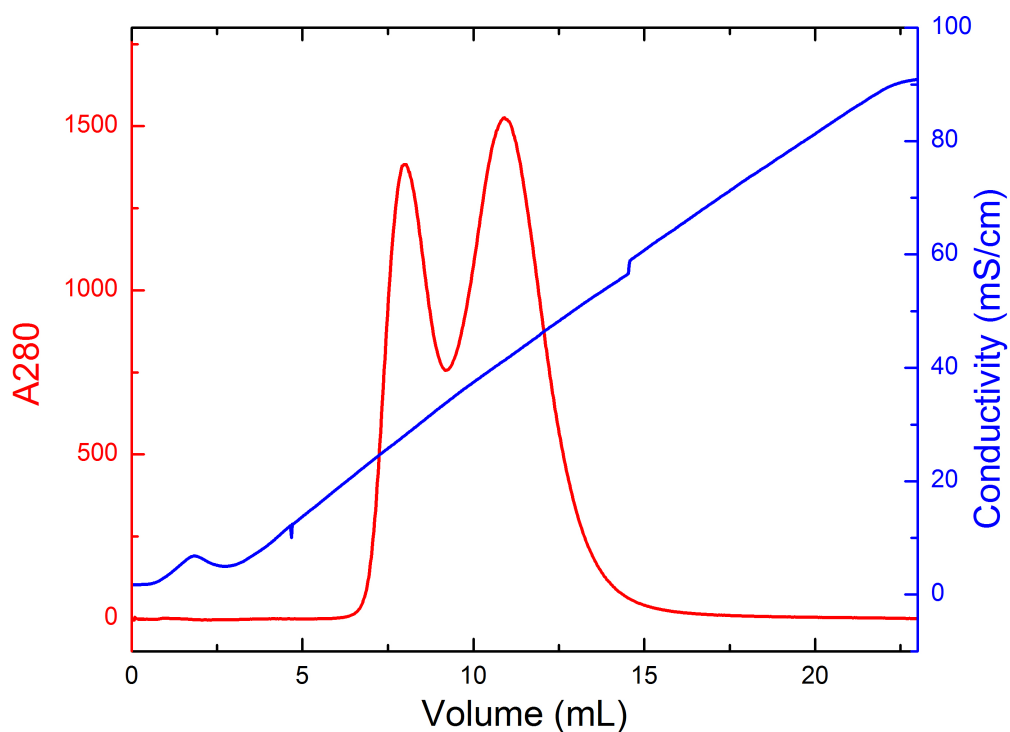


Figure C.2: Chromatographic purification of mAb C Fc on SP Sepharose FF at pH 4.5 with a linear gradient from 0 to 1 M NaCl over 20 CVs. The first peak is Fc and the second peak is intact mAb. Subsequent runs at more gradual gradient resulted in better peak separation.

### C.3 IDEC-152 Fc Chromatographic Purification

IDEC-152 Fc fragments were purified from undigested mAb after protein A purification using anion exchange chromatography. QAE 550 resin with a linear salt gradient elution was run at pH 8.5. The chromatogram is in Figure C.3. The majority

of material is in the flow-through fraction. This is due to both exclusion of the intact mAb and low binding affinity of IDEC-152 on the anion exchange resin; the mAb has low net charge at pH 8.5 because it is close to the pI. The peak that elutes at the start of the gradient elution contains purified IDEC-152 Fc fragment. As discussed above, the relative size of the Fc and mAb peaks demonstrates the low efficiency of papain cleavage.

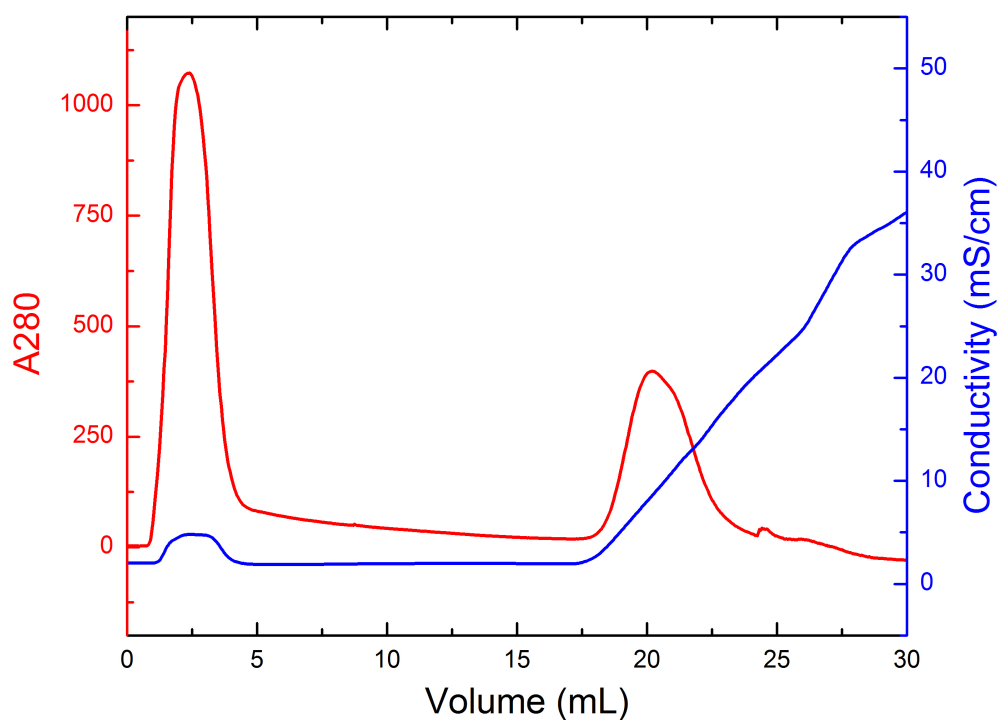


Figure C.3: Chromatographic purification of IDEC-152 Fc on QAE 550 at pH 8.5 with a linear salt gradient from 0 to 0.4 M NaCl over 15 CVs. Undigested mAb is found in the 'flow-through' and Fc fragment is in the elution fraction.

#### **C.4 Mill04 Fc Fragment Purification**

Mill04 Fc fragments were purified from undigested mAb and partially digested mAb after protein A purification of the papain digest. SP 650S resin was used at pH 5.5 with a linear gradient elution from 0 to 0.5 M NaCl over 20 CVs. The chromatogram is in Figure C.4. The Mill04 Fc purification has different features than any of the previously discussed Fc purifications. There are three main peaks across the gradient elution. The earliest eluting peak contains the purified Fc domain. The next two peaks are not well resolved from each other. The middle peak contains a 100 kDa species; this is most likely a mAb with a single Fab domain removed. The latest eluting peak is the undigested mAb. Papain enzymatic cleavage of Mill04 has a similar efficiency compared to the other mAbs discussed here.

Although papain efficiency was low and the yield for some of the Fc purification processes used here is low, sufficient material was produced for self- and cross- interaction chromatography applications.

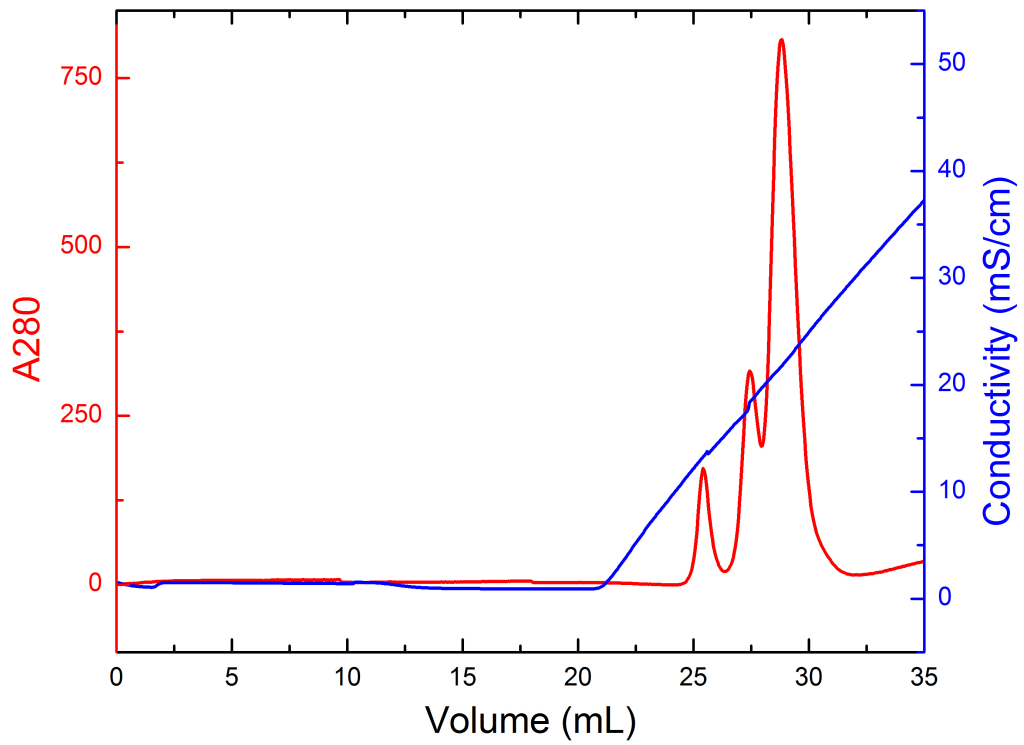


Figure C.4: Chromatographic purification of Mill04 Fc on SP 650S at pH 5.5 with a linear salt gradient from 0 to 0.5 M NaCl over 20 CVs. The first peak is Fc, the second peak is Fc-Fab and last peak is full mAb.

## Appendix D

### LIPOPROTEIN LIPASE DNA SEQUENCE

#### D.1 Synthesized CHO LPL Sequence

The Chinese hamster LPL gene sequence (UniProKB entry G3H6V7) was synthesized by Life Technologies. The synthesized LPL sequence is in Figure D.1. The synthesized sequence included NdeI and BamHI restriction enzyme sites at the 5' and 3' ends respectively. To assist the purification of LPL, a six His tag sequence was also added between the last codon of LPL and the BamHI site. The sequence was optimized for expression in *E. coli* using GeneOptimizer® software. Although the gene was optimized for expression in *E. coli*, this same gene was also used for YSD experiments in Chapter 5.

1. CATATG M A A A D G G R D F T D I E S K F A L R T  
 70. P D D T A E D N C H L I P G I A E S V S N C H  
 CCGGATGATACCGCAGAAGATAATTGTCATCTGATTCCGGGTATTGCAGAAAAGCGTTAGCAATTGCCAT  
 139. F N H S S K T F V V I H G W T V T G M Y E S W  
 TTTAACCATAGCAGCAAAACCTTTGGTGGTATTCATGGTTGGACCGTTACCGGTATGTATGAAAGCTGG  
 208. V P K L V A A L Y K R E P D S N V I V V D W L  
 GTTCCGAAACTGGTTGCAGCACTGTATAAACGTGAACCGGATAGCAATGTTATTGTTGTGGATTGGCTG  
 277. Y R A Q Q H Y P V S A G Y T K L V G N D V A R  
 TATCGTGCACAGCAGCATTATCCGGTTAGCGCAGGTTATACCAAACCTGGTGGTAATGATGTTGCCCGT  
 346. F I N W M E E E F N Y P L D N V H L L G Y S L  
 TTTATCAATTGGATGGAAGAAGAATTTAACTATCCGCTGGATAATGTTTCATCTGCTGGGTTATAGCCTG  
 415. G A H A A G V A G S L T N K K V N R I T G L D  
 GGTGCATAGCAGCCGGTGTTCAGGTAGCCTGACCAACAAAAAGTTAATCGTATTACCGGTCTGGAC  
 484. P A G P N F E Y A E A P S R L S P D D A D F V  
 CCTGCAGGTCCGAATTTTGAATATGCAGAAACCCGAGCCGTCTGAGTCCGGATGATGCAGATTTTGT  
 553. D V L H T F T R G S P G R S I G I Q K P V G H  
 GATGTTCTGCATACCTTTACCGTGGTAGTCCGGGTCGTAGCATTGGTATTAGAAAACCGGTTGGTCAT  
 622. V D I Y P N G G T F Q P G C N I G E A I R V I  
 GTTGATATTTTCCGAATGGTGGCACCTTTAGCCTGGTTGTAATATTGGTGAAGCCATTCGTGTTATT  
 691. A E R G L G D V D Q L V K C S H E R S I H L F  
 GCCGAACGTGGTCTGGGTGATGTTGATCAGCTGGTTAAATGTAGCCATGAACGTAGCATTACCTGTTT  
 760. I D S L L N E E N P S K A Y R C N S K E A F E  
 ATTGATAGCCTGCTGAATGAAGAAAATCCGAGCAAGCATATCGCTGCAATAGCAAGAAGCCTTTGAA  
 829. K G L C L S C R K N R C N N V G Y E I N K V R  
 AAAGGTCTGTGCTGAGCTGTCGTAATAATCGTTGTAATAACGTGGGCTACGAGATCAATAAAGTTTCGT  
 898. A K R S S K M Y L K T R S Q M P Y K V F H Y Q  
 GCAAAACGTTCCAGCAAAATGTATCTGAAAACCCGTAGCCAGATGCCGTATAAAGTTTTTCATTACCAG  
 967. V K I H F S G T E S D K Q L N Q A F E I S L Y  
 GTGAAAATCCACTTTAGCGGCACCGAAAAGCGATAAACAGCTGAACCGGCATTTGAAATTAGCCTGTAT  
 1036. G T V A E S E N I P F T L P E V S T N K T Y S  
 GGCACCGTTGCGGAAAGCGAAAATATCCGTTTACCCTGCCGGAAGTTTCAACCAATAAAACCTATAGC  
 1105. F L I Y T E V D I G E L L M M K L K W K S D S  
 TTCCTGATCTATACCGAAGTGGATATTGGCGAACTGCTGATGATGAAACTGAAATGGAAAAGCGATAGC  
 1174. Y F S W S D W W S S P G F V I E K I R V K A G  
 TACTTCAGCTGGTCAGATTGGTGGTCAAGTCCGGGTTTTGTGATTGAAAAAATTCGTGTGAAAAGCCGGT  
 1243. E T Q K K V I F C A R E K V S H L Q K G K D S  
 GAAACCCAGAAAAAAGTGATTTTTGTGCCCGTAAAAAGTGAGCCATCTGCAGAAAAGGTAAGATAGC  
 1312. A V F V K C H D K S L K K S G H H H H H H \*  
 GCAGTTTTTGTGAAATGCCATGATAAAAGCCTGAAAAAAGCGGTCATCATCACCATCACCCTAA GGA  
 1381. TCC

Figure D.1. CHO LPL sequence synthesized by Life Technologies. N-del (1-6) and BamH1 (1378-1383) restriction enzyme sites are highlighted in yellow.

**Appendix E**  
**PERMISSION LETTERS**

The following is the official permission for the reprint of content that was previously published by John Wiley and Sons and is contained in Chapter 3.

**JOHN WILEY AND SONS LICENSE  
TERMS AND CONDITIONS**

Jun 19, 2014

---

This is a License Agreement between Nicholas E Levy ("You") and John Wiley and Sons ("John Wiley and Sons") provided by Copyright Clearance Center ("CCC"). The license consists of your order details, the terms and conditions provided by John Wiley and Sons, and the payment terms and conditions.

**All payments must be made in full to CCC. For payment instructions, please see information listed at the bottom of this form.**

License Number	3412580860842
License date	Jun 19, 2014
Licensed content publisher	John Wiley and Sons
Licensed content publication	Biotechnology & Bioengineering
Licensed content title	Identification and characterization of host cell protein product-associated impurities in monoclonal antibody bioprocessing
Licensed copyright line	© 2013 Wiley Periodicals, Inc.
Licensed content author	Nicholas E. Levy, Kristin N. Valente, Lella H. Choe, Kelvin H. Lee, Abraham M. Lenhoff
Licensed content date	Dec 11, 2013
Start page	904
End page	912
Type of use	Dissertation/Thesis
Requestor type	Author of this Wiley article
Format	Electronic
Portion	Full article
Will you be translating?	No
Title of your thesis / dissertation	HOST CELL PROTEIN IMPURITIES AND PROTEIN-PROTEIN INTERACTIONS IN DOWNSTREAM PURIFICATION OF MONOCLONAL ANTIBODIES
Expected completion date	Jun 2014
Expected size (number of pages)	250
Total	0.00 USD
Terms and Conditions	

**TERMS AND CONDITIONS**

This copyrighted material is owned by or exclusively licensed to John Wiley & Sons, Inc. or one of its group companies (each a "Wiley Company") or handled on behalf of a society with

which a Wiley Company has exclusive publishing rights in relation to a particular work (collectively "WILEY"). By clicking  accept  in connection with completing this licensing transaction, you agree that the following terms and conditions apply to this transaction (along with the billing and payment terms and conditions established by the Copyright Clearance Center Inc., ("CCC's Billing and Payment terms and conditions"), at the time that you opened your Rightslink account (these are available at any time at <http://wvaccount.copyright.com>).

#### **Terms and Conditions**

- The materials you have requested permission to reproduce or reuse (the "Wiley Materials") are protected by copyright.
- You are hereby granted a personal, non-exclusive, non-sub licensable (on a stand-alone basis), non-transferable, worldwide, limited license to reproduce the Wiley Materials for the purpose specified in the licensing process. This license is for a one-time use only and limited to any maximum distribution number specified in the license. The first instance of republication or reuse granted by this licence must be completed within two years of the date of the grant of this licence (although copies prepared before the end date may be distributed thereafter). The Wiley Materials shall not be used in any other manner or for any other purpose, beyond what is granted in the license. Permission is granted subject to an appropriate acknowledgement given to the author, title of the material/book/journal and the publisher. You shall also duplicate the copyright notice that appears in the Wiley publication in your use of the Wiley Material. Permission is also granted on the understanding that nowhere in the text is a previously published source acknowledged for all or part of this Wiley Material. Any third party content is expressly excluded from this permission.
- With respect to the Wiley Materials, all rights are reserved. Except as expressly granted by the terms of the license, no part of the Wiley Materials may be copied, modified, adapted (except for minor reformatting required by the new Publication), translated, reproduced, transferred or distributed, in any form or by any means, and no derivative works may be made based on the Wiley Materials without the prior permission of the respective copyright owner. You may not alter, remove or suppress in any manner any copyright, trademark or other notices displayed by the Wiley Materials. You may not license, rent, sell, loan, lease, pledge, offer as security, transfer or assign the Wiley Materials on a stand-alone basis, or any of the rights granted to you hereunder to any other person.
- The Wiley Materials and all of the intellectual property rights therein shall at all times remain the exclusive property of John Wiley & Sons Inc, the Wiley Companies, or their respective licensors, and your interest therein is only that of having possession of and the right to reproduce the Wiley Materials pursuant to Section 2 herein during the continuance of this Agreement. You agree that you own no right, title or interest in or to the Wiley Materials or any of the intellectual property rights therein. You shall have no rights hereunder other than the license as provided for above in Section 2. No right, license or interest to any trademark, trade name, service mark or other branding ("Marks") of WILEY or its licensors is granted hereunder, and you agree that you shall not assert any such right, license or interest with respect thereto.
- NEITHER WILEY NOR ITS LICENSORS MAKES ANY WARRANTY OR

REPRESENTATION OF ANY KIND TO YOU OR ANY THIRD PARTY, EXPRESS, IMPLIED OR STATUTORY, WITH RESPECT TO THE MATERIALS OR THE ACCURACY OF ANY INFORMATION CONTAINED IN THE MATERIALS, INCLUDING, WITHOUT LIMITATION, ANY IMPLIED WARRANTY OF MERCHANTABILITY, ACCURACY, SATISFACTORY QUALITY, FITNESS FOR A PARTICULAR PURPOSE, USABILITY, INTEGRATION OR NON-INFRINGEMENT AND ALL SUCH WARRANTIES ARE HEREBY EXCLUDED BY WILEY AND ITS LICENSORS AND WAIVED BY YOU

- WILEY shall have the right to terminate this Agreement immediately upon breach of this Agreement by you.
- You shall indemnify, defend and hold harmless WILEY, its Licensors and their respective directors, officers, agents and employees, from and against any actual or threatened claims, demands, causes of action or proceedings arising from any breach of this Agreement by you.
- IN NO EVENT SHALL WILEY OR ITS LICENSORS BE LIABLE TO YOU OR ANY OTHER PARTY OR ANY OTHER PERSON OR ENTITY FOR ANY SPECIAL, CONSEQUENTIAL, INCIDENTAL, INDIRECT, EXEMPLARY OR PUNITIVE DAMAGES, HOWEVER CAUSED, ARISING OUT OF OR IN CONNECTION WITH THE DOWNLOADING, PROVISIONING, VIEWING OR USE OF THE MATERIALS REGARDLESS OF THE FORM OF ACTION, WHETHER FOR BREACH OF CONTRACT, BREACH OF WARRANTY, TORT, NEGLIGENCE, INFRINGEMENT OR OTHERWISE (INCLUDING, WITHOUT LIMITATION, DAMAGES BASED ON LOSS OF PROFITS, DATA, FILES, USE, BUSINESS OPPORTUNITY OR CLAIMS OF THIRD PARTIES), AND WHETHER OR NOT THE PARTY HAS BEEN ADVISED OF THE POSSIBILITY OF SUCH DAMAGES. THIS LIMITATION SHALL APPLY NOTWITHSTANDING ANY FAILURE OF ESSENTIAL PURPOSE OF ANY LIMITED REMEDY PROVIDED HEREIN.
- Should any provision of this Agreement be held by a court of competent jurisdiction to be illegal, invalid, or unenforceable, that provision shall be deemed amended to achieve as nearly as possible the same economic effect as the original provision, and the legality, validity and enforceability of the remaining provisions of this Agreement shall not be affected or impaired thereby.
- The failure of either party to enforce any term or condition of this Agreement shall not constitute a waiver of either party's right to enforce each and every term and condition of this Agreement. No breach under this agreement shall be deemed waived or excused by either party unless such waiver or consent is in writing signed by the party granting such waiver or consent. The waiver by or consent of a party to a breach of any provision of this Agreement shall not operate or be construed as a waiver of or consent to any other or subsequent breach by such other party.
- This Agreement may not be assigned (including by operation of law or otherwise) by you without WILEY's prior written consent.
- Any fee required for this permission shall be non-refundable after thirty (30) days from

receipt by the CCC.

- These terms and conditions together with CCC's Billing and Payment terms and conditions (which are incorporated herein) form the entire agreement between you and WILEY concerning this licensing transaction and (in the absence of fraud) supersedes all prior agreements and representations of the parties, oral or written. This Agreement may not be amended except in writing signed by both parties. This Agreement shall be binding upon and inure to the benefit of the parties' successors, legal representatives, and authorized assigns.
- In the event of any conflict between your obligations established by these terms and conditions and those established by CCC's Billing and Payment terms and conditions, these terms and conditions shall prevail.
- WILEY expressly reserves all rights not specifically granted in the combination of (i) the license details provided by you and accepted in the course of this licensing transaction, (ii) these terms and conditions and (iii) CCC's Billing and Payment terms and conditions.
- This Agreement will be void if the Type of Use, Format, Circulation, or Requestor Type was misrepresented during the licensing process.
- This Agreement shall be governed by and construed in accordance with the laws of the State of New York, USA, without regards to such state's conflict of law rules. Any legal action, suit or proceeding arising out of or relating to these Terms and Conditions or the breach thereof shall be instituted in a court of competent jurisdiction in New York County in the State of New York in the United States of America and each party hereby consents and submits to the personal jurisdiction of such court, waives any objection to venue in such court and consents to service of process by registered or certified mail, return receipt requested, at the last known address of such party.